CENTER FOR INFRASTRUCTURE ENGINEERING STUDIES

Strengthening of Masonry Elements with FRP Composites

by

University of Missouri-Rolla
Antonio Morbin, Visiting Scholar

University of Missouri-Rolla

Disclaimer

The mission of CIES is to provide leadership in research and education for solving society's problems affecting the nation's infrastructure systems. CIES is the primary conduit for communication among those on the UMR campus interested in infrastructure studies and provides coordination for collaborative efforts. CIES activities include interdisciplinary research and development with projects tailored to address needs of federal agencies, state agencies, and private industry as well as technology transfer and continuing/distance education to the engineering community and industry.

Center for Infrastructure Engineering Studies (CIES)
University of Missouri-Rolla
223 Engineering Research Lab
1870 Miner Circle
Rolla, MO 65409-0710
Tel: (573) 341-6223; fax -6215
E-mail: cies@umr.edu
www.cies.umr.edu

ABSTRACT

The worldwide engineering community has identified failures of URM walls as one of the major causes of material damage and loss of human life due to seismic events. Therefore, the development of effective and affordable retrofitting techniques for masonry members is an urgent need. Fiber Reinforced Polymer (FRP) composites provide solutions for the strengthening of URM walls subjected to in-plane and out-of-plane overstresses caused by high wind pressures or earthquake loads. The presented research, part of the effective collaboration between the Department of Construction and Transportation (DCT) of University of Padua (Italy) and the Center for Infrastructure Engineering Studies (CIES) of University of Missouri-Rolla (U.S.A.), deals with the mechanical behavior of masonry walls strengthened with FRP composites and subjected to out-of-plane and in-plane loading. Two series of walls were tested for this research study. The first series studied the behavior of masonry wallettes under out-of-plane loads; the second series analyzed the performance in terms of shear capacity of masonry panels. FRP composites in the form of laminates and rods were used as strengthening materials. The results showed that both flexural and shear capacity of masonry walls can be notably increased by strengthening with FRP composites. A strengthening method denominated "FRP structural repointing" demonstrated that besides increasing the wall capacity it can preserve its aesthetics. Analytical models to predict the behavior of strengthened walls, as well as provisional guidelines to design the FRP strengthening for shear and flexure are also presented. Finally, conclusions are provided and future research needs on the area of masonry strengthening are outlined.

ACKNOWLEDGEMENTS

To Chiara, for her love

TABLE OF CONTENTS

x

1.
INTRODUCTION

1.1 GENERAL

Being one of the oldest and most widely used types of construction system in the world, masonry deserves to be rediscovered by modern engineering technology. Inherent advantages, like aesthetic, architectural appearance, effective heat and sound isolation, fire resistance and economical construction, will contribute to the use of masonry as the prime material specially for residential construction once its behaviour be well understood (*Sucuoglu et al.* 1991).

Masonry buildings have historically been designed with little or no regard for the effects of seismic loadings or high speed winds.

Recent earthquakes in California, Japan, Italy, Turkey and other areas of the world have demonstrated that these older masonry structures are extremely susceptible to the forces imposed during such events. With each new earthquake, reinforcement strategies have been update. However, existing masonry buildings still remain at risk because, with few exceptions, these older structures have not been improved to meet the current standards. The upgrading of such structures has become a priority in the fields of earthquake engineering and retrofitting old historical buildings.

Fig.1.1 *Debris on Pioneer Square*
Seattle,U.S.A., Feb 2001

1.1.1 <u>Background</u>

Structural weakness or overloading, dynamic vibrations, settlement, and in-plane and out-of-plane deformations can cause failure of masonry structures. Unreinforced masonry (URM) buildings have features that can threaten human lives. These include unbraced parapets, inadequate connections to the roof, and the brittle nature of the URM elements. As a matter of fact, organizations such as *The Masonry Society (TMS)* and *the Federal Emergency Management Agency (FEMA)*, have identified that failures of URM walls result in more material damage and loss of human life during earthquakes than any other type of structural element. This was evident from the recent post-earthquake observation in Turkey.

Nowadays, in the United States, large investments are being directed to retrofitting projects. It is estimated that the national average spending on reconstruction is about 25% of new construction investment (*U.S. Census Bureau* 1998). For example, under the URM Building Law of California, passed in 1986, approximately 25,500 URM buildings were inventoried throughout the state. Even though this number is relatively small percentage of the total building inventory in California, it includes many cultural icons and historical buildings. The building evaluation showed that 96% of the URM buildings in California needed to be retrofitted. To date, it has been estimated that only half of the owners have taken remedial actions, which may be attribute to the retrofitting cost. Thereby, the development of effective and affordable retrofitting techniques for masonry elements is an urgent need.

Seismic loadings induce ***out-of-plane*** bending of walls between the restraining floors. Analysis of the failure modes must take into account many different factors, such as boundary conditions, wall compressive strengths, joint tensile strengths, wall stiffness, and applied loadings. Walls will typically remain stable under dead load and after cracking if they are within the specified height-to-thickness ratio. In the slenderness ratio is exceeded, the wall needs bracing by either a horizontal brace or vertical columns. Parapets, chimneys, and similar elements extending above the topmost line of restraint are most vulnerable to out-of-plane forces.

Fig.1.1.1 a-b *Out-of-plane collapse of bearing walls*
Umbria, Italy, 1997

In-plane resistance of unreinforced masonry walls is based on mortar strength and brick proportions. If the forces are strong enough to exceed the in-plane strength capacity of the wall, a shear failure will occur. This failure mode is characterized by brittle tensile cracking through the mortar and the masonry unit and a sudden loss of lateral load capacity.

Earthquake forces cause walls to push against and pull away from the floors that they are connected to. Failure to have a secure *connection* between the two elements can cause failure by falling brick as well as floor collapse. This type of problem can be corrected and work can be performed while the building is occupied.

Fig.1.1.1c *In-plane failure of load-bearing walls*
Umbria, Italy, September 1997

Current methods of retrofitting masonry structures have proved to be effective , but have many drawbacks. These methods usually include the addition of framing elements such as steel columns, pilasters, beams, or surface treatments such as shotcrete or ferrocement to increase the strength and ductility of the walls. Such procedures are often time consuming to apply, not cost-effective, add significant mass to the structure, encroach upon available working space, and adversely affects the aesthetics of the repaired area and in many cases the building as a whole. The extra mass added to the structure can also increase the earthquake-induced inertia forces and may require strengthening of the footing as well.

These problems may be overcome by using *fiber reinforced polymers (FRP)* reinforcement instead of the conventional methods. Because of the corrosion of metal reinforcement in concrete structures, alternative procedures are being studied and FRP products have proved to be a successful solution. Supporting research and development in the use of FRP for reinforcement, repair and strengthening was conducted for reinforced concrete applications, especially in United States and Japan for the last 20 years.

While extensive research was conducted and reported for reinforced and prestressed concrete structures, much less has been reported for masonry structures.

1.1.2 <u>Objectives and scope</u>

Many failures can occur in unreinforced masonry (URM) buildings when they are subjected to dynamic or static actions such as those caused by moderate earthquakes, high speed winds, deterioration, construction or design mistakes.

During a seismic event, walls located at the bottom story of the building may be overstressed because the shear forces at that level are larger than any other story. On the other hand, walls located at the upper stories are prone to fail under out-of-plane loading because the maximum seismic accelerations occur at those levels.

This research, as a part of the collaboration between University of Missouri-Rolla, U.S.A., and University of Padua, Italy, investigates the mechanical behavior of masonry walls reinforced with FRP composites (in particular, rods and laminates) and subjected to out-of-plane and in-plane loading.

The first series of walls deals with the flexural behavior of members strengthened with FRP laminates and with high height/thickness ratios. Different widths of reinforcement

are evaluated and depending of the amount of FRP applied remarkable differences in the mode of failure are observed.

In the second series of walls a new technique, called "structural repointing", less intrusive in terms of aesthetics, has been explored; variables such as different configurations of strengthening and masonry typologies are investigated.

For both of the series static load tests to failure are performed in order to understand the behavior of the specimens.

Because of the urgent need of an international code for the design of FRP reinforcement for masonry structures, one of the most important goals of this study is to provide provisional design guidelines to be implemented by practitioners when retrofitting URM walls.

1.1.3 <u>Thesis Layout</u>

The research is organized according to the stages followed for the development of the investigation. Thus, ***Chapter 1.1*** introduces the significance of the strengthening of masonry elements, which led to setting the objectives of the research.

There is a great diversity of masonry systems around the world. Masonry differs from region to region. Furthermore, it can be said that in addition to architectural and structural requirements, the construction practice of a region or country plays a role in selecting a determined typology.

In that context ***Chapter 1.2*** provides a brief description of the masonry walls typologies used through United States.

Also, strengthening methods using "conventional" materials are presented.

Chapter 1.3 deals with the main properties of composite materials, focusing on fiber reinforced polymers, and in particular FRP laminates and FRP rods, typologies of reinforcement being used in this research.

The behavior of masonry walls subjected to out-of-plane and in-plane is studied and discussed in ***Chapter 2*** and ***Chapter 3***, respectively.

The walls are strengthened with different composite systems such as Aramid FRP (AFRP), Glass FRP (GFRP) laminates and GFRP rods.

The specimens, test setups and test procedures are thoroughly described. The test results are interpreted and mechanisms of failure are identified.

Assumptions and expressions used for the development of analytical models are presented; the analytical values are confronted with the experimental values. With the premise that further research needs to be conducted, ***Chapter 4*** presents provisional design guidelines for flexural and shear strengthening of URM walls with FRP composites, developed through recent U.S. codes for masonry structures.

Chapter 5 provides conclusions and recommendations for future work in the area of masonry strengthening with FRP composites.

In ***Appendix A*** different tests for a mechanical characterization of the materials being used in the present research are described and discussed.

Finally, ***Appendix B*** and ***Appendix C*** gather all the graphs related to the study and the pictures taken when performing the tests for out-of-plane and in-plane tests respectively.

1.2 MASONRY

1.2.1 MASONRY IN THE UNITED STATES

Masonry constitutes approximately 70% of the existing building inventory in the United States. Most of these buildings are constituted by unreinforced masonry, in special to the east of the Rocky Mountains. During the formation of the United States as a new nation, bearing unreinforced masonry walls were a very common form of construction. These walls had thickness ranging from 12 to 40 inches, and were multi-wythe walls, where sometimes rubble was used for the interior wythes. The walls were commonly built with hand-made and fired clay units, bonded by sand-lime mortar. A good example of this kind of construction is the *Monadnock Building* in Chicago (see Figure 2.1). This 16-story building completed in 1891 had 6 feet thick walls at the base, decreasing 4 inches in thickness per floor, to a minimum thickness of 12 inches at the top. The thick walls occupied a valuable floor space and impose a heavy load on the foundations; that is why that by 1940, the building had settled 20 inches in the soft clay soil.

Fig.1.2.1 *Monadnock Building*

The transition from traditional to modern methods was a consequence of the severe damage to URM walls due to the earthquake of 1933 in Long Beach, California. This seismic event forced to take preventive actions for future earthquakes. Through the California's Field Act, the use of masonry was prohibited in all the public buildings throughout the state of California. In the late 1940's and early 1950's, the masonry construction was revitalized in California. It was required that new masonry edifications complied with the newly developed Uniform Building Code, which was based on the reinforced concrete design practice of the time. Those provisions required that minimum seismic lateral forces be considered in the design of masonry elements, that tensile stresses in masonry be resisted by reinforcement; and that at least a minimum percentage of horizontal and vertical reinforcement be used.

In contemporary North American commercial construction, masonry walls include panel, curtain, and bearing walls, which can be unreinforced or reinforced (Klingner, 1994).

1.2.1.1 **Panel, curtain and bearing walls**

Panel walls are single-story walls meant to primarily resist out-of-plane loads generated by either earthquakes or wind; and vertical loads primarily due to self-weight. Panel walls are a common façade element in buildings conformed by frames of steel or reinforced concrete. This kind of walls may consist of two wythes separated by at least 2-inch air space, commonly referred as to cavity walls. Panel walls may also consist of single wythe or multiple wythes in contact with each other. In the latter case are also denominated composite walls. When built within steel or RC frames

these walls are called *infill walls*, and are commonly found forming the envelope of the building to protect the interior from the external environment; for this reason are also called *barrier walls*. Infill walls can be subjected to in-plane loads caused by their interaction with the surrounding frame. Due to vertical spans of 12 feet or less, panel walls can satisfactorily resist out-of-plane loading and are generally unreinforced.

Curtain walls are multi-story walls that also resist out-of-plane loads due to earthquakes or wind. If a single wythe is used, horizontal steel, in the form of welded reinforcement, is placed in the mortar joints to increase the wind resistance. This kind of construction is commonly referred to as "partially reinforced".

Bearing walls are arranged at a fairly uniform spacing to resist out-of-plane loads, in-plane loads (traditionally called "shear walls" when having this function); and vertical loads from self-weight and upper tributary floor areas. Cavity and composite walls can also lie on this category. Depending on the load solicitations bearing walls can be unreinforced or reinforced.

In the United Stated, differences of masonry systems can be categorized according to the geographical region. Thus, in contrast to the eastern United Stated, masonry in the western United State has been primarily developed for earthquake resistance criteria, and secondarily for architectural and fire resistance criteria. Because of the seismic considerations the majority of the masonry construction in that part of the country consists of reinforced and fully grouted walls built with concrete masonry units (CMU), which are meant to act as shear and bearing elements.

1.2.1.2 Masonry in backup walls

Commonly two different masonry units are found in backup or inner walls, clay tiles and concrete units. Structural clay tile has been first manufactured in the United States approximately since 1875. A clay tile is a hollow unit, which is characterized by possessing parallel cores and thin webs and face shells. In the beginning, structural tile was used in building floors and as a fireproofing material for steel frame construction. Owing to its lightweight, large unit size and ease of handling during construction, the use of clay tiles was extended to load-bearing walls, wall facings, silos, columns, etc. In the early 1900's, structural clay tiles were used in infill walls throughout the United States. Some notable structures were it is possible to observe this kind of construction are *the New York Chrysler Building*, *Los Angeles City Hall*

Building, and *the Oakland City Hall Building* in California, which is considered a historic structure.

Figure 5 illustrates information, made available by the U.S. Department of Commerce Census of Manufacturers, on the production of clay tile in the 20th century. As can be observed, the maximum peak in the production of clay tiles was in the 1920's. As a consequence of the Great Depression, the production suffered a dramatic decrease. As World War II began, the economy was revitalized and large public works were performed. Some of military facilities built primarily with clay tiles included Fort Benning in Georgia, and the Women's Army Auxiliary Corps Barracks in Iowa. From the same figure, it is observed that the production of clay tiles decreased during the 1960's, when concrete units began to be widely used.
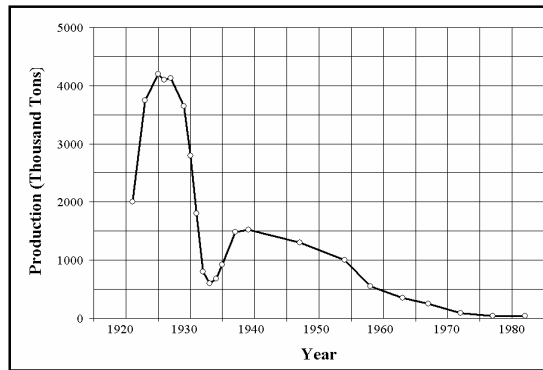
Fig.1.2.1.2 *Production of Clay Tile during the 20th Century*

It is important to point out that the use of concrete units was not new in the United States. Concrete blocks were first manufactured in the United States at about the turn of the 20th century in small one-at-a-time machines that could be operated by hand and purchased from Sears and Roebuck catalogs. Using this kind of machines, the production was limited to 10 blocks per man-hour. Due to manufacturing and aesthetic limitations, and because the architects preferred the use of stone because of its integrity, the use of concrete units was limited. The concrete block were not widely used until the 1920's when the manufacturing processes were improved; however due to the big recession many plants had to close or merge. It was not until the 1960's that the market started to change. This change is attributed to the automation of plant equipment, which increased the production capability of concrete blocks. The increase in production capability led to low unit cost and increased available quantity. In

addition, the manufacturing process of concrete units allowed a better quality control of the products. For instance, concrete units show more uniformity since they are not fired during their manufacture process. Also, due to the brittle characteristics of clay tiles when being handled and transported, made that the demand of concrete units was increased. Another cause for the decrease of clay tiles production was the efforts driven by *the Environmental Protection Agency (EPA)* to reduce the environmental costs associated with the manufacture of clay masonry units. This led to the closing of many old plants where the kilns generated emissions above the standards.

1.2.2 TRADITIONAL REPAIRING TECHNIQUES

In this section, the most common retrofitting techniques are reviewed.

1.2.2.1 <u>Repointing</u>

Over time, mortar joints may spall or erode due to freeze-thaw cycles or water drainage paths or the joints may not have been well filled or not filled with durable mortar. Also, debonding and separation cracks along the joints may occur due to differential movement. In most cases, deteriorated or unsatisfactory mortar joints can be repaired by *repointing*. Note that the term "repointing" is not applied consistently across the masonry industry and in some geographic areas may be taken to mean simply replacing missing mortar. The cutting out, filling, and retooling of masonry joints is sometimes called *tuck pointing*.

A common practice is to hose down the wall about one hour before repointing to remove debris and to wet masonry units. The fresh mortar, matching the original material as closely as possible, is placed in layers and tooled when thumb print hard. The new mortar should match as closely as possible the existing mortar in color, texture, and physical properties. In major restoration projects of historic buildings, comprehensive investigations may be justified to ensure the compatibility and long term durability of the repaired joints (see Fig. 1.2.2.1).

| (1) | (2) |
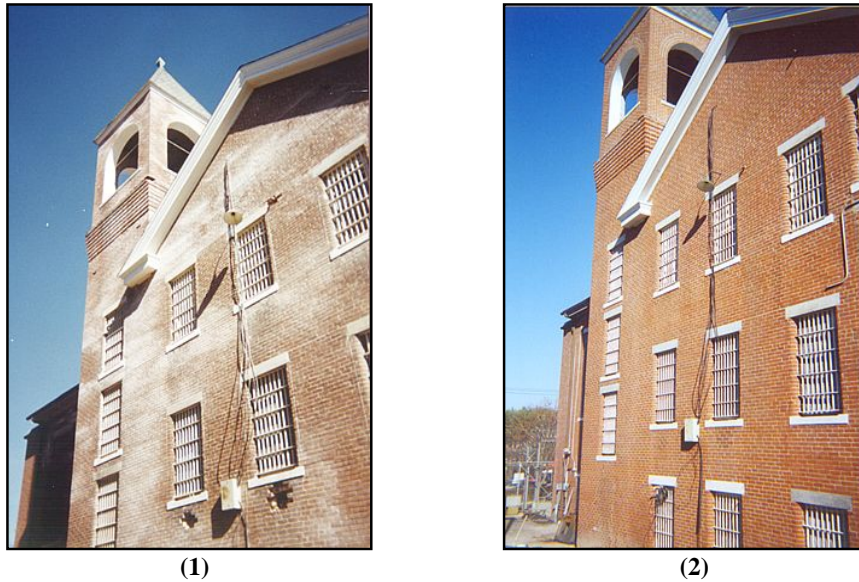
Fig. 1.2.2.1 *A masonry facade before (1) and after (2) a repointing application*

1.2.2.2 <u>Grout Injection</u>

Grout can be injected into walls to anchor other components or to strengthen and stiffen a wall by solidly filling hollow masonry. Whether using a non-shrink Portland cement grout (preferably an expanding grout) or an epoxy or polymer-modified grout, it is important to ensure complete filling and avoid later shrink-back as water is adsorbed from the grout. Experience has shown that the effectiveness depends on the compatibility of physical, chemical, and mechanical properties of the original masonry and the injected material (*Binda et al.* 1993).

The grout material should be selected to maximize the following desirable properties:

- high water retentivity
- minimum shrinkage or even slight expansion
- highly fluid grout but not subjected to segregation of constituent materials
- high tensile strength (greater than standard mortars)
- high bond to mortar and units (greater than bond of standard mortars)

1.2.2.3 <u>Grout Filling of Hollow and Cavity Walls</u>

Filling the cells of hollow units with grout increases the compressive capacity and, because of the greater tensile strength of grout compared to mortar bond, also produces a significant improvement in flexural and in-plane shear capacities. Filling voids with grout can also improve the resistance to water penetration, particularly for single-wythe construction. Except for very large cells or cavity widths, gravity placement of grout is typically not reliable due to obstructions from mortar fins and droppings and because of the difficulty of providing vibration for consolidation. Therefore, pressure grouting from the bottom up is usually the most reliable method for achieving complete filling. The vertical spacing is limited by the ability of the masonry to withstand internal pressure., by the capacity of the pump, and by the desire to limit the height of lifts to allow for some consolidation due to water absorption and compaction of the grout. Fine grout, often incorporating a plasticizer, is typically used and commercially available products that also recommended to avoid shrink-back of the grout and creation of voids in the grout or between the grout and the masonry.

1.2.2.4 <u>External Reinforcing Overlay</u>

Prawel et al. (1985) conducted an investigation on masonry panels retrofitted with ferrocement overlays. Ferrocement is an orthotropic composite material, which consists of a high-strength cement mortar matrix and layers of fine steel wires configured in the form of a mesh. The overall thickness usually varies between 0.5 and 1 in. The tensile strength of the ferrocement layer ranges from 500 to 2000 psi, and it is dependable on mesh type, and the amount and orientation of the reinforcement. These overlays are used to increase in-plane and out-of-plane resistance. This study was focused on masonry specimens subjected to in-plane loading. The specimens consisted of 25.5 in. by 25.5 in. brick panels laid in a stack bond pattern, having a thickness of 8 in. A 0.5 in.-wide layer of ferrocement, with different amounts of reinforcement, were attached to both sides of the masonry to increase the shear strength.
The specimens were subjected to diagonal in-plane loading. Two modes of failure were observed, a ductile one caused by yielding of the steel wire and a brittle failure caused by debonding of the ferrocement overlay from the masonry surface. The experimental results indicated that the strength and ductility were almost doubled in

the coated walls compared to the unstrengthened wall. Fig. 1.2.2.4 illustrates the test results of three specimens. In the testing of panel 2, which had a 0.5 in. mesh wire spacing, it was observed that the layer of ferrocement debonded from masonry after substantial cracking. In contrast, in panel 3, with a mesh wire spacing of 0.125 in., complete yielding and tensile failure of the mesh was observed.
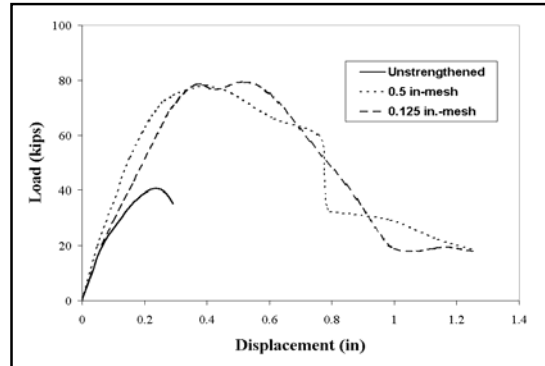
Fig. 1.2.2.4 *Test Results-External Reinforcing Overlay*

1.2.2.5 <u>Internal Steel Reinforcing</u>

Manzouri et.al. (1996) evaluated the efficiency of repairing URM walls by grout injection in combination with horizontal and vertical steel reinforcement. URM walls were built in three whites with clay bricks for an overall dimension of 8 ft.-6 in by 5 ft. The walls were tested under in-plane loading. First, the behavior of the walls in their original condition was investigated. Then, the walls were retrofitted to be tested once again. All the retrofitted walls were injected with grout. The severely damaged areas were repaired by replacement with similar materials. Crack widths larger than 0.06 in were injected with a coarse aggregate; whereas, crack widths ranging between 0.008 to 0.06 in. were injected with a fine grout. Steel ties for use as dry-fix remedial anchor were placed as vertical reinforcement used for the pinning of the wythes in the toe area; and horizontal reinforcement as can be observed in Fig. 1.2.2.5a. The ties were made of Type 304 stainless steel with a helical design, similar to a self-tapping screw, which cuts a spiral groove as it is tapped into a pilot hole. The installation procedure included cutting of certain bed joints to a depth of 3-in. followed by placement of the tie in the slot and sealing with mortar.
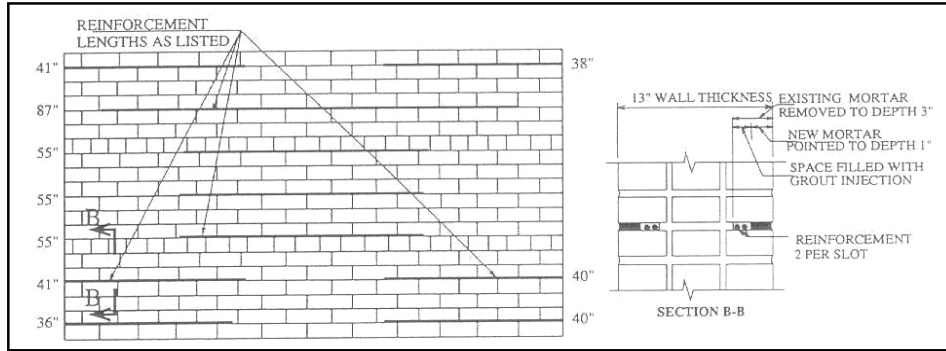
Fig. 1.2.2.5a *Location of Horizontal Reinforcement-Internal Steel Reinforcing*

The test results demonstrated that the injection of grout accompanied by repair of localized damaged areas can restore the original strength and stiffness of retrofitted walls. The introduction of horizontal reinforcement increased the strength and ductility of the wall system, since shear failure was prevented. It was also observed that the vertical reinforcement increased the lateral resistance and ductility.

Fig. 1.2.2.5b illustrates the test results for a wall before and after being strengthened.
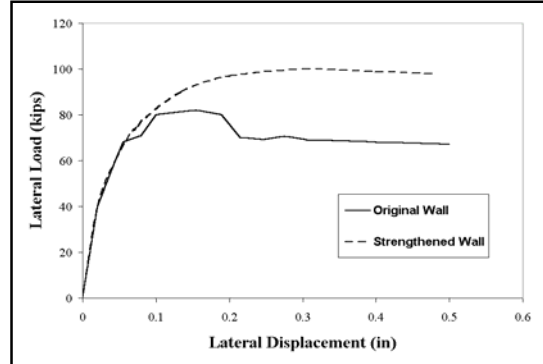
Fig. 1.2.2.5b *Test Results-Internal Steel Reinforcing*

In old structures, load bearing masonry elements are prone to vertical cracking due to the combined effect of the gravitational sustained load and cyclic loads. This phenomenon has been observed in masonry towers and pillars throughout Europe, and can eventually lead to the collapse of the structure. *Binda et al.* (1999) investigated a technique to repair and strengthen masonry elements subjected to the aforementioned mechanism. This technique consisted of grooving the bed joints, placing of mortar along with the steel reinforcement (bars or plates) as shown in Figure 1.2.2.5c.

14

10x20x 44 in. panels were built for this research program. Initially, the specimens were pre-cracked by compressive loads representing the 80% of their capacity. After this, the specimens were repaired by placing two #6 bars every three bed joints in grooves 2.5 in.-deep grooves. The test results of the repaired specimens showed that the strength was not improved. However, significant results in terms of deformation were attained, which was evident from the reduced cracking observed. In the repaired walls, reductions in the strains ranging between 40% and 50% were recorded. It was concluded that the structural degradation process of a masonry element can be detained; especially if the overall conditions are improved by other strengthening techniques such as injections and replacement of damaged sections.
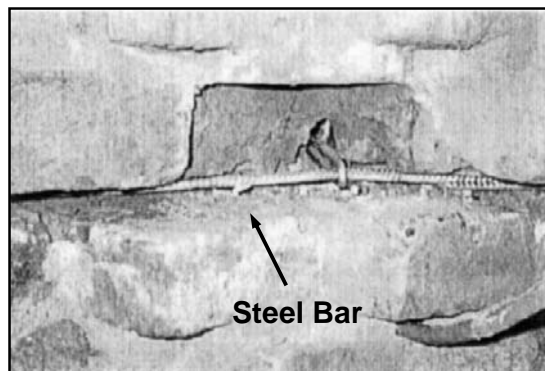
Fig. 1.2.2.5c *Internal Reinforcement*

1.2.2.6 <u>External Steel Plate Reinforcing</u>

Taghdi et al. (2000) proposed a strengthening method which consisted of placing diagonal and vertical steel strips on both sides of lightly reinforced masonry walls, as illustrated in Figure 1.2.2.6a.
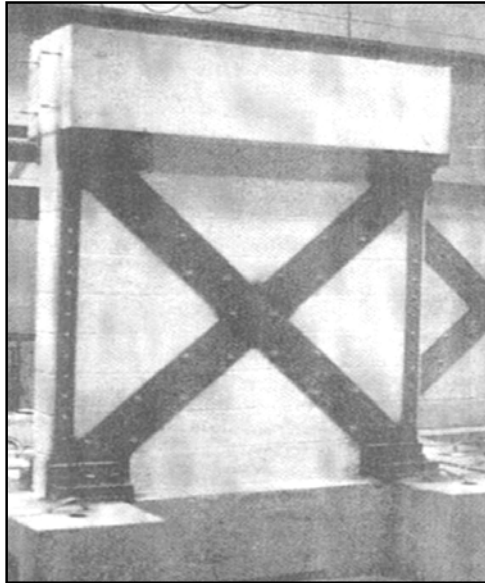
Fig. 1.2.2.6a *Steel Plate Reinforcing*

The walls were built with standard concrete masonry units, being their overall dimensions 72 in. by 72 in. The walls were internally reinforced with No.8 gauge ladder reinforcement every 2 courses, and Canadian M15 vertical steel placed at the edges and at the center of the wall. The retrofitting strategy consisted of two 9-in wide diagonal steel strips with a thickness of 0.15 in. The diagonal steel strips were welded at the intersection. Structural steel bolts were used to fasten the steel strips to the walls. Also, steel angles and high strength anchors connected the strips to the floor to prevent sliding of the walls. Fig.1.2.2.6b illustrates the test results of an unstrengthened wall and a wall strengthened with the described method. Although the primary objective of this experimental program was to study the in-plane behavior of strengthened walls, it was suggested that the proposed technique could also be effective for walls subjected to out-of-plane loading. A shear failure with crushing of the masonry diagonal struts was observed in the unstrengthened wall. In the strengthened wall, the diagonal steels strips delayed the crushing of masonry until

excessive yielding, which led to buckling in the strips, occurred. It was observed that the vertical strips provided a ductile flexural behavior to the walls; and the steel strip system prevented the development of rigid body rotation and allowed cracks to spread the cracks.
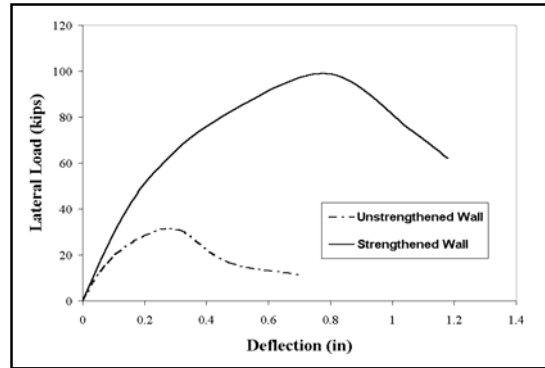
Fig. 1.2.2.6b *Test Results-Internal Steel Reinforcing*

1.3 FIBER REINFORCED COMPOSITES

1.3.1 OVERVIEW

Although the concept of fiber reinforced materials can be traced back to the use of straw as reinforcement in bricks manufactured by the Israelites in 800 B.C., and in more recent times to the use of short glass fiber reinforcement in cement in United States in the early 1930's, fiber reinforced resin matrix materials (or ***fiber reinforced composites*** as we know them today) were not developed until the early 1940's.

After World War II, US manufacturers began producing *fiberglass* and *polyester resin* composite boat hulls and radomes (radar cover). The automotive industry first introduced composites into vehicle bodies in the early 1950s. Because of the highly desirable light weight, corrosion resistance, and high strength characteristics in composites; research emphasis went into improving the material science and manufacturing process. That effort led to the development of two new manufacturing techniques known as *filament winding* and *pultrusion*, which helped advance the composite technology into new markets. There was a great demand by the recreation industry for composite fishing rods, tennis rackets, ski equipment and golf clubs. The aerospace industry began to use composites in pressure vessels, containers, and non-structural aircraft components. The US Navy applied composites in mine sweeping vessels, crew boats and submarine parts. The domestic consumers began installing composite bath tubs, covers, railings, ladders and electrical equipment. The first civil application in composites was a dome structure built in Benghazi in 1968, and other structures followed slowly.

1.3.2 GENERAL PROPERTIES OF COMPOSITES

A composite is a combination of two or more materials into a single system that exhibits combined properties of its individual components. The system constituents retain their distinct identities (they do not dissolve or merge completely into each other) and act in concert as a hybrid to provide new, desirable properties. Reinforced concrete, for example, is a composite consisting of steel reinforcement, sand and gravel fillers, and a cement matrix.

Composite materials are composed of a ***matrix*** material reinforced with any of a variety of fibers (reinforcing phase) made from ceramics, metals, or polymers. The

reinforcing fibers are the primary load carriers of the material, with the matrix component transferring the load from fiber to fiber. Reinforcement of the matrix material may be achieved in a variety of ways: fibers may be either continuous or discontinuous, and the reinforcement may also be in the form of particles (see Fig.1.3.2a). The matrix material is usually one of the many available engineering plastics/polymers.

Selection of the optimal reinforcement form and material is dependent on the property requirements of the finished part.
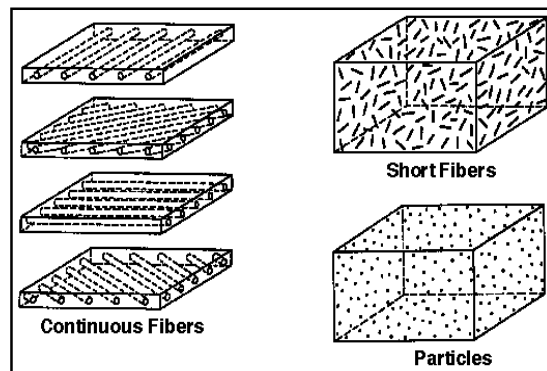
Fig.1.3.2a Reinforcement of matrix material

The advantages of composite materials over metals are:

- Light weight
- Can tailor the fiber/resin mix to meet
- Meet stiffness/strength/manufacturing requirements
- Reduced machining
- Resistance to corrosion
- Resistance to fatigue damage
- Good damping characteristics
- Low coefficient of thermal expansion

Weight: A weight savings of 27% is attainable in most structures. This is due to the lower density of composites, which range (depending on material form) from 0.045 lb/in^3 (1246 daN/m^3) to 0.065 lb/in^3 (1800 daN/m^3) as compared to 0.10 lb/in^3 (2768

daN/m^3) for aluminum. Some applications may require thicker composite sections to meet strength/stiffness requirements, however, a weight savings will still result.

Cost: Low cost, high volume manufacturing methods are used to make composites cost competitive with metals: tooling costs for high volume production of metals and composites parts are similar and also the production labor time is similar, so the higher cost of composite parts is mostly due to high raw material costs; a judicious selection of the optimal material for the part (not the best material) and of the suppliers will control these costs and can minimize the cost penalty.

Composite performance: Composites have inherent properties that provide performance benefits over metals. A wide range of fibers and resins are available to select the optimal material combination to meet the structural requirements. The strength-to-weight and stiffness-to-weight ratios are the primary reasons composites are used. The fiber reinforcements provide good damping characteristics and high resistance to fatigue and most resins provide very good resistance to chemicals and corrosion. The fracture toughness of composites is better than aluminum castings; by their nature, castings basically have built-in notches that can catastrophically fracture under impact. The fiber reinforcement of composites alter this failure sequence; resulting in an increased resistance to impact. The impact toughness of composites can be maximized by fiber selection, length of fiber and use of tougher resin such as thermoplastics.

Composite materials will provide structure that saves weight and has better performance over the competing metallic structure. The structure will be more durable and tougher. Composites will enable the consolidation of parts thus improving the reliability of the structure and keeping the costs competitive with metallic structure.

The composite industry associations and materials producers track the FRP's composites material shipments in eight primary markets like shown in the follow figure:

U.S. Composite Shipments 1998 Market Share - Volume

- ■ Marine
- ■ Other
- □ Transportation
- □ Construction
- ■ Corrosion/Resistant
- ■ Aircraft
- ■ Consumer
- □ Appliance/Buisness Equipment
- ■ Electrical/Electronic

11.8%   0.6%   6.3%   5.5%   10.0%   10.1%   3.3%   20.8%   31.6%
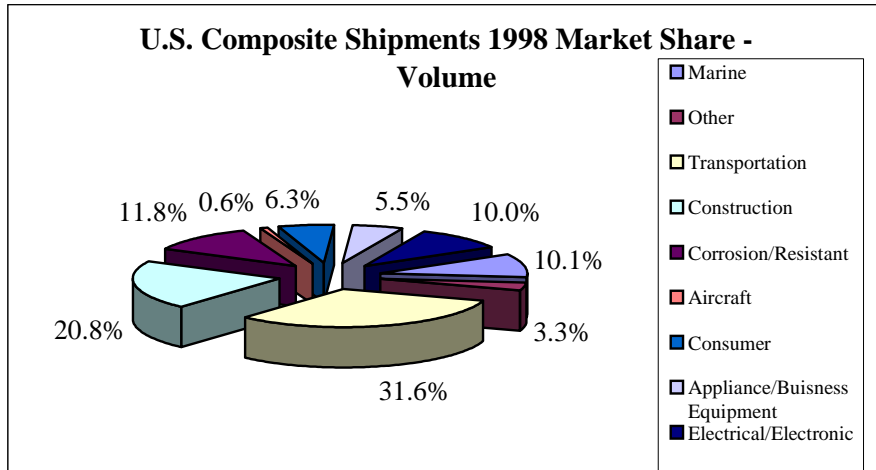
Fig. 1.3.2b *SPI Composites Institute, May 1999 – Includes shipments of reinforced thermoset and thermoplastic resin composites, reinforcements and fillers*

The composites industry has shown growth over the past ten years and is projected to increase as FRP composites are accepted in new markets. The FRP increase is presented in the figure below:

Growth of FRP Composites From 1970 to 2000

Pounds Shipped (in millions)

4000
3000
2000
1000
0

1969   1979   1989   1999

Years
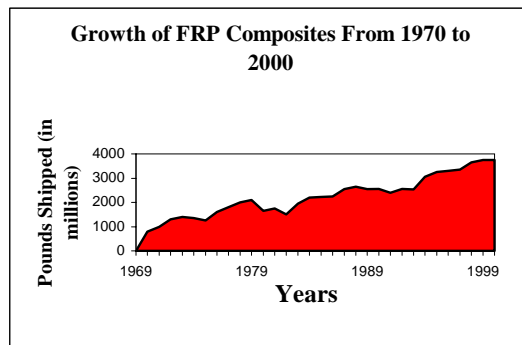
Fig. 1.3.2c *Growth of FRP composites from 1970 to 2000*

1.3.3 FIBER REINFORCED POLYMERS

Fiber reinforced polymers (**FRP**) are a particular typology of composite materials, made of high resistance fibers impregnated with polymeric resins. The mixing result is a material with properties between fiber and resin.
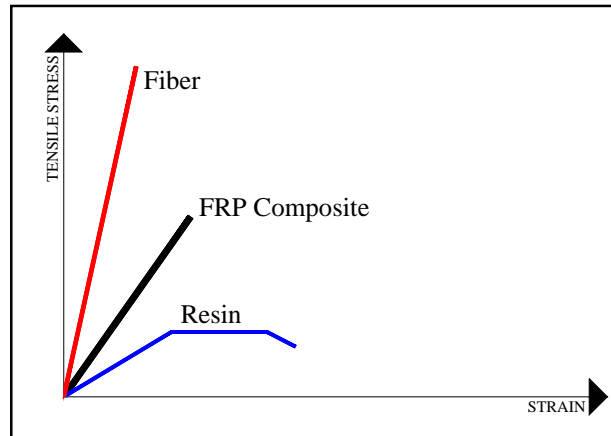
Fig. 1.3.3a *Comparison among fiber's, resin's and composite's tensile properties*

FRP materials are characterized by excellent tensile strength in the direction of the fibers and by negligible strength in the direction transverse to the fibers; this illustrates the anisotropic nature of these materials. FRP composites do not exhibit yielding, but instead are elastic up to failure and they are also characterized by relatively low modulus of elasticity in tension and low compressive properties.

Their function usually consists in adsorbing tensile stress due to shear and flexural actions. Often, among the reachable advantages, are also the increase of the overall stiffness and ductility.

FRP properties make these materials particularly suitable for structural applications, especially in support or substitution of steel.

The general advantages of FRP reinforcement compared to steel are:

- Durability in aggressive environments

- High strength-to-density ratio

- Magnetic and electric neutrality

- Low specific weight

- Low axial coefficient of thermal expansion

Without underlining the importance of a lower installation cost, the use of FRP composites possesses some advantages compared to traditional retrofitting methods; as an example, the disturbance of the occupants and the facilities are minimal and there is no loss of valuable space. In addition, from the structural point of view, the dynamic properties of the structure remain unchanging because there is no addition of weight that would lead to increases in seismic forces.

FRP products are commercialized in different shapes: rods, tendons, laminates and three-dimensional components.

FRP reinforcement comes in the shape of rods of circular cross-sections, strips of rectangular cross-sections, strands, and laminates, which enable different types of applications.
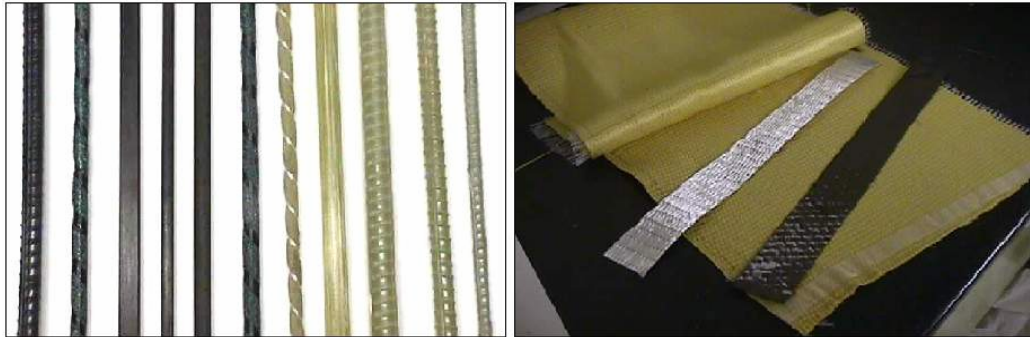
Fig. 1.3.3b *FRP rods (left) and laminates (right)*

1.3.3.1 <u>Reinforcing phase:fibers</u>

The three most common types of FRP used in construction are made of ***carbon***, ***aramid*** or ***glass fibers***.

- ***Carbon Fibers***: Fiber produced by heating organic precursor materials containing a substantial amount of carbon (93÷95%), such as rayon, polyacrylonitrile (PAN), or pitch (a black residue from the distillation of petroleum) in an inert environment. This kind of fibers is the strongest, stiffest, and most durable; they are more expensive than glass fibers but offer an excellent combination of strength, low weight, high modulus and fatigue properties.

- *Aramid Fibers (ex. Kevlar)***:**   Highly oriented organic fiber derived from polyamide incorporating into aromatic ring structure. This kind of fibers offers excellent impact resistance, a good electric and temperature insulating properties and they are also resistant to organic solvents, fuels and lubricants.

  They have a medium modulus and a very low density as compared to glass and carbon.

  It is available in tows, yarns and various woven cloth products.

- *Glass Fibers***:** Fiber drawn from an inorganic product of fusion that has cooled without crystallizing. **E-Glass** fibers are considered the predominant reinforcement for polymer matrix composites, due to their high electrical insulating properties and low susceptibility to moisture. Other commercial composition includes **S-Glass,** with higher strength, heat resistance and modulus, as well as some specialized glass reinforcements with improved chemical resistance, such as AR Glass (alkali resistant). On the other hand, these products are very expensive. Glass produces a common, low-cost reinforcing fiber, but they weight more than carbon or aramid and the lower modulus requires special design treatment where stiffness is critical. Glass has been the predominant fiber for many civil engineering applications because of an economical balance of cost and specific strength properties.

A comparison based on fiber area only among sheets made of carbon (CFRP), aramid (AFRP), glass (GFRP) and reinforcing steel in terms of stress-strain relationship is illustrated in figure 1.3.3c:
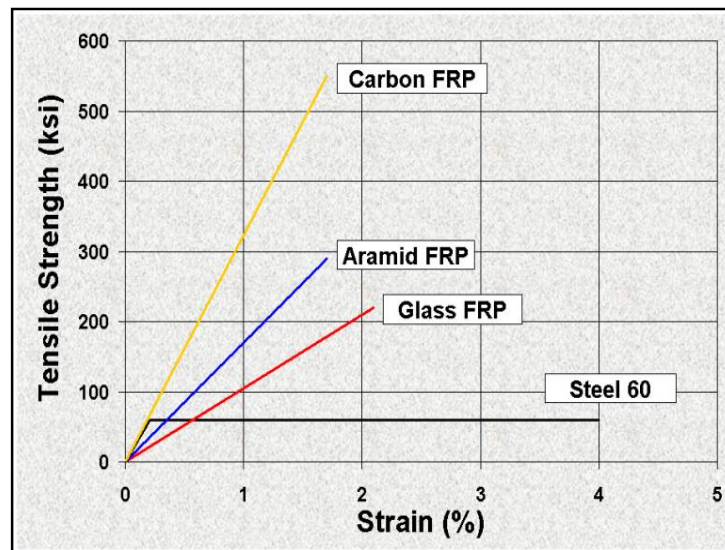
Fig. 1.3.3c *Comparison among AFRP, CFRP, GFRP and Steel*

1.3.3.2 <u>Matrix</u>

The ***FRP matrix*** consists of a polymer, or resin, used as a binder for the reinforcing fibers, and it has two main functions: it enables the load to be transferred among fibers and protects them from environmental effects.

The resin is fundamental for interlaminate and in-plane shear strength: the interlaminate strength is important for the structures inflection and the in-plane strength is important for the torsion. Furthermore, FRP workability and defects depend of some physical-thermal resin's properties   like viscosity, vulcanization temp and melting point. Polymeric resins are subdivided in two big categories, thermosetting and thermoplastic:

- The ***thermosetting polymers*** after the vulcanization (with energy under appearances of heat energy or with catalysts) are insoluble and not melt also with high temperature.

- The ***thermoplastic polymers*** are instead soluble, because they have a low molecular bond; so, these resins can be weak, melted and mold all times you want.

The ***glass transition temperature (T_g)*** is used to measure the softening of cured resin. Generally the resins are isotropic and they have an elastic-brittle behavior.

Also if the thermoplastic resins had a large development as for thermosetting polymers, there are still many problems to soak the fibers, so, in the building's field, there are three types of commonly available thermo-setting resins: epoxy, vinyl ester and phenolic.

- ***Epoxy*** resins are the most common and have excellent structural properties as well as excellent adhesion characteristics; a major benefit of epoxy resins is their lower shrinkage. Epoxy can also be formulated with different materials or blended with other epoxy resins to achieve specific performance features. Epoxies are used primarily for fabricating high performance composites with superior mechanical properties and good performance at elevated temperatures; this kind of resin has particularly good UV resistance and their maximum use temperature is on the order of 200° F (93.3° C). Epoxy resins are available in a

range of viscosity, and will work with a number of curing agents or hardeners.

- *Vinyl ester* resins are a lower cost matrix material with good durability characteristics, excellent corrosion resistance and very good mechanical toughness, but have lower structural performance and low resistance to heat. Vinyl esters were developed to combine the advantages of epoxy resin with the better handling/faster cure, which are typical for unsaturated polyester resins.
- *Phenolic* are a class of resins commonly based on phenol and formaldehyde. Phenolic composites have many desirable performance qualities include high temperature resistance, creep resistance, excellent thermal insulation and sound damping properties, corrosion resistance and excellent fire/smoke toxicity properties.

Phenolic appears the most important resin, but epoxy and vinylester are the most commonly used because of durability and adhesion properties.

The main mechanical properties of a typical epoxy resin are shown below:

Density	0.043 lb/in^3 (1200 Kg/m^3)
Elastic modulus	493128 Psi (3.4 GPa)
Shear modulus	189710 Psi (1.308 Gpa)
Tensile strength	10443 Psi (72 Mpa)

Tab. 1.3.3d *Typical epoxy resin properties*

Thermosetting resins are generally heat activated, or cured, from an initial liquid state. Resins are often combined with additives and fillers for environmental resistance, flame resistance, appearance, and cost reduction.

1.3.3.3 <u>Fillers</u>

The use of inorganic fillers in composites is increasing; they not only reduce the cost of composites, but also frequently impart performance that might not otherwise be achieved by the reinforcement and resin ingredients alone. These materials improve the following performance:

- They reduce the shrinkage of the composites part
- They influence the fire resistance of laminates
- Fillers can influence the mechanical strengths of composites

- Crack resistance and crack prevention properties are improved with filled resin systems
- Uniformity of the laminate can be enhanced by use of fillers

There are a lot of inorganic filler materials that can be used with composites including *Calcium Carbonate* (the most used), *Kaolin*, *Alumina trihydrate*, *Calcium sulfate* etc…

1.3.3.4 Additives

A wide of additives are used in composites to modify materials properties and tailor the FRP performance. Additive used in thermosetting composites include the following:

- Fire resistance (in place of fillers)
- Viscosity control
- Toughness
- Heat stabilizers
- Ultraviolet stabilizers

1.3.3.5 Reinforcement forms

Reinforcements are available in forms to serve a wide range of processes and end-product requirements and they can be obtained using multi-end or single-end roving.

Multi-end roving consists of many individual strands or bundles of filaments, which are than chopped and randomly deposited into the resin matrix; these products can be used in pultrusion application.

The single-end roving consists of many individual filaments wound into a single strand. The product is generally used in processes that utilize a unidirectional reinforcement.

Materials supplied as reinforcement include:

- Mats
- Woven, stitched, braided & 3D fabrics
- Unidirectional
- Rods/Laminates

1.3.3.5.1 Mats

Reinforcing mats are usually described by weight-per-unit-of-area; the type and amount of binder that is used to hold the mat together dictate differences between mat products.

1.3.3.5.2 Woven, stitched, braided & 3D fabrics

There are many type of fabrics that can be used to reinforce resin in a composite. Multidirectional reinforcements are produced by weaving, knitting, stitched or braiding continuous fibers into a fabric form twisted and plied yarn.

Fabrics allow the precise placement of the reinforcement.

- **Woven** fabrics are fabricated on looms in a variety of weights, weaves and widths. In a plain weave, each fill yarn or roving is alternately crosses over and under each warp fiber. This work allows the fabric to be more drapeable and conform to curved surface.

- **Stitched** fabrics have optimized strength properties because of the fiber architecture. Stitched fabrics are produced by assembling successive layers of aligned fibers. Typically, the available fiber orientations include the 0° direction (warp), 90° direction (weft) and 45° direction (bias). This type of construction allows for load sharing between fibers so that a higher modulus, both tensile and flexural, is typically observed. Multiple orientation provide a quasi-isotropic reinforcement. The following figure shown the typical fiber's orientation:
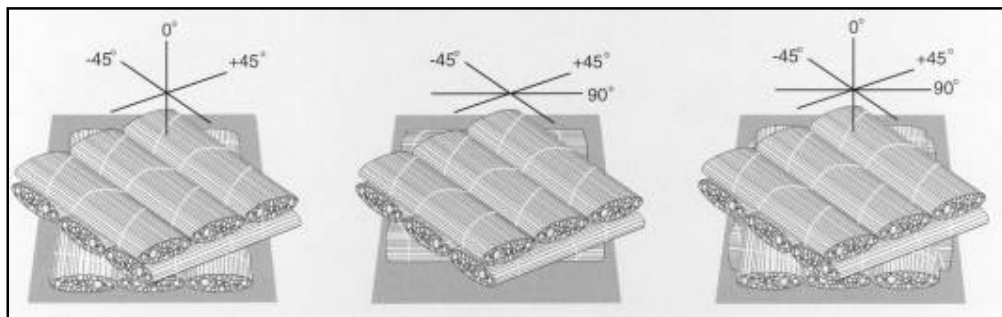
Fig. 1.3.3.5.2a *Diagram of stitched triaxial and quadriaxial fabrics*

- **Braided** fabrics are engineered with a system of two or more yarns intertwined in such a way that all of the yarns are interlocked for optimum load distribution. Biaxial braids provide reinforcement in the bias direction only with fiber angles ranging from ± 15° to ± 95°; triaxial braids provide reinforcement in the bias direction with fiber angles ranging from ± 10° to ± 80° and axial (0°) direction.
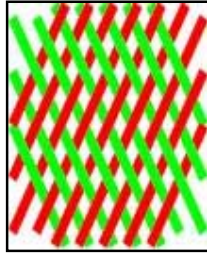
Fig. 1.3.3.5.2b Biaxial braided fabric   *Fig. 1.3.3.5.2c Triaxial braided fabric*
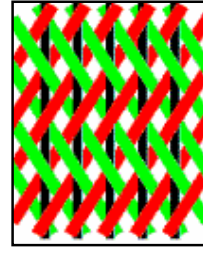
- **3-D** fabric uses a special weaving process that ties multiple layers and multiaxial fibers together with "Z-yarns". This Z improves the integrity of the fabric. This technology is capable to make forms for panels and structural profiles.
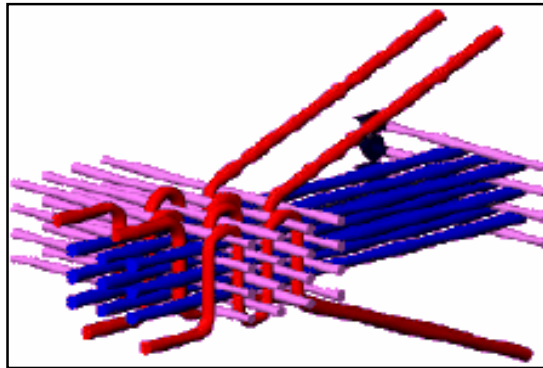
Fig. 1.3.3.5.2d 3-D fabric weaving process

1.3.3.5.3 Unidirectional

Unidirectional reinforcements include tapes, tows and rovings. Fibers in this form are all aligned parallel in one direction and the composites that use this method have high strength in the direction of the fiber. Unidirectional sheets are thin and multiple layers are required for most structural application.

1.3.3.5.4 Rods

FRP rods are anisotropic, with the longitudinal axis being the major axis. Their mechanical properties can vary significantly from one manufacturer to another and within the same product. They are made for braiding, weaving or *pultrusion* that is a continuous molding process that combines fiber reinforcements and thermosetting resin.

In order to improve the bond performance through mechanical interlock, the rods are produced by manufacturers in various types and with different deformation systems, including exterior wound fibers, sand coating and separately formed deformations.

Fig. 1.3.3.5.4 *Different types of FRP rods*

1.3.3.5.5 Laminates

Lamination technology is based on the joining or bonding of two or more layers to form a laminate. The materials can vary in type and mechanical properties in addition to property specific orientation; there are three types of laminated construction, these include sandwich lamination consisting of at least two high stiffness and strength outer layers connected by a core.

All laminate constructions utilize relatively high strength/stiffness materials.

Below we have an example of multi-ply construction: the figure shows the different orientation of the layers.
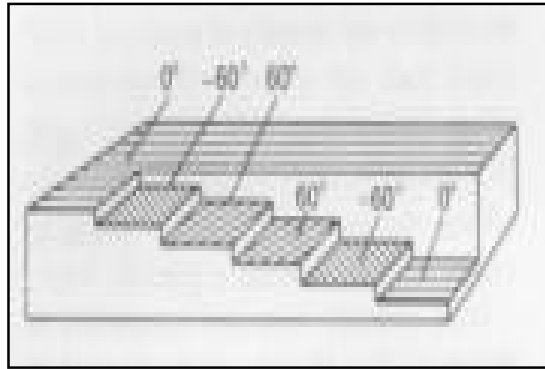
Fig. 1.3.3.5.5a Multi-ply Construction

Fig. 1.3.3.5.5b *E-Glass sheet*

Properties of FRP rods and laminates will be widely illustrated in the next chapters.

1.3.3.6 <u>FRP Manufacturing Processes Overview</u>

In this section, those manufacturing processes typically used to make products found in construction/civil infrastructure market are covered. Unique to the composites industry is the ability to create a product from many different manufacturing processes. There are a wide variety of processes available to the composites manufacturer to produce cost efficient products. Each of the fabrication processes has characteristics that define the type of products to be produced. This is advantageous because this expertise allows the manufacturer to provide the best solution for the customer. In order to select the most efficient manufacturing process, the manufacturing team considers several factors such as:

- user needs
- performance requirements
- size of the product
- surface complexity
- appearance
- production rate
- total production volume
- economic targets/limitations
- labor
- materials
- tooling/assembly
- equipment

1.3.3.6.1 Pultrusion

Pultrusion is a continuous molding process that combines fiber reinforcements and thermosetting resin. The pultrusion process is used in the fabrication of composite parts that have a constant cross-section profile. Typical examples include various rods and bar section, ladder side rails, tool handles, and electrical cable tray components and now bridge beams and decks. Most pultruded laminates are formed using rovings aligned down the major axis of the part. Various continuous strand mats, fabrics

(braided, woven and knitted), and texturized or bulked rovings are used to obtain strength in the cross axis or transverse direction.
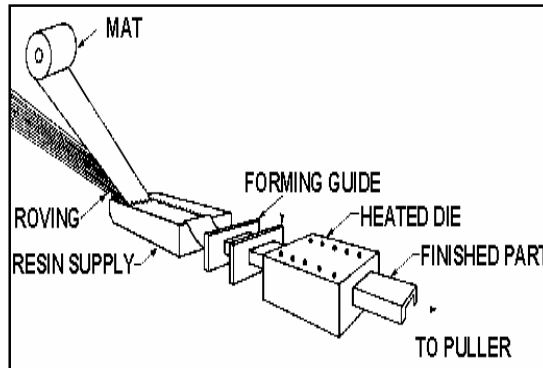
Fig. 1.3.3.6.1 *Pultrusion process*

The process is normally continuous and highly automated. Reinforcement materials, such as roving, mat or fabrics, positioned in a specific location using preforming shapers or guides to form the profile. The reinforcements are drawn through a resin bath or wet-out where the material is thoroughly coated or impregnated with a liquid thermosetting resin. The resin-saturated reinforcements enter a heated metal pultrusion die. The dimensions and shape of the die will define the finished part being fabricated. Inside the metal die, heat is transferred initiated by precise temperature control to the reinforcements and liquid resin. The heat energy activates the curing or polymerization of the thermoset resin changing it from a liquid to a solid. The solid laminate emerges from the pultrusion die to the exact shape of the die cavity. The laminate solidifies when cooled and it is continuously pulled through the pultrusion machine and cut to the desired length. The process is driven by a system of caterpillar or tandem pullers located between the die exit and the cut-off mechanism.

1.3.3.6.2 Resin Transfer Molding (RTM)

Resin Transfer Molding or RTM as it is commonly referred to is a "Closed Mold Process" in which reinforcement material is placed between two matching mold surfaces – one being male and one being female. The matching mold set is then closed and clamped and a low-viscosity thermoset resin is injected under moderate pressures (50 – 100 psi typical) into the mold cavity through a port or series of ports

within the mold. The resin is injected to fill all voids within the mold set and thus penetrates and wets out all surfaces of the reinforcing materials. The reinforcements may include a variety of fiber types, in various forms such as continuous fibers, mat or woven type construction as well as a hybrid of more that one fiber type. Vacuum is sometimes used to enhance the resin flow and reduce void formation. The part is typically cured with heat. In some applications, the exothermic reaction of the resin may be sufficient for proper cure.
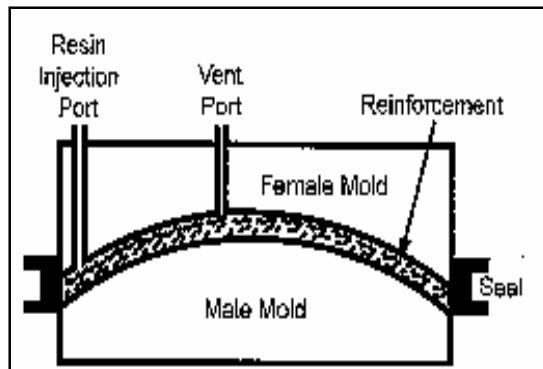
Fig. 1.3.3.6.2 *Resin Transfer Molding*

1.3.3.6.3 Vacuum Assisted Resin Transfer Molding (VARTM)

In the traditional RTM process, a matched set of molds or "closed mold" is used. The fiber reinforcements are usually preformed off line to enhance the production cycle time of the molds to perform at a respectable production rate. Resin is injected at high pressures and the process is sometimes assisted with vacuum.

However, Vacuum Assisted Resin Transfer Molding (VARTM) is different for many reasons. First, the fabrication of parts can be accomplished on a single open mold. Second, the process uses the injection of resin in combination with a vacuum and captured under a bag to thoroughly impregnate the fiber reinforcement. In the late 1980's, Bill Seemann invented and patented a variation to the VARTM process called SCRIMP[TM], which is Seemann Composite Resin Infusion Molding Process. This process has been used in many new and large applications ranging from turbine blades and boats to rail cars and bridge decks. Unique to this process is the manufacturing method that allows the efficient processing of VARTM to produce large structural shapes that are virtually void-free. This process has been used to make both thin and

very thick laminates. In addition, complex shapes with unique fiber architectures allow the fabrication of large parts that have a high structural performance.
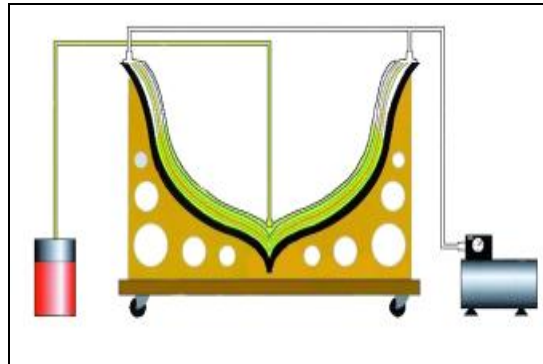
Fig.1.3.3.6.3 *VARTM process*

Parts using VARTM are made by placing dry fiber reinforcing fabrics into a mold, applying a vacuum bag to the open surface and pulling a vacuum while at the same time infusing a resin to saturate the fibers until the part is fully cured. This process allows for easy visual monitoring of the resin to ensure complete coverage to produce good parts without defects.

1.3.3.6.4 Hand Lay-up, Open Molding Process

Hand lay up is the oldest and simplest method used for producing reinforced plastic laminates. Capital investment for hand lay up processes is relatively low. The most expensive piece of equipment typically is a spray gun for resin and gel coat application. Some fabricators pour or brush the resin into the molds so that a spray gun is not required for this step. There is virtually no limit to the size of the part that can be made. The molds can be made of wood, sheet metal, plaster, and FRP composites.

In a particular hand lay up process (otherwise known as *wet lay up*), high solubility resin is sprayed, poured, or brushed into a mold. The reinforcement is then wet out with resin. The reinforcement is placed in the mold. Depending upon the thickness or density of the reinforcement, it may receive additional resin to improve wet out and allow better drapeability into the mold surface. The reinforcement is then rolled, brushed, or applied using a squeegee to remove entrapped air and to compact it against the mold surface.

Chopped strand mat is the lowest cost form of reinforcement used in wet lay up. It also provides equal reinforcing strength in all directions due to the random orientation of the fibers that form the mat. Woven roving is especially suitable for thick laminates requiring greater strength. Woven fabric and braid can also provide a low cost reinforcement. Once the reinforcement is thoroughly wet out with resin, it can be easily formed into complex shapes.

A key component to a successful lamination is the ***bonding process*** of the layers. There are three basic components, which make up the bonding process. First is the surface preparation of the laminate, which improves the substrate's ability to accept and adhere to an adhesive. Surface preparation varies depending on material type. Composites use sanding and grinding, surface texturing, or solvent cleaning. The second component is the adhesive itself, including epoxies, urethanes, phenolics, polyesters, solvents, acrylics and others. Each adhesive has its attributes depending on substrate type, in use requirements and process constraints. As a general rule, a maximum bond is achieved for a given substrate type when the material itself fails during an ultimate strength test. The maximum lap shear strength of an adhesive is achieved when the adhesive exhibits a cohesive failure in the bond line. The third component of lamination is the process by which the materials are bonded together. This involves a host of parameters primarily time, heat pressure, mixture, moisture and catalysts (initiators). It is important that the three basic components of bonding are properly employed to achieve a successful lamination.

1.3.3.6.5 Compression molding

Compression molding is the most common method of molding thermosetting materials such as SMC (sheet molding compound) and BMC (bulk molding compound). This molding technique involves compressing materials containing a temperature-activated catalyst in a heated matched metal die using a vertical press. The molding process begins with the delivery of high viscosity uncured composite material to the mold. Mold temperatures typically are in the range of 350° - 400° F. As the mold closes, composite viscosity is reduced under the heat and pressure approximating 1000 psi. The resin and the isotropically distributed reinforcements flow to fill the mold cavity. While the mold remains closed, the thermoset material undergoes a chemical change (cure) that permanently hardens it into the shape of the mold cavity.

Mold closure times vary from 30 seconds up to several minutes depending on part design and material formulation.

When the mold opens, parts are ready for finishing operations such as deflashing, painting, bonding, and installation of inserts for fasteners. By varying the formulation of the thermoset material and the reinforcements, parts can be molded to meet applications ranging from automotive class 'A' exterior body panels to structural members such as automobile bumper beams.

1.3.3.6.6 Filament winding

The filament winding process is used in the fabrication of tubular composite parts. Typical examples are composite pipe, electrical conduit, and composite tanks. Fiberglass roving strands are impregnated with a liquid thermosetting resin and wrapped onto a rotating mandrel in a specific pattern. When the winding operation is completed, the resin is cured or polymerized and the composite part is removed from the mandrel. Capital investment is relatively higher compared to open mold processes. The primary expense for an existing filament winder would be the cost of the winding mandrel for a specific application.
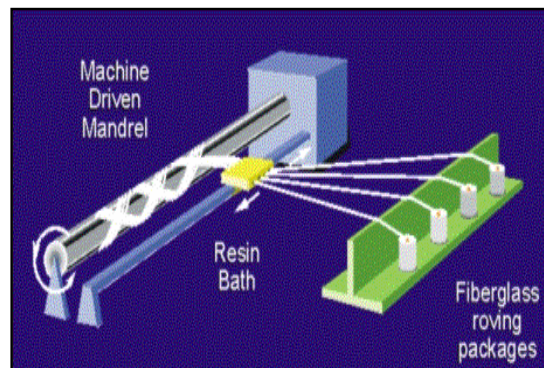
Fig. 1.3.3.6.6 *Filament winding process*

1.3.3.7 <u>Durability of FRP composites</u>

The most significant technical obstacle preventing the extended use of FRP is a lack of long-term and durability performance data comparable to the data available for more traditional construction materials. Although there have been numerous studies on creep, stress corrosion, fatigue, environmental fatigue, chemical and physical ageing and natural weathering of composites, most of these are not related for civil engineering application. Therefore the lack of durability data generate, at the moment, a big obstacle: a majority of civil engineers are not familiar with composites and are skeptical about using of FRP to replace conventional materials in the structures.

It was already mentioned that corrosion problems of steel reinforcement and the good mechanical properties of FRP materials opened a large field for the use of composite in new constructions and for repairing purposes, but the determination of the durability is one of the most important issues.

Durability of material can be defined as its ability to resist cracking, oxidation, chemical degradation, delamination, wear and the effects of foreign object damage for a specified period of time under specified environmental conditions.

Damage tolerance is defined as the ability of a material or structure to resist failure and continue performing at prescribed levels of performance in the presence of damage for a specified period of time under specified environmental conditions.

The performance of FRP composites is given on the interactions between the selected constituent materials (fibers, resin, fillers and additives), determination of microstructure/architecture and geometrical configuration and influences of the appropriate manufacturing process.

1.3.3.7.1 Moisture (water) absorption

All resins adsorb moisture with the percentage of moisture absorption depending on the resin structure, degree of cure and water temperature. In general moisture effects over the short-term cause degradation in strength rather than stiffness levels in a composite.

Moisture absorption in FRP composite depends on type of resins, laminate composition, thickness, laminate quality, curing condition, fiber/resin interface and manufacturing process. In some applications, performance is improved with the use of corrosion barrier.

1.3.3.7.2 Alkaline solutions

Alkaline solutions, such as the pore water of concrete, have a high PH and high concentration of alkali ions; this combination has no relevant effect on carbon reinforcement but may lead to degradation at the resin matrix and/or interface levels (strength and stiffness have been reported to each decrease between 0-20%).

Tensile strength reductions in GFRP bars ranging from zero to 75% of initial values have been reported in literature, while tensile stiffness reductions in GFRP bars range between zero and 20%.

Tensile strength and stiffness of AFRP rods in elevated temperature alkaline solutions either with and without tensile stress applied have been reported to decrease between 10-50% and 0-20% of initial values, respectively.

Resin damage via alkali is generally more severe than that due to moisture.

1.3.3.7.3 Aggressive chemical solutions

FRP composites generally exhibit a variable performance when exposed to solution such as acids or corrosives; the resin type primarily influences this performance.

In the case of CFRP immersed in hydrochloric acid at the temperature of 80°C, the tensile strength reduced about 20% after 120 days.

The tensile of glass fiber reduced rapidly with time when immersed in any of the solution (NaOH, HCl, H_2O) at the temperature of 80°C; when immersed in sodium hydroxide, the strength reduction is tremendous: 96% within 9 hours at the same temperature.

For the AFRP (Technora fiber), after immersing for 90 days, strength reduced about 80% in hydrochloric acid and about 45% in sodium hydroxide solution.

However no particular sign of degradation were observed when the FRP were immersed in distilled water at temperatures of 20, 40 and 80°C (T.Uomoto and T.Nishimura,1999).

1.3.3.7.4 Sub-zero and freeze-thaw exposure

Composites display excellent freeze-thaw resistance and are expected to withstand years of sub-zero conditions and hundreds of freeze-thaw cycles, with minimal loss of properties.

In general, freeze-thaw exposure does not affect fibers although it can affect the resin and the fiber/resin interface.

1.3.3.7.5 Temperature and thermal cycling (above zero)

The primary effects of temperature are on viscoelastic response of the resin and hence of the composites; if the temperature exceeds the glass transition temperature (T_g), FRP composite performance can be expected to drop.

Thermal cycling in general does not cause deleterious effects, although extended cycles of brittle resin systems can result in microcrack formation.

1.3.3.7.6 Creep and relaxation

FRP subjected to a constant load over time can suddenly fail after a time period called the **endurance time**; this phenomenon is known as creep rupture (or static fatigue).

Creep rupture is not an issue with steel bars in reinforced concrete except in extremely high temperatures such as those encountered in a fire.

The creep rupture endurance time can also irreversibly decrease under sufficiently adverse environmental conditions, such as high temperature, ultraviolet radiation exposure, high alkalinity, wet and dry cycles, or freezing-thawing cycles. In general, carbon fibers are the least susceptible to creep rupture, aramid fibers are moderately susceptible, and glass fibers are most susceptible to creep rupture.

Results indicated that a linear relationship exists between creep rupture strength and the logarithm of time for times up to nearly 100 hr. The ratios of stress level at creep rupture to the initial strength of the GFRP, AFRP, and CFRP bars after 500,000 hours (more than 50 years) were linearly extrapolated to be 0.29, 0.47, and 0.93, respectively.

Creep will not be a significant factor if the load to the structure are kept within manufacturer recommended stress levels.

For a typical civil infrastructure composite application, the creep-stress relaxation properties are dominated by the resin-dependent properties, rather than on the fiber or interfacial properties.

Traditionally glass-fiber reinforced composites have been designed to ensure that stress levels under sustained do not exceed 25-30% of ultimate to avoid premature failure due to stress rupture.

1.3.3.7.7 Fatigue

FRP composites show significantly enhanced fatigue resistance over metallic materials. However, FRP composites structures are still susceptible to failure at joints and connections under fatigue loading and must be designed to reduce stress concentrations and geometrical discontinuities, which decrease overall fatigue resistance.

Fatigue failure in FRP composites is usually initiated through fiber/matrix debonding and matrix microcracking.

Although the data on fatigue is in large structural application is limited, the data that is available indicates that fatigue failure is unlikely to occur at the lower stress levels used in design except at the joints and connection details.

Of all types of current FRP composites for infrastructure application, CFRP is generally thought to be the least prone to fatigue failure like E-glass and S-glass, but, for the last two types, environmental factors play an important role in the fatigue behavior due to their susceptibility to moisture, alkaline and acidic solutions.

Aramid fibers, for which substantial durability data are available, appear to behave similarly to carbon and glass fibers in fatigue.

1.3.3.7.8 Ultraviolet (UV) radiation

In general, effects are rarely sever in terms of mechanical performance, although some resins can show significant embrittlement and surface erosion.

The most deleterious effect of UV exposure is probably not the UV-related damage, but the potential for increased penetration of moisture and other agents via the damaged region.

FRP composites can be protected from UV-related degradation through the use of appropriate additives in the resin and/or use of appropriate coatings.

1.3.3.7.9 Fire and high thermal exposure

All polymeric system degrade in the presence of extreme heat over prolonged periods. The primary effect in most fires is that of resin degradation and softening followed by charring of surface layers, which often causes the FRP composites to self-extinguish.

In critical applications, the FRP may be fireproofed with the use of special fire-resistant additives, intumescent coatings and the addition of inorganic fillers, but these increases the costs and however depending on the application (may not be possible). The usual method to achieve the necessary structural fire rating is to use the FRP reinforcement as supplemental reinforcement: with this concept, the existing structure will not be able of total collapse without FRP reinforcement.

In FRP reinforced concrete the concrete itself acts as a thermal barrier reducing effects of thermal load.

1.3.4 FRP LAMINATES

1.3.4.1 <u>Mechanical properties</u>

FRP composites in the form of sheets were used throughout this research to strengthen masonry walls. Three basic component materials are commonly used for the installation process of the FRP sheets, namely: primer, putty and impregnating resin or saturant. The combination of the latter and the fibers form the FRP laminate.

The impregnating resin forms the matrix, which acts a binder for the reinforcing fibers. The matrix has two functions: to enable the load to be transferred among fibers and and to protect the fibers from environmental effects.

Properties for primer, putty and saturant are shown in Table 1.3.4.1.

Material	Tensile Strength, psi, (kPa)	Tensile Elastic Modulus, ksi (MPa)	Tensile Strain (%)	Compressive Strength psi, (kPa)	Compressive Modulus ksi, (MPa)	Bond Strength psi, (MPa)
Primer	1800 (12400)	105 (723.5)	3	3500 (24100)	95 (654.5)	NA
Putty	1800 (12400)	260 (1791.4)	1.5	3500 (24100)	155 (1068.0)	NA
Saturant	7900 (54400)	440 (3031.6)	2.5	12500 (86100)	380 (2618.2)	NA

Table 1.3.4.*1 Mechanical properties for primer, putty and saturant*

It is important to highlight that for the strengthening of masonry walls, the surface is commonly primed with the saturant used to bond and impregnate the fibers rather than the conventional primer used for concrete surfaces. This is due to the absortive characteristics of masonry, which requires a high amount of primer. Two types of commercially available FRP sheets constituted of aramid and glass were used in this research to strengthen the masonry walls. Their engineering properties according to the manufacturers are summarized in Table 1.3.4.2.

Designation	Fiber Type	Guaranteed Ultimate Strength, ksi (MPa)	Load per Sheet width, lbs/in (kN/mm)	Tensile Modulus, ksi (MPa)	Guaranteed Ultimate Strain (%)
AK60	Aramid	290(1998)	3190(0.56)	17000(117130)	1.7
EG 900	E-Glass	220(1516)	3050(0.53)	10500(72345)	2.1

Table 1.3.4.2 *Mechanical properties for Aramid and E-Glass Fibers*

1.3.4.2 <u>Tensile and Compressive Behavior</u>

When loaded in tension, FRP materials do not exhibit any plastic behavior (yielding) before rupture. The tensile behavior of FRP materials consisting of one type of fiber material is characterized by a linearly elastic stress-strain relationship until failure.

The tensile strength and stiffness of an FRP material is dependent of several factors. Because the fibers in an FRP material are the main load-carrying constituent, the type of fiber, the orientation of the fibers, and the quantity of fibers primarily govern the tensile properties of the FRP material. Due to the primary role of the fibers and methods of application, the properties of an FRP repair system are sometimes reported based on the net-fiber area. In other instances, the reported properties are based on the gross-laminate area.

The gross-laminate area of an FRP system is calculated using the total cross-sectional area of the cured FRP system, including all fibers and resin. Gross-laminate area is typically used for reporting precured laminate properties where the cured thickness is constant and the relative proportion of fiber and resin is controlled.

The net-fiber area of an FRP system is calculated using the known area of fiber, neglecting the total width and thickness of the cured system; thus, resin is excluded. Net-fiber area is typically used for reporting properties of wet lay-up systems that use manufactured fiber sheets and field-installed resins. The wet lay-up installation process leads to a controlled fiber content and a variable resin content.

System properties reported using the gross-laminate area have higher relative thickness dimensions and lower relative strength and modulus values; while system properties reported using the net-fiber area have lower relative thickness dimensions and higher relative strength and modulus values. Regardless of the basis for the reported values, the load-carrying capacity ($f_{fu}A_f$) and stiffness (A_fE_f) remain constant. Properties reported based on the net-fiber area are not the properties of the bare fibers. The properties of an FRP system should be characterized as a composite, recognizing not just the material properties of the individual fibers but also the efficiency of the fiber-resin system and fabric architecture. The mechanical properties of all FRP systems, regardless of form, should be based on the testing of laminate samples with a known fiber content.

Tests on FRP laminates used for repair on concrete have shown that the compressive strength is lower than the tensile strength (*Wu* 1990). The mode of failure of FRP subjected to longitudinal compression can include transverse tensile failure, fiber microbuckling, or shear failure. The mode of failure depends on the type of fiber, the fiber volume fraction, and the type of resin. In general, compressive strengths are higher for materials with higher tensile strengths, except in the case of AFRP where the fibers exhibit non-linear behavior in compression at a relatively low level of stress. The modulus of elasticity is usually smaller than the tensile modulus of elasticity of FRP materials as well. Test reports on samples containing 55 to 60% volume fraction of continuous E-glass fibers in a matrix of vinyl ester or isophthalic polyester resin have reported a compressive modulus of elasticity of 5000 to 7000 kip/in.^{2} (34000 to 48000 Mpa) (*Wu* 1990). According to reports, the compressive modulus of elasticity is approximately 80% for GFRP, 85% for CFRP, and 100% for AFRP of the tensile modulus of elasticity for the same product (*Ehsani* 1993).

1.3.4.3 <u>Time-dependent behavior</u>

FRP materials subjected to a constant load over time can suddenly fail after a time period referred to as the endurance time. This failure is known as creep-rupture and is similar to fatigue in metals except that the stresses are sustained instead of cycled. As the ratio of the sustained tensile stress to the short-term strength of the FRP laminate increases, endurance time decreases.

The endurance time also decreases under adverse environmental conditions, such as high temperature, ultraviolet-radiation exposure, high alkalinity, wet and dry cycles, or freezing-thawing cycles. In general, carbon fibers are the least susceptible to creep-rupture; aramid fibers are moderately susceptible, and glass fibers are most susceptible. Creep rupture tests have been conducted on 0.25 in.(63.5 mm) diameter FRP bars reinforced with glass, aramid, and carbon fibers. The bars were tested at different load levels at room temperature. Results indicated that a linear relationship exists between creep-rupture strength and the logarithm of time for all load levels. The ratios of stress level at creep-rupture after 500000 hours (about 50 years) to the initial ultimate strength of the GFRP, AFRP and CFRP bars were extrapolated to be 0.3, 0.47, and 0.91, respectively (*Yamaguchi et al*. 1997). Similar values have been determined elsewhere (*Malvar* 1998).

1.3.4.4 <u>Installation techniques: Manual Lay-Up</u>

The *Manual Lay-Up* technique for the installation of FRP laminates is described. FRP laminates are formed by manual lay-up onto the surface of the member being strengthened. Prior to the fibers installation, the surface is usually prepared by grinding or sandblasting, application of primer, and puttying. Depending on the characteristics of the masonry surface, it may not need be sandblasted because the surface exhibits sufficient roughness.

This is particularly evident in concrete units, which are extruded and thereby do not have laitance on their surface. The surface of the walls, particularly at the joints, is levelled with putty. After applying a first coat of saturant, the fibers are attached to the wall surface. The fibers are impregnated by a second coat of saturant, which after hardening enables the newly formed laminate to become integral part of the strengthened member.

In the following pictures a typical Manual Lay-Up process using CFRP laminates applied to infill walls is presented.

(1) *Surface Preparation*

(2) *Primer/Putty Application*

(3) *Fibers Installation*

(4) *Saturant Impregnation*

Fig. 1.3.4.4 *Installation of FRP laminates* **(From Tumialan 1999)**

1.3.5 FRP rods

1.3.5.1 <u>Mechanical properties</u>

FRP rods used in civil engineering are unidirectional composites. The direction parallel to the fibers is called the longitudinal direction, in which the mechanical properties are controlled by the fibers strength. The transversal direction, perpendicular to the fibers, presents lower mechanical properties, controlled by resin and fiber/matrix interface properties. It means that the mechanical properties depend on the nature and content of fibers in the longitudinal direction.

It is commonly assumed that the use of FRP rods in concrete and masonry structures is concerned with the longitudinal properties of these materials, but in durability studies, like those performed recently at University of Mi` ssouri-Rolla (*Micelli* 2001), resin properties are significant too, because of the load is transferred to the fibers by means of the matrix, and because the resin constitute a chemical and physical protection to the fibers. Therefore, the damage and cracking of the resin do not allow the desired stress distribution, and open a preferential way for degradation of fibers. This reflects to longitudinal properties in ultimate strength and stiffness lower than assumed for design purposes.

FRP composites in form of GFRP rods were used in this research.

GFRP rebars of fiberglass rebars are manufactured from E-glass fibers encapsulated in a vinyl ester resin matrix.

It features a deformed and sand-coated surface to facilitate bond with the concrete, mortar or epoxy-based paste. Deformations are slight undulations that take best advantage of the glass fiber structural element, constituting a minimum of 70% volume by weight of the end product.

Typical mechanical properties of GFRP rods used in the experimentation program are shown below.

BAR SIZE # (mm)	Cross-Sectional Area, $in^2(mm^2)$	Nominal Diameter, in (mm)	Tensile Strength, ksi (MPa)	Tensile Modulus of Elasticity, ksi (MPa)	Max Bond Stress to Concrete psi (kPa)
2(6)	0.0515 (33.23)	0.250 (6.35)	110 (760)	5920 (40789)	1679 (11568)

Fig. 1.3.5.1 *Mechanical properties of GFRP rod #2*

1.3.5.2 <u>Tensile and compressive behavior</u>

When loaded in tension, FRP bars do not exhibit any plastic behavior (yielding) before rupture. The tensile behavior of FRP bars consisting of one type of fiber material is characterized by a linearly elastic stress-strain relationship until failure.

The tensile strength and stiffness of an FRP bar are dependent on several factors.

Because the fibers in an FRP bar are the main load-carrying constituent, the ratio of the volume of fiber to the overall volume of the FRP (fiber-volume fraction) significantly affects the tensile properties of an FRP bar. Strength and stiffness variations will occur in bars with various fiber-volume fractions, even in bars with the same diameter, appearance, and costituents. The rate of curing, the manufacturing process, and the manufacturing quality control also affect the mechanical characteristics of the bar.

The tensile properties of a particular FRP bar should be obtained from the bar manufacturer. Usually, a normal (Gaussian) distribution is assumed to represent the strength of a population of bar specimens, although at this time additional research is needed to determine the most generally appropriate distribution for FRP bars.

An FRP bar cannot be bent once it has been manufactured (an exception to this would be an FRP bar with a thermoplastic resin that could be reshaped with the addition of heat and pressure). FRP bars can be fabricated with bends. In FRP bars produced with bends, a strength reduction of 40 to 50% compared to the tensile strength of a straigth bar can occur in the bend portion due to fiber bending and stress concentration (*Nanni et al.* 1998)**.**

Tests on FRP bars with a length to diameter ratio from 1:1 to 2:1 have shown that the compressive strength is lower than the tensile strength (*Wu* 1990). The mode of failure for FRP bars subjected to longitudinal compression can include transverse tensile failure, fiber microbuckling, or shear failure. The mode of failure depends on the type of fiber, the fiber-volume fraction, and the type of resin. Compressive strengths of 55%, 78% and 20% of the tensile strength have been reported for GFRP, CFRP and AFRP respectively (*Mallick* 1998 and *Wo* 1990). In general, compressive strengths are higher for bars with higher tensile strengths, except in the case of AFRP where the fibers exhibit nonlinear behavior in compression at a relatively low level of stress.

The compressive modulus of elasticity of FRP reinforcing bars appears to be smaller than its tensile modulus of elasticity. Standard test methods are not yet established to

characterized the compressive behavior of FRP bars. If the compressive properties of a particular FRP bar are needed, these should be obtained from the bar manufacturer.

1.3.5.3 **Bond behavior**

Bond performance of an FRP bar is dependent on the design, manufacturing process, mechanical properties of the bar itself, and the enviromental conditions (*Al-Dulaijan et al.* 1996*, Nanni et al.* 1997*, Bakis et al.* 1998*, Bank et al.* 1998*, Freimanis et al.* 1998).

When anchoring a reinforcing bar in concrete, the bond force can be transferred by:

- adhesion resistence of the interface, also known as chemical bond;
- Frictional resistance of the interface against slip;
- Mechanical interlock due to irregularity of the interface

In FRP bars, it is postulated that bond force is transferred through the resin to the reinforcement fibers, and a bond-shear failure in the resin is also possible. When a bonded deformed bar is subjected to increasing tension, the adhesion between the bar and the surrounding concrete breaks down and deformations on the surface of the bar cause inclined contact forces between the bar and the surrounding concrete. The stress at the surface of the bar resulting from the force component in the direction of the bar can be considered the bond stress between the bar and the concrete. Unlike reinforcing steel, the bond of FRP rebars appears not to be significantly influenced by the concrete compressive strength provided adequate concrete cover exists to prevent longitudinal splitting. (*Nanni et al.* 1995*, Benmokrane et al.* 1996*, Kachlakev and Lundy* 1998).

The bond properties of FRP bars have been extensively investigated by numerous researchers through different types of tests, such as, pullout tests, splice tests, and cantilever beams, to determine an empirical equation for embedment length (*Faza and GangaRao* 1990*, Ehsani et al.* 1996*, Benmokrane* 1997).

1.3.5.4 **Time-dependent behavior**

Creep rupture is not an issue with steel bars in reinforced concrete except in extremely high temperatures such as those encountered in a fire. An investigation of creep rupture in GFRP bars in room temperature laboratory conditions was reported by *Seki et al.* in 1997. The molded E-glass/vinyl ester bars had a small (0.0068 in^2, 4.4

mm^2) rectangular cross-section and integral GFRP tabs. The percentage of initial tensile strength retained followed a linear relationship with logarithmic time, reaching a value of 55% at an extrapolated 50-yr endurance time.

Creep rupture data characteristics of a 0.5-in-diameter (12.5-mm) commercial CFRP twisted strand in an indoor environment is available from the manufacturer (*Tokyo Rope* 2000). The rupture strength at a projected 100 yr endurance time is reported to be 85% of the initial strength. An extensive investigation of creep deformation (not rupture) in one commercial AFRP and two commercial CFP bars tested to 3000 hr has been reported (*Saadatmanesh and Tannous* 1999). The bars were tested in laboratory air and in room-temperature solutions with pH equal to 3 and 12. The bars had diameters between 0.313-0.375 inch (8-10 mm) and the applied stress was fixed at 40% of initial strength. The results indicated a slight trend towards higher creep strain in the larger diameter bars and in the bars immersed in the acidic solution. Bars tested in air had the lowest creep strains of the three environments. Considering all enviroments and materials, the range of strains recorded after 3000 hr was 0.002%-0.037%. Creep strains were slightly higher in the AFRP bar than in the CFRP bars.

1.3.5.5 <u>Durability</u>

FRP bars are susceptible to varying amounts of strength and stiffness changes in the presence of enviroments prior to, during, and after construction.

These enviroments can include water, ultraviolet exposure, elevated temperature, alkaline or acidic solutions, and saline solutions. Strength and stiffness may increase, decrease, or remain the same, depending on the particular material and exposure conditions. Tensile and bond properties of FRP bars are the primary parameters of interest for reinforced concrete construction.

The enviromental condition that has attracted the most interest by investigators concerned with FRP bars is the highly alkaline pore water found in outdoor concrete structures (*Gerritse* 1992, *Takewaka and Khin* 1996, *Rostasy* 1997, *Yamaguchi et al.* 1997).

Aqueous solutions with high values of pH are known to degrade the tensile strength and stiffness of GFRP bars (*Porter and Barnes* 1998), although particular results vary tremendously according to differences in test methods. Higher temperatures and longer exposure times exasperate the problem. Most data have been generated using

temperatures as low as slightly sub-freezing and as high as a few degrees below the T_g of the resin. The degree to which the resin protects the glass fibers from the diffusion of deleterious hydroxyl (OH-) ions figures prominently in the alkali resistence of GFRP bars (*Bank and Puterman* 1997, *Coomarasamy and Saadatmanesh* 1999, *Uomoto* 2000). Most researchers are of the opinion that vinyl ester resins have superior resistance to moisture ingress in comparison with other commodity resins. The type of glass fiber also appears to be an important factor in the alkali resistance of GFRP bars (*Devalapura et al.* 1996). Tensile strength reductions in GFRP bars ranging from zero to 75% of initial values have been reported in the cited literature. Tensile stiffness reductions in GFRP bars range between zero and 20% in many cases. Tensile strength and stiffness of AFRP rods in elevated temperature alkaline solutions either with and without tensile stress applied have been reported to decrease between 10-50% and 0-20% of initial values, respectively (*Takewaka and Khin* 1996, *Rostasy* 1997, *Sen et al.* 1998). In the case of CFRP, strength and stiffness have been reported to each decrease between 0-20% (*Takewaka and Khin 1996*).

Some results from combined ultraviolet and moisture exposure tests with and without applied stress applied to the bars have shown tensile strength reductions of 0-20% of initial values in CFRP , 0-30% in AFRP and 0-40% in GFRP (*Sasaki et al.* 1997, *Uomoto* 2000). An extensive study of GFRP, AFRP and CFRP bars kept outdoors in a rack by the ocean showed no significant change of tensile strength or modulus of any of the bars (*Tomosowa and Nakatsuji* 1996,1997).

Adding various types of salts to the solutions in which FRP bars are immersed has been shown to not necessarily make a significant difference in the strength and stiffness of many FRP bars, in comparison to the same solution without salt (*Rahman et al. 1996*). Most studies do not separate the effects of water and salt added to water, however. One study found a 0-20% reduction of initial tensile strength in GFRP bars subjected to a saline solution at room-temperature and cyclic freeze/thaw temperatures (*Vijay and GangaRao* 1999) and another has found a 15% reduction in the strength of AFRP bars in a marine environment (*Sen et al*. 1998).

Studies of the durability of bond between FRP and concrete have been mostly concerned with the moist, alkaline environment found in concrete. Bond of FRP reinforcement relies upon the transfer of shear and transverse forces at the interface between bar and concrete and between individual fibers within the bar. These resin-dominated mechanisms are in contrast to the fiber-dominated mechanisms that control

properties such as longitudinal strength and stiffness of FRP bars. Enviroments that degrade the polymer resin or fiber/resin interface are thus also likely to degrade the bond strength of an FRP bar. Numerous bond test methods have been proposed for FRP bars, although the direct pullout test remains rather popular due to its simplicity and low cost (*Nanni et al.* 1995). Pullout specimens with CFRP and GFRP bars have been subjected to natural enviromental exposures and have not indicated significant decreases in bond strength over periods of time between one and two years (*Clarke and Sheard* 1998, *Sen et al.* 1998). Positive and negative trends in pullout strength with respect to shorter periods of time have been obtained with GFRP bars subjected to wet elevated-temperature enviroments in concrete, with or without artificially added alkalinity (*Al-Dulaijan et al.* 1996, *Bakis et al.* 1998, *Bank et al.* 1998, *Porter and Barnes* 1998). Longitudinal cracking in the concrete cover can seriously degrade the apparent bond capability of FRP bars and sufficient measures must be taken to prevent such cracking in laboratory tests and field applications (*Sen et al.* 1998).The ability of chemical agents to pass through the concrete to the FRP bar is another important factor thought to affect bond strength (*Porter and Barnes* 1998).

1.3.5.6 <u>Installation techniques: Near Surface Mounted Rods</u>

A new FRP-based strengthening technique is now emerging as a valid alternative to externally bonded FRP laminates. From this point forward, it will be referred to as Near-Surface-Mounted (NSM) rods. Embedment of the rods is achieved by grooving the surface of the member to be strengthened along the desired direction. The groove is filled half-way with epoxy-based paste, the FRP rod is then placed in the groove and lightly pressed, so forcing the paste to flow around the bar and fill completely between the bar and the sides of the groove. The groove is then filled with more paste and the surface is leveled. Although the use of FRP rods for this application is very recent (*De Lorenzis* 2000, *Tinazzi* 2000, *Tumialan* 2000-2001), NSM steel rods have been used in Europe for strengthening of RC structures since the early 50's.

The advantage in using FRP instead of steel for NSM rods is primarily the resistance of FRP to corrosion. This property is particularly important in this case due to the position of the rods very close to the surface, which exposes them to the enviromental attacks. The use of NSM FRP rods is an attractive method for increasing the flexural

and the shear strength of deficient RC members and masonry walls and, in certain cases, can be more convenient than using FRP laminates.

When the FRP rods are installed in either the horizontal or vertical (only for stack bond patterns) masonry joints, the aforementioned technique receives the name of **FRP Structural Repointing.** Repointing is a traditional retrofitting technique, commonly used in the masonry industry, which consists in replacing missing mortar in the joints. The term "structural" is added to describe a strengthening method aimed at restoring the integrity and/or upgrading the capacity of walls. This is achieved by placing into the joints deformed FRP rods, which are bonded to the masonry wall by the paste.
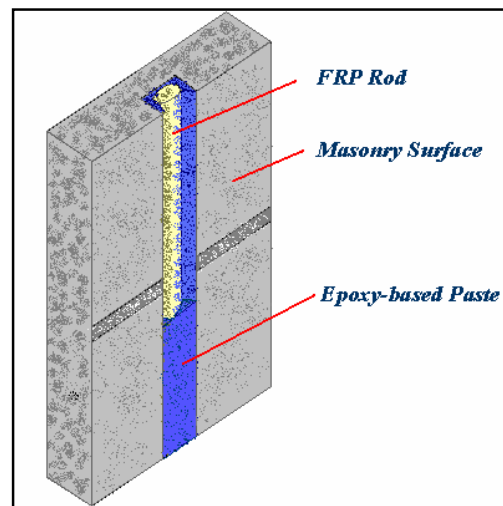
Fig. 1.3.5.6a *NSM rod system*

Structural repointing offers advantages compared to the use of FRP laminates. The method itself is simpler since the surface preparation is reduced (sandblasting and puttying are not required). In addition the aesthetic of masonry is preserved. The diameter size of the FRP rods is limited by the thickness of the mortar joint, which usually is $^3/_8$ inches. The FRP rods are placed into the joints by using a technique known as *tuck pointing*, which consists of: (1) cutting out part of the mortar using a grinder, the depth of the cut depends on the shell thickness of the masonry unit, (2) masking of the masonry surface to avoid staining with the epoxy-based paste, (3) filling the joints with an epoxy-based paste, (4) embedding the rods in the joint, and (5) retooling. To ensure a proper bonding between the epoxy-based paste and masonry,

it is recommended to remove the dust by means of an air blower once the grinding of the mortar joints has been completed (See Fig.1.3.5.6b).

(1) *Grinding of joints*   **(2)** *Masking to avoid staining*

(3) *Application of epoxy-based paste*   **(4)** *Installation of FRP rods*

Fig. 1.3.5.6b *Strengthening of masonry walls with FRP Structural Repointing*
(From *Tumialan* **2000)**

2.
OUT-OF-PLANE BEHAVIOR OF MASONRY WALLS STRENGTHENED WITH FRP LAMINATES

2.1 Problem statement and general objectives

Masonry walls may be subjected to lateral loads normal to the faces of the walls causing them to bend out-of-plane. These walls are referred to as "flexural walls" since the mode of deformation is primarily flexure with little or no externally applied axial load. The loads can be permanent, such as earth pressure against a retaining wall or basement wall, or they can be transient, such as from wind or earthquake.

In ancient masonry buildings, where the masonry units often were not bonded together, walls were generally thick enough that flexural stresses from the lateral loads were much lower than axial compressive stresses from self-weight and other gravity loads.

It is only in the latter half of the twentieth century that the tensile strength of masonry has become relied upon to provide flexural resistance to out-of-plane lateral loads.

Gradually, rules of thumb were developed to describe accepted limits for heigth-to-thickness or length-to-thickness. In general, these empirical provisions have worked well, except where very high wind or seismic loads have been experienced or where the normal redundancy of masonry construction was eliminated from the design.

Engineered masonry often relies on reinforcement to resist tensile stress from lateral loads.

Since FRP materials have proven to be a successful solution for the retrofitting and structural upgrading of masonry structures (*Velazquez* 1998,*Tumialan et al.*1999-2000,*Tinazzi* 2000,*Barbieri* 2001), this study deals with the flexural performance of masonry walls reinforced with FRP laminates.

Different types of FRP reinforcement and masonry units are used in this investigation.

The effectiveness of FRP materials in terms of capacity and the influence of different amounts of FRP reinforcement in the modes of failure of the masonry walls are evaluated in order to identify which are the factors to be controlled in developing provisional design guidelines.

2.2 **Previous results**

Ehsani et al. (1996) investigated the flexural behavior of URM walls strengthened with GFRP sheets. Their dimensions were 8.5in.(0.22 m) wide, 4in.(0.1 m) high, and 57in.(1.48 m) long. Two different kind of mortars were used for their construction, type M with cement: lime: sand ratios of $1:^1/_4:3$ and a compressive strength of 4.65 ksi (32.04 MPa); and type M* with ratios of $1:^1/_4:5$ and a compressive strength of 4.1 ksi (28.25 MPa). The specimens were subjected to four-point bending. The primarily failure was a tension failure, which was observed when low amount of strengthening was used. When the number of plies was increased, the masonry failed in compression. It was observed that the flexural capacity was increased up to 24 times compared to the control specimen. As observed in Figure 2.2a, the effect of the mortar strength appeared to be negligible, both specimens failed by crushing of the masonry.
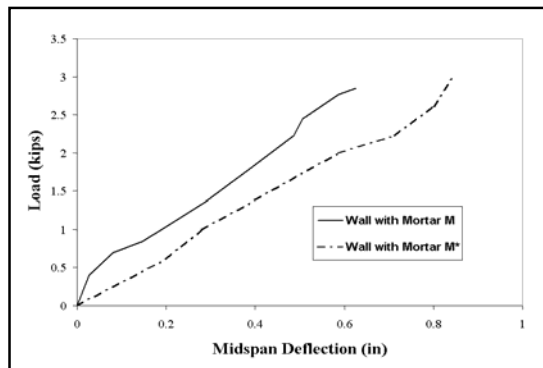
Figure 2.2a *Test Results* **(Ehsani 1996)**

Hamilton et al. (1999) investigated the flexural behavior of URM walls strengthened with different composite materials. The walls were built with standard concrete blocks, with an overall dimension of 2 ft (0.61 m) by 6 ft (1.83 m). The use of high strength composite materials such as CFRP and AFRP led to undesirable modes of failure such as delamination and shear in the masonry. In order to use the material efficiently, two alternatives were recommended. The first one was to increase the spacing of the material until observing the rupture of the laminate. The second one was to use less expensive materials such as GFRP. Four modes of failure were identified: debonding, laminate rupture, shear, and face shell pull out. It was reported that debonding from the masonry substrate caused the failure of most of the test spe specimens (see Figure 2.2b).
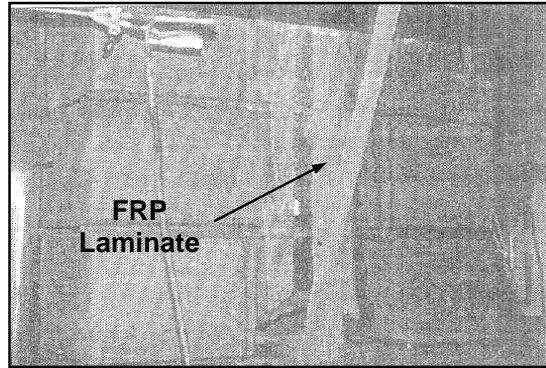
Figure 2.2b *Debonding of FRP Laminate* **(Hamilton 1999)**

Velazquez et al. (2000) reported test results of half-scale URM walls tested under out-of-plane cyclic loading. The test specimens had a width of 48 in. (1.22 m) and a height of 56 in. (1.42 m), with a slenderness ratio of 28. Two of the walls were strengthened on both faces with GFRP strips. By understanding that the balanced condition represents the failure of masonry and rupture of composite laminate at the same time, one wall had the reinforcement equivalent to the balanced ratio (100% ρ_b). The other wall had three times the amount of reinforcement as compared as the first wall (300% ρ_b). The specimen reinforced with 100% ρ_b showed extensive delamination at failure. The first delaminated areas where observed on the central strip above the middle brick course. The specimen with 300% ρ_b failed due to high in-plane shear stresses along the lower brick course. Substantial increases in strength and deformation capability were achieved. It was observed (see Figure 2.2c) that the retrofitted walls resisted pressures up to 24 times the weight of the wall and deflected as much as 5% of the wall height. To avoid very stiff behavior and improve the hysteretic response, it was recommended to limit the reinforcement ratio to two times the balanced condition.
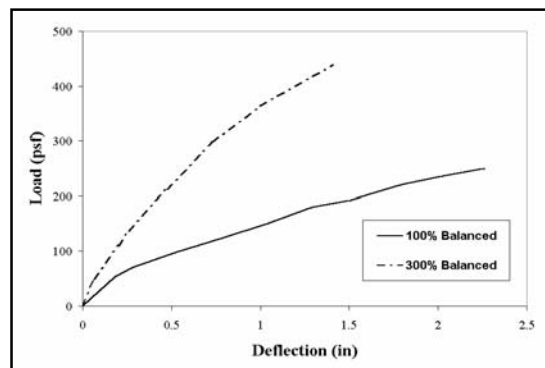
Figure 2.2c *Test Results* **(Velazquez 2000)**

57

Tumialan (1999) tested ten full-scale infill panels at Malcolm Bliss Hospital, a forty years old building scheduled for demolition in the late 90's.

The nominal dimensions of the walls were 8 by 8 ft (2.44x2.44 m); their overall thickness, including the two wythes and plaster was 13 in. (0.33 m). The upper and lower boundaries for these walls were RC beams which were cast integrally with the floor system.

The walls under investigation consisted of two wythes of masonry units spaced at 0.75 in. (0.019 m), joined only by header units placed at each fourth course, and at each fourth unit within that course. The outer wythe, corresponding to the veneer wall, was built using cored units with width of 4 in. (0.1 m), height of 2.25 in. (0.057 m), and length of 8 in. (0.2 m).

Two walls, identified as OF1 and OF2, were left unstrengthened as control walls, one with plaster and one without; walls OF3 and OF4 were strengthened with three 20 in. (0.50 m) wide GFRP laminates (one with plaster, one without), OF5 with three 10 in. (0.25 m) wide GFRP laminates (with plaster). Walls OF6 and OF7, both with plaster, were reinforced with three 20 in. (0.50 m) wide laminates, CFRP and AFRP respectively.

Wall OF8, with plaster, was strengthened with three 20 in. wide GFRP laminates anchored with GFRP rods . Finally walls OF9 and OF10, both with plaster, were strengthened with #3 GFRP NSM rods, unanchored and anchored at the floor respectively. The masonry walls were tested under two out-of-plane loads, which were distributed by 12x12x1/2 in. (0.30x0.30x0.012 m) steel plates to the external face of the walls.
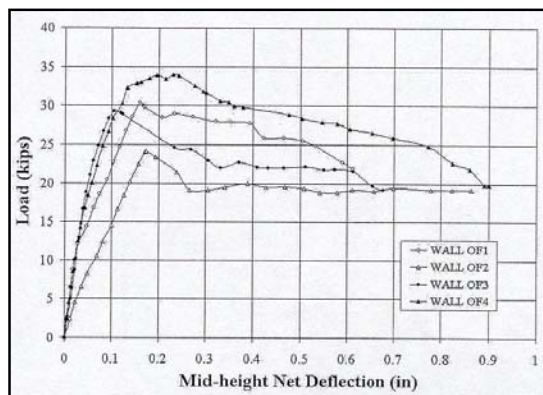
Fig. 2.2d *Test results* **(Tumialan 1999)**
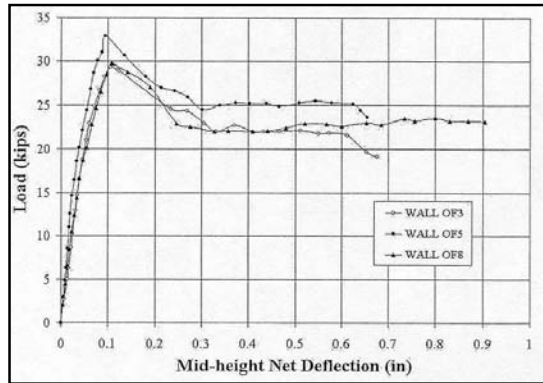
Fig. 2.2e *Test results* **(Tumialan 1999)**

A mechanism of failure that is not commonly observed in tests performed in a laboratory environment was identified. This action, called ***arching effect***, induces an in-plane compressive force (F_V in Fig. 2.2f) which accompanied by the shear force (F_H in Fig. 2.2f) in the support creates a resultant force that causes the fracture of the tile (F_R in Fig. 2.2f). The walls where the FRP laminates were applied directly to the masonry surface, after the removal of plaster, exhibited a better performance than their counterparts, strengthened without the removal of plaster. The increase in capacity was about 17% compared to the wall strengthened with the presence of plaster, and 45% compared to the control wall without plaster.

A critical influence of the height/thickness (slenderness) ratio in the mechanical performance of the panels was recognized.

For values of slenderness at around 12 the clamping forces generated by the so called arching effect were found to be so decisive to induce the failure on the corners of the infill panels. As reported by *Angel et al.* (1994), for slenderness ratios (h/t) larger than 20, the effect of the arching action can be so small to be ignored.
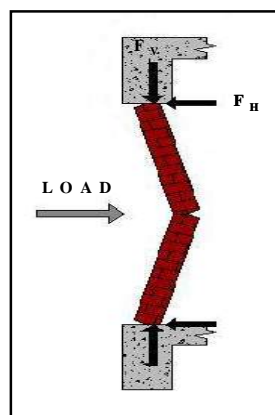
Fig. 2.2f *Arching effect on infill panels* **(Tumialan 1999)**

Albert et al (1999) tested ten full-scale masonry walls reinforced with externally applied FRP and subjected to primarily monotonically increasing lateral out-of-plane loads. One wall was loaded cyclically. Some walls were also concurrently subjected to moderate constant axial loads. All walls were 12 ft (4 m) high and 4 ft (1.20 m) wide, all tested in an upright position. Two out-of-plane concentrated loads were applied at two lines, 4 ft (1.20 m) from each reaction point. The parameters investigated were the type (carbon strap, carbon sheet and glass sheet), amount and layout of fiber reinforcement, axial load effects and cyclic behavior.

A full ancillary test series was performed. Masonry units showed a mean compressive strength of 2.88 ksi (19.90 MPa) and 2.30 ksi (15.90 MPa) respectively for the two series of walls investigated.

Each specimen was 20 courses high with #9 gauge joint reinforcement every third course. The walls were laid in running bond using factory mix Type S mortar.

Series 1 involved seven tests on the four walls and focused on varying the type of fiber reinforcement. Wall MU1 was first tested without fiber reinforcement , then tested again as a partially cracked wall reinforced with carbon straps, MCS2-1, and finally as a fully cracked wall, MCS3-2. One was reinforced on one side with carbon sheet and tested until fully cracked, MCST4, then additional carbon sheet fiber reinforcement was placed on the opposite side and the wall was tested again in a cyclic manner, MCST7-4. One test in the series involved a wall reinforced with four carbon straps , MCS-6, and another was reinforced with two glass sheets, MGST5.

Overall results showed that the strength and ductility of the specimens were increased significantly when strengthened. The overall behavior of the specimens was similar.

The load-midspan deflection response for all the specimens was found to be divided into two phases. The first phase, nonlinear, represented the stiffness contribution of the masonry materials. The second phase was linear and represented the stiffness contribution from the fiber reinforcement.

The type and amount of reinforcement used affected the overall stiffness of a specimen. The layout of the fiber reinforcement had more of a direct effect on the local joint strain behavior than the overall behavior. The introduction of axial load increased the first phase stiffness and reduced the second phase stiffness. Series 2 involved six tests on the six walls and focused on varying the layout and amount of carbon fiber sheet. The fiber reinforcement was primarily oriented in the vertical direction to optimize the strength of the fibers. ICST12 was tested with the strips oriented

diagonally. The purpose of this test was to determine the out-of-plane resistance of a wall reinforced primarily for in-plane loads. Axial load effects were also investigated in the series, ICST9 and ICST13.
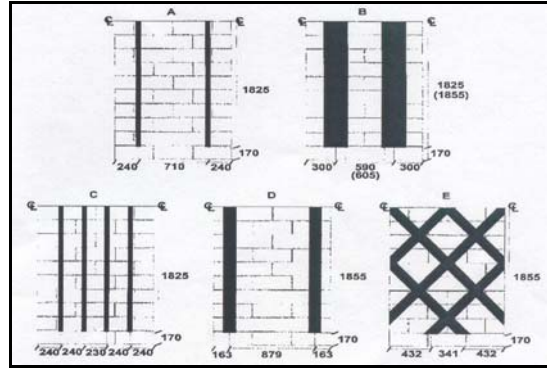

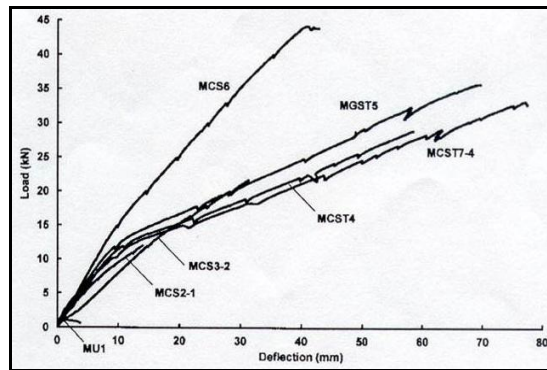**Fig. 2.2f** *Patterns and placement of FRP* (**Albert 1999**)

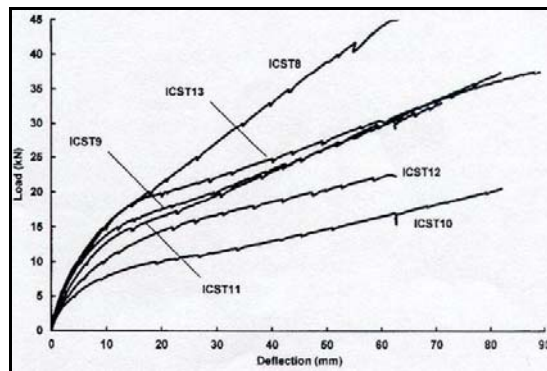**Fig. 2.2g** *Load-Deflection Response for Series 1* (**Albert 1999**)

**Fig. 2.2h** *Load-Deflection Response for Series 2* (**Albert 1999**)

2.3 <u>Experimental program</u>

The present research presents the results for simply supported wallettes, meaning that boundary conditions such as presence of slabs or surrounded concrete frames are not taken into consideration (see Fig. 2.2f); in other words, masonry walls with high slenderness ratio (height/thickness) in which the arching effect can be ignored are investigated. As shown in the previous results, delamination of the FRP reinforcement controlled the mode of failure of the majority of the tested specimens; therefore, longitudinal tensile strain in composite strips, deflections at mid-height, and the reinforcement ratio are considered to be the most representative parameters for the purpose of this study.

2.3.1 Description of the specimens

Twenty-six unreinforced masonry wallettes were constructed for this experimental program: half of them were built with 4x8x12in. (0.102x0.203x0.305 m) concrete blocks and half with 2.5x4x8in. (0.64x0.102x0.203m) dark molded clay bricks (see Fig. 2.3.1 a-b) in a running bond pattern, six and eighteen courses respectively. As shown in Fig. 2.3.1c the specimens were 48 in. (1.22 m) high, 24 in. (0.610 m) wide and 4 in. (0.102 m) thick ,therefore with a constant slenderness of 12, and they were built by qualified masons to not introduce additional variables, such as handwork and different mortar workability that may arise from the construction of the specimens.

The mortar used for the wallettes was available in bags in a dry premixed composition of cement and sand, and was classified as Type N according to the standard ASTM C270 (see Appendix A).
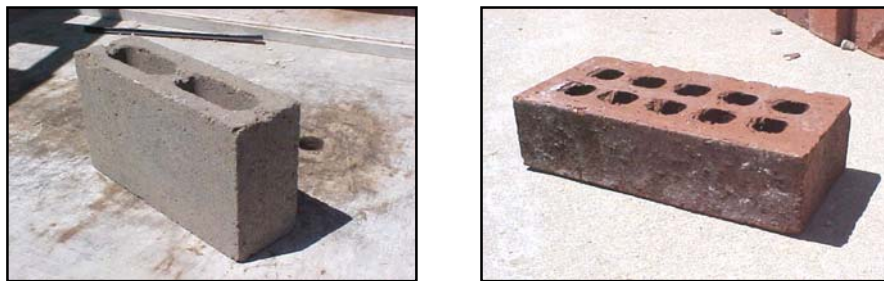
Fig. 2.3.1a-b *Masonry Units: concrete blocks (left), dark clay bricks (right)*

In order to characterize the mechanical properties of masonry compression tests on prisms made of concrete blocks and clay bricks were performed (see Appendix A). The average compressive strength of the concrete masonry was found to be 1414 psi (9.74 MPa) with a standard deviation of 151 psi (1.04 MPa), whereas the compressive strength of the clay masonry was 2500 psi (17.22 MPa) with a standard deviation of 50 psi (0.35 MPa).
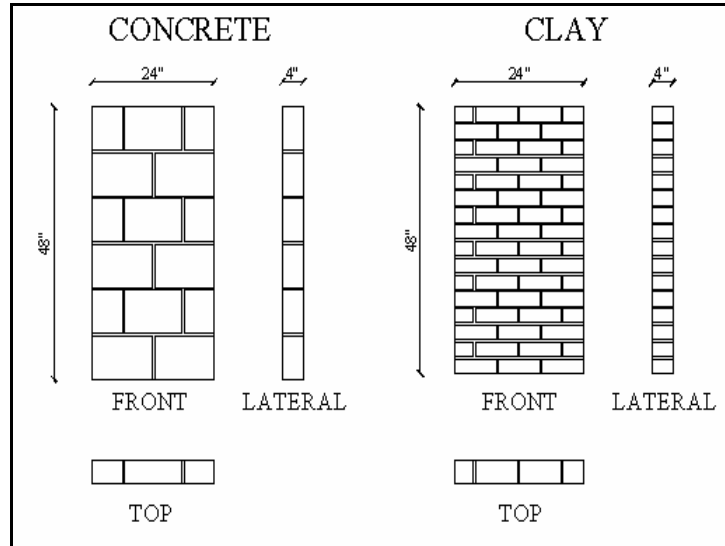
Fig. 2.3.1c *URM wall patterns*
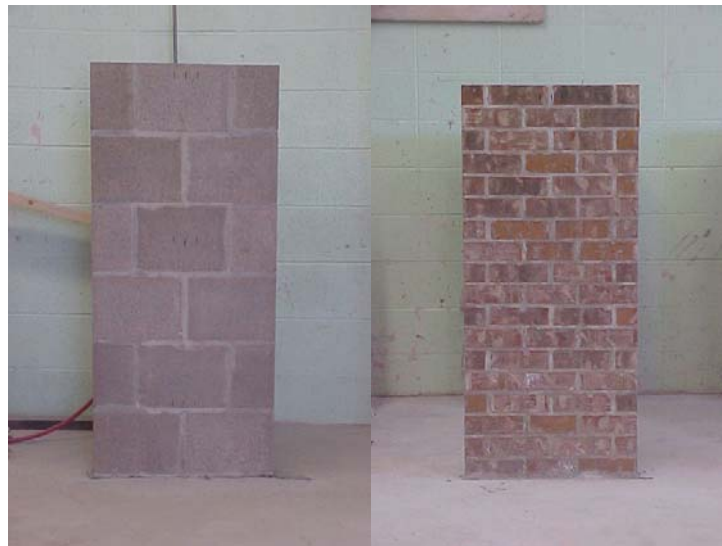
Fig. 2.3.1d Unreinforced specimens to be strengthened
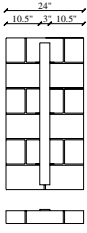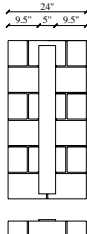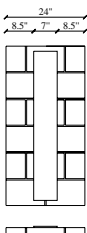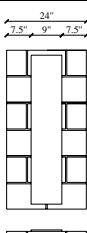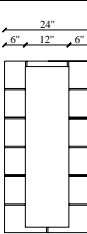
The investigated small-scale walls belong to a masonry typology commonly used across the United States, known as *infill panels*, typically utilized as exterior walls in reinforced concrete frame structures to form part of the building envelope. Where these walls are intended to be non-load-bearing, they are not design to contribute to the axial load-carrying or lateral load-resisting capacity of the structure.

2.3.2 Fiber Reinforcement Strategy

2.3.2.1 SERIES CO

Series CO involved 13 wallettes built with concrete blocks (see Section 2.3.1) and focused on varying the type and the amount of fiber reinforcement. At the beginning of the study it was decided to test 5 specimens reinforced with AFRP (Aramid) and 5 with GFRP (Glass) laminates, one FRP strip per specimen on one side. A summary of the experimental program for Series CO is shown in Table 2.3.2.1. The mechanical properties of the reinforcement were provided first by the manufacturer and the calculation of the amount of reinforcement was carried out based on these values (see Section 1.3.4.1).By understanding that the balanced condition for the flexural behavior of masonry walls represents the failure of masonry and rupture of composite laminate at the same time, two walls had the reinforcement equivalent to the balanced ratio (100% ρ_b), one for AFRP, one for GFRP. A plane section analysis was conducted to determine the calculated value. It was assumed that the masonry is ineffective in tension and that only the face shell can carry compression. For simplicity and similarly to the flexural analysis of RC members, a parabolic distribution of the stresses was used: thus it was found a FRP reinforcement consisting of one strip 7 in. (0.178 m) wide for both the types of FRP materials. For the rest of the wallettes it was decided to apply 40%, 70%, 130%, 170% of the ρ_b , namely 3 in. (0.0762 m), 5 in. (0.127 m), 9 in. (0.228 m) and 12 in. (0.305 m) respectively, with the obvious assumption that for percentages of reinforcement over the ρ_b a theoretically shear failure, whereas for percentages under the same value a typical flexural collapse of the specimens are expected. The purpose of testing this group of wallettes was to observe the difference in the mode of failure, if any, in wallettes reinforced with different amount and different types of FRP reinforcement, and ,in light of previous studies, to better understand which are the critical factors that can affect the theoretical flexural capacity of the walls. All the strips were 46 in. (1.17 m) wide.

Table 2.3.2.1a *Test Matrix for Series CO*

Specimen	Strengthening System	Reinforcing Scheme	Specimen Layout
COA3	AFRP laminates	One strip (w=3 in.) 40% of ρ_b	
COG3	GFRP laminates		
COA5	AFRP laminates	One strip (w=5 in.) 70% of ρ_b	
COG5	GFRP laminates		
COA7	AFRP laminates	One strip (w=7 in.) 100% of ρ_b	
COG7	GFRP laminates		
COA9	AFRP laminates	One strip (w=9 in.) 130% of ρ_b	
COG9	GFRP laminates		
COA12	AFRP laminates	One strip (w=12 in.) 170 % of ρ_b	
COG12	GFRP laminates		

In order to verify the longitudinal tensile strains in the composite strips, three other concrete wallettes were tested. It was decide to use only Glass fibers, for simplicity, compared with Aramid fibers, in applying them on the surfaces. Therefore one wall, called COG3R, was strengthened with the lowest amount of reinforcement, namely one 3 in. wide strip; COG5R was reinforced with a 5 in. wide strip as well as COG5A. However in the latter case a special anchorage for the FRP laminate was utilized, consisting in grooving a slot in the upper and lower courses of the wallette, at 2.5 in. (0.064 m) from the edges, rounding a GFRP #3 rod (mechanical properties are shown in Appendix A) which acted as anchorage after being bounded by epoxy-based paste. Pictures and schemes of the anchorage system previously described are presented in the next section. Details about the use of FRP rods as anchorage of FRP externally bonded sheets in RC and masonry members are clearly exposed elsewhere (*Khalifa et al.*, 1999). The program for the last three specimens in shown in Table 2.3.2.1b.

Table 2.3.2.1b

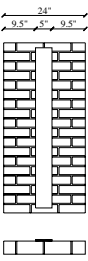| Specimen	Strengthening System	Reinforcing Scheme	Specimen Layout
COG3R	GFRP laminates	One strip (w=3 in.)	
COG5R	GFRP laminates	One strip (w=5 in.)	
COG5A	GFRP laminates GFRP rods	One strip (w=5 in.) Two GFRP #3 rods	

2.3.2.2 SERIES CL

As well as Series CO, <u>Series CL</u> involved 13 wallettes constructed of clay units. It's important to note that dark clay bricks used for these tests were molded and not extruded; *Roko et al.* (1999) observed that the absorption of the epoxy is limited in the extruded brick units as compared to the absorption in molded bricks. This is attributed to the glazed nature of their surface, which leads to a reduction of the bond strength between the FRP laminate and the masonry surface. A summary of the experimental program is shown in Table 2.3.2.2. In consequence of the compression tests performed on clay prisms built during the construction of the specimens (therefore with the same type of clay units and the same type and quality of mortar, see Appendix A), it was found that for the balanced condition a 9 in. (0.229 m) wide AFRP or GFRP sheet satisfied the equation. Even if Young's tensile modulus of elasticity of Aramid fibers is different from Young's modulus of Glass fibers (117000 MPa and 72350 MPa respectively) the different values obtained from the calculation can be considered equal with an approximation of 4%, more than acceptable for our research.

Instead of applying two reinforcements over the balanced amount and two under the calculated value, it was decided to put only one over, corresponding to 130% of the ρ_b (12 in.).
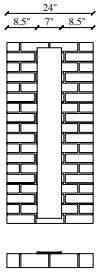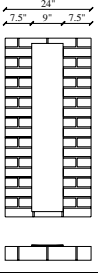
Table 2.3.2.2 *Test matrix for Series CL*
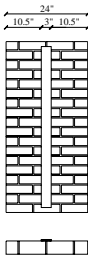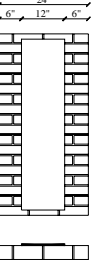
Specimen	Strengthening System	Reinforcing Scheme	Specimen Layout
CLA3	AFRP laminates		
CLG3	GFRP laminates	One strip (w=3 in.) 30% of ρ_b	
CLG3R	GFRP laminates		
CLA5	AFRP laminates		
CLG5	GFRP laminates	One strip (w=5 in.) 50% of ρ_b	
CLG5R	GFRP laminates		

Table 2.3.2.2 *Test matrix for Series CL (continued)*

Specimen	Strengthening System	Reinforcing Scheme	Specimen Layout
CLA7	AFRP laminates	One strip (w=7 in.) 80% of ρ_b	
CLG7	GFRP laminates		
CLG7R	GFRP laminates		
CLA9	AFRP laminates	One strip (w=9 in.) 100% of ρ_b	
CLG9	GFRP laminates		
CLA12	AFRP laminates	One strip (w=12 in.) 130% of ρ_b	
CLG12	GFRP laminates		

Technical remarks

In order to leave enough room for the reaction points, similarly to Series CO all the composite strips were 46 in. (1.17 m) wide. Particularly for Series CL the FRP reinforcements were applied just overlapping the mortar joint (see Fig. 2.3.3g).

2.3.3 Installation of FRP reinforcement

According to Section 1.3.4.4 and following protocols provided by the manufacturers, a typical *manual lay-up* technique was utilized in order to strengthen the specimens. After the construction of the wallettes, built by qualified masons to not introduce additional variables, the composite strips (Aramid and Glass laminates) were bonded with an epoxy resin on the faces of the walls. A more detailed description of the steps involved in retrofitting a wall with fiber composites is given elsewhere (*Ehsani and Saadatmanesh* 1996, *Tumialan* 1999). It is noted that, similar to many other construction practices, this technique has been patented (*Lester* 1998, *Ehsani and Saadatmanesh* 1996).

The wall is first cleaned with a steel brush (Fig. 2.3.3a), then dust and any loose particles are removed with high air pressure (Fig. 2.3.3b). A thin layer of primer is coated to the wall surface where the composite strips are to be attached (Fig. 2.3.3c). The surface of the walls, particularly at the joints, is leveled with putty (Fig. 2.3.3d). A first coat of saturant is applied on the surface (Fig. 2.3.3e); next, the composite strips are cut to size (Fig. 2.3.3f) and bonded to the wall face by hand pressure (Fig. 2.3.3g) and pressed with a roller to eliminate air bubbles (Fig. 2.3.3h) and to ensure that the fabric is saturated with the saturant. Finally, the exterior surface of the fabric is coated with a small layer of saturant for protection and instrumentation purposes. In the following pictures all the steps previously described are illustrated.

Fig. 2.3.3a *Cleaning of the wallettes with a steel brush*

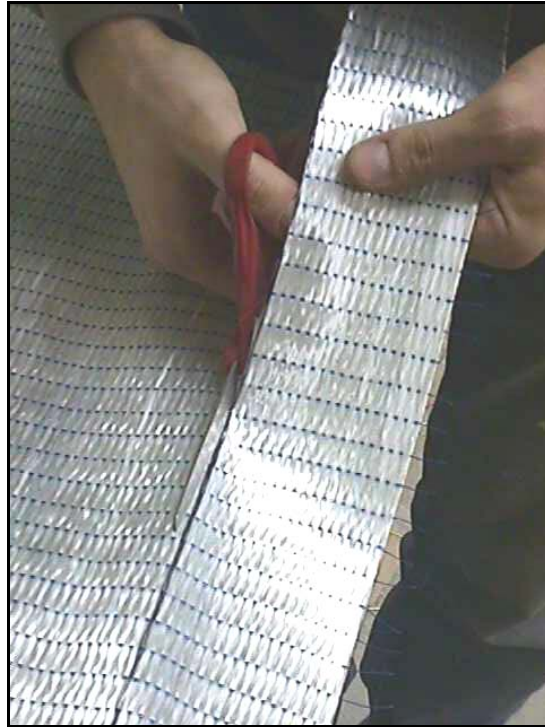**Fig. 2.3.3b** *Removing of dust and any loose particles*

Fig. 2.3.3c *Application of primer on clay*

Fig. 2.3.3d *Leveling with putty*

Fig. 2.3.3e *First coat of saturant*

Fig. 2.3.3f *Cutting of Glass fibers*

Fig. 2.3.3g *Fiber installation*

Fig. 2.3.3h *Elimination of air bubbles*

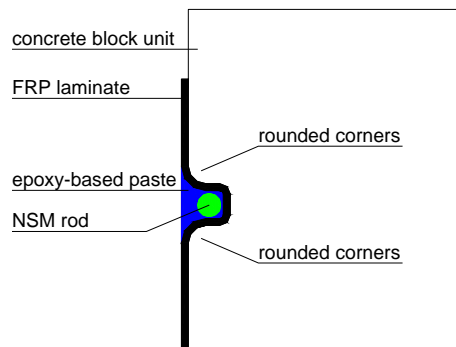**Fig. 2.3.3i** *Second coat of saturant*

Fig. 2.3.3j *Reinforced specimen before testing*

Fig. 2.3.3k Installation of GFRP rod as anchorage

Fig. 2.3.3l Injection of epoxy-based paste into the groove and final retooling

Fig. 2.3.3m Scheme of NSM rod acted as anchorage

2.3.4 Test set up

2.3.4.1 Test frame

Masonry specimens were tested under four point bending, following the ASTM standard E518. All specimens were loaded in the test steel frame shown in Fig. 2.3.4a-b-c. Each was tested as a simply supported beam, meaning that boundaries conditions such as presence of corners or joint interferences were not take into consideration. The loads were generated by means of a 100 kN (20 kip) hydraulic jack, centered on the distribution beam of the steel frame, which then separated the concentrated load into two line loads both located at 4 in. (0.102 m) from the mid-height of each wallette.

Therefore a constant moment region 8 in. (0.203 m) long was created. The line loads rested along the full width of the wallettes. Knife edges and rollers were used for the loading and gravity supports (See Fig.2.3.4d-e).
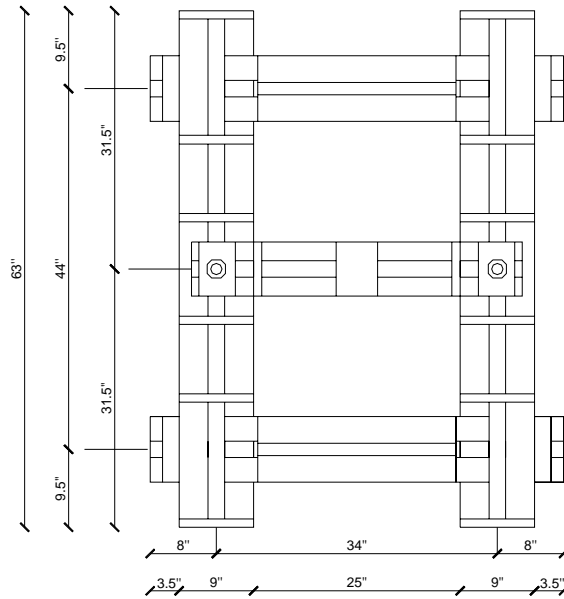
**Fig. 2.3.4a** *Steel Frame for wall testing-FRONT VIE W(scale 1:20)*
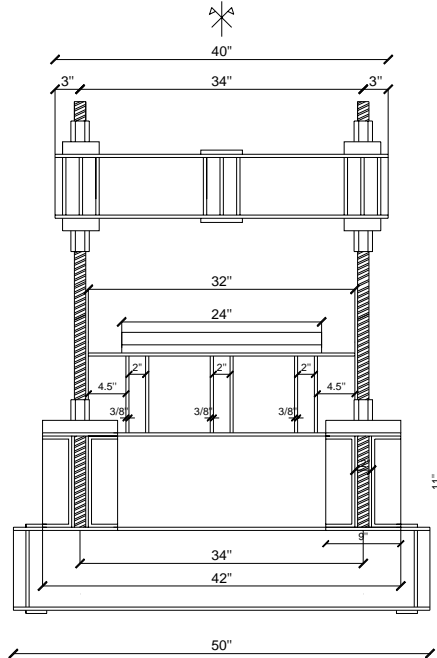
Fig.2.3.4b *LONGITUDINAL VIEW (scale 1:20)*
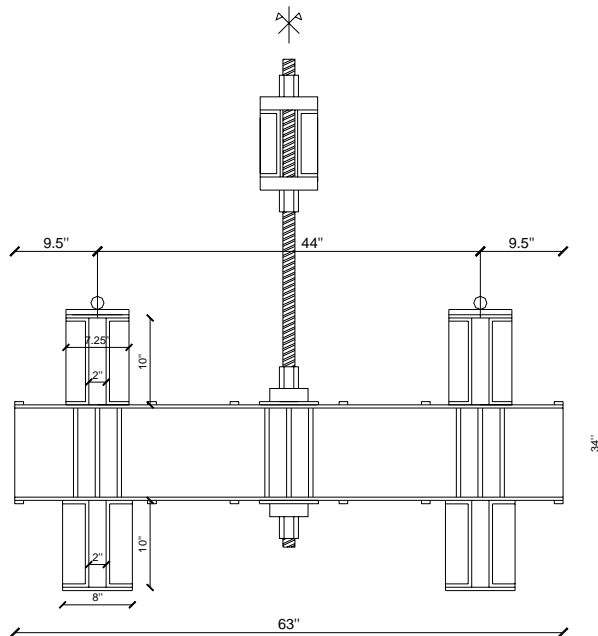
Fig. 2.3.4c *PLANT VIEW (scale 1:20)*

The force created by the hydraulic jack reacted against a 40 in. (1.02 m) steel girder made of two C5x8, hereafter called reaction beam, in its turn connected by means of two high strength steel rods 5 foot (1.52 m) long to two C5x10(couples) and two C5x11(couples), the first couple of beams supported by the second one, acted as gravity supports to the wallettes. The entire structure was finally sustained by means of two C5x10, playing the role of basement beams. All the connections among the various couple of steel girders were effective using suitable C-clamps which generated friction on the interfaces.
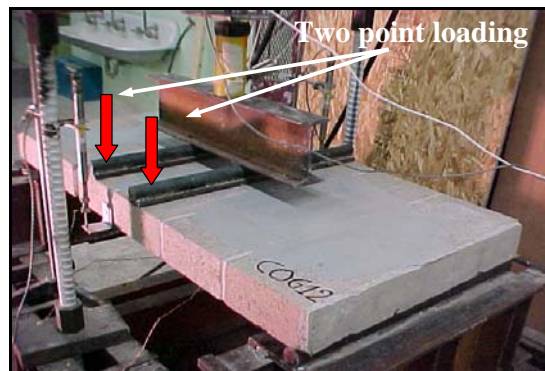
Fig. 2.3.4d *Test set up with two point loading*
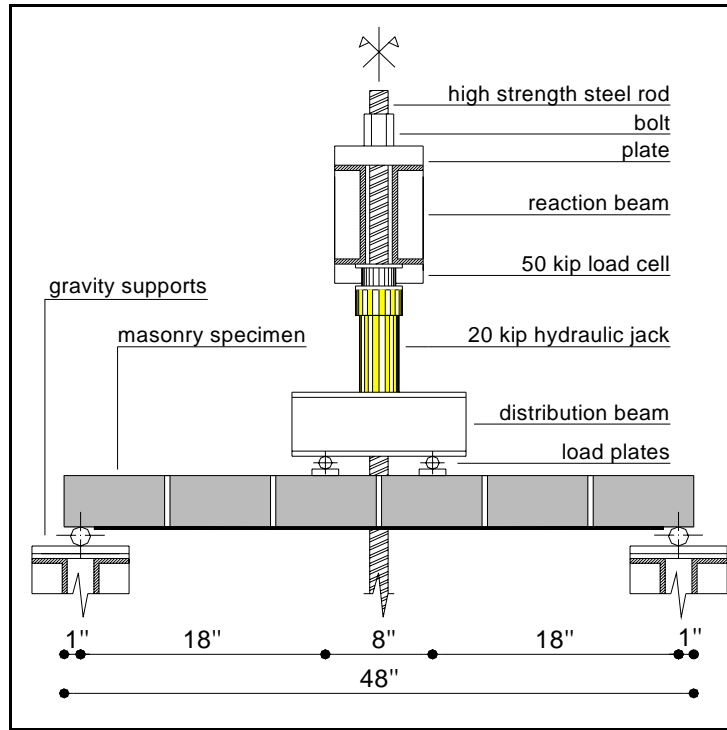
Fig. 2.3.4e *Generated load scheme*

Fig. 2.3.4f *Reinforced specimen before testing*

Technical remarks   Due to the remarkable number of specimens to be tested, a fast and practical procedure was developed in order to put the wallettes on the test frame without causing any damages to the masonry units as well as the FRP reinforcement. Each wallette was first precompressed using two small beams applied on the edges and forced in tension with two deformed steel rods. Thus it was wrapped into a special cover consisting of two 2 in. by 4 in. (0.05 by 0.1 m) wood poles, acted as supporting beams after being rounded with the wallette itself by four elastic straps which created a suitable state of confinement to rotate the wall from vertical to horizontal and then to move it into the test frame as shown in Fig. 2.3.4f.

2.3.4.2 Instrumentation

The instrumentation used consisted of a 50 kips (250 kN) load cell to measure the force generated by the hydraulic jack, two linear variable differential transducers (LVDT's) to register deflections at mid-height, one LVDT for each side of the specimen being tested. In order to monitor the strain distribution along the FRP reinforcement (laminate) five strain gages per wall were employed, placed on the longitudinal axis of the sheet , each one relating with a mortar joint below the fabric. In this manner it was found that the strain gages were placed at every mortar joint for the concrete unit walls (Fig. 2.3.4.2a), at every three mortar joints for the clay unit walls. All the data were collected by a data acquisition system at a frequency of 1 Hz (see Fig. 2.3.4.2b).

Fig. 2.3.4.2a *Placing of strain gages on FRP*   **Fig. 2.3.4.2b** *Data Acquisition System*

2.3.4.3 Test procedure

The load was applied in cycles of loading and unloading. Each wallette was loaded to 0.5 kips (2.22 kN) and then holded to this value prior to continuing with the test. This procedure allowed checking the instrumentation and loading system. The specimens were loaded in increments of 1 kip (4.45 kN), and unloaded to a low threshold of 0.5 kips. A summary of the load cycles is presented below.

Table 2.3.4.3 *Load cycles*

Cycle	Load Range (kips)
1	0-0.5
2	0.5-1.5-0.5
3	0.5-2.5-0.5
4	0.5-3.5-0.5
5	0.5-failure (?)

2.3.5 Test results

2.3.5.1 <u>SERIES COG</u>

Wall COG3

The first specimen to be tested was strengthened with a GFRP 3 in. (0.076 m) wide sheet. At 2.22 kN a first major crack was visible at mid-height, along the full mortar joint. At an applied load of 3.38 kN two cracks appeared along the full mortar joints adjacent the one corresponding to the middle of the wall (Fig. 2.3.5b). The peak load was reached at 8.66 kN for a midspan deflection of 20 mm as can be observed in Fig. 2.3.5a.
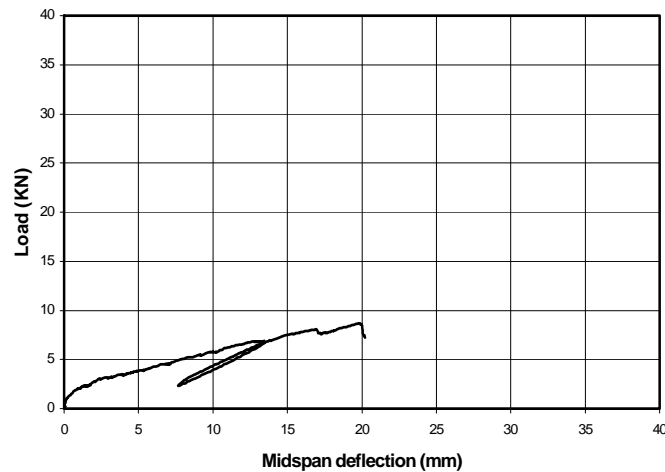

Fig. 2.3.5a *Load vs. Midspan net deflection Curve-Wall COG3*

80

At the final stage, starting from the mid-height, a progressive delamination of the FRP reinforcement occurred, moving to one of the two edges of the wallette, therefore causing the final failure due to complete lack of bond between the masonry surface and the FRP sheet. In order to better understand the final mechanical behavior of the wall part of debris resulted from the collapse was formed again and two 45 degrees fractures were found to have been developed just before the complete failure, taking origin from the longitudinal axis, at the middle of the second course of masonry units, and moving to the longitudinal borders, obviously stopping at the nearest mortar joint that cannot support tensile stresses (Fig. 2.3.5c).This phenomenon, revealed in the majority of the specimens of Series CO, can be attributed to the high-stress condition provided by the bond stresses between the masonry surface and the FRP reinforcement in the constant moment region, in which the tensile stresses developed in the sheet are maximized.
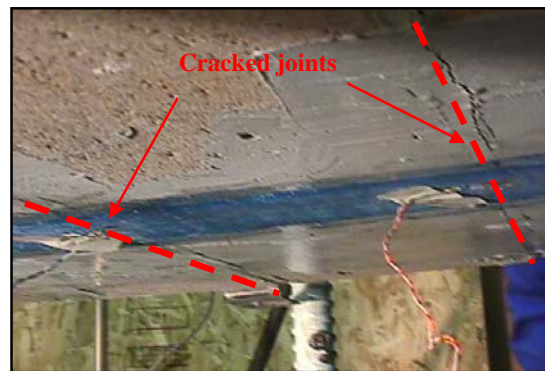
Fig. 2.3.5b *Developing of cracks along the full mortar joints*

Fig. 2.3.5c 45° *Fractures on the second course of concrete units*

WALL COG3R

A specimens with same characteristics of the previous one was investigated. The first visible crack was observed at a load of 2.2 kN, running along the middle mortar joint, for the entire length. The peak load was reached at 11.84 kN, 30% higher than the first one, for a midspan deflection of 26.81 mm, as shown in Fig. 2.3.5d. The failure, similar to that observed in COG3, was caused by a debonding effect which involved in this case not only the FRP reinforcement but the concrete unit surfaces either. Therefore in this case the failure mode should be identified as a combination of debonding and peeling of concrete. The increase of the peak load should be attribute to a better bond between the concrete surface and the FRP laminate, which means a better penetration of primer and saturant into the porous surface of the bricks. Strain channels revealed that at mid-height FRP laminate reached a strain value of 1.5 % before delamination occurred.
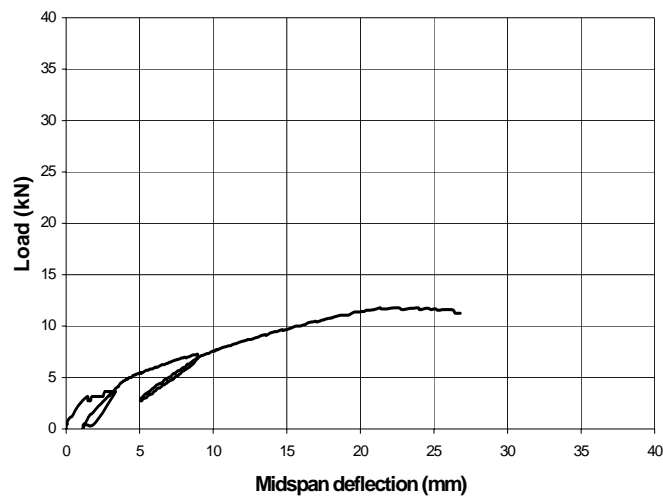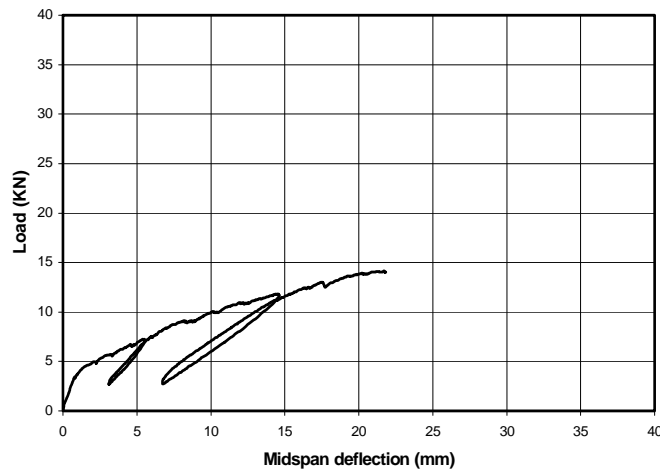

Fig. 2.3.5d *Load vs. Midspan net deflection Curve-Wall COG3R*

WALL COG5

This wall was strengthened with one GFRP 5 in. (0.127 m) wide strip. The first visible crack was observed at a load of 4.45 kN running along the mid-height mortar joint. At a load of 6.09 kN two cracks appeared on the mortar joints adjacent to the previous one and at a load of 6.91 another crack, located along the joint between the first and the second course of the wallette, on one side, was opened. As shown in Fig. 2.3.5e, the specimen failed at a load of 14.15 kN for a midspan deflection of 22 mm.

The collapse, similarly to COG3R, was caused by a combination of debonding of the FRP reinforcement followed by peeling of the concrete unit surfaces.

Fig. 2.3.5e *Load vs. Midspan net deflection Curve-COG5*

Fig. 2.3.5f *Developing of flexural-shear crack under a loading point*

WALL COG5R

Similarly to COG3R, COG5R presented the same amount of reinforcement of COG5. As shown in Fig. 2.3.5g the peak load was reached at 14.56 kN for a deflection of 26.89 mm. The first visible crack was found at a load of 5.2 kN, as for the previous wallettes running along the mid-height mortar joint. Two cracks developing from the adjacent joints were observed at a load of 6.1 kN. One of these moved to the loading point above assuming a 45 degrees slope, meaning that a combination of flexural-shear behavior was occurring. As for COG5, the wall failed for debonding of the FRP laminates, however a typical flexural-shear behavior was identified at the final stage. Strain channels registered a maximum strain value on the FRP sheet at the mid-height of 1.2% before collapse.
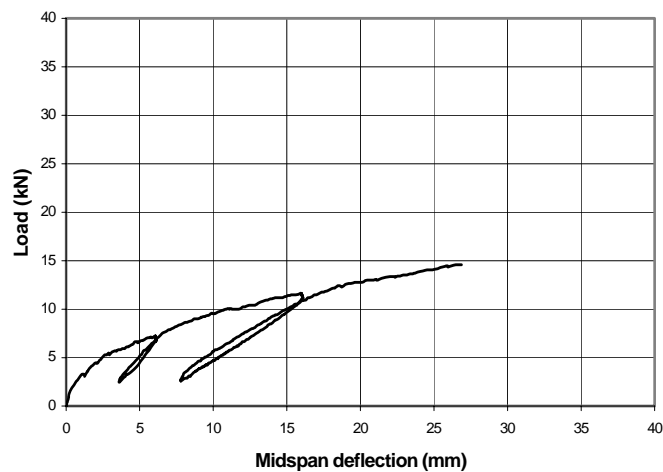
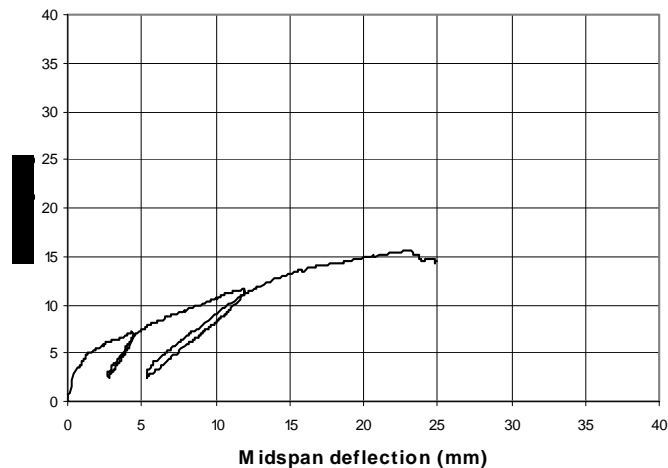**Fig. 2.3.5g** *Load vs. Midspan net deflection Curve-COG5R*

Fig. 2.3.5h *Flexural-shear behavior at the final stage*

84

WALL COG5A

This wall had a similar strengthening scheme to COG5 and COG5R. The significant difference consisted in the use of two NSM GFRP rod acted as anchorages for the FRP strip (see Section 2.3.3) at the edges. As shown in Fig. 2.3.5i the maximum load recorded was 14.47 kN with a corresponding midspan deflection of 25 mm.

No differences in terms of crack patterns and ultimate capacity were observed until the final stage, compared with COG5 and COG5R. However the failure was caused in this case by the collapse of one of the anchorages. Strain channels recorded a maximum strain value in the mid-height of 1%.

Fig. 2.3.5i *Load vs. Midspan net deflection Curve-COG5A*

Fig. 2.3.5j *Pull-out of NSM rod from the groove*

WALL COG7

This wall was strengthened with the amount of reinforcement corresponding to the balanced condition. Similarly to the previous walls reinforced with 70% of ρ_b , the failure was caused by a combination of debonding of the FRP laminate and peeling of concrete surfaces. The peak load was reached at 15.78 kN with a midspan deflection of 19 mm, as shown in Fig. 2.3.5k. The first crack running along the mid-height mortar joint was registered at 5.25 kN. By comparing this wall with the previous ones, a larger presence of cracks spread for all the mortar joints was observed (Fig. 2.3.5l).
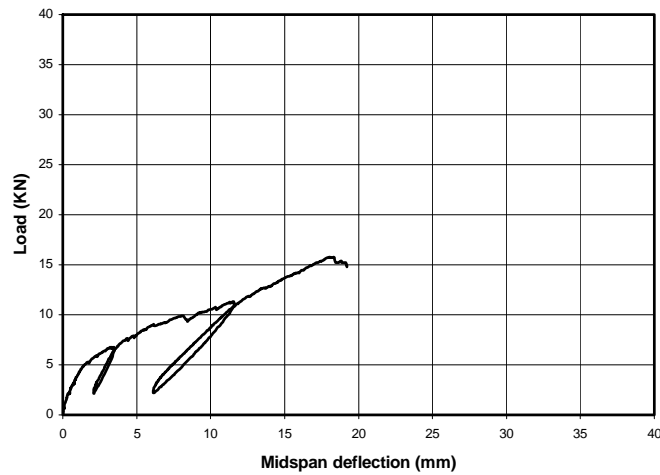
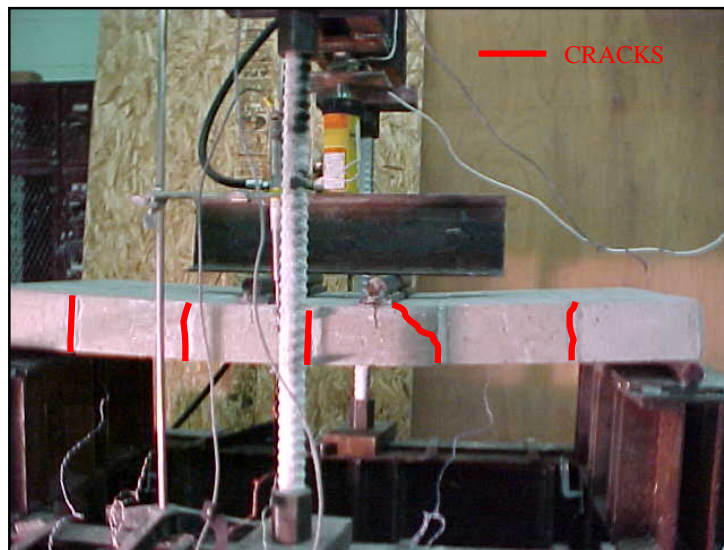**Fig. 2.3.5k** *Load vs. Midspan net deflection Curve-COG7*

Fig. 2.3.5l *Crack patterns at the ultimate stage*

WALL COG9

This wall was strengthened with an amount of reinforcement corresponding to 130% of the ρ_b. A shear failure was so expected. The peak load was reached at 21.95 kN with a midspan deflection of 18 mm, as shown in Fig. 2.3.5m. A first major crack was identified at a load of 6.1 kN; once the load increased after this value, as for COG7, a presence of cracks spread for all the mortar joints was observed. The failure of the specimens was due to a combination of debonding of the FRP reinforcement and shear developed in the concrete units.
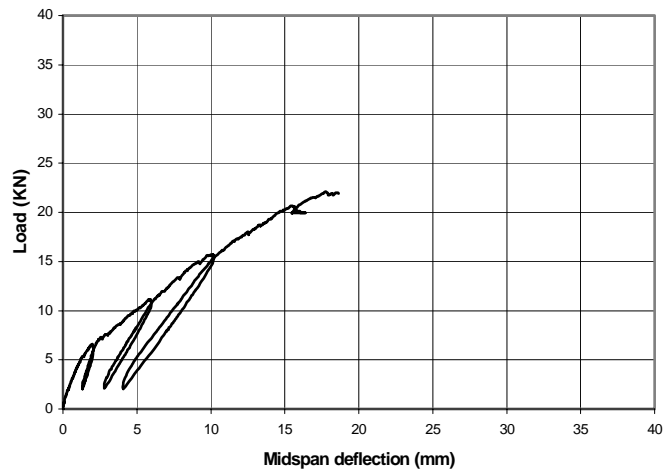

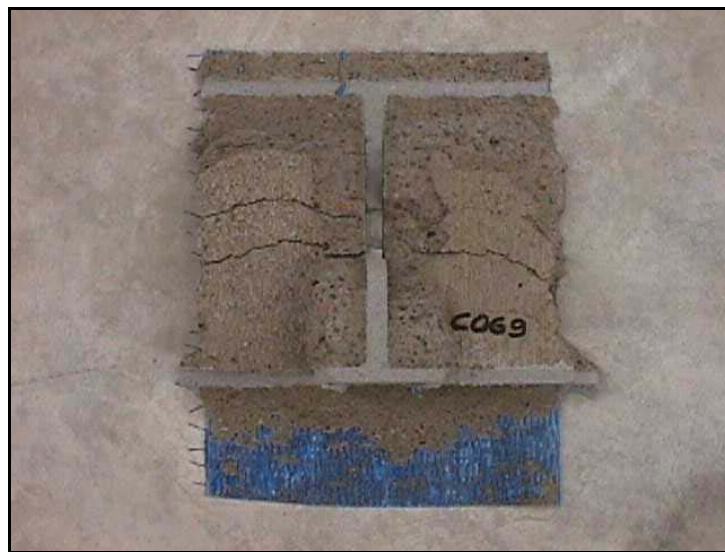**Fig. 2.3.5m** *Load vs. Midspan net deflection Curve-COG9*

Fig. 2.3.5n *FRP sheet sample after failure*

WALL COG12

This wallette had the highest amount of GFRP reinforcement, corresponding to 170% of the ρ_b. A major horizontal crack was observed at a load of 7.03 kN. The wall exhibited a peak load of 25.62 kN for a midspan deflection of 17.5 mm, as presented in Fig. 2.3.5o. This specimen exhibited a very stiff behavior during the loading cycles and showed a typical shear brittle failure, without revealing any lack of bond between the FRP sheet and the concrete surface. A huge presence of 45° cracks , from both sides of the wall, moving from the longitudinal axis to the borders in the bottom face was observed, meaning that the FRP laminate was able to transfer tensile stresses by means of the interface to the masonry units.
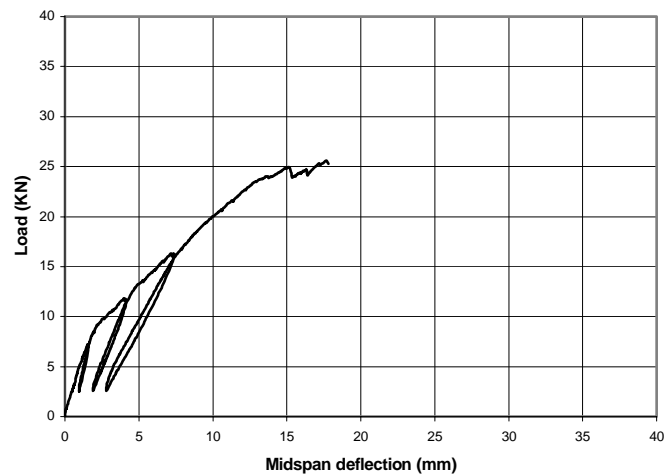

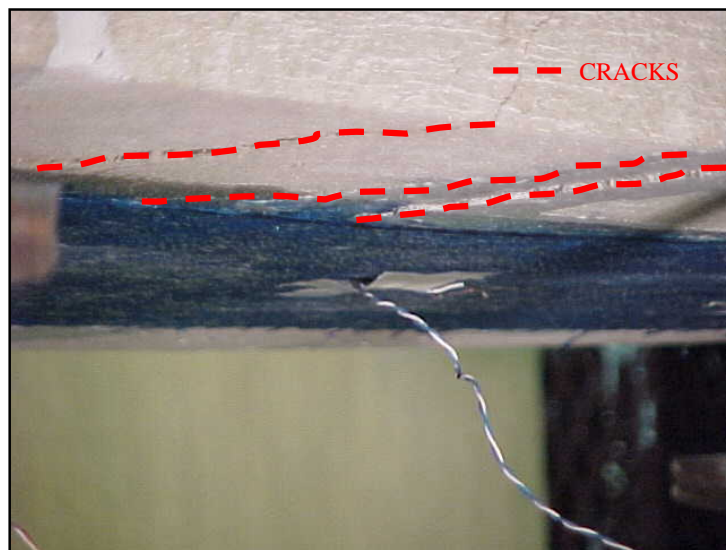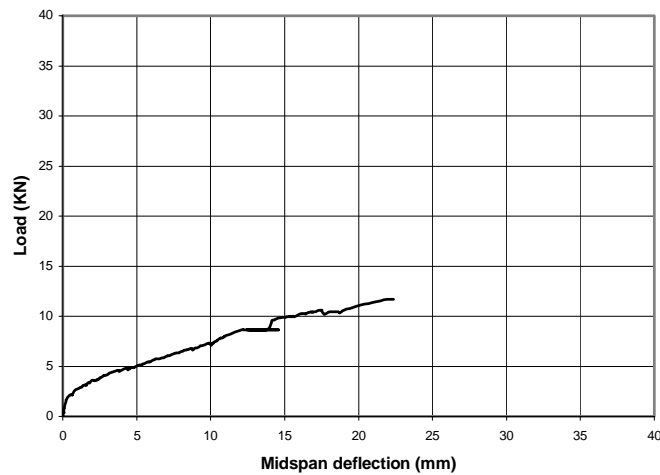**Fig. 2.3.5o** *Load vs. Midspan net deflection Curve, COG12*

**Fig. 2.3.5p** *Transfer of tensile stresses from FRP to masonry units*

2.3.5.2 <u>SERIES COA</u>

WALL COA3

The strengthening scheme of this wall was similar to COG3, only that in this case AFRP laminates were used. This wall did not show large areas of cracking, only a major horizontal crack running along the mid-height mortar joint was detected at a load of 2.25 kN. The peak load was 11.69 kN, much higher than COG3 (obviously the differences in the mechanical properties of the FRP have to be taken into consideration), and the recorded midspan deflection was 22 mm, as observed in Fig. 2.3.5a*.

Fig. 2.3.5a* *Load vs. Midspan net deflection-COA3*
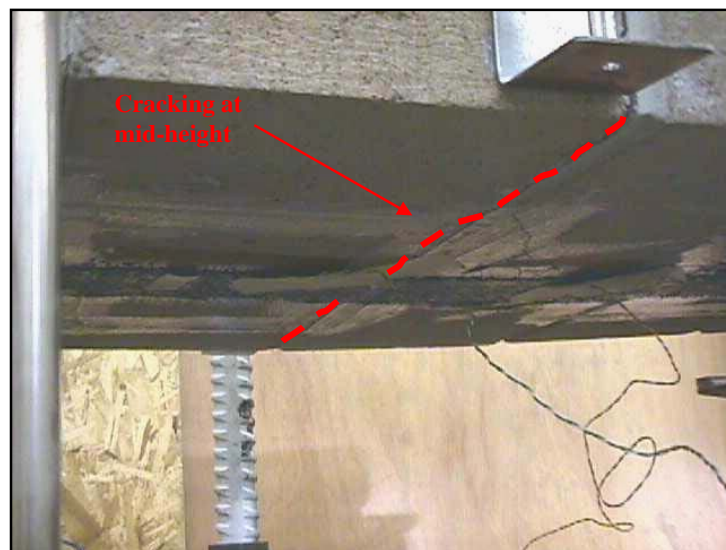
Fig. 2.3.5b* *Major horizontal crack at mid-height*

WALL COA5

The strengthening geometry of COA5 and COG5 were similar. The only difference in this case was the employment of AFRP laminates. No remarkable differences in terms of crack patterns, ultimate capacity or mode of failure, compared with COG5 and COG5R, were observed. As shown in Fig. 2.3.5c* the peak load was reached at 14.83 kN for a midspan deflection of 23 mm. The failure was caused by debonding of the laminate moving from the middle of the specimen to the edges. Presence of 45 degrees cracks on the bottom face, starting from the longitudinal axis, revealed a good transmission of tensile stresses through the interface FRP-masonry units.
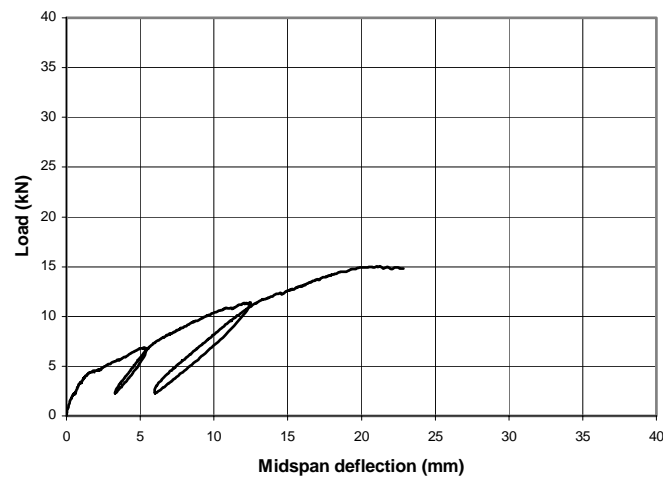

Fig. 2.3.5c* *Load vs. Midspan net deflection Curve-COA5*

Fig. 2.3.5d* *Edge of the specimen after debonding failure*

WALL COA7

This wall was strengthened with one AFRP sheet 7 in. (0.178 m) wide, corresponding to 100% of ρ_b. The first visible crack was observed at a load of 5.16 kN, running along the full mid-height mortar joint. Two other cracks, starting from the adjacent mortar joints and moving to the loading points were observed for a load of 8.59 kN. The peak load was reached at 19.73 kN for a midspan deflection of 22 mm, as shown in Fig. 2.3.5e*. The wallette failed for a combination of debonding of the FRP laminate and shear in the masonry which caused 45 degrees fractures in concrete units.
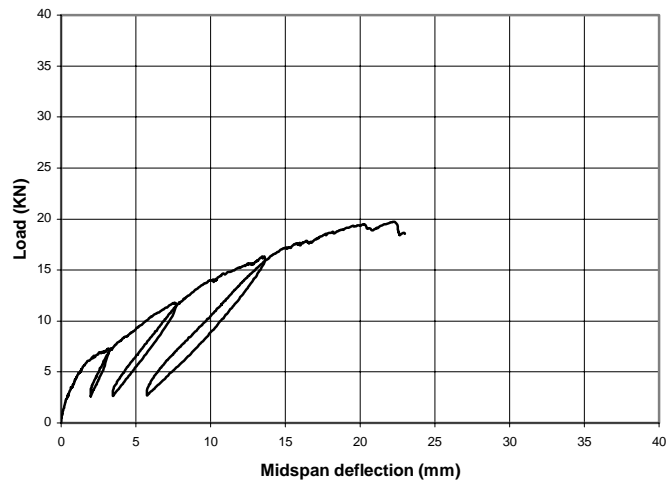

Fig. 2.3.5e* *Load vs. Midspan net deflection Curve-COA7*

Fig. 2.3.5f* *45• fractures in concrete units*

WALL COA9

This wall was reinforced with an amount of AFRP corresponding to 130% of ρ_b. A first crack was observed at a load of 6.67 kN. As for COA7, two cracks, revealing a combined action between tensile stresses on the bottom face and shear stresses corresponding to the loading points, were detected at 8.90 kN. The peak load was reached at 22.18 kN for a midspan deflection of 16 mm, as observed in Fig. 2.3.5g*. Compared with the previous specimens reinforced with AFRP laminates, COA9 exhibited a stiffer behavior and the failure occurred for the shear collapse of the concrete units in correspondence of the loading points, meaning that the tensile stress limit in the masonry was reached.
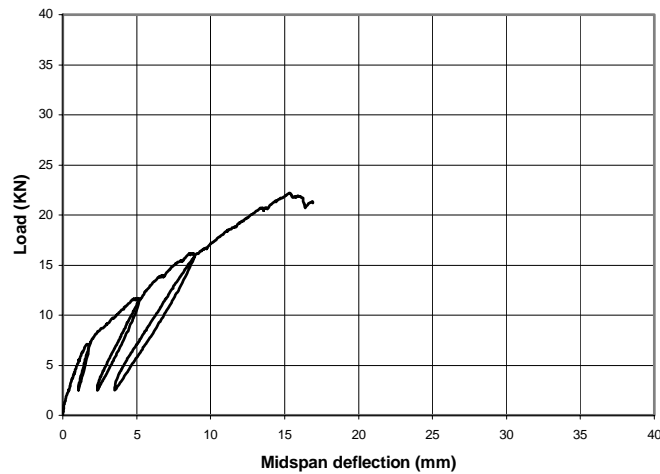

**Fig. 2.3.5g*** *Load vs. Midspan net deflection Curve-COGA9*

Fig. 2.3.5h* *Shear fractures on masonry units*

WALL COA12

This wall was the most strengthened using Aramid fibers. The strengthening geometry was similar to COG12, with the difference of using AFRP instead of GFRP.

No differences were observed in terms of mechanical behavior compared to COA9. However, a larger presence of cracks spread for all the mortar joints were detected. The maximum load was registered at 26.98 kN for a midspan deflection of 15 mm; the big difference with COG9 was that the failure was caused by the shear collapse of the concrete units located at the edge of the specimen, as shown in Fig. 2.3.5i*.
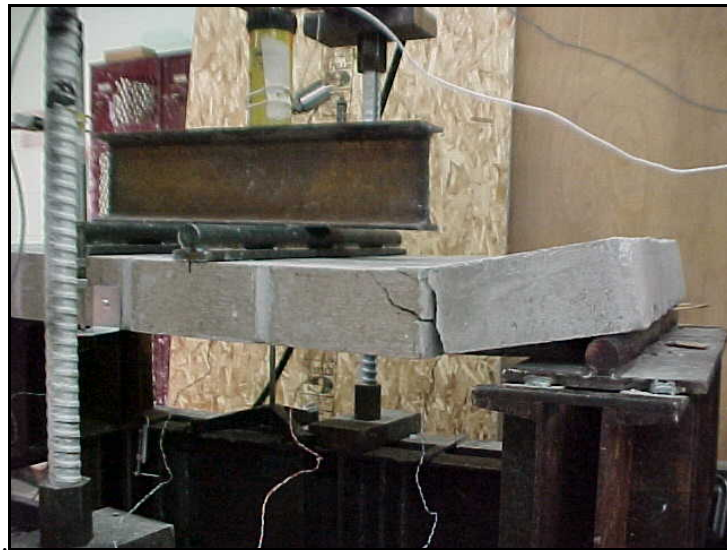
Fig. 2.3.5i* *Failure at the edge*

Fig. 2.3.5j* *Developing of shear cracks for the entire length*

2.3.5.3 <u>SERIES CLG</u>

WALL CLG3

This wall, constructed of clay units, was tested as the first wall of Series CL. As clearly exposed elsewhere (*Roko et al.* 1999) clay molded units exhibit better porosity than concrete units, caused by manufacturing processes (concrete units are extruded) and furthermore by the microscopic structure of clay which allow primer and saturant to deeply penetrate into the material; therefore bonding may be significantly increase and FRP laminates may perform much better in terms of ultimate capacity and strain distribution at the ultimate stage. This specimen failed for debonding of the laminate, reaching a peak load of 15.87 kN for a midspan deflection of 31 mm.
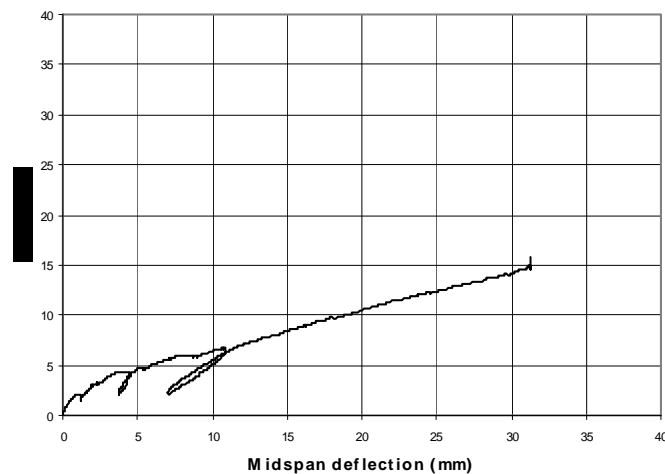

Fig. 2.3.5a** *Load vs. Midspan net deflection Curve-CLG3*

Fig. 2.3.5b** *Debonded FRP laminate after failure*

94

WALL CLG3R

In order to verify the values registered by strain channels on the FRP strip, CLG3R was strengthened identically to CLG3. Since the controlling factor in the previous specimens was debonding of FRP laminate, a similar failure mode was so expected; however, due to the significant increase of bond in the interface FRP-masonry the specimen collapsed for rupture of the FRP laminate occurred at mid-height (Fig. 2.3.5d**). The peak load was reached at 15.92 kN for a midspan deflection of 30 mm. Strain recordings revealed a maximum strain corresponding to the rupture region of 2.25%, higher than the value provided by the manufacturers.
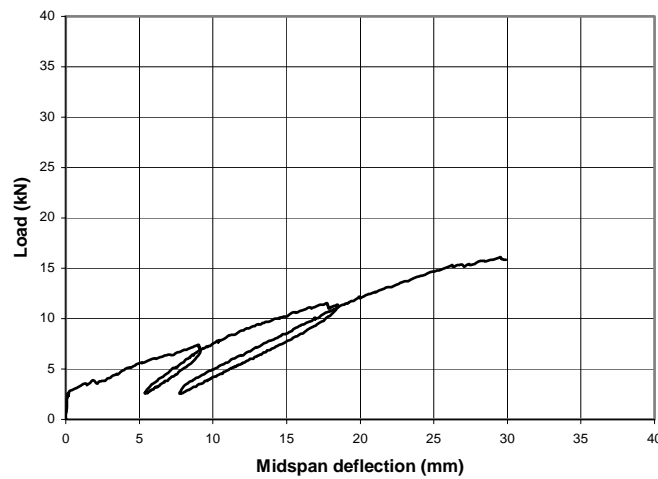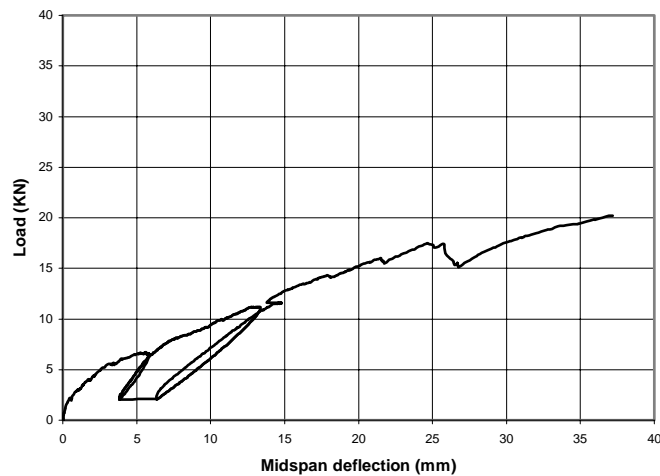

**Fig. 2.3.5c**** *Load vs. Midspan net deflection Curve-CLG3R*

Fig. 2.3.5d** *Rupture of GFRP laminate at mid-height*

95

WALL CLG5

This wall was reinforced with a 5 in. (0.127 m) wide AFRP strip. A major crack was visible at 4.45 kN running along the mid-height, followed at 8.9 kN by other cracks observed in the adjacent joints. No other areas of cracking were detected until the final stage. As shown in Fig. 2.3.5e**, the peak load was reached at 20.18 kN for a midspan deflection of 37 mm. The higher values of deflection compared with the concrete wallettes may be attributed to the different nature of the clay masonry structure, which is characterized by a suitable distribution of mortar joints and clay units that can provide more flexibility and deformability to the entire wallette. The failure was caused by debonding of the laminate as shown in Fig. 2.3.5f**.
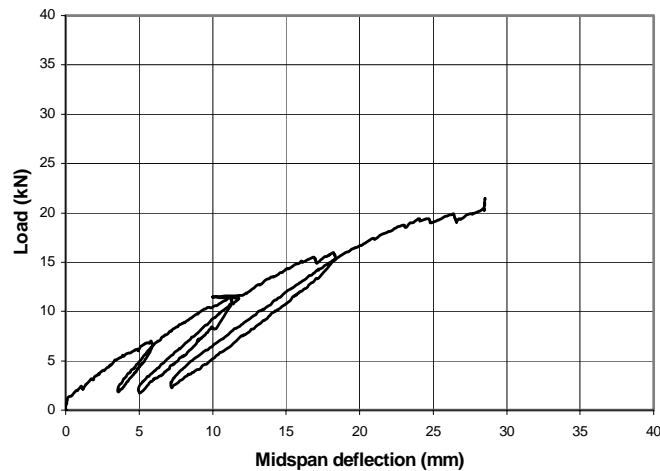

Fig. 2.3.5e** *Load vs. Midspan net deflection Curve-CLG5*
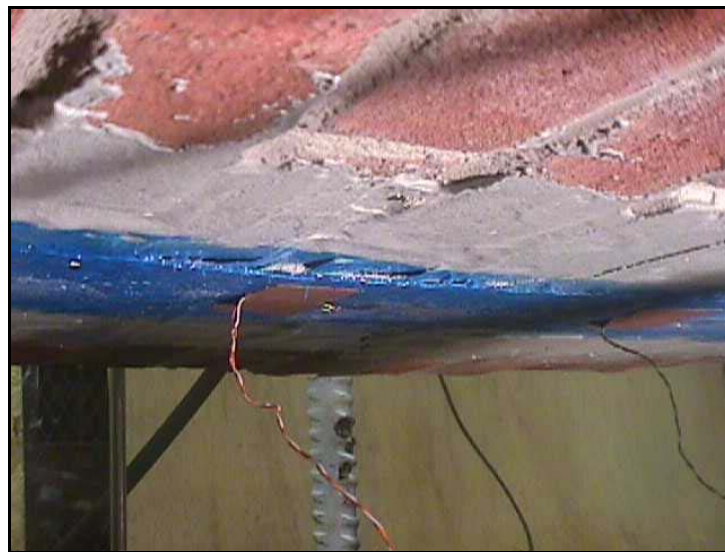
Fig. 2.3.5f** *Delamination of the FRP sheet at mid-height*

96

WALL CLG5R

The strengthening geometry of this wall was identical to the previous one. No remarkable differences were observed in terms of crack patterns and ultimate capacity. However in this case a different loading procedure was performed, consisting in applying three loading cycles instead of two as shown in Fig. 2.3.5g**. The peak load was reached at 21.51 kN for a midspan deflection of 28.5 mm. The collapse was caused by rupture of the laminates and shear fractures in the mid-height courses. Comparing the Load vs. Deflection Curves of CLG5 and CLG5R it can be observed that at the ultimate stage the first specimen exhibited a sudden drop of the load-carrying capacity, corresponding to the initial delamination, followed by a reprise which leaded to the failure with the same slope of the previous phase, whereas in the second wallette this phenomenon was not visible. Similarly to CLG3R, the maximum strain was recorded at mid-height showing a value of 2%, therefore very close to the ultimate strain (2.1%) guaranteed by the manufacturers.

Fig. 2.3.5g* *Load vs. Midspan net deflection Curve-CLG5R*

Fig. 2.3.5h** *Rupture of the GFRP laminate*

WALL CLG7

This wall was strengthened with an amount of reinforcement corresponding to 80% of ρ_b, therefore close to the balanced condition. As expected the specimen revealed a stiffer behavior compared with the previous clay wallettes during the load cycles as can be observed in Fig. 2.3.5h** analyzing the slope of the load-deflection curve. In this case the first visible crack was observed at a load of 7.12 kN at mid-height course. Adjacent courses were subjected to cracking at 8.9 kN. No more cracks were observed and the peak load was reached at 27.62 kN for a midspan deflection of 34 mm (Fig. 2.3.5h**). The failure occurred for debonding of the FRP sheet.
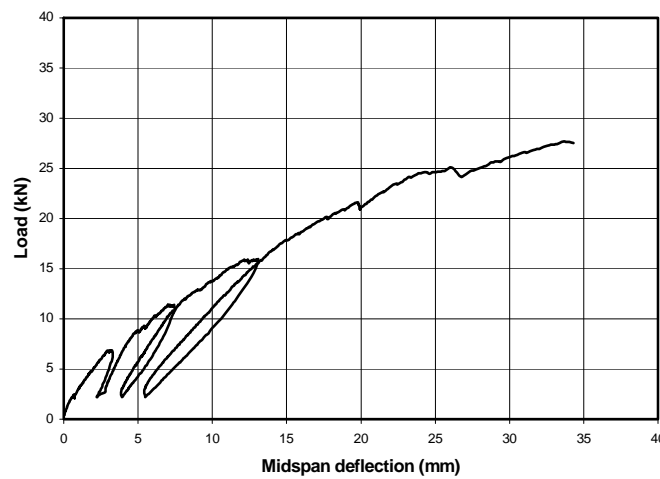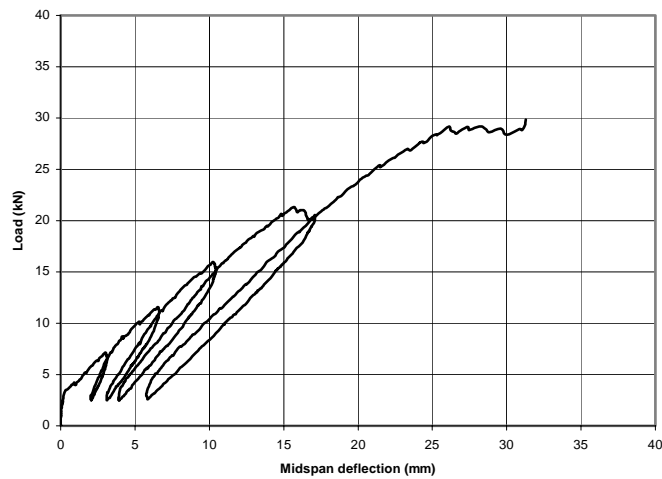

Fig. 2.3.5i* *Load vs. Midspan net deflection-CLG7*

Fig. 2.3.5j* *Wall deflection at the ultimate stage*

WALL CLG7R

This specimen had the same strengthening scheme of CLG7, in order to verify the mechanical behavior of the wall up to failure and to check the strain values on the FRP strip. No differences were observed in terms of crack patterns. The first visible crack was detected at 6.64 kN. The peak load was registered at 29.84 kN corresponding to a midspan deflection of 31 mm. The failure was caused by shear collapse of the masonry, as shown in Fig. 2.3.5l**, namely for reaching the ultimate tensile strength in the masonry members. Strain channels revealed a maximum strain value at mid-height of 1.5%.
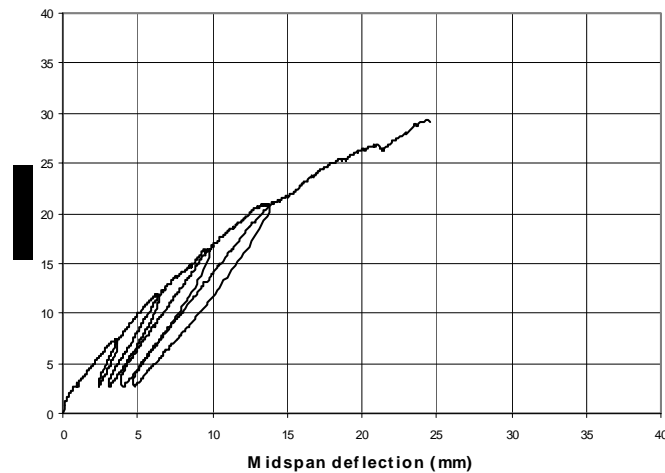

Fig. 2.3.5k** *Load vs. Midspan net deflection Curve, CLG7R*

Fig. 2.3.5l *Shear failure with separation of masonry elements*

WALL CLG9

This wall was strengthened with an amount of FRP corresponding to the balanced condition. No differences were observed in terms of crack opening compared to CLG7 and CLG7R. The peak load was reached at 29.16 kN for a midspan deflection of 25 mm. As shown in Fig. 2.3.5l the wall failed for slipping of the first joint from one of the two edges in the vertical direction. This mode of failure occurred because the fiber reinforcement did not have sufficient bonded area to restrain the shear forces. This was determined to be an undesirable mode of failure.

Fig. 2.3.5k** *Load vs. Midspan net deflection Curve-CLG9*

Fig. 2.3.5l** *Slipping in the vertical direction of the first mortar joint*

WALL CLG12

The most strengthened wall using GFRP laminates exhibited the same undesirable mode of failure observed for CLG9 (Fig. 2.3.5n**). No differences were observed in terms of crack patterns up to failure. The wall revealed a significant stiff behavior during the load cycles, due to the largest amount of FRP reinforcement applied in this case. The peak load was reached at 26 kN for a midspan deflection of 13 mm.
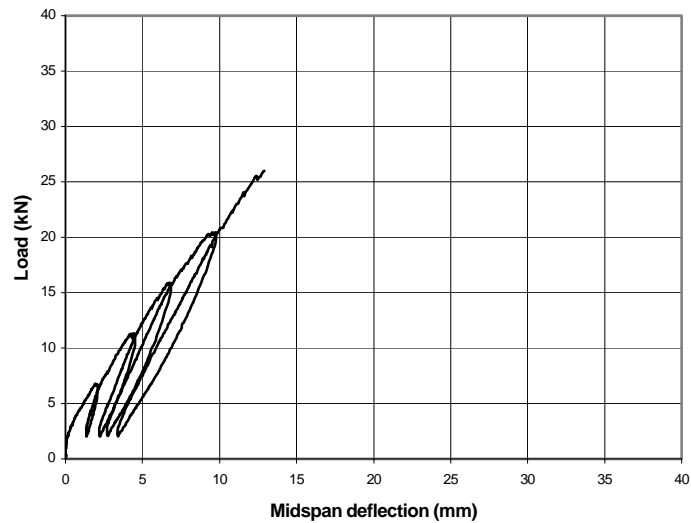
Fig. 2.3.5m* *Load vs. Midspan net deflection Curve,CLG12*

Fig. 2.3.5n* *Slipping of the mortar joint at the border*

2.3.5.4 SERIES CLA

WALL CLA3

The first clay wall reinforced with Aramid fibers was also the less strengthened. A first visible crack was observed at mid-height mortar joint at 4.45 kN, followed, according to CLG3 behavior, by cracking spread to adjacent joints corresponding to a load of 5.78 kN. The peak was registered at 12.02 kN for a midspan deflection of 23 mm. As observed in CLG3, the failure occurred for debonding of the Aramid laminate starting from mid-height and migrating to the edge, as shown in Fig. 2.3.5b***.
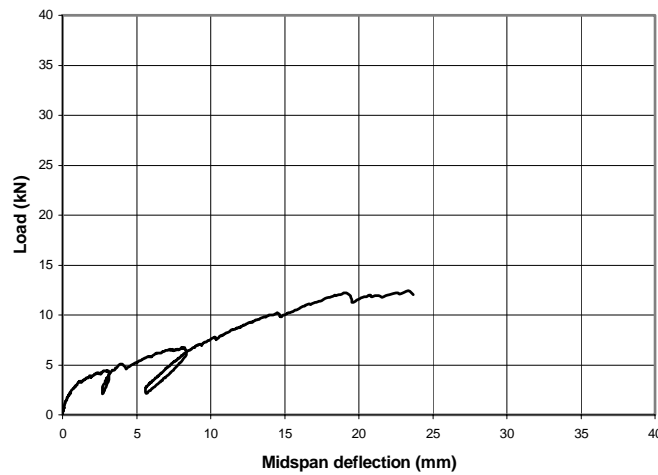
Fig. 2.3.5a*** *Load vs. Midspan net deflection Curve, CLA3*

Fig. 2.3.5b*** *Debonded laminate after failure*

102

WALL CLA5

This wall had a similar strengthening scheme to CLG5, the only difference was in using AFRP instead of GFRP. No differences were observed in terms of crack patterns compared with CLA3. The peak load was reached at 22.04 kN for a midspan deflection of 28mm. It was observed that the wall collapsed at mid-height for rupture of the fibers, as shown in Fig. 2.3.5d***.
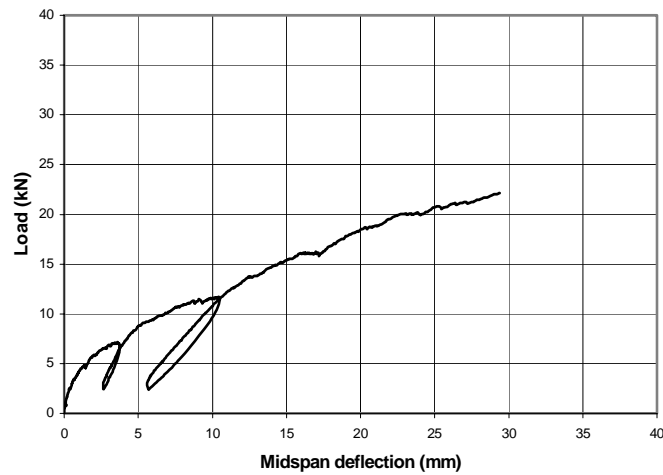
Fig. 2.3.5c*** *Load vs. Midspan net deflection Curve, CLA5*
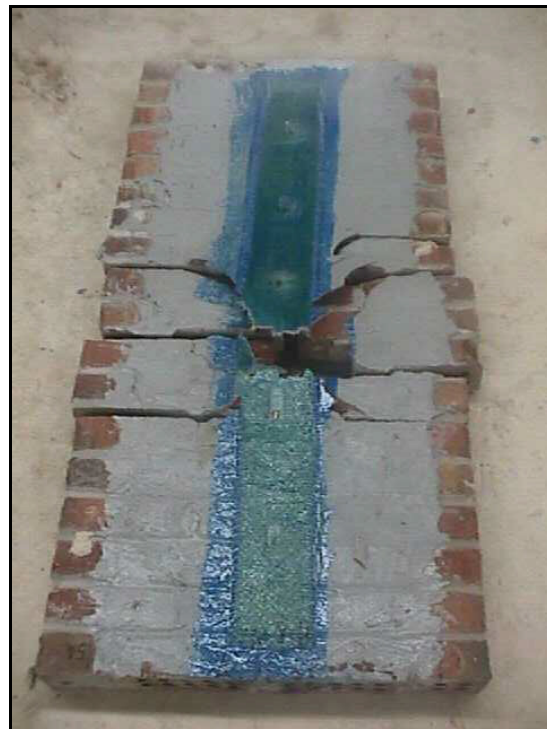
Fig. 2.3.5d*** *Forming of the specimen after failure*

WALL CLA7

This wall was reinforced with a similar strengthening scheme to CLG7. The only difference was the AFRP instead of GFRP. Only one visible crack was observed at a load of 8.9 kN. The maximum load was reached at 25.9 kN for a midspan deflection of 23.5 mm. The failure was caused by the well-known debonding of the laminate moving from mid-height to the edge of the specimen. As shown in Fig. 2.3.5f*** the debris resulted from the collapse revealed a good engagement of the FRP to the masonry surface.
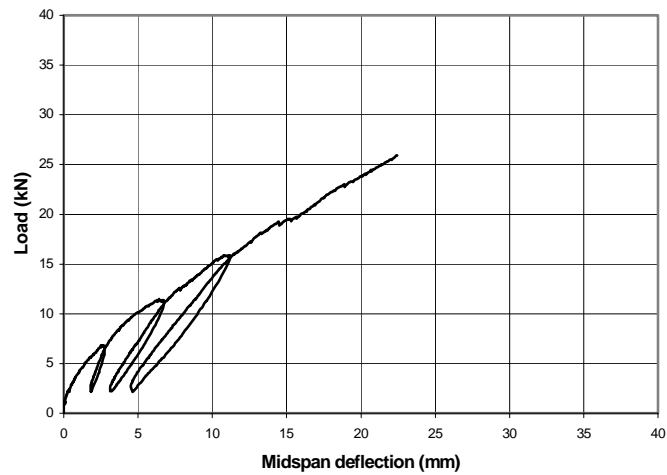
Fig. 2.3.5e*** *Load vs. Midspan net deflection Curve, CLA7*

Fig. 2.3.5f*** *Debonded laminate at the edge after failure*

WALL CLA9

The wall was strengthened with the amount of AFRP corresponding to the balanced condition. A first visible crack was observed at 8 kN, running along the mid-height mortar joint, as detected in most of the clay specimens, followed by another on the top face in the adjacent joint, meaning that high shear stresses were developing. The failure was caused, similarly to CLA5, for complete rupture of the AFRP laminate. No signs of compression in the masonry units were observed up to failure. The peak was reached for a load of 35.65 kN corresponding to a midspan deflection of 36mm.
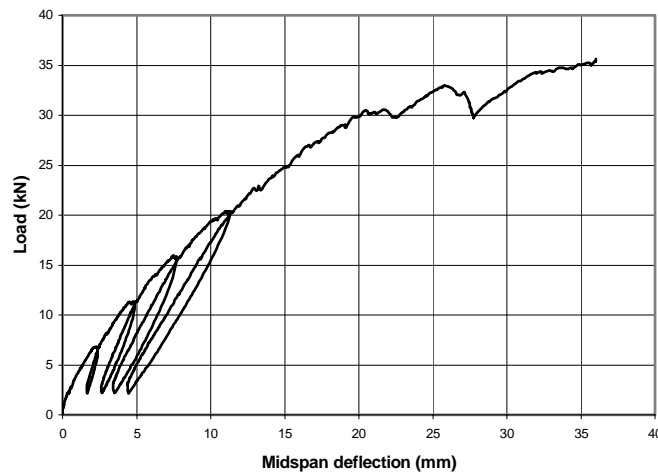
Fig. 2.3.5g*** *Load vs. Midspan net deflection Curve-CLA9*

Fig. 2.3.5h*** *Rupture of the AFRP laminate*

CLA12

This wall had the largest amount of AFRP reinforcement; similarly to CLG12 the specimen exhibited a very stiff behavior during the loading cycles, as shown in Fig. 2.3.5i***. A unique major crack at mid-height was observed at 7.12 kN. The wall collapsed for the high shear stresses developed at the edges and in consequence of this the second mortar joint from the border, as shown in Fig. 2.3.5j***, slipped in the vertical direction, similarly to what registered for CLG9 and CLG12. In order not to have this undesirable mode of failure, when preparing design guidelines, a reasonable limit to the amount of reinforcement has to be assessed.
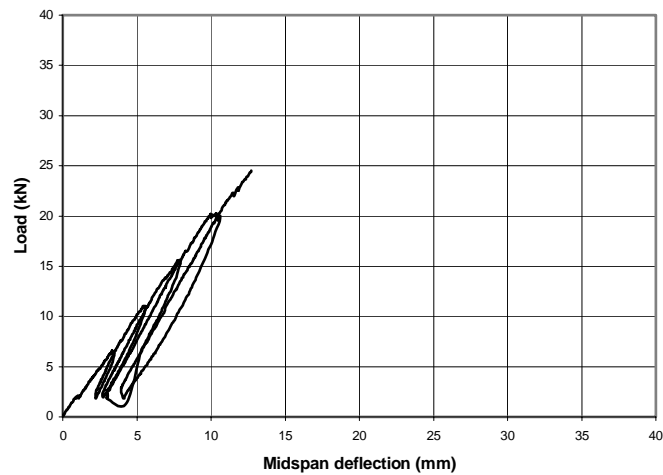
Fig. 2.3.5i*** *Load vs. Midspan net deflection Curve-CLA12*

Fig. 2.3.5j*** *Shear failure at the edge*

106

2.3.6 Test discussion

In Figure 2.3.6a-b the envelopes of load vs. midspan net deflection curves for concrete masonry specimens reinforced with GFRP and AFRP laminates respectively are presented. During the tests a malfunction to the Data Acquisition System occurred and caused the complete loss of the load-deflection trend for the specimen COA12.

Fig. 2.3.6a-b *Envelopes of Series COG (top) and COA (bottom)*

Similarly to the previous figures, the behavior of clay wallettes strengthened with GFRP and AFRP sheets respectively is also shown in Figure 2.3.6c-d.
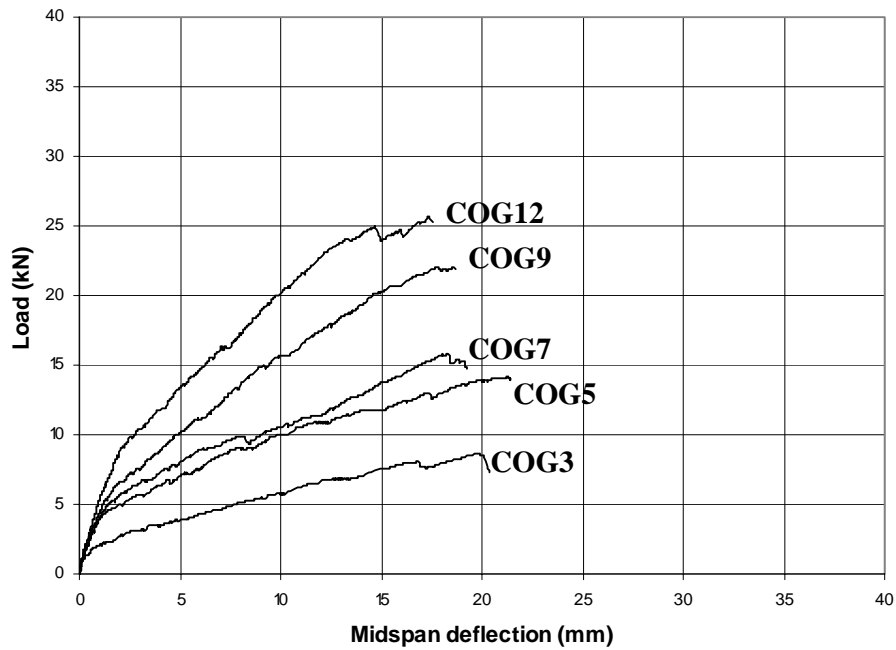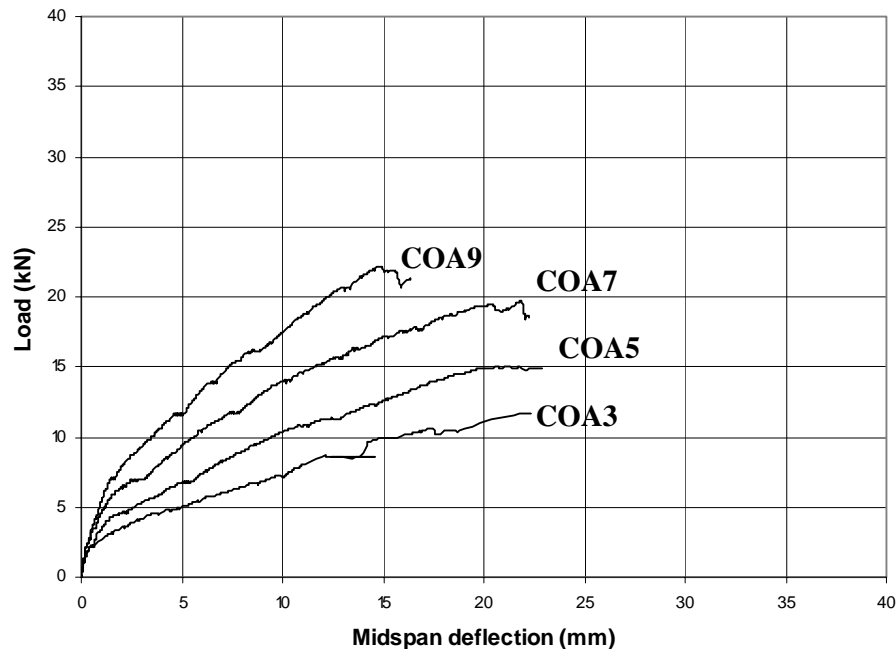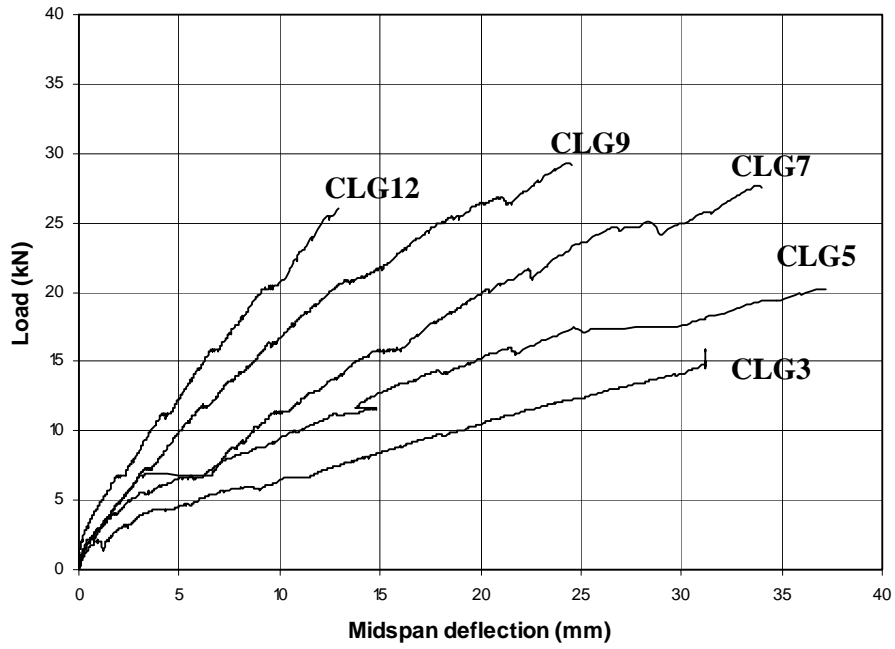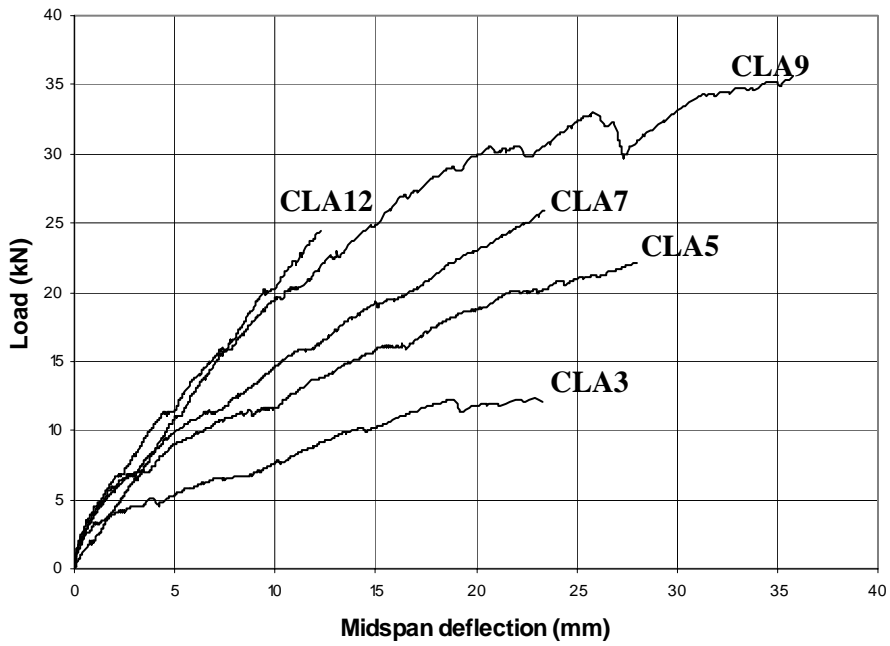

Fig. 2.3.6 c-d *Envelopes of Series CLG (top) and CLA (bottom)*

2.3.6.1 Load-deflection behavior

Comparing the combined load-deflection results for Series COG, Series COA, Series CLG and Series CLG, it is evident that the strength and the stiffness increase dramatically with the introduction of fiber reinforcement to an unreinforced wall. Furthermore it appears that the initial stiffness and final stiffness are primarily functions of the amount of FRP reinforcements. Moreover, the load vs. midspan deflections for all the 26 reinforced specimens, without any visible differences between Glass or Aramid fibers, reveals a definite behavior pattern. The overall shape of response can be divided into two distinct phases: the first phase of the response is a gradual arc that ends at 2.5-5 mm of midspan deflection.

This initial portion of the response curves is a result of the mortar reaching the tensile capacity and cracking. As one joint separates the load is transferred to the next joint and so on until the joints are completely separated in the constant moment region. This was particularly evident for clay specimens with an amount of reinforcement under the balanced condition, therefore with a typical flexural behavior up to failure. In this case, separation means the mortar loses its bond to the adjacent masonry block. Only occasionally did a crack form within the mortar itself.

The second portion of the curve is simulated by a straight line, approximately. This part of the curve represents the contribution of the fiber reinforcement to the behavior of the specimen. At this stage, the mid-height joint and ,in most of the specimens, the adjacent bed joints within the constant moment region are partially separated. For the rest of the test the crack widths in the mortar joints simply increases as the wall experiences more deflection. Because the joints have already lost their ability to resist tensile forces, and therefore their ability to contribute to the wall stiffness, they no longer have an effect on the load-deflection behavior of the wall. It should be noted that masonry is a material that has a significant amount of "built-in" variability. While direct comparisons are made between the load-deflection curves they should be understood to indicate ranges of behavior rather than exact values. However, the grouping of each series of tests suggests that a comparison of the overall behavior can be made.

Because of the different stiffness of each fiber type, different types of masonry units, and the presence of variables such as handwork for the construction of the masonry specimens and discrepancy in the effective widths of the FRP reinforcement

and different amount of saturant involved during the installation procedure, which can dramatically modify the mechanical properties of the composites, it should be introduced a special factor, namely the reinforcement ratio ω_f, expressed as $(\rho_f\, E_f)/\, (f'_m\, (h/t))$, in which the presence of a normalized stiffness is combined with the mechanical properties of the masonry. The introduction of the slenderness ratio (h/t) is justified since this parameter is identified as one of the most important in the out-of-plane behavior of masonry walls. The concept will be widely expressed in the next sections.

2.3.6.2 Failure modes

Out of the 26 tests three general modes of failure were observed:

(1) <u>Debonding of the FRP laminates</u>

(2) <u>Tension failure of the FRP reinforcement</u>

(3) <u>Shear failure in the masonry units</u>

Fig. 2.3.6.2a and Fig. 2.3.6.2b show typical FRP sheet tensile behavior under loading for specimens COG3R and COG5R respectively. In both the wallettes the failure was caused by debonding of the FRP laminate, starting from the mid-height, in which due to the configuration of the test set up the highest bond stresses between FRP and masonry surface were developed, and then spread the middle brick course to one of the edges. This visual observation may be validate by analyzing the strain development of the FRP strips presented in Fig. 2.3.6.2a and Fig. 2.3.6.2b. Assuming that the load is correctly applied, at the initial stages the strain distribution can be assumed symmetric to the transverse axis of the masonry wall, meaning that masonry surface provides a good engagement to the FRP laminate along the entire length of the strip. Once the delamination starts at mid-height, corresponding to the so-called peeling load, the effective bonded length of the laminate aims to move from the middle of the wall to the edge. As the strip is completely detached at the mid-height courses, the specimen can no longer carry the applied load and the failure occurs.

In Appendix A a detailed characterization of FRP laminates bonded to masonry surfaces is provided and an analytical procedure to calculate the proper bonded length is developed. Experimental observations suggest that surface preparation of the masonry members plays a fundamental role in determining which is the mode of failure of concrete or clay walls strengthened with externally bonded FRP overlays.
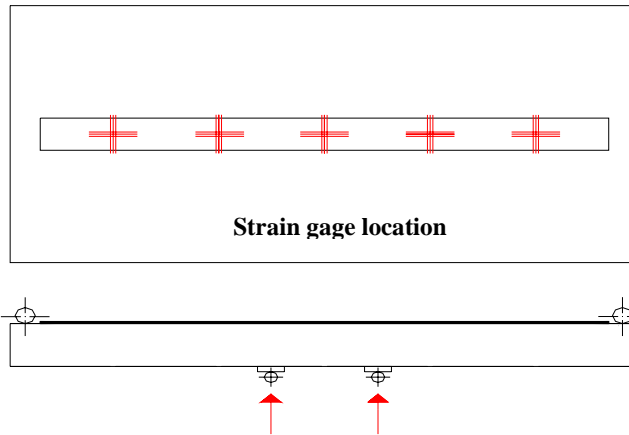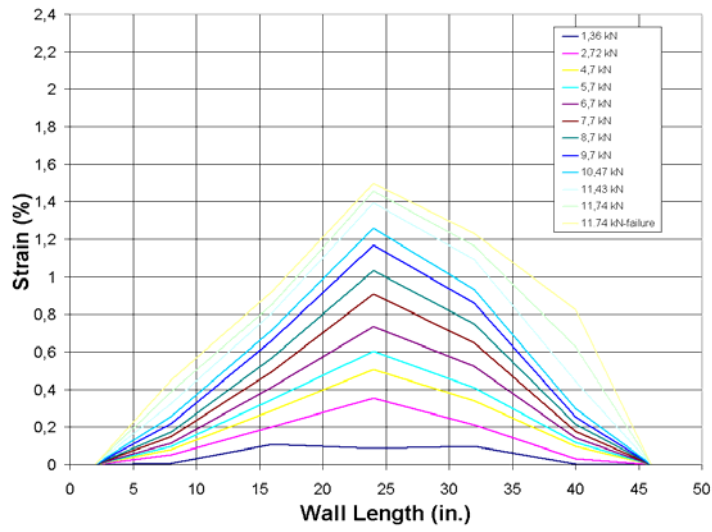
Fig. 2.3.6a *Tensile behavior of FRP reinforcement-COG3R*
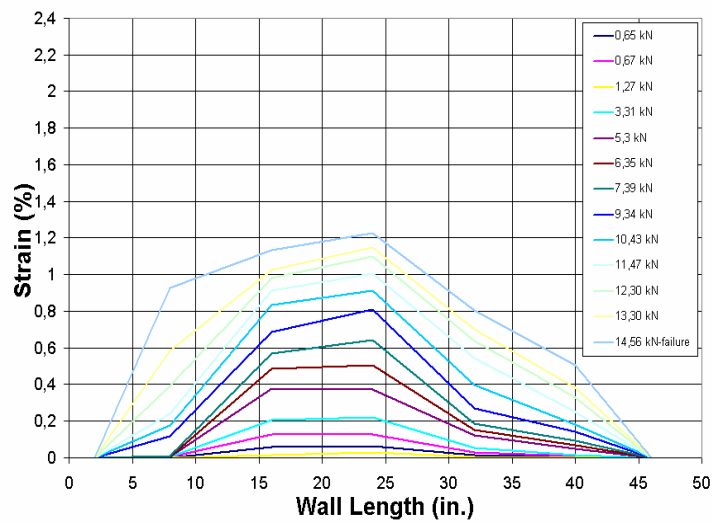
Fig. 2.3.6.1b *Tensile behavior of FRP reinforcement –COG5R*

In particular variables such as the amount of primer and putty applied to the masonry members prior to FRP application, porosity of the masonry units as well as quantity of saturant combined with fibers should be investigated in further research and correlated with the mechanical performance of the walls.

Fig. 2.3.6.1c presents the strain development along the FRP strip of CLG3R, which failed for rupture of the laminate at the final stage. Differently from COG3R and COG5R, the strain distribution exhibited a perfect symmetrical behavior up to failure, validating the experimental observations on the debonding phenomenon.
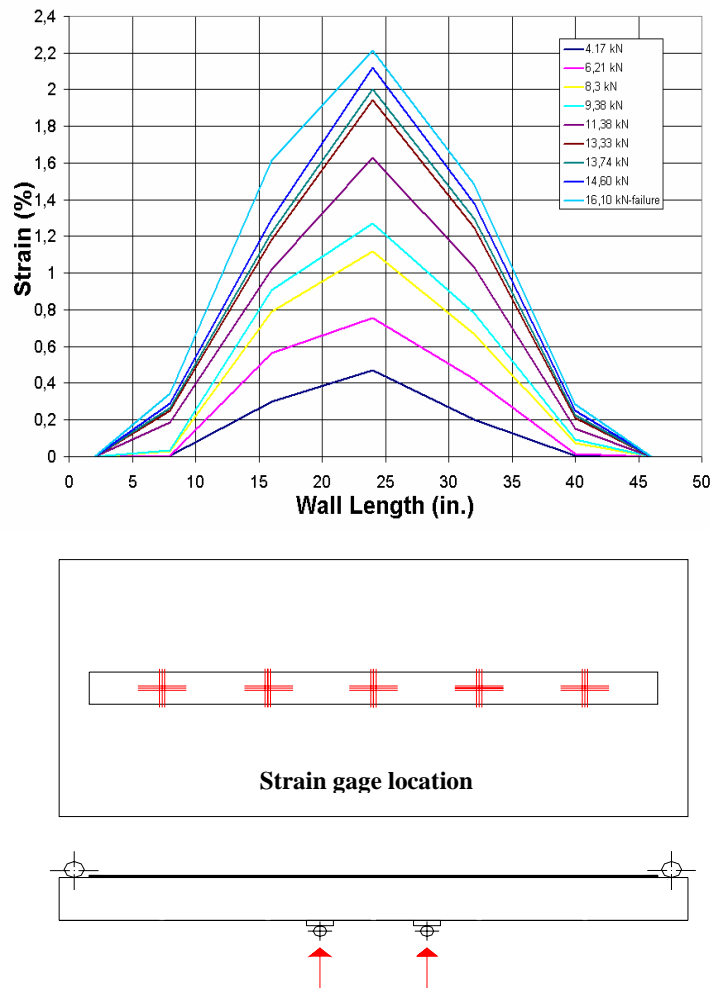
Fig. 2.3.6.1c *Tensile behavior of FRP reinforcement-CLG3R*

Similar strain distributions were registered for all the specimens failed by tension failure, namely CLA5, CLA7, CLG3R, CLG5R.

2.3.6.3 Data summary

All the experimental data are summarized in Table 2.3.6.3. Columns 2,3,4 refer to the masonry engineering properties, whereas columns 5,6,7,8,9 refer to the FRP specifications. Last columns provide analyzed data in order to give a complete response of the research. It's important to note that before testing, the FRP mechanical properties used to calculate the theoretical flexural capacity of the walls, were provided by the manufacturers. Only in a second moment the theoretical moments were calculated by means of the FRP specifications come out from the material characterization (see Appendix A).

Table 2.3.6.3 *Summary of the experimental research*

Wall	f'_m (ksi)	h/t	t_m (in)	t_f (in)	w_f (in)	ρ_f	E_f (ksi)	$\rho_f E_f$	$(\rho_f E_f)/(f'_m (h/t))$	$M_{exp.}$ (ft-kips)	$M_{the.}$ (ft-kips)	$M_{exp.}/M_{the.}$	$\varepsilon_{eff}/\varepsilon_{ult}$	Failure
COG3	1,5	12,3	3,75	0,014	3	0,00047	12056	5,6	0,31	1,48	3,10	0,48	NA	Delamination
COG3R	1,5	12,3	3,75	0,014	3	0,00047	12056	5,6	0,31	2,08	3,10	0,69	0,80	Delamination
COG5	1,5	12,3	3,75	0,014	5	0,00078	12056	9,4	0,51	2,45	5,20	0,47	NA	Delamination
COG5R	1,5	12,3	3,75	0,014	5	0,00078	12056	9,4	0,51	2,61	5,20	0,50	0,68	Delamination
COG5A	1,5	12,3	3,75	0,014	5	0,00078	12056	9,4	0,51	3,49	5,20	0,67	0,53	Delamination
COG7	1,5	12,3	3,75	0,014	7	0,00109	12056	13,1	0,71	2,77	6,80	0,41	NA	Delamination
COG9	1,5	12,3	3,75	0,014	9	0,00140	12056	16,9	0,92	3,88	7,60	0,51	NA	Shear
COG12	1,5	12,3	3,75	0,014	12	0,00187	12056	22,5	1,22	4,40	8,60	0,51	NA	Shear
COA3	1,5	12,3	3,75	0,011	3	0,00037	17570	6,4	0,35	1,87	2,70	0,69	NA	Delamination
COA5	1,5	12,3	3,75	0,011	5	0,00061	17570	10,7	0,58	2,61	4,50	0,58	NA	Delamination
COA7	1,5	12,3	3,75	0,011	7	0,00086	17570	15,0	0,82	3,38	6,30	0,54	NA	Shear
COA9	1,5	12,3	3,75	0,011	9	0,00110	17570	19,3	1,05	3,82	8,00	0,48	NA	Shear
COA12	1,5	12,3	3,75	0,011	12	0,00147	17570	25,8	1,40	4,67	9,10	0,51	NA	Shear
CLG3	2,5	12,3	3,75	0,014	3	0,00047	12056	5,6	0,18	2,85	4,80	0,59	NA	Delamination
CLG3R	2,5	12,3	3,75	0,014	3	0,00047	12056	5,6	0,18	3,88	4,80	0,81	1,23	Rupture
CLG5	2,5	12,3	3,75	0,014	5	0,00078	12056	9,4	0,31	3,61	6,10	0,59	NA	Delamination
CLG5R	2,5	12,3	3,75	0,014	5	0,00078	12056	9,4	0,31	5,69	6,10	0,93	1,09	Rupture
CLG7	2,5	12,3	3,75	0,014	7	0,00109	12056	13,1	0,43	4,84	7,00	0,69	NA	Delamination
CLG7R	2,5	12,3	3,75	0,014	7	0,00109	12056	13,1	0,43	6,80	7,00	0,97	0,70	Shear
CLG9	2,5	12,3	3,75	0,014	9	0,00140	12056	16,9	0,55	5,10	7,80	0,65	NA	Shear
CLG12	2,5	12,3	3,75	0,014	12	0,00187	12056	22,5	0,73	4,54	8,80	0,52	NA	Shear
CLA3	2,5	12,3	3,75	0,011	3	0,00037	17570	6,4	0,21	2,17	2,70	0,80	NA	Delamination
CLA5	2,5	12,3	3,75	0,011	5	0,00061	17570	10,7	0,35	3,86	4,50	0,86	NA	Rupture
CLA7	2,5	12,3	3,75	0,011	7	0,00086	17570	15,0	0,49	4,52	6,20	0,73	NA	Delamination
CLA9	2,5	12,3	3,75	0,011	9	0,00110	17570	19,3	0,63	7,80	8,30	0,94	NA	Rupture
CLA12	2,5	12,3	3,75	0,011	12	0,00147	17570	25,8	0,84	4,04	9,30	0,43	NA	Shear

2.3.7 Analytical model

A simplified analytical method was implemented to predict the ultimate flexural strength of the fiber-reinforced masonry wall systems. Theoretical flexural capacities of the strengthened walls were estimated based on the assumption that no premature failure was to be observed. This means that either rupture of the laminate or crushing of masonry would control the wall behavior. According to the flexural analysis of RC members, a parabolic distribution was used in the computation of the flexural capacity of the strengthened masonry. Thus the method is based on the following assumptions:

- Linear strain distribution through the full depth of the wall

- Small deformations

- Tensile strength of masonry neglected

- No interfacial slip between the fiber-reinforced composites and the masonry wall

The stress-strain relationship of the fiber-reinforced composites systems is generally considered to be linear elastic up to failure, while the stress-strain behavior of the masonry is modeled based on the idealized uniform stress block, derived as shown in Fig. 2.3.7a. According to the diagram presented below, the coefficients α and β_1 should be calculated using the following equations.
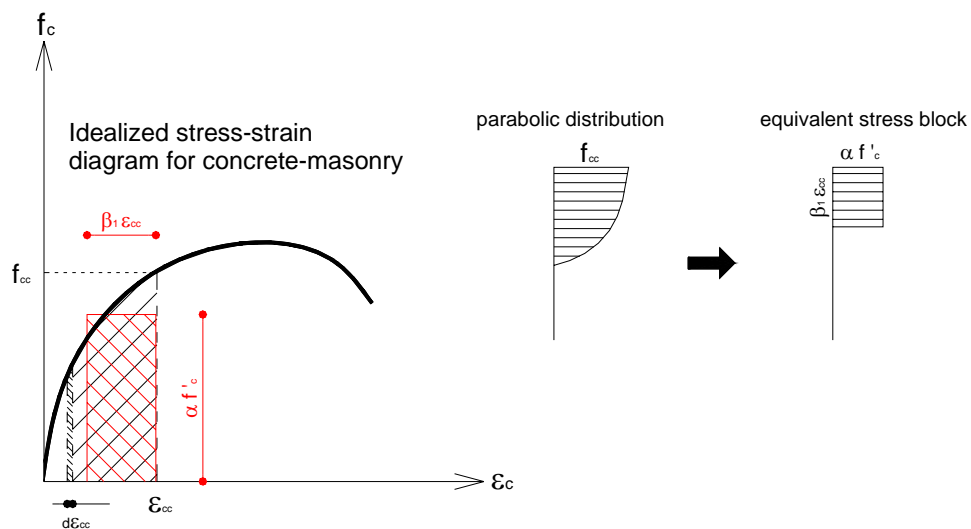

Fig. 2.3.7a *Stress block derivation*

In order to satisfy the force equilibrium:

$$\beta_1\,\varepsilon_{cc}\,\alpha\,f'_c = \int_0^{\varepsilon_{cc}} f_c \cdot d\varepsilon_{cc} \qquad (2.3.7.1)$$

where:

f'_c = compressive strength of masonry

ε_{cc} = maximum strain value in the masonry compressed face shell

For the equilibrium of the moments about O:

$$\beta_1\,\varepsilon_{cc}\,\alpha\,f'_c\,(\varepsilon_{cc} - \tfrac{1}{2}\,\beta_1\,\varepsilon_{cc}) = \int_0^{\varepsilon_{cc}} f_c \cdot \varepsilon_{cc} \cdot d\varepsilon_c \qquad (2.3.7.2)$$

The relationship between f_c and f'_c can be expressed as:

$$f_c = f'_c\left[2\left(\frac{\varepsilon_c}{\varepsilon'_c}\right)-\left(\frac{\varepsilon_c}{\varepsilon'_c}\right)^2\right] \qquad (2.3.7.3)$$

From (2.3.7.1):

$$\beta_1\,\alpha\,\varepsilon_{cc}\,f'_c = f'_c\left[\frac{\varepsilon_{cc}^2}{\varepsilon'_c} - \frac{1}{3}\frac{\varepsilon_{cc}^3}{\varepsilon'^2_c}\right] \qquad (2.3.7.4)$$

obtaining

$$\alpha\,\beta_1 = \frac{\varepsilon_{cc}}{\varepsilon'_c} - \frac{1}{3}\left(\frac{\varepsilon_{cc}}{\varepsilon'_c}\right)^2 \qquad (2.3.7.5)$$

From (2.3.7.2):

$$\alpha\,\beta_1\,(1-\tfrac{1}{2}\,\beta_1)\,f'_c\,\varepsilon_{cc}^2 = f'_c\left[\frac{2}{3}\frac{\varepsilon'^3_{cc}}{\varepsilon'_c} - \frac{1}{4}\frac{\varepsilon_{cc}^4}{\varepsilon'^2_c}\right] \qquad (2.3.7.6)$$

obtaining

$$\alpha\,\beta_1\,(1-\tfrac{1}{2}\,\beta_1) = \frac{2}{3}\frac{\varepsilon_{cc}}{\varepsilon'_c} - \frac{1}{4}\left(\frac{\varepsilon_{cc}}{\varepsilon'_c}\right)^2 \qquad (2.3.7.7)$$

The strain and stress distributions in a masonry cross-section strengthened with FRP laminates are illustrated in Fig. 2.3.7b.
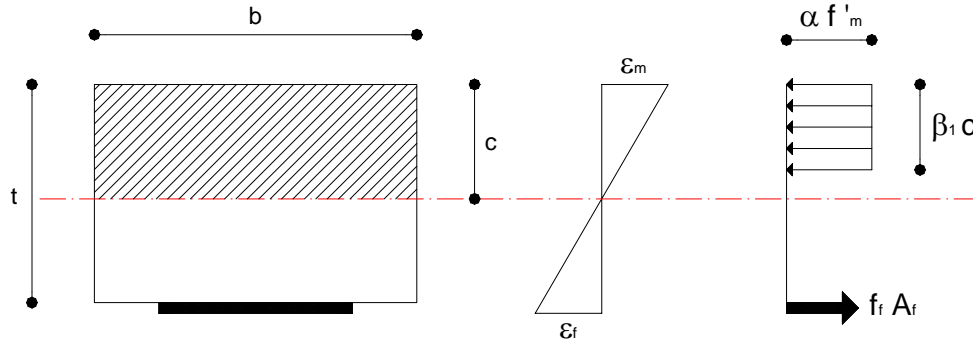

Fig. 2.3.7b *Strain and stress distribution*

In the case of masonry members, according to the previous equations:

$f'_c \equiv f'_m$

$\varepsilon_{cc} \equiv \varepsilon_m$

In order to satisfy the internal force equilibrium:

$$(\alpha f'_m)(\beta_1 c) b = A_f f_f \tag{2.3.7.8}$$

$$f_f = E_f \varepsilon_f \tag{2.3.7.9}$$

The effective strain in the reinforcement ε_f and the strain in the masonry are related by:

$$\frac{\varepsilon_m}{c} = \frac{\varepsilon_f}{t-c} \tag{2.3.7.10}$$

The following assumptions provided by MSJC (1999) are considered:

- The maximum usable strain ε_{mu} is assumed to be 0.0035 in./in. for clay masonry and 0.0025 in./in. for concrete masonry.
- The tensile strength of masonry is neglected

116

Using the previous relationships, the depth of the neutral axis 'c', the theoretical flexural capacity can be estimated by:

$$M_{theoretical} = A_f f_f \left(t - \frac{\beta_1 c}{2} \right)$$ (2.3.7.11)

In Table 2.3.7a theoretical and experimental moments of the 26 masonry wallettes subjected to out-of-plane loading are shown.

Table 2.3.7a *Comparison between theoretical and experimental moments*

Wall	Mexp. (ft-kips)	Mthe. (ft-kips)	Mexp./ Mthe.	Failure
COG3	1,48	3,1	0,48	Delamination
COG3R	2,08	3,1	0,69	Delamination
COG5	2,45	5,2	0,47	Delamination
COG5R	2,61	5,2	0,5	Delamination
COG5A	3,49	5,2	0,67	Delamination
COG7	2,77	6,8	0,41	Delamination
COG9	3,88	7,6	0,51	Shear
COG12	4,4	8,6	0,51	Shear
COA3	1,87	2,7	0,69	Delamination
COA5	2,61	4,5	0,58	Delamination
COA7	3,38	6,3	0,54	Shear
COA9	3,82	8	0,48	Shear
COA12	4,67	9,1	0,51	Shear
CLG3	2,85	4,8	0,59	Delamination
CLG3R	3,88	4,8	0,81	Rupture
CLG5	3,61	6,1	0,59	Delamination
CLG5R	5,69	6,1	0,93	Rupture
CLG7	4,84	7	0,69	Delamination
CLG7R	6,8	7	0,97	Shear
CLG9	5,1	7,8	0,65	Shear
CLG12	4,54	8,8	0,52	Shear
CLA3	2,17	2,7	0,8	Delamination
CLA5	3,86	4,5	0,86	Rupture
CLA7	4,52	6,2	0,73	Delamination
CLA9	7,8	8,3	0,94	Rupture
CLA12	4,04	9,3	0,43	Shear

Based on the $M_{experimental}$-$M_{theoretical}$ ratios observed in Table 2.3.7a, it can be considered that the actual ultimate capacity of the strengthened walls can be calculated from a

cracked section under elastic stresses, where the two materials behave elastically, or very nearly so in the case of masonry (see Fig. 2.3.7c).
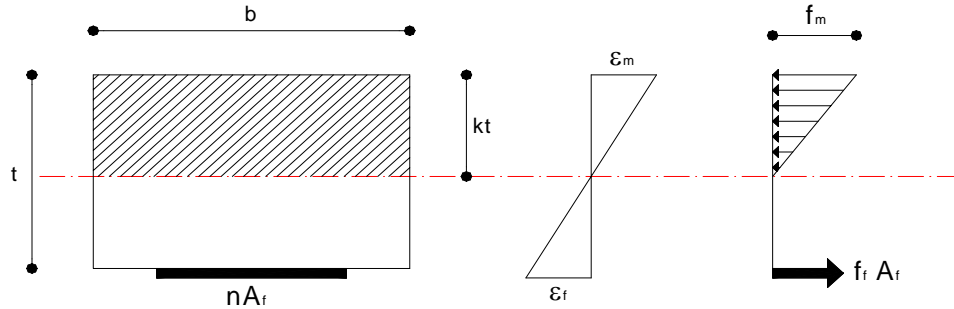

Fig. 2.3.7c *Strain and stress distribution in cracked transformed section*

Thus, the depth of the neutral axis and the flexural capacity can be estimated from the equilibrium of forces:

$$\frac{1}{2}\ (\ f_m\ k\ t)\ b =\ A_f\ f_f \tag{2.3.7.12}$$

and the following relationships:

$$f_m = \varepsilon_m\ E_m \tag{2.3.7.13}$$

$$f_{fe} = \varepsilon_f\ E_{fe} \tag{2.3.7.14}$$

$$n = \frac{E_{fe}}{E_m} \tag{2.3.7.15}$$

where:

f_{fe}= effective tensile strength in the FRP laminate

E_{fe}= effective modulus of elasticity in the FRP laminate

Thus, the coefficient 'k' is obtained from the following relationship:

$$k = \sqrt{(n\rho_f)^2 + 2(n\rho_f)}\ -\ n\rho_f \tag{2.3.7.16}$$

Finally the flexural capacity is estimated as:

$$M_n = A_f\ f_f\ \left(t - \frac{kt}{3}\right) \tag{2.3.7.17}$$

Validating correlations between experimental and theoretical values are presented in Appendix C.

118

3.
IN-PLANE BEHAVIOR OF MASONRY PANELS REINFORCED WITH FRP RODS AND LAMINATES

3.1 <u>Problem statement and general objectives</u>

Masonry structures have been constructed since the earliest days of civilization. They still constitute a significant percentage of the current building stock. Many of these buildings are located in seismic regions and were built before the establishment of any building-code requirements for earthquake-resistant construction. These structures are usually constructed from concrete blocks or clay bricks. The block or brick units are tied together by a cement mortar; little or no steel is used in these structures. In fact, it has been reported that the use of steel as reinforcement for masonry structures was introduced in the United States in the 1930s to the 1940s (*Amrhein* 1992). While properly reinforced masonry structures can and do perform well during earthquakes, the lack of reinforcement in the large inventory of existing masonry buildings is a major concern of the profession.

The in-plane (shear) resistance in load-bearing unreinforced masonry (URM) walls is provided by the shear bond strength of the mortar and the friction shear due to the vertical load. The aging and often deteriorated mortar joints have little shear capacity. Under severe earthquake loads the shear capacity of the mortar in exceeded, resulting in failure of the wall. Regarding those walls which go under the name of *infill panels,* it is recognized that the behavior of these panels would be different in presence of a surrounding concrete frame. Masonry walls are commonly used as interior partitions or exterior walls bound by steel or concrete frames conforming the building envelope. For the latter case , depending on the design considerations, the infill walls may or not resist lateral and vertical loads. In order to simplify the design, the potential interaction between the infill walls and the structural frame has been ordinarily ignored. Ignoring the contribution of the masonry infill walls does not always represents a conservative design. The presence of infill walls can lead to stiffening their frames and thereby cause a redistribution of lateral loads in the building plan. The increase in stiffness of the frame can attract higher lateral loads than those expected according to the design. This may cause cracking of the wall and overstressing of the frame. Previous investigations (*Sabnis* 1976, *Drysdale et al.* 1979-1994) have demonstrated that the

composite action between the masonry infill and the surrounding frame is depending on the level of the in-plane load, bonding or anchorage at the interfaces, and geometry and stiffness of both the masonry infill and the structural frame. At a very low level of in-plane loading, a full composite action between the infill wall and the frame is observed. Once the load increases, the infill wall and the frame are no longer in contact, except in surrounding areas of the two corners where compression stresses are transmitted from the frame to the masonry which lead to the formation of a diagonal compression strut (see Fig. 3.1a).
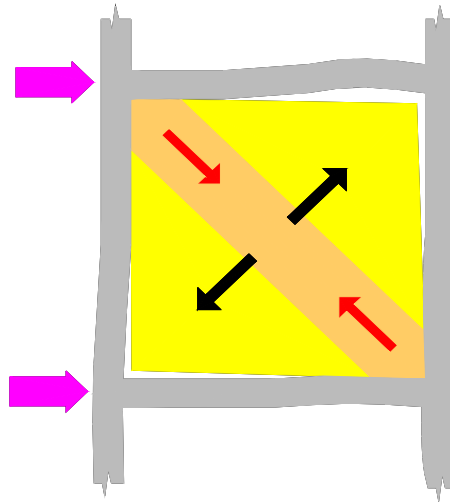

Fig. 3.1a *Diagonal Strut*

The resulting structural system is usually analyzed as a truss. The stiffness of the infill starts decreasing once cracking is developed. At a stage when higher in-plane loads are present, the contribution of the compressive strut begins to reduce as further cracking is developed. Also, the gap separating masonry from frame is increased, which eventually leads to shear failure (*diagonal tension*) of masonry as observed in Fig. 3.1b and flexure (yielding) failure of the columns. Depending on the compressive strength of the masonry, the units in the corner areas may be crushed prior to developing diagonal cracking. Alternatively to the diagonal tension failure, a shear failure along a horizontal joint can be observed at a lower load level as compared to the load causing the latter mentioned failure. The resulting shear crack divides the infill in two parts, where the behavior is controlled by either the flexural or shear capacity of the columns. This failure mechanism is commonly known as *Knee Brace or Joint-Slip* (see Fig. 3.1c).

120

Fig. 3.1b *Diagonal tension failure (Turkey 1999)*
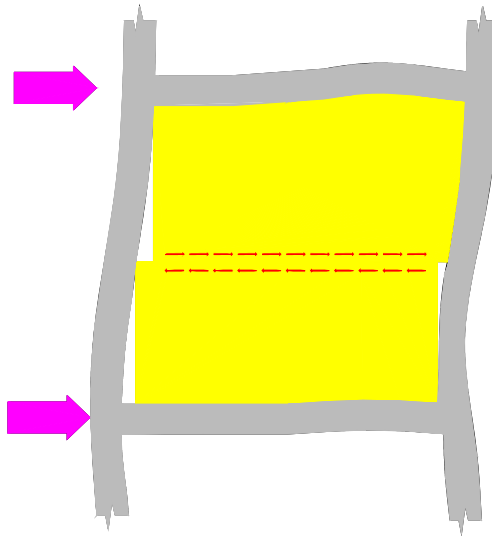
Fig. 3.1c *Joint-slip failure*

Single-story buildings, such as schools and shopping centers, are very common in the United States. In these buildings, vertical and horizontal loads are resisted by shear walls. These unreinforced or lightly reinforced walls are prone to failing during an earthquake. Their capacity to withstand horizontal loads is limited by the strength of the masonry units and the mortar in the bed joints. At low axial loads, two modes of

failure may be observed. One is *sliding* of the wall along the bed joints (Fig. 3.1d); the other is *rocking* on a horizontal crack at the wall bottom (see Fig. 3.1e). The overall stability of the building is not compromised as long as the deformation are small. If the masonry wall bears high axial loads, the bed joint friction is increased and therefore sliding or rocking will not be observed. Instead, diagonal shear crack will be developed.
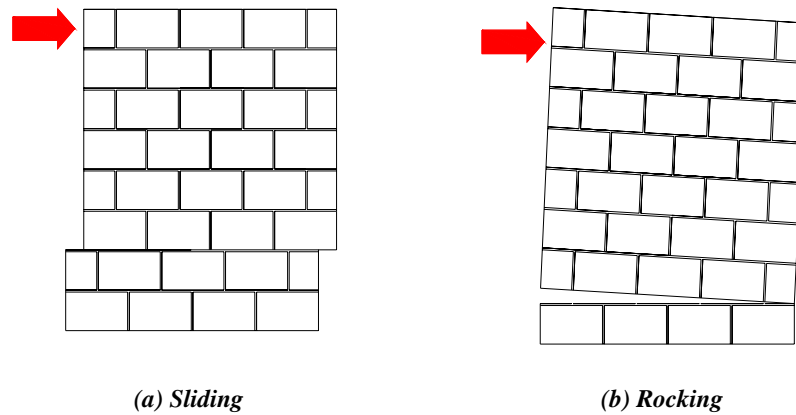
(a) Sliding   *(b) Rocking*

Fig. 3.1d *Potential failures in walls with no axial load: Sliding (a) and Rocking (b)*

Lenczer (1972) has reported that the shear strength of a bearing wall, in the case of a sliding failure mode, can be calculated as

$$\tau = \tau_o + \mu\sigma_n \tag{3.1}$$

where:

τ= shear stress at the shear bond failure

τ_o= shear bond strength at zero normal stress due to the adhesive strength of mortar

μ= coefficient of friction between brick and mortar

σ_n= normal stress

Controlling shear failure is a key issue in masonry strengthening because after the wall is cracked due to in-plane loads, it can easily collapse due to movement perpendicular to the plane and jeopardize human lives. This kind of behavior has been evident from post-earthquake observations. In this context, fiber reinforced polymer (FRP) composites can provide viable solutions for the strengthening of URM walls subjected to stresses caused by wind or earthquake loads. The use of FRP materials offers important advantages in addition to their mechanical characteristics and ease of

122

installation. To name some, the disturbance of the occupants of the facility is minimized and there is minimal loss of usable space during strengthening. Furthermore, from the structural point of view, the dynamic properties of the structure remain unchanged because there is no addition of weight and stiffness. Any alteration to the aforementioned properties would result in an increase in seismic forces on the walls themselves.

This section describes an experimental program on shear strengthening of URM panels. FRP materials in the form of GFRP (Glass) laminates and GFRP bars were used to strengthen the walls. In addition, to the use of FRP laminates, a novel technique denominated **FRP Structural Repointing** is investigated. This technique consists in placing FRP bars in the mortar joints (*Tumialan et al.,* 2000). Repointing is a traditional retrofitting technique commonly used in the masonry industry, which consists in replacing missing mortar in the joints (See Section 1.2.2). The term "structural" is added because the proposed method does not merely consist of filling the joints as the traditional technique, but allows for restoring the integrity and/or upgrading the shear and/or flexural capacity of walls. Masonry panels made of concrete blocks and clay bricks reinforced through the employment of different strengthening configurations are investigated, in order to come up with suitable design guidelines.
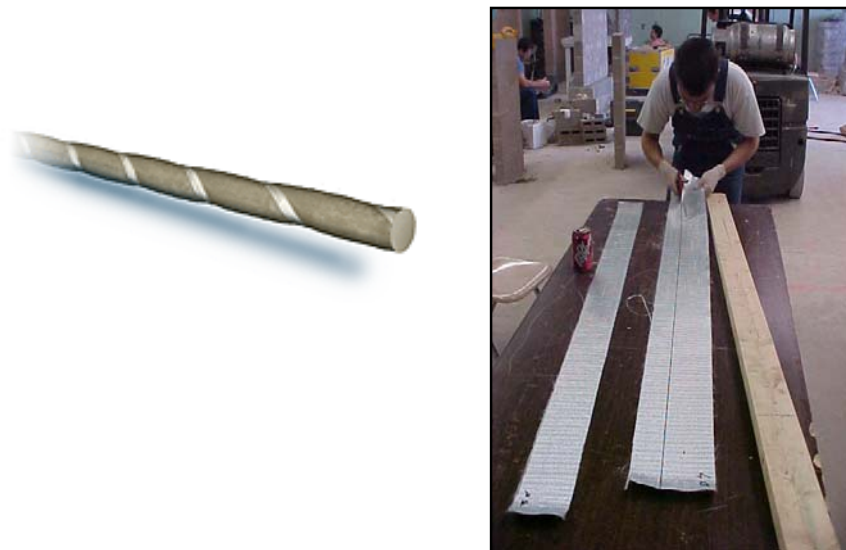

**Fig. 3.1e** *GFRP rod (left) and laminates (right)*

3.2 **Previous results**

Schwegler (1995) investigated strengthening methods for masonry shear walls. The objectives of this study were to increase the system ductility, generate uniform crack distribution, and increase the load carrying capacity of the system. The dimensions of the walls were 12 ft.(3.66 m) x 6ft.(1.83 m) x 8 in.(0.2 m) CFRP sheets were bonded diagonally to the masonry walls as shown in Figure 3.2a, and mechanically anchored to the adjoining slabs.
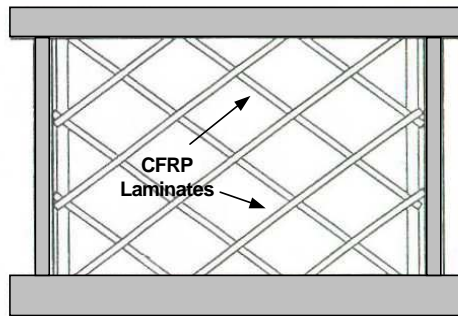

Fig. 3.2a *Strengthened wall (Schwegler)*
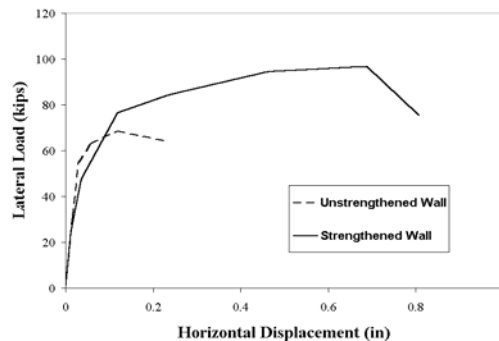
Fig. 3.2b *Test results (Schwegler)*

As observed in Figure 3.2b, the test results showed that the strengthened wall exhibited elastic behavior up to 70% of the maximum shear force. It was also observed that the carrying capacity decreased as a consequence of massive crack formation in the masonry. By comparing walls strengthened in one side and two sides, it was observed that if only one side of the masonry wall is strengthened, the capacity could be halved. In addition, the eccentricities caused by this strengthening scheme had a minimum effect on the shear carrying capacity. In all the strengthened walls fine cracks were observed perpendicular to the sheets. The crack separation was constant and the crack widths remained small.

Laursen et.al. (1995) studied the shear behavior of masonry walls strengthened with CFRP laminates. The walls were built with concrete blocks; the walls were fully grouted. The overall dimensions were 72 in. by 72 in. (1.82x1.82 m). The walls were internally reinforced; horizontally with a low shear reinforcement ratio of 0.14%, and vertically with a ratio of 0.54%. The "original" wall failed in shear. The specimen was re-tested after being repaired. The repair was performed by closing the large diagonal shear cracks with epoxy filler and epoxy injection, and repairing the crushed compression toes with epoxy mortar. The "repaired" wall was then strengthened with CFRP laminates, which covered the two sides of the wall; an additional layer was applied in the end regions as confinement. The amount of strengthening in the "retrofitted" wall was similar to the previous wall but applied to only one side of the wall.
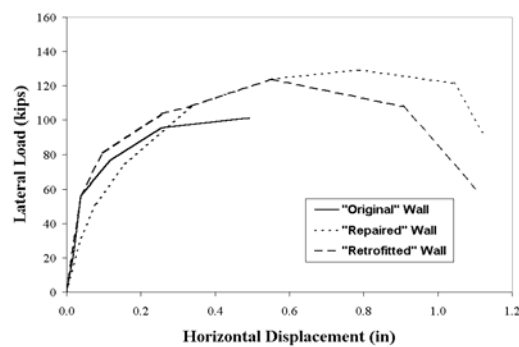
Fig. 3.2c *Test results (Laursen)*

It was observed that the presence of the FRP laminates improved the wall performance by changing the failure from a shear-controlled failure to a flexural-controlled failure. This change caused an increase in the capability of deformation of approximately 100% by preventing a brittle failure mode. The test results of this wall, shown in Figure 3.2c, also proved that even though the wall failed in shear, it could be repaired to restore the initial stiffness and strength compared to the standard of the "original" and "retrofitted" walls.

Tinazzi et al. (2000) introduced the term Structural Repointing and investigated the use of FRP rods to increase the shear capacity of masonry panels made of clay bricks. This technology consisted of placing # 2 GFRP rods in grooved horizontal joints as shown in Figure 3.2d. The rods were embedded in an epoxy-based paste. The nominal dimensions of the panels were 3.5x24x24 in. (0.09x0.61x0.61 m). The failure of unreinforced panels consisted of the joint sliding along the compressed

125

diagonal. In contrast, strengthened with FRP rods at each joint, showed increases in capacity of about 45% higher as compared to the unreinforced wall. The failure mode changed since joint sliding was prevented. The mechanism of failure indicated the sliding of the masonry-paste interface.


Fig. 3.2d *GFRP rods in mortar bed joints (Tinazzi)*

3.3 <u>Experimental program</u>

3.3.1 Description of the specimens

A total of ten masonry walls were manufactured for this experimental program: six were built with 6x8x16 in. (0.15x0.20x0.41 m) concrete blocks in a running bond pattern, four walls were constructed by means of light extruded clay bricks, having the nominal dimensions of 2.5x4x8in. (0.64x0.10x0.20 m), in a common bond pattern. All the walls were built by qualified masons to not introduce additional variables such as handwork and different mortar workability that may arise from the construction of the specimens. The panels had a nominal dimension of 64 in. by 64 in. (1.63 x 1.63 m). In Fig. 3.3.1a-b masonry patterns are illustrated.

CONCRETE BLOCK PANEL

FRONT VIEW   SIDE VIEW
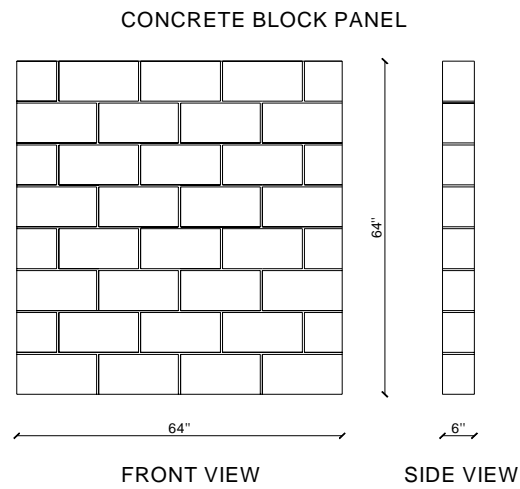
Fig. 3.3.1 a-b *Concrete block panel (top) and clay brick panel (bottom)*

CLAY BRICK PANEL

FRONT VIEW   SIDE VIEW
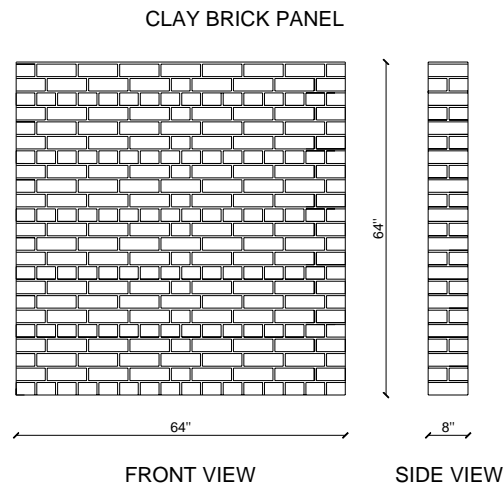
Fig. 3.3.1a *Concrete block panels in the testing room*

Fig. 3.3.1b *Clay panels*

3.3.2 Materials

Tests were performed to characterize the engineering properties of the materials used in this investigation. The average compressive strength of concrete masonry obtained from the testing of prisms was 2430 psi (16.74 MPa) with a standard deviation of 345 psi (2.37 MPa). Clay prisms instead showed an average compressive strength of 2129 psi (14.67 MPa) with a standard deviation of 193 psi (1.33 MPa). ASTM C1314 was followed. In order to determine the shear stresses along the mortar joints two series of triplets were tested. Cohesion and coefficient of friction according to Coulomb criterion, expressed by the equation $\tau = \tau_o + \mu \, \sigma_n$, were obtained by means of linear interpolation of the experimental data. Thus for concrete blocks it was found $\tau = 57.43 + 0.6679\sigma_n$ (psi) for $\sigma_n < 216$ psi, whereas for clay bricks $\tau = 119.57 + 1.35\sigma_n$ (psi) for $\sigma_n < 70$ psi. The walls were strengthened with #2 glass FRP (GFRP) bars having a diameter of 0.25 in.(6 mm), a tensile strength of 107 ksi (737 MPa) and modulus of elasticity of 5900 ksi (40651 ksi), and GFRP laminates with a tensile strength of 245 ksi (1688 MPa) and modulus of elasticity equal to 12056 ksi (83066 MPa). In the case of bars the mechanical properties were provided by the manufacturers, instead in the case of laminates tensile tests following ASTM D3039 standard protocol were performed in laboratory environment. All the characterizations are summed up in Appendix A.

The GFRP bars are deformed by a helical wrap with a sand coating to effect bond between concrete or structural epoxy (see Fig. 3.1e). The bars are produced using a variation of the pultrusion process using 100% vinylester resin and e-glass fibers. Typical fiber content is 75% by weight. The rods are commercially available in high volumes with stocking locations in several points throughout North America and Europe. The GFRP bars were embedded into an epoxy-based paste. According to the manufacturer, the paste had the following mechanical properties: compressive strength of 12.5 ksi (86 MPa), tensile strength of 4 ksi (28 MPa), and modulus of elasticity of 450 ksi (3101 MPa) (see Appendix A).

3.3.3 Strengthening Strategy

3.3.3.1 Series COW

A total of six masonry walls were manufactured as part of this experimental program, which were built with 6x8x16 in. concrete blocks following a running bond pattern. One Unreinforced Masonry (URM) wall, COW1, was the control specimen. COW2 was strengthened with GFRP bars at every horizontal only on one side. Walls COW2 and COW3 had similar amounts of reinforcement. In the latter specimen, the reinforcement was distributed in the two faces, following an alternate pattern, to observe the influence of the reinforcement eccentricity. Wall COW4 was strengthened with GFRP bars at every second horizontal joint to observe the behavior of a wall with half the amount of strengthening. Wall 5 was strengthened with GFRP laminates; the amount of strengthening reinforcement was equivalent to that of Wall 2 in terms of axial stiffness EA (Modulus of Elasticity x Reinforcement Cross Sectional Area). Thus four GFRP strips 64 in. (1.63 m) long and 4 in. (0.1 m) wide were applied on the panel surface. Wall 6 was strengthened with a combination of GFRP bars and laminates. The bars were placed in every horizontal joint, whereas, the laminates were applied in the vertical direction. The amount of reinforcement for both directions was similar in terms of EA; as for wall COW5 four strips 64 in. long and 4 in. wide were cut. For the case of walls strengthened by "FRP structural repointing", grooving of the mortar joints is a simpler task than grooving the masonry units. If grooving of the units is not carefully carried out, there may be local fractures. That is the reason why the spacing of FRP bars is practically dictated by the height of the blocks or bricks.   The test matrix used in this investigation for Series COW is summarized in Table 3.3.3.1.
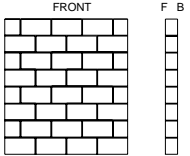
Table 3.3.3.1 *Test matrix for Series COW*

Specimen	Strengthening	Front Side	Back Side	Layout
COW1	None	None	None	

Table 3.3.31 *Test matrix (continued)*

Specimen	Strengthening	Front Side	Back Side	Layout
COW2	#2 GFRP bars	1HJ	None	
COW3	#2 GFRP bars	2HJ	2HJ	
COW4	#2 GFRP bars	2HJ	None	
COW5	4in. GFRP laminates	4HS	None	
COW6	#2 GFRP bars 4in. GFRP laminates	HJ/4VS	None	

LEGEND: 1HJ= every horizontal joint, 2HJ= every second horizontal joints
4HS=four horizontal strips @ 16 in. o.c., 4VS= four vertical strips @ 16 in. o.c

3.3.3.2 Series CLW

Four walls made of light extruded clay bricks were constructed for the second part of the experimental program. Wall CLW1, unstrengthened, was selected as control specimen. For the first strengthened panel, CLW2, it was decided to put an amount of reinforcement equivalent to that of COW2 in terms of reinforcement ratio, which can be defined as:

$$\rho = \frac{A_f \bullet E_f}{A_m \bullet E_m} \tag{3.3.1}$$

where:

A_f = cross area of FRP reinforcement

131

A_m= net area of masonry unit

E_f = modulus of elasticity of FRP reinforcement

E_m= modulus of elasticity of masonry

In the modulus of elasticity of masonry is unknown, it can be estimated as $700f'_m$ for clay masonry, and $900f'_m$ for concrete masonry, according to MSJC Code (1999).

Following this procedure CLW2 was reinforced placing on both sides of the panel, therefore in a symmetrical configuration, GFRP rods every two joints and four vertical GFRP strips 64 in. long and 4.5 in. wide. In this manner the horizontal reinforcement was equal in terms of axial stiffness to the vertical one. CLW3 presented the same amount of vertical GFRP laminates of CLW2, but half of the horizontal FRP reinforcement, thus GFRP rods placed every four mortar joints. The purpose was to check the efficiency of the horizontal strengthening with the same amount of vertical. Finally CLW4 was reinforced with the lowest amount of FRP, namely half of the horizontal reinforcement of CLW2 and no vertical GFRP strips, in order to check the influence of the vertical reinforcement in clay panels, which present significant differences in terms of masonry unit geometry and bed joint distribution compared to walls made of concrete blocks. The test matrix for Series CLW is summarized in Table 3.3.3.2.

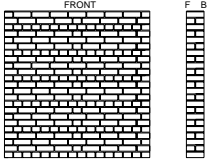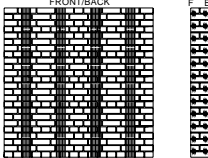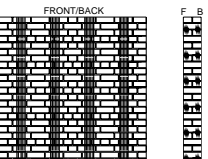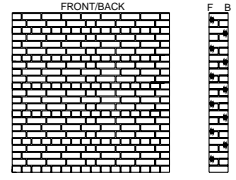**Table 3.3.3.2** *Test matrix for clay panels*

Specimen	Strengthening	Front Side	Back Side	Layout
CLW1	None	None	None	
CLW2	#2 GFRP bars 4.5 in. GFRP laminates	2HJ/4VS	2HJ/4VS	
CLW3	#2 GFRP bars 4.5 in. GFRP laminates	4HJ/4VS	4HJ/4VS	

Table 3.3.3.2 *Test matrix (continued)*

Specimen	Strengthening	Front Side	Back Side	Layout
CLW4	#2 GFRP bars	4HJ	4HJ	

LEGEND: 2HJ=every second mortar joint, 4HJ= every fourth mortar joint
               4VS= four vertical strips @ 16 in. o.c

3.3.4 Strengthening procedure

FRP Structural Repointing offers advantages compared to the use of FRP laminates. The method itself is simpler since the surface preparation is reduced (sandblasting and puttying) is not required. The installation procedure of FRP laminates for the strengthening of masonry structures (manual lay-up) was widely described in Section 1, therefore in this chapter it will be described only by means of pictures taken during the installation on the panels.

For the "FRP structural repointing" technique, the diameter size of the FRP bars is limited by the thickness of the mortar joint, which usually is not larger than $^3/_8$ inches (see Fig. 3.3.4a). The strengthening procedure consisted of: (1) cutting out part of the mortar using a grinder (Fig. 3.3.4b), (2)cleaning the grooved mortar joint by means of an air blower (Fig. 3.3.4c), (3)masking of masonry to avoid staining (Fig. 3.3.4d), (4)filling the joints with a epoxy-based paste (Fig. 3.3.4e), (5)embedding the bars in the joint (Fig. 3.3.4f), (6)final retooling (Fig. 3.3.4g) and (7)removing masking tapes (Fig. 3.3.4h). To ensure a proper bonding between the epoxy-based paste and masonry, dust must be removed from the grooved by means of an air blower.
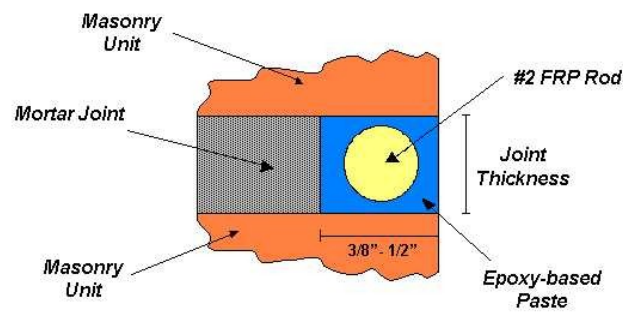

Fig. 3.3.4a *FRP Structural Repointing*

133

Fig. 3.3.4b *Grooving along the mortar joint*

Fig. 3.3.4c *Removal of dust by air pressure*

Fig. 3.3.4d *Masking of masonry to avoid staining*

Fig. 3.3.4e *Injection of epoxy-based paste into the groove*

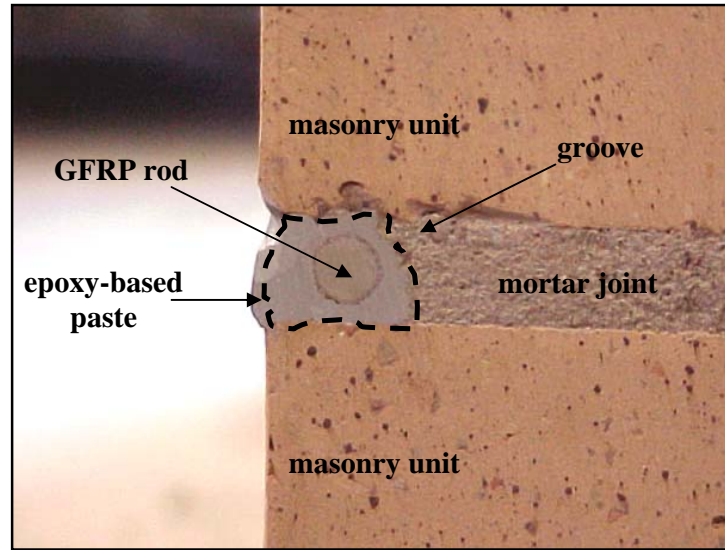**Fig. 3.3.4f** *Embedding of GFRP bar into the joint*

Fig. 3.3.4g *Final retooling of the joint*

Fig. 3.3.4h *Removal of the masking tape*

Fig. 3.3.4i *Masonry surface after strengthening*

Fig. 3.3.4p *GFRP rod embedded into the groove*

In the following pictures the manual lay-up technique, utilized to apply GFRP laminates, is illustrated.

Fig. 3.3.4j *Surface preparation*

Fig.3.3.4j *Removal of any loose parts from the masonry surface*

Fig. 3.3.4k *Primer application*

**Fig. 3.3.4l** *1st coat of saturant*

Fig. 3.3.4m *Installation of GFRP laminates*

140

Fig. 3.3.4n *2ⁿᵈ coat of saturant*

**Fig. 3.3.4o** *Strengthened panel with GFRP laminates and rods*

141

3.4 Test Setup

The specimens were tested in a close loop fashion, following the ASTM E518 standard protocol (Standard Test Method for Diagonal Tension in Masonry Assemblages). Two 30-ton-capacity hydraulic jacks activated by a manual pump were used to load the specimen along one diagonal. The force was applied to the wall by steel shoes placed at the top corner, and transmitted to similar shoes at the bottom corner through high-strength steel bars. Fig. 3.4a-b illustrate the test setup for Series COW and CLW respectively.
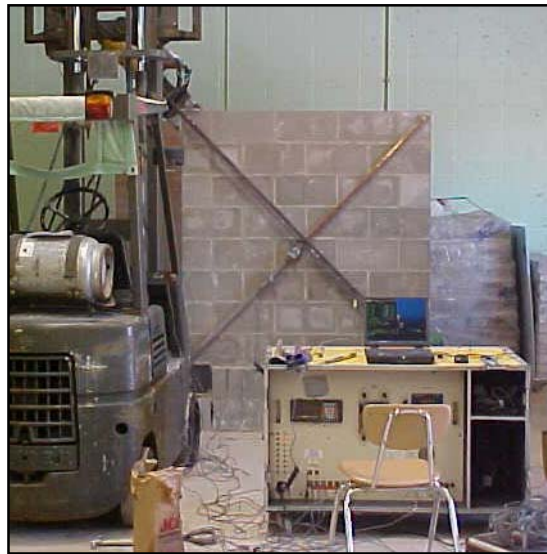
Fig. 3.4a *Concrete panel being tested*

Fig. 3.4b *Test setup for clay panel*

142
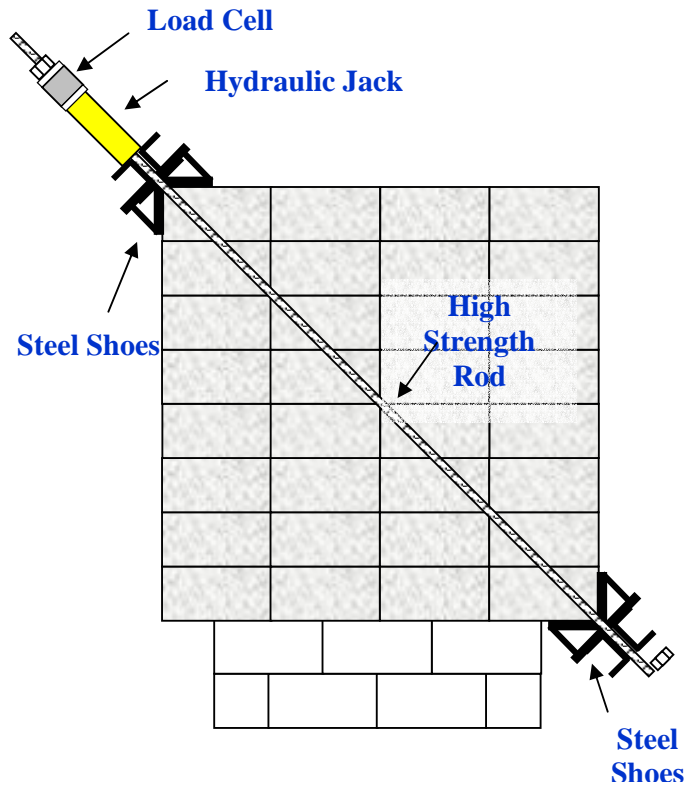
Fig. 3.4c *Test setup scheme*

The load was applied in cycles of loading and unloading, except for the control walls. An initial cycle for a low load was performed in every wall to verify that both the mechanical and electronic equipment was working properly (see Table 3.4a). The data acquired by a 200 kip load cell and the Linear Variable Differential Transducers (LVDT's) were collected by a Daytronic Data Acquisition System at a frequency of one Hz. A total of four LVDT's were used to register displacements in the walls along the wall diagonals. Two LVDT's were placed on each side of the walls: one oriented along the force line to measure the wall shortening, and the other perpendicular to the force line to record the crack opening. In addition strain gauges were attached to the FRP bars and laminates, located in correspondence to the loaded diagonal of the panels (for the recorded values see Appendix B).

	Cycle	Load Range (kips)
	1	0-30-10
	2	10-40-10
	3	10-50-10
Table 3.4a *Load cycles*	4	10-failure(?)

143

3.5 Test results

3.5.1 SERIES COW

Wall COW1

This wall was tested as first of Series COW. It was made of concrete blocks 6 in. (0.15 m). After a low load cycle to check the instrumentation applied on the panel surfaces, the specimen was loaded up to failure. No visible cracks were observed before failure, which was brittle and caused by the lack of bonding between concrete units and mortar in the joints. Only one major crack was found after failure running along the loaded diagonal on both sides of the wall (Fig. 3.5.1b). The peak load was reached at 108 kN, as shown in Fig. 3.5.1a.
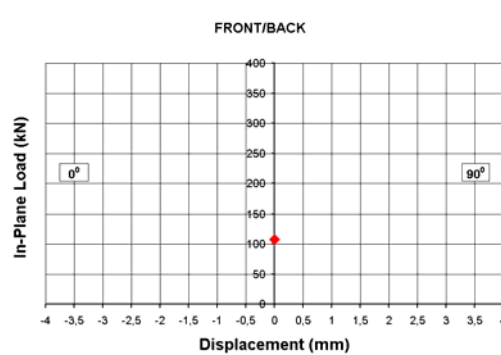

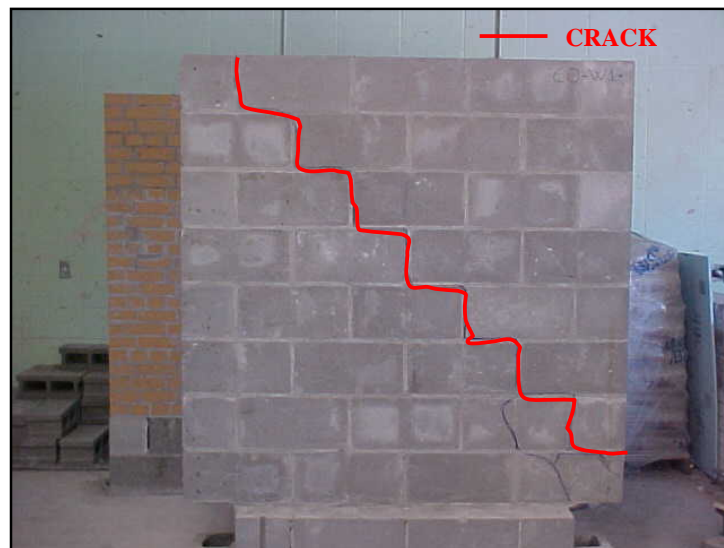**Fig. 3.5.1a** *Load vs. Diagonal displacement Curve-COW1*

Fig. 3.5.1b *Developed crack along the diagonal mortar joints*

Wall COW2

This panel was strengthened with GFRP rods placed at every joint only on one side. Therefore the strengthening configuration was asymmetrical. A significant increment of 85% in terms of shear capacity was registered as shown in Fig. 3.5.1c. The peak load was reached at 199.6 kN. The first major crack was observed at 180 kN, running along the loaded diagonal on the mortar joints. After that the load-displacement curve tended to be flat. The failure occurred due to the progressive lack of bonding on the interface masonry-epoxy based paste in reinforced joints (see Section 3.5.2).
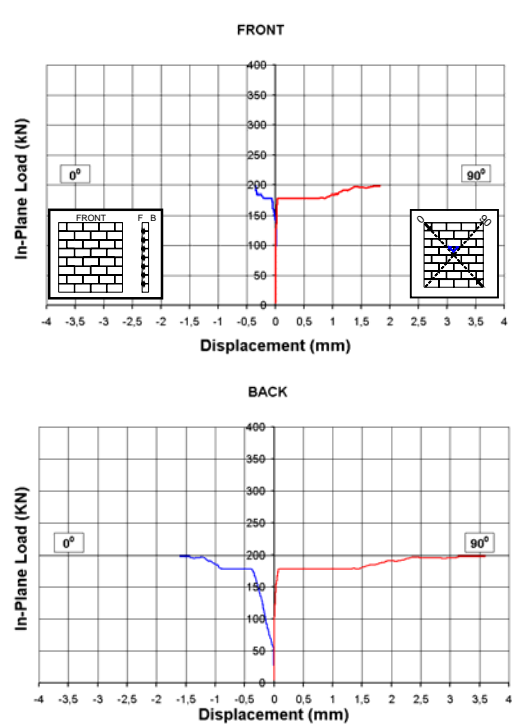

Fig. 3.5.1c *Load vs. Diagonal displacement Curves-COW2*

Fig. 3.5.1d *Unstrengthened side of the wall after failure*

Wall COW3

This wall was strengthened with the same amount of GFRP rods of COW2. The significant difference was in the strengthening configuration. In this case the GFRP rods were placed at every joint but alternated on the two facades of the specimen.

Even if the ultimate shear capacity was the same of COW2, as observed in Fig. 3.5.1e, the panel exhibited at the ultimate stage more stability than COW2, due to the symmetrical configuration of the reinforcement, which led to similar crack openings on the two faces of the wall.
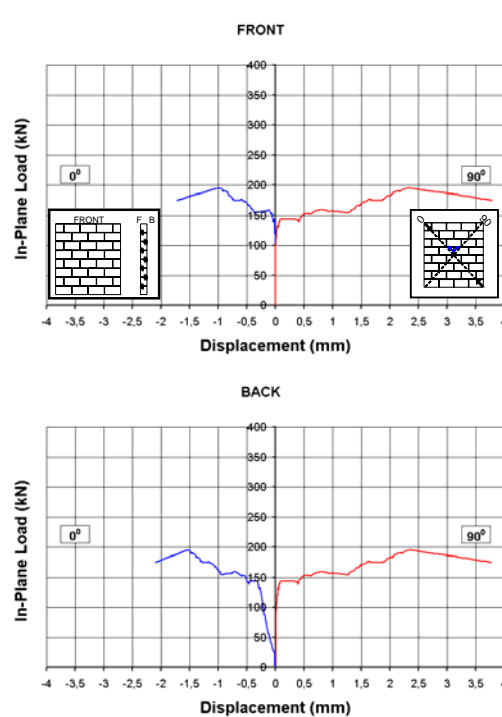

Fig. 3.5.1e *Load vs. Diagonal Displacement Curves-COW3*

Fig. 3.5.1f *Panel after failure*

146

Wall COW4

Instead of placing GFRP rods every horizontal joint on one side, this specimen was strengthened with bars placed every two joints. Compared to the control wall an increment of only 20% in terms of shear capacity was observed, due to the sliding failure occurred along the unstrengthened mortar joint at the second course. The peak load was reached at 139 kN. After that a major crack was detected running along the loaded diagonal and the wall could carry no more capacity up to failure.
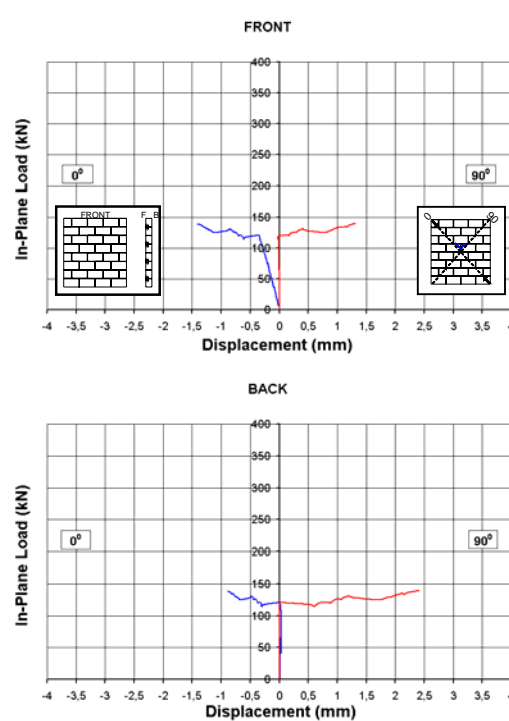

Fig. 3.5.1g *Load vs. Diagonal Displacement Curves-COW4*

Fig. 3.5.1h *Cracked wall after failure*

Wall COW5

This wall was retrofitted with the same amount of FRP in terms of axial stiffness EA of COW4 in the horizontal direction; the difference was that instead of using GFRP rods GFRP laminates were employed. Four strips 64 in. long and 4 in. wide were attached on the concrete masonry surface every 2 courses. The peak load was registered at 187 kN, higher compared to the previous specimen. Similarly to COW4 the failure was caused by sliding of the second course of the concrete units.
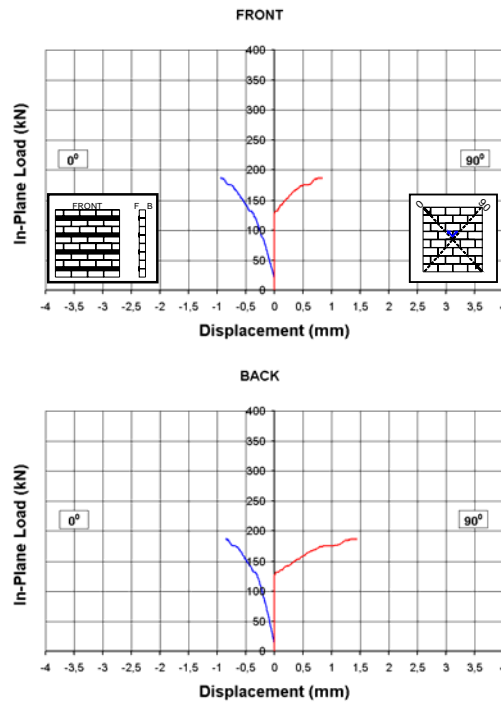

Fig. 3.5.1i *Load vs. Displacement Curves-COW5*

Fig. 3.5.1j *Unstrengthened side after failure*

148

Wall COW6

The wall was reinforced with a combination of GFRP rods placed at every joint on one side and GFRP laminates applied in vertical direction with the same spacing of the rods and on the same face. Compared to COW2, no increments of shear capacity were recorded, therefore demonstrating that vertical reinforcement combined with horizontal is not effective. At the ultimate stage both progressive debonding of the epoxy from the concrete unit surfaces and partial delamination of the GFRP sheets were observed.
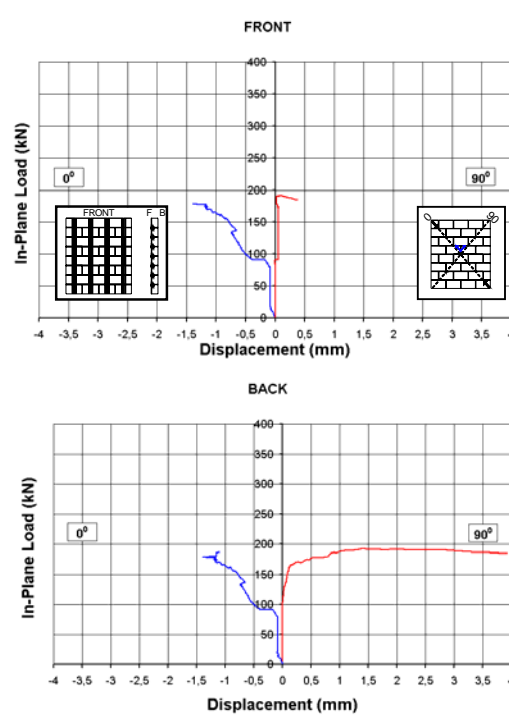

Fig. 3.5.1k *Load vs. Diagonal Displacement Curves-COW6*

Fig. 3.5.1l *Strengthened side of the panel after collapse*

3.5.2 SERIES CLW

Wall CLW1

Similarly to COW1 this wall was left unstrengthened and selected as control wall. After a low load cycle in order to verify the proper function of the monitoring instrumentation, the wall was brought to failure. Due to the brittle nature of the unstrengthened clay masonry the failure was caused by complete collapse of the loaded diagonal for splitting of the clay units, as shown in Fig. 3.5.1n. No visible cracks were detected until reaching the maximum load, which was 341 kN.
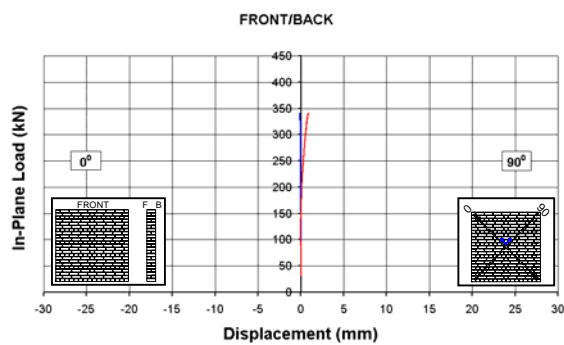

Fig. 3.5.2a *Load vs. Diagonal Displacement Curve-CLW1*

Fig. 3.5.2b *Collapse of the unstrengthened wall*

Wall CLW2

This panel presented the equivalent reinforcement ratio of COW2. In this case the reinforcement was equally distributed in horizontal and vertical direction, by means of GFRP rods and GFRP laminates respectively. The first visible cracks were detected along the diagonal mortar joints and in the clay units at 300 kN. The peak was reached at 408 kN. The specimen, compared with the control wall, exhibited a significant ductile behavior, which allowed the panel to keep the maximum load for a mean tensile displacement of 30 mm, as shown in Fig. 3.5.2c.
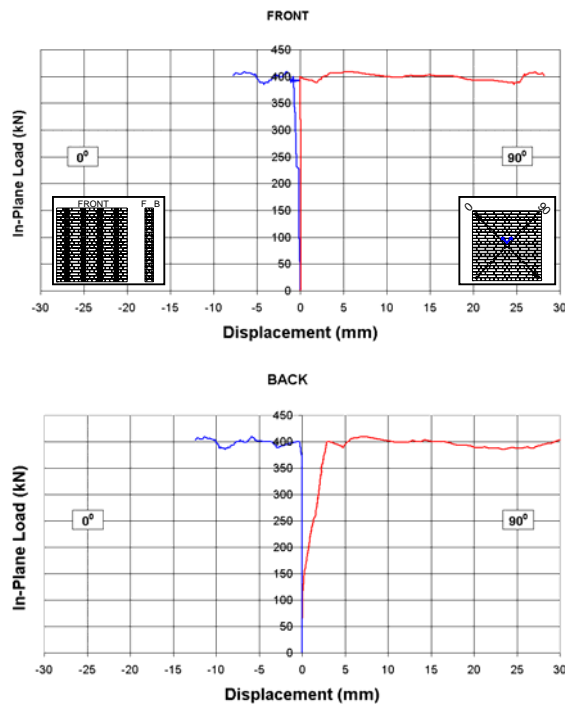

Fig. 3.5.2c *Load vs. Displacement Curves-CLW2*

Fig. 3.5.2d *Crack pattern of CLW2*

Wall CLW3

This wall was strengthened with the same amount of vertical reinforcement of CLW2 but half of the horizontal. No substantial differences in the mechanical behavior during the load cycles and in the mode of failure at the ultimate stage were observed. The collapse was caused, similarly to concrete block walls reinforced at every mortar joints, for the progressive lack of bonding between the epoxy-based paste in the reinforced joints and the clay unit surfaces, starting from the loaded diagonal; in addition, delamination of the GFRP laminates was detected. The peak was 319 kN.
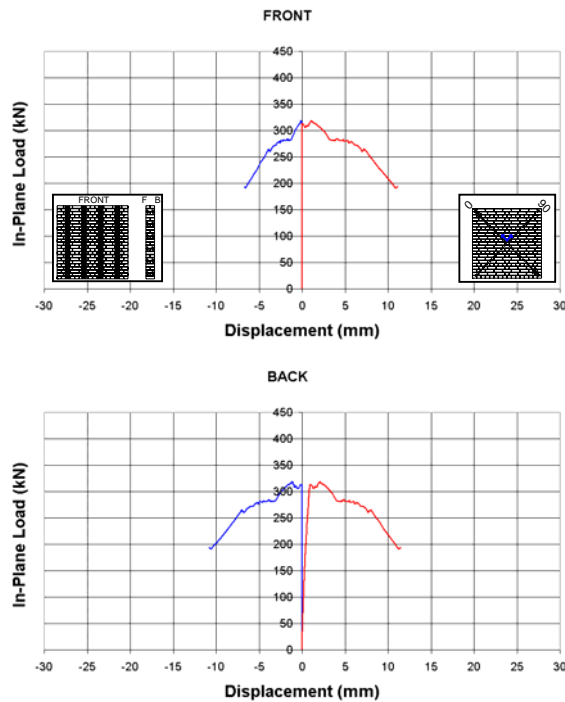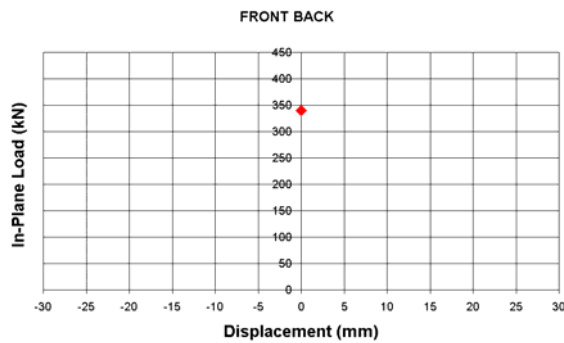

Fig. 3.5.2e *Load vs. Diagonal Displacement Curves-CLW3*

Fig. 3.5.2f *Panel after failure*

Wall CLW4

The last wall of Series CL was strengthened placing only GFRP rods every two mortar joints distributed on the two faces of the panel. The peak load was reached at 340 kN, therefore even less than the control wall and without showing any ductile behavior. This fact may be attributed to undesirable variables such as handwork or mortar workability; however, in this case the GFRP rods had no effect in terms of shear capacity, meaning that ,due to the high compressive strength of clay masonry, a lower limit for FRP reinforcement should be identified for the shear strengthening of clay masonry walls. In this panel the rods embedded in the joints provided the unique function to hold the wall at the ultimate stage.

Fig. 3.5.2g *Load vs. Diagonal Displacement Curve-CLW4*

Fig. 3.5.2h *Crack pattern of CLW4*

3.5.3 Test discussion

3.5.3.1 Mechanisms of failure and analysis in Series COW

It was observed that the mechanism of failure of walls strengthened with GFRP bars placed at every bed joint consists of two phases. From the test observations, the in-plane phase was the most critical.

- **In-Plane Phase:** When the tensile strength of masonry is overcome, the wall cracks along the diagonal, following the mortar joints (stepped crack vertical/horizontal, see Fig.3.5.3.1a) For the reinforcement placed in the horizontal joint, the crack is typically at the top side (see item 1 – Fig. 3.5.3.1a). Wall failure occurs only when a second crack develops below the reinforcement at the epoxy/block interface (see item 2 – Fig. 3.5.3.1a)
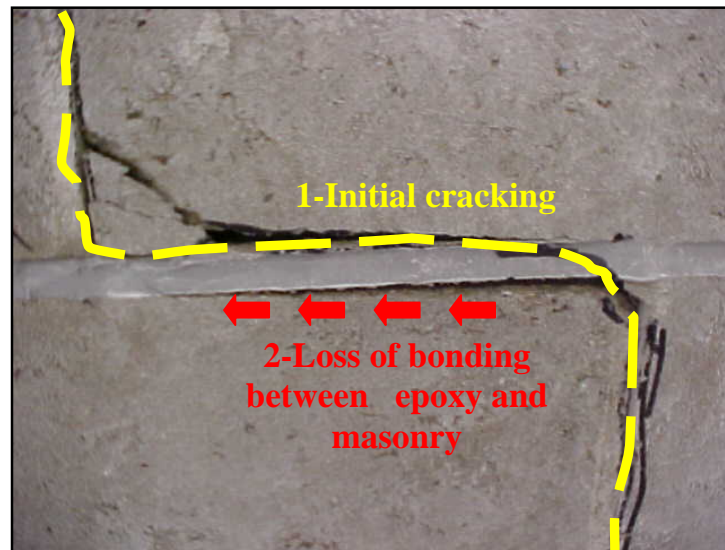

Fig. 3.5.3.1a *In-Plane failure component*

- **Out-of-Plane Phase:** This phase influences the stability of the wall, which is observed in specimens strengthened only on one side (see Fig. 3.5.3.1b-c). Comparing the recorded crack openings on the front (strengthened) and back (unstrengthened) sides, the crack growth on the unstrengthened side increased at a higher rate than the strengthened side (see Fig. 3.5.3.1d).

For walls where not all the joints were strengthened, such is the case of Walls COW4 and COW5, the specimen failed by sliding shear along one of the bottom bed joints

(see Fig. 3.5.3.1e). Sliding shear can significantly reduce wall pseudo-ductility. Test results of Series CLW have demonstrated that in walls built with clay units, this mode of failure is not observed. This can be attributed to better bonding between clay units and mortar.

Fig. 3.5.3.1b
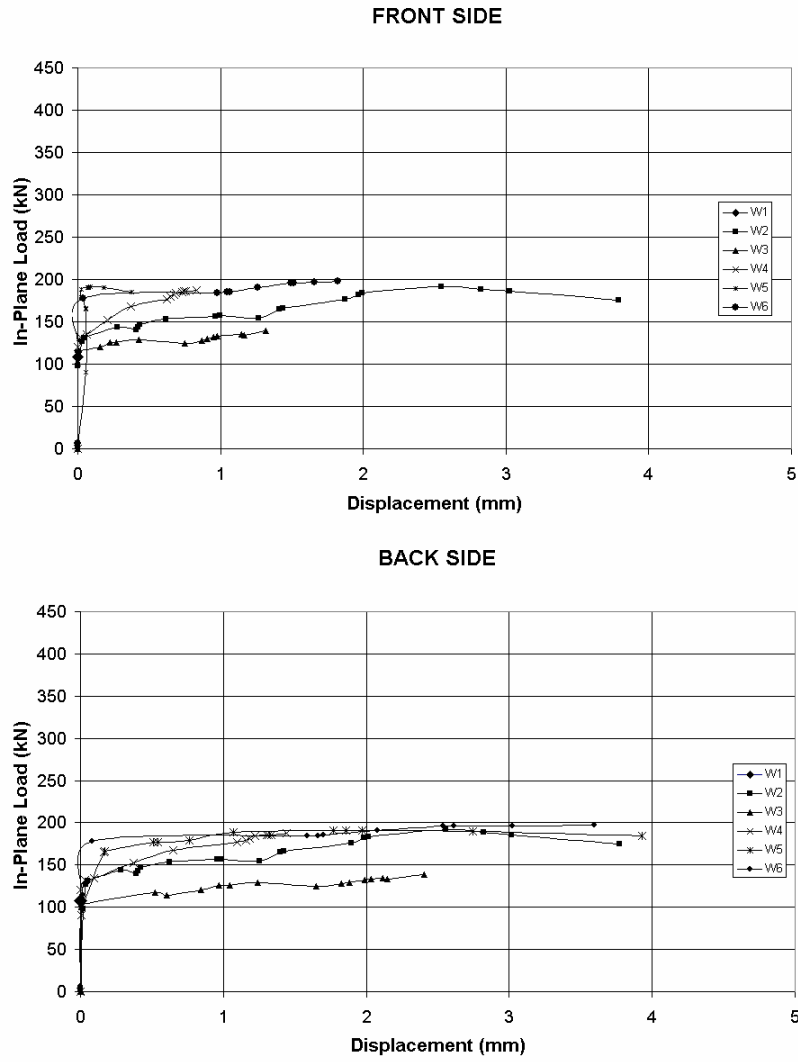

Fig. 3.5.3.1c *Strengthened specimens after collapse*

155

FRONT SIDE

BACK SIDE

Fig. 3.5.3.1d *Crack openings*

Fig. 3.5.3.1e *Shear Sliding Failure*

156

In the control Wall 1 the failure was brittle, controlled by bonding between the masonry units and mortar (see Fig. 3.5.1b and 3.5.3.1f). For the specimens strengthened with the "FRP structural repointing" technique the maximum increment in shear capacity was about 80%, which was registered in Walls COW2 and COW3, strengthened with GFRP bars placed at every bed joint. At the final stage, the walls failed due to the formation of a second crack below the reinforcement (Item 2 in Fig 5). Strengthened walls showed stability (i.e. no loose material was observed) after failure. This fact can reduce risk of injuries due to partial or total collapse of walls also subjected to out-of-plane loads (see Fig. 3.5.3.1g).
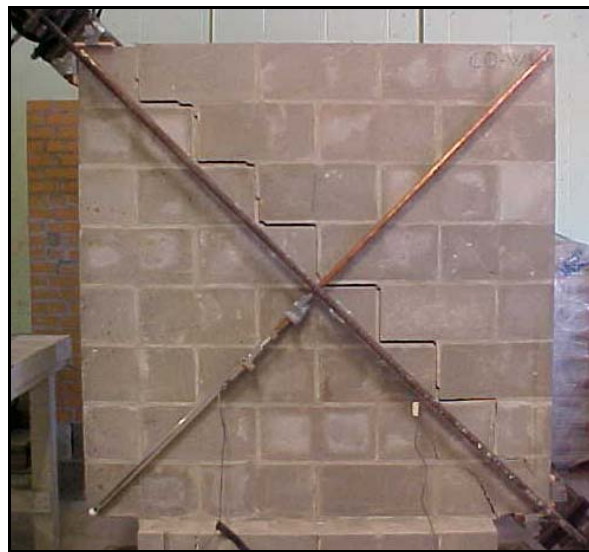
Fig. 3.5.3.1f *Unstrengthened wall before collapse*

Fig. 3.5.3.1g *Strengthened wall after failure*

157

Failure in Walls COW4 and COW5 was due to sliding shear along an unstrengthened joint (see Fig. 3.5.3.1e). However, in the case of Wall COW5 a larger increase in shear capacity was recorded due to the fact that the horizontal laminates engaged the masonry layers where the sliding occurred, and that cracks running along the head joints were bridged. This failure mechanism is also commonly known as *knee brace* or *joint-slip*. Due to its premature characteristic and negative effect to the boundary elements (i.e. columns in an infill wall), this kind of failure should be avoided. A potential way to prevent it would be to place of vertical FRP reinforcement on the masonry infill, which would act as a dowel action. Wall 6 showed that vertical reinforcement was not effective. In this specimen failure was also caused by occurrence of a second crack below the horizontal reinforcement. Local delamination in the laminates was also observed in the debonded regions.

The test setup configuration did not allow estimating pseudo-ductility as conventionally done ($\mu = \delta_u/\delta_y$), where δ_u and δ_y are the horizontal displacements at ultimate and "yielding" caused by an in-plane load. Instead a criterion using the shear strain was adopted. Thus, the pseudo-ductility, 'μ', was quantified as the ratio γ_u/γ_y; where γ_u is the shear strain at ultimate and γ_y is the shear strain, corresponding to the point where the in-plane load vs. shear strain curve tends to be flat. Considering the strains generated by the diagonal in-plane load as principal strains, the maximum shear strain is expressed as:

$$\gamma = \left|\varepsilon_0\right| + \left|\varepsilon_{90}\right|$$

where ε_0 and ε_{90} are the strains associated to the wall diagonals. The shear strain values are shown in Table 3.5.3.1a.

Table 3.5.3.1a *Comparison of Pseudo-ductility for Series COW*

Specimen	In-Plane Load	γ_u	γ_y	μ
COW1	108 kN	0.09	0.09	1.0
COW2	200 kN	1.71	0.13	13.1
COW3	195 kN	1.82	0.09	20.2
COW4	189 kN	0.40	0.08	5.0
COW5	137 kN	0.94	0.17	5.5
COW6	191 kN	0.72	0.14	5.1

Fig. 3.5.3.1d illustrates the in-plane load vs. shear strain curves for the test walls. It can be observed that Wall COW3 exhibited the largest pseudo-ductility value, which can be attributed to reinforcement staggering on the two wall sides. Because of this strengthening configuration, the effect of the out-of-plane component in the wall stability was inexistent. The pseudo-ductility values estimated from Walls COW4 and COW5 were the smallest of all the strengthened walls. As it was mentioned before, this is caused by the occurrence of sliding shear. In Wall COW6, the large amount of reinforcement led to a reduction of pseudo-ductility.

3.5.3.2 Mechanisms of failure and analysis for Series CLW

A critical in-plane mechanism of failure was detected in all the clay unit panels, except for CLW1, which failed for splitting of the clay units, as observed in Fig. 3.5.3.2a and Fig. 3.5.3.2b.

Fig. 3.5.3.2a(left)-b(right) *Splitting of clay units in CLW1*

In CLW2 and CLW3 non substantial differences were observed in terms of developed cracks and mechanism of failure, which could be divided in two different phases that occurred at the same time:

- **Horizontal phase**: Similarly to what observed in Series COW, when the tensile strength of masonry is overcome, the wall cracks along the diagonal, following the mortar joints (stepped crack vertical/horizontal, see Fig.3.5.3.2c) For the reinforcement placed in the horizontal joint, the crack is typically at the top

side (see item 1 – Fig. 3.5.3.2c). Wall failure occurs only for a progressive loss of bonding due to a second crack which develops in this case above and below the reinforcement at the epoxy/block interface (see item 2 – Fig. 3.5.3.2c).
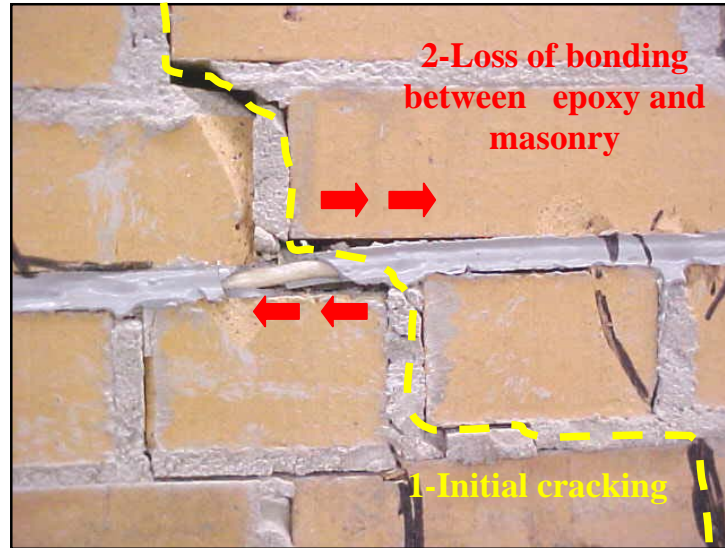

Fig. 3.5.3.2c *Horizontal component*

- **Vertical component**: Once the major diagonal crack is formed, simultaneously to the horizontal, a vertical phase, consisting in the progressive delamination of the GFRP sheets from the clay surface, starts moving from the loaded diagonal to the upper or lower borders of the panel. As described in Appendix A, it is assumed that an effective bonded length exists for Aramid but also for Glass fibers, and once the delamination occurs, it starts spreading to the boundaries, as shown in Fig. 3.5.3.2d-e.

Wall CLW4 was reinforced only with GFRP rods and no vertical reinforcement in form of GFRP laminates was applied. Due to the presence of a low amount of GFRP rods, the wall did not exhibit more shear capacity compared to the control wall CLW1, but failed for the occurring of the horizontal phase previously explained. In order to achieve a significant increment in shear capacity utilizing for an aesthetic purpose only the FRP Structural Repointing technique, a larger amount of rods embedded in the mortar joints should be provided for clay walls. CLW3 exhibited the lowest shear capacity due to significant imperfections detected during the tests such as large number of thick mortar joints and great differences in the mortar workability. For further
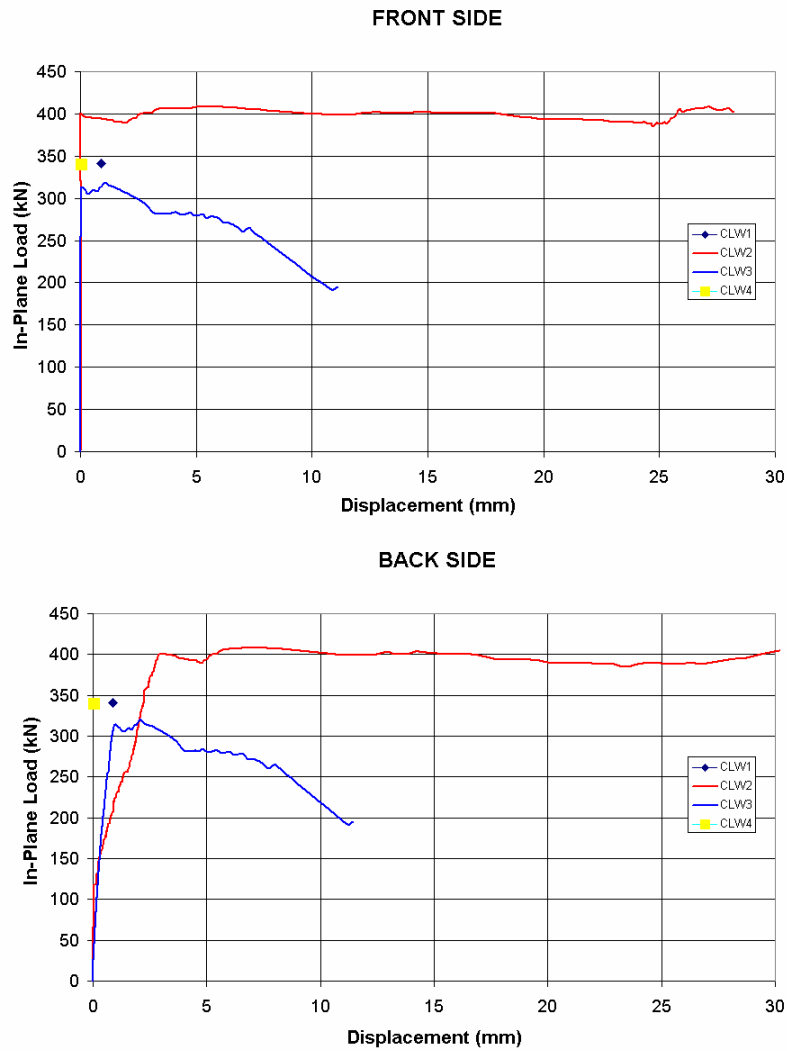
research, these type of imperfections that affected the average shear capacity should be avoided.

Fig. 3.5.3.2d *Delamination of GFRP laminates from clay surface*
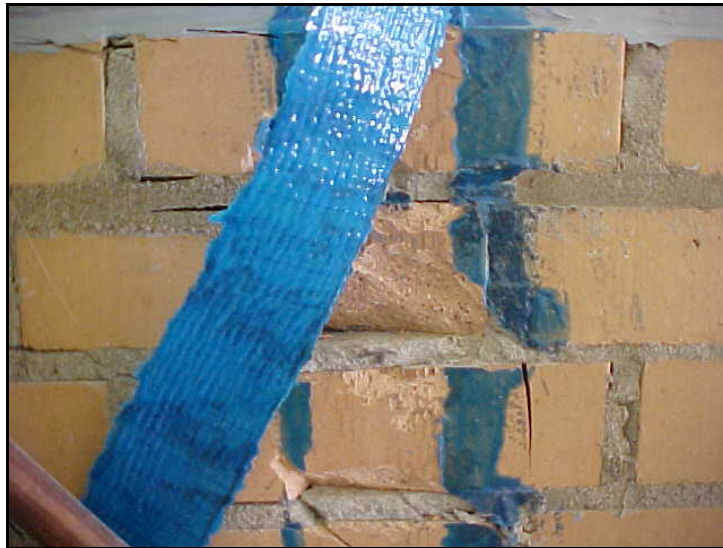
Fig. 3.5.3.2e *Clay unit surface after delamination*

Fig. 3.5.3.2f *Crack openings*

In Table 3.5.3.2a, similarly to Series COW, a comparison of the pseudo-ductilities is presented: the most strengthened specimens showed the highest values.

Table 3.5.3.2a *Comparison of pseudo-ductility for Series CLW*

Specimen	In-Plane Load	γ_u	γ_y	μ
CLW1	351 kN	0.09	0.09	1.0
CLW2	408 kN	1.79	0.2	8.9
CLW3	319 kN	2.1	0.3	7.0
CLW4	340 kN	0.24	0.08	3.0

3.5.4 Analytical Study

A simplified method in order to estimate the shear capacity of a masonry panel strengthened with FRP rods is presented.

3.5.4.1 Evaluation of shear strength of strengthened walls

Generally, the nominal shear strength of a reinforced masonry wall can be estimated as the sum of the shear contributions of the masonry and the steel shear reinforcement. The shear strength of a wall strengthened with FRP systems can be quantified by adding a third term to account for the contribution of the new reinforcement:

$$V_n = V_m + V_s + V_f \tag{1}$$

CALCULATION OF V_f

V_f depends on the shear contribution of reinforcing rods developing their full tensile capacity and rods being debonded. Thus, two areas can be identified in a masonry panel (see Fig. 3.5.4.1a).

The following assumptions are considered:

- Inclination angle of the shear cracks constant and equal to 45°.

- Constant distribution of bond stresses along the FRP rods at ultimate.

- The ultimate bond strength is reached in all the rods intersected by the crack at ultimate.
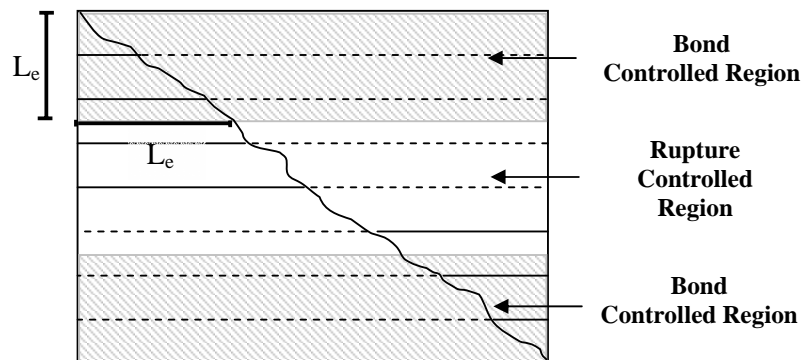
- The spacing between rods is the layer height.

Fig. 3.5.4.1a *Controlling areas to calculate V_f*

The bond behavior is dependent on the type of the rod; thereby, the assumption of constant bond stresses at ultimate may not result adequate. In this case, the value of the average bond strength would depend on the bonded length and could be computed from the local bond stress–slip relationship of the given type of FRP rod.

L_e is defined as the length at which the rod breaks, and can be derived from Fig. 3.5.4.1b:
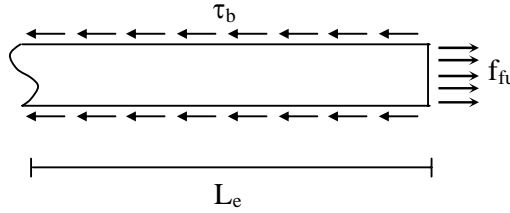

Fig. 3.5.4.1b *Effective Length L_e*

By equilibrium the force due to the bonding stress is equal to the force generated by the tensile stresses in the rod; thus:

$$\tau_b \, A_f = f_{fu} \, A_b$$

$$\tau_b (\pi \, d_b L_e) = f_{fu} \left(\frac{\pi \, d_b^2}{4} \right)$$

Then the effective length can be expressed as:

$$L_e = \frac{d_b f_{fu}}{4 \, \tau_b} \tag{2}$$

SHEAR IN BOND CONTROLLED REGION (V_b)

The number of rods (r_b) in the bond controlled region can be quantified as:

$$r_b' = \frac{L_e}{s} \tag{3a}$$

$$r_b = 2r_b' \tag{3b}$$

The value obtained using equation (3a) is rounded to the immediate inferior integer.

The shear force resisted by the FRP rods in this region can be calculated as:

$$V_b = n \, \pi \, d_b \tau_b L_t \tag{4}$$

where all these parameters are known:

  n = number of the strengthened sides of the wall (1 or 2)

  τ_b = assumed bond stress (*De Lorenzis*, 2000)

L_t = sum of the bonded lengths of all the rods crossed by the crack, calculated in the most unfavorable crack position (minimum total length).

The value of L_t is calculated as:

$$L_t = r_b \ s \tag{5}$$

SHEAR IN RUPTURE CONTROLLED REGION (V_t)

The number of rods (r_t) in the rupture controlled region can be quantified as:

$$r_t = r - r_b \tag{6}$$

The shear force resisted by the FRP rods in this region are calculated as:

$$V_t = n \ r_t \ A_i \ f_{fu} \tag{7}$$

Since long-term exposure to various types of environments may reduce the tensile properties of the FRP reinforcement, the material properties used in design equations should be reduced based on the environmental exposure condition by an appropriate environmental reduction factor C_E (ACI-440, 2000). Thus:

$$f_{fu} = C_E f_{fu}^* \tag{8}$$

where f_{fu}^* is the guaranteed ultimate tensile strength of the FRP rod as reported by the manufacturer. Finally, the shear force resisted by the FRP rods in both regions can be estimated as:

$$V_f = V_b + V_t \tag{9}$$

3.5.4.2 Validation of the analytical study

The validation of the strengthening of Wall COW2, strengthened with GFRP rods at every horizontal joint in one side is presented.

Computation of V_m

The net area of a concrete block with dimensions of 6x8x16 in. including the mortar in one of the head joints is: $A_{cb} = 55.5$ in^2

Then, the net area of the horizontal masonry section: $A_{mv} = 4\,(55.5\text{ in}^2) = 222\text{ in}^2$

The contribution of masonry to the shear strength is computed by the 1997 Unified Building Code (UBC, 1997) as follows:

$$V_m = C_d A_{mv} \sqrt{f'_m} = 1.2\,(222\ in^2)\sqrt{2490\ psi} = 132930\ lbs = 13.3\ kips$$

where according to UBC the nominal shear strength coefficient C_d is estimated as 1.2.

Computation of V_F

As previously mentioned, the bond stresses are limited to half of those estimated by De Lorenzis. Following the same criterion, the strength in the rods is limited to half of the ultimate tensile strength, thus:

$$f_{fu} \leq C_E f_{fu}^* = 0.5[(0.8)(110\,ksi)] = 44\,ksi$$

$$\tau_b \leq 0.5(0.45\,\text{ksi}) = 0.225\,\text{ksi}$$

C_E is equal to 0.8 for GFRP rods in a closed space environment. Also, to be consistent with the approach previously described, so-called "bond-controlled" and "rupture-controlled" areas are considered, with the understanding that neither debonding nor breaking of the rods were observed.

Calculation of V_b

Determine L_t:

The effective length can be calculated from equation 2 as follows:

$$L_e = \frac{d_b f_{fu}}{4\,\tau_b} = \frac{(0.25in)(44\,ksi)}{4(0.225ksi)} = 12.2\,in > spacing\ 's' = 8\,in$$

Thus, from Eq. (3a) the number of rods in the "bond-controlled" area is:

$$r_b' = \frac{L_e}{s} = \frac{12.2}{8} = 1.5,\ \text{then}\ r_b' = 1$$

From Eq. (3b): $r_b = 2r_b' = 2$ (1) = 2 rods in the "bond-controlled" area.

From Eq. (4), the shear force carried by the rods in this region is:

$V_b = n \pi d_b \tau_b L_t = (1)(\pi)(0.25 \text{in})(0.225 \text{ksi})(16 \text{in}) = 2.8 \text{kips}$

Calculation of V_t

The rods in the "rupture-controlled" area are the remaining rods; thus in Eq. (6):

$r_t = r - r_b = 7 - 2 = 5$ rods

From Eq. (7):

$V_t = n r_r A_i f_{fu} = (1)(5 rods)(0.05 in^2)(44 ksi) = 11\ kips$

The shear contribution of the GFRP rods estimated from Eq. (9) is:

$V_f = V_b + V_t = 2.8\ kips + 11\ kips = 13.8\ kips$

Finally the capacity of the strengthened wall is:

$V_{st} = V_m + V_F = 12.2\ kips + 13.8\ kips = 26.0\ kips$

By comparing the horizontal component of the ultimate loads with the expected loads the following results are found:

Control Wall 1: $V_{\text{m-exp.}} = V_{max} \sin 45^o = (24.3 kips)\left(\dfrac{1}{\sqrt{2}}\right) = 17.1 kips$

Strengthened Wall 2: $V_{\text{st-exp.}} = V_{max} \sin 45^o = (44.4 kips)\left(\dfrac{1}{\sqrt{2}}\right) = 31.4 kips$

Comparing expected and experimental shear strengths it can be observed that the presented methodology provides reasonable values.

4.
PROVISIONAL DESIGN APPROACHES

4.1 FLEXURAL STRENGTHENING WITH FRP LAMINATES

Three ultimate states can be considered in a masonry wall strengthened with FRP laminates:

- State 1: debonding of the FRP laminate from the masonry substrate
- State 2: rupture of the FRP laminate/crushing of masonry in compression
- State 3: shear failure in the masonry units

The flexural capacity of a FRP strengthened masonry wall can be determined based on strain compatibility, internal force equilibrium, and the controlling mode of failure. Previous investigations (*Velazquez* 1998, *Hamilton et al.* 1999, and *Roko et al.* 1999) and the present research suggest that most of the times, the controlling state is the debonding of the FRP laminate (State 1). If a large amount of FRP is provided, shear failure may be observed.

As demonstrated in the experimental program (see Section 2.3) debonding may have a direct relationship with the porosity of the masonry unit, which is characterized by initial rate of absorption tests. *Roko et al.* (1999) observed that the absorption of the epoxy is limited in the extruded brick units as compared to the absorption in molded bricks. This is attributed to the glazed nature of their surface, which leads to a reduction of the bond strength between the FRP laminate and the masonry surface.

Figure 4.1a illustrates the relationship between the experimental-theoretical flexural capacity ratio, and the reinforcement ratio ω_f, expressed as $\dfrac{\rho_f E_f}{f'_m (h/t)}$. The introduction of the slenderness ratio h/t is justified since this parameter is identified as one of the most important in the out-of-plane behavior of masonry walls. The slenderness ratios and the out-of-plane capacity are inversely proportional. As the slenderness ratios decrease, the out-of-plane strength becomes very large (*Angel et al.* 1994). Since the strength is directly proportional to the compressive strength, then the slenderness ratio and the compressive strength are inversely proportional. Therefore, it is reasonable to express the relation between the compressive strength and the slenderness factor as a product. The experimental data used for plotting Fig. 2.4.1a was obtained from previous research (*Velazquez* 1998, and *Hamilton et al.*1999) and

from the specimens tested during the present investigation. The test specimens were
built with clay and concrete masonry units. AFRP and GFRP laminates were used as
strengthening material. Mostly, the tests showed that the strengthened specimens failed
due to debonding of the laminate. These masonry assemblages were built with
standard concrete blocks, and had nominal dimensions of 24-in. by 48-in.   The
reinforcement consisted of GFRP and AFRP laminates. The characteristics of the
specimens being considered as well as the calculations conducted to developing Figure
4.1a are presented in Section 2.
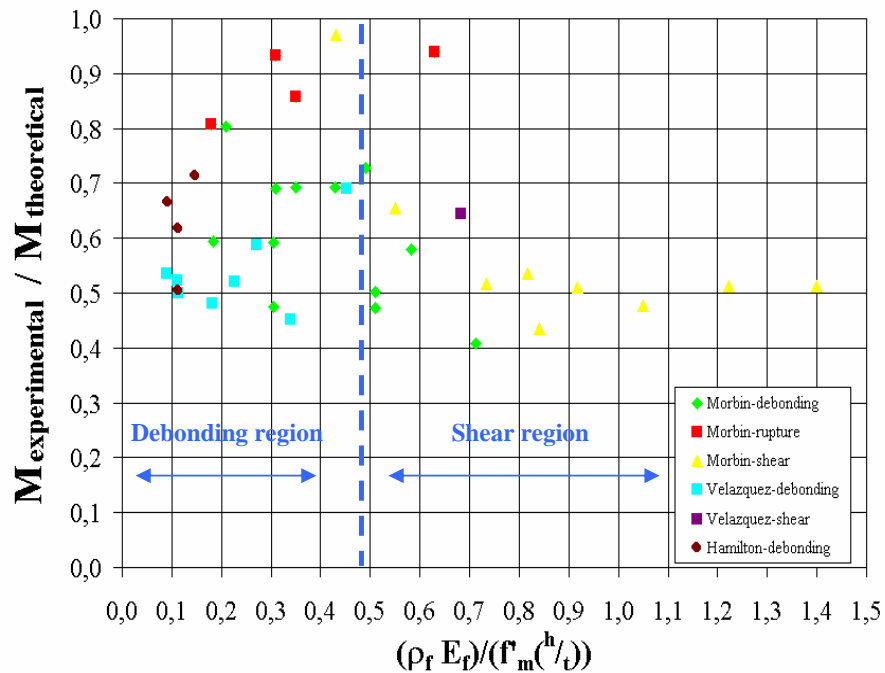
Fig. 4.1a *Influence of amount of FRP reinforcement*

According to Section 2.3.7 theoretical flexural capacities of the strengthened walls
were estimated based on the assumption that no premature failure was to be observed.
This meant that either rupture of the laminate or crushing of masonry would control
the wall behavior. A parabolic distribution was used in the computation of the flexural
capacity of the strengthened masonry. Based on the $M_{experimental}$-$M_{theoretical}$ ratios, it
was considered that the actual ultimate capacity of the strengthened wall could be
calculated form a cracked section under elastic stresses, where the two materials
behave elastically. For detailed equations see Section 2.3.7.

If the modulus of elasticity of masonry, E_m, is unknown, it can be estimated as $E_m=700$ f'_m for clay masonry and $E_m=900$ f'_m for concrete masonry (MSJC, 1999). As shown in Fig. 2.4.1a, since the ratio $M_{experimental}$-$M_{theoretical}$ averages in the range 0.5-0.7, for design considerations the effective strain ε_{fe} in the FRP laminate can be limited as about half of the strain at ultimate in the laminate ε_{fu}.

Because of the use of both GFRP and AFRP laminates, it is suggested to use a value equal to 0.008 for e_{fe} for limit strain. As observed in Fig. 4.1a, the index ω_f may be limited to 0.5 to prevent the occurrence of shear failure. These assumptions are taken with the premise that further research needs to be conducted to fully validate the veracity of the assumed limits.

During strong seismic events the strengthened walls can displace as a whole or partially collapse under out-of-plane loads. To avoid this, anchorage systems can be installed. Some anchorage systems include the use of steel angles (see Figure 4.1b), steel bolts (see Figure 4.1c), and NSM rods. The use of steel angles can locally fracture the wall in the anchorage regions due to the restraint caused when the wall starts deflecting. Thereby, it is advisable that the anchorage system is not in contact with the masonry surface. *Schwegler et al.(*1996) investigated the use of bolts, which even though showed effectiveness, represent a demanding installation effort.
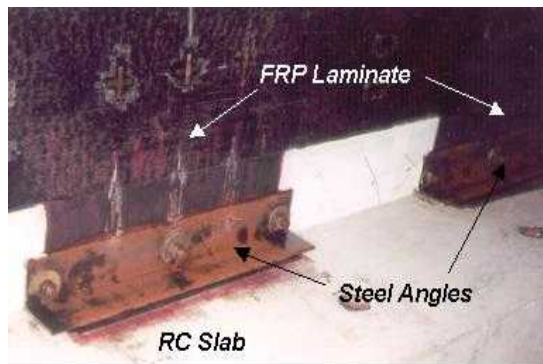

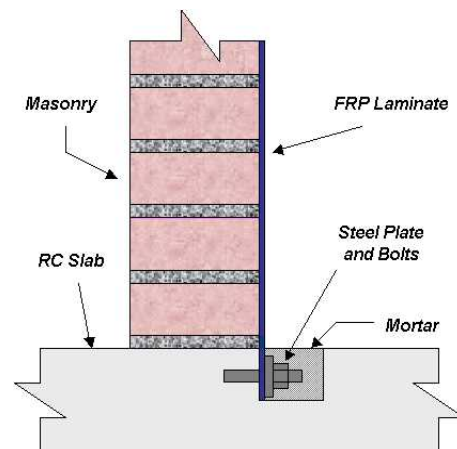**Fig. 4.1b** *Steel Angles*   **Fig. 4.1c** *Steel bolts*

The nature of the NSM installation technique and the shortened installation time make their use suitable to be used as part of the strengthening strategy of masonry walls. NSM rods have been successfully used for anchoring FRP laminates in RC joists strengthened in shear (*Anaiah et al.*,2000). The installation technique consists of

grooving a slot in the upper and lower boundary members. The fibers are then placed in the slot, rounding a FRP rod which will act as anchorage after being bounded by a suitable epoxy-based paste (see Figure 4.1d).
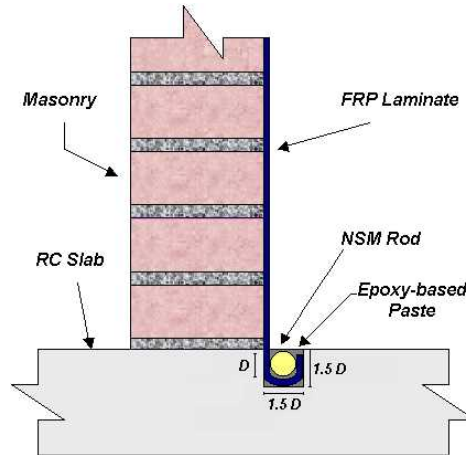

Fig. 4.1d *Anchorage with NSM rods*

4.1.1   Design Protocol

The ultimate strength design criteria states that the design flexural capacity of a member must exceed the flexural demand.

$$M_u \leq \phi M_n \tag{4.1}$$

The following assumptions are taken:

- The strains in the reinforcement and masonry are directly proportional to the distance from the neutral axis.
- The maximum usable strain, ε_{mu}, at the extreme compressive fiber is assumed to be 0.0035 in./in. for clay masonry and 0.0025 in./in for concrete masonry.
- The maximum usable strain is the FRP reinforcement is assumed to be 0.0008 in./in.
- The tensile strength of masonry is neglected.
- The FRP reinforcement has a linear elastic stress-strain relationship up to failure.

The design protocol can be outlined as follows:

171

1.Compare the allowable tensile stresses provided by MSJC with the acting stresses to determine the need for strengthening.

2.The nominal flexural capacity is computed by considering a reduction factor ϕ equal to 0.70.

The approach for the reduction factor is similar to that of the ACI-318, where a section with low ductility must be compensated with a higher reserve of strength. The higher reserve of strength is attained by applying a strength reduction factor of 0.70 to sections prone to have brittle or premature failures such as debonding of the laminate. The amount of FRP reinforcement is estimated by modifying equation 2.3.7.17 as follows:

$$M_n = \rho_f f_{fe} b t_m^{\,2}\left(1 - \frac{k}{3}\right) \tag{4.2}$$

where ρ_f is the FRP reinforcement ratio, b is the width of the section being analyzed, and t_m is the overall wall thickness.

A maximum usable strain FRP strain is used based on experimental observations. Thus, the effective usable stress can be computed as:

$$f_{fe}^* = 0.008 E_f \tag{4.3}$$

Similarly, to the shear design protocol, an environmental reduction factor C_E (ACI-440, 2000) is also considered. The C_E factors are estimated from Table 4.1.1a.

$$f_{fe} = C_E f_{fe}^* \tag{4.4}$$

Exposure Condition	Fiber Type	C_E
Enclosed Conditioned Space	Carbon	1.00
	Glass	0.80
	Aramid	0.90
Unenclosed or Unconditioned Space	Carbon	0.90
	Glass	0.70
	Aramid	0.80

The maximum clear spacing between FRP strips can be defined as follows:

$$s_f = \min\{2t_m, L\} \tag{4.5}$$

For block units: $L = l_b$

For brick units: L= $2l_b$

Where t_m is the thickness of the wall being reinforced without including the wall veneer, and l_b is the length of the masonry unit.

There is no scientific evidence for the recommendations on maximum clear spacing. s_f equal to two times the wall thickness is based on stress distribution criteria along the thickness. For s_f equal to the length of the masonry unit, the rationale is to engage most of the masonry units and avoid loosening of units, which could cause the partial collapse of the wall. Additional reinforcement, no needed to satisfy load demands, would have to be placed.

Design Example

The flexural capacity of a non-bearing URM concrete block wall needs to be verified due to increased wind load demands. The nominal dimension of the concrete units is 8x8x16-in. The wall has only two boundary elements (i.e. lower and upper beams), and it can be assumed to have only one-way bending behavior. The dimensions of the wall are 12-ft. by 12-ft. The moment demand has been estimated as 1.15 ft-kips/ft. If strengthening is needed, a glass/epoxy system will be used to upgrade the shear capacity.

Masonry Properties: $f'_m = 2000$ psi

$\varepsilon_{mu} = 0.0035$ in./in.

$t_m = 8$-in.

FRP Properties: $f_{fu}^* = 120$ ksi

$E_f = 10500$ ksi

GFRP Sheet thickness, $t_t = 0.0139$-in.

- Check the flexural tension stress:

    Assuming face shell mortar bedding, the moment of inertia of the section is estimated by the ASTM C90 to be equal to 309 in^4 per foot of wall.

    According to the MSJC provisions the allowable flexural tension is 25 psi. Considering the $^1/_3$ increase for wind loading, the allowable stress is 33.3 psi. The acting tensile stress is:

$$f_t = \frac{M(t_m/2)}{I} = \frac{(1.15\,ft - kips/ft)(12)(7.625\,in/2)}{309\,in^4} = 170\,psi, \quad \text{which} \quad \text{greatly}$$

exceeds the allowable tensile stress. Therefore, the URM wall needs upgrading.

- Compute the nominal flexural capacity

The ultimate moment due to wind loads can be estimated as:

$$M_u = 1.3(1.15\,ft - kips/ft) = 1.5\,ft - kips/ft$$

The nominal flexural capacity is calculated as:

$$M_n = \frac{M_u}{\phi} = \frac{(1.5\,ft - kips/ft)}{0.7} = 2.1\,ft - kips/ft$$

The effective usable stress is estimated from equation (4.4) as:

$$f_{fe}^* = 0.008E_f = 0.008(10500\,ksi) = 84\,ksi$$

Considering an environmental factor C_E equal to 0.8, the effective stress is:

$$f_{fe} = C_E f_{fe}^* = 0.8(84\,ksi) = 67.2\,ksi$$

To determine the ratio n between the modulus of elasticity of FRP reinforcement and masonry, the latter can be estimated as $E_m = 900f'_m$ (MSJC, 2000). Thus:

$$E_m = 900(2000\,psi) = 1800\,ksi, \text{ and } n = \frac{E_f}{E_m} = \frac{(10500\,ksi)}{(1800\,ksi)} = 5.83$$

The coefficient k is computed by equation 2.3.7.16 as:

$$k = \sqrt{(5.83\rho_f)^2 + 2(5.83\rho_f)} - 5.83\rho_f$$

The amount of required reinforcement is computed by solving equation (4.2):

$$(2.1\,ft - kips/ft) = \rho_f(67.2\,ksi)(12\,in)(7.625\,in)^2 \left(1 - \frac{\sqrt{(5.83\rho_f)^2 + 2(5.83\rho_f)} - 5.83\rho}{3}\right)$$

Solving for trial and error or another numerical method: $\rho_f = 0.00056$

The amount of strengthening is estimated as: $A_f = (0.00056)(8 \text{ in})(12 \text{ in}) = 0.054$ in^2/ft

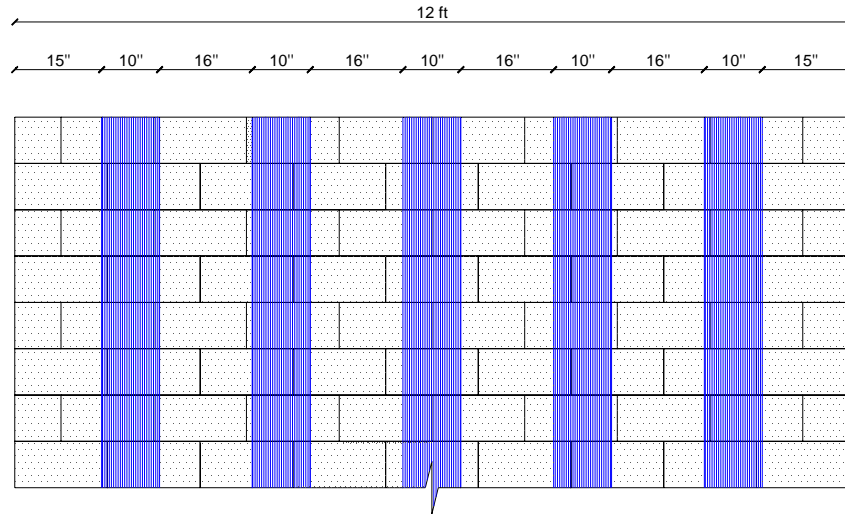The width of GFRP is: $w_f = \dfrac{A_f}{t_f} = \dfrac{(0.054\,in^2)}{(0.0139\,in)} = 3.8\,in/ft \therefore Use\,4.0\,in/ft$

The total length of required reinforcement is: (12 ft)(4.0 in/ft) = 48-in. The strengthening layout is illustrated in Figure 4.1.1a.

- Determine the clear spacing s_f

t_m and l_b are equal to 8-in. and 16-in., respectively.

Thus, in the relationship 6.16 the clear spacing can be calculated as:

$$s_f = \min\{2(8in.),16in.\} = 16in.$$

Fig. 4.1.1a *Strengthening Layout*

The presented design protocol did not take into account boundary regions, namely the possible occurring of local crushing in the boundaries of the masonry walls. *Tumialan* (2000) developed a method to predict the out-of-plane load causing local crushing in the masonry. This behavior is critical in walls constituted of brittle units with a very low compressive strength and with slenderness ratios averaging under 20: in this case in fact the so called arching effect is able to dramatically decrease the flexural performance of the walls. Therefore the presented protocol may be verified for walls with low slenderness ratios.

175

4.2 SHEAR STRENGTHENING WITH FRP RODS

Load reversal causes cracking and reduction in compression-shear transfer, aggregate interaction, and dowel action (*Priestley*, 1986). Therefore, for design purposes it may not bee too conservative to carry all the shear demand by the FRP reinforcement (i.e. $R_n = R_f$). The ultimate strength design requires that the design shear capacity must exceed the shear demand:

$$R_u \leq \phi R_n \tag{1}$$

The following assumptions are considered:

- Inclination angle of the shear cracks is constant and equal to 45°.

- The effective strength is reached in all the rods intersected by the diagonal crack.

- The effective strength is one half of that reported by the manufacturer.

4.2.1 Protocol

1. Determine the critical diagonal compression force in a masonry infill

A building with infill walls laterally loaded can be idealized as a diagonally braced frame, where the diagonal compression struts have an area bounded by the effective width w_m and the wall thickness. The diagonal strut is idealized as a truss element, which is connected by pins to the frame corners (see Figure 4.2a). There are different approaches to estimate w_m; for example the New Zealand Code (1990) suggests taking w_m as one-fourth of the length of the infill diagonal, d_m. The expressions showed herein intend to determine the forces in the infill wall for three failure conditions. These failure conditions are diagonal tension, sliding shear, and compression failure of diagonal strut. The lowest value initiates the failure of the infill panel. Figure 4.2b illustrates the geometry of the infill panel.
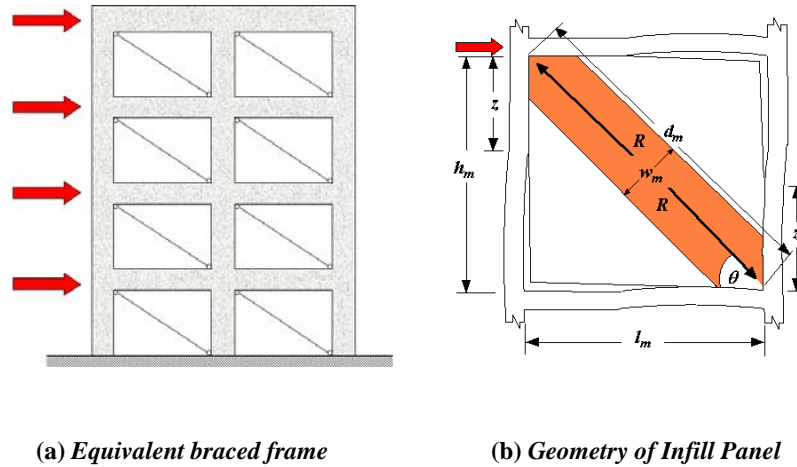
(a) *Equivalent braced frame*   (b) *Geometry of Infill Panel*

Fig. 4.2a-b *Equivalent Bracing Action of Infill Panel*

Diagonal Tension Failure

The diagonal force to initiate diagonal cracking (R_d) can be estimated by equating the shear stress caused by R_d and the allowable in-plane shear stresses provided by MSJC. Defining the horizontal net area as A_n, The acting stresses are computed based on the diagonal net area, which is expressed as A_n divided by the cosine of the angle θ. Assuming that $1.5\sqrt{f'_m}$ controls, the following derivations can be made:

$$\frac{R_d}{A_n / \cos\theta} = 1.5\sqrt{f'_m} \tag{2a}$$

$$R_d = 1.5\sqrt{f'_m} A_n \left(\frac{d_m}{l_m}\right) \tag{2b}$$

Sliding Shear Failure

It is assumed that the masonry panel does not carry vertical loads due to gravity effects. The assumption is based on the absence of a tight connection with the surrounding frame, and the separation of the frame and infill panel when the members are laterally loaded.

The maximum shear force resisted by the infill, V_p, can be expressed as:

$$V_p = \tau_o A_n + \mu N \tag{3a}$$

where τ_o is a shear bond, μ is a coefficient of friction, and, N is a normal (clamping) force to the shear plane. The vertical component of the diagonal force

to initiate sliding shear (R_s) is the only normal force across the sliding plane. V_p is the horizontal component of R_s. Thus:

$$R_s \cos \theta = \tau_o A_n + \mu R_s \sin \theta \qquad (3b)$$

$$R_s = \frac{\tau_0 A_n d_m}{l_m - \mu h_m} \qquad (3c)$$

Consider $\tau_o = 0.03 f'_m$ and $\mu = 0.3$ (*Paulay et al.*, 1992) or use the values provided by MSJC.

Compression Failure of Diagonal Strut

The following expression to determine the force causing compression failure of the diagonal strut has given a conservative agreement with test results (*Paulay at al.,* 1992)

$$R_c = \frac{2}{3} z\, t\, f'_m \sec \theta \qquad (4a)$$

where z is the vertical contact length between infill and column, and it can be estimated as:

$$z = \frac{\pi}{2} \left(\frac{4 E_c I_g h_m}{E_m t \sin 2\theta} \right)^{1/4} \qquad (4b)$$

where E_c and I_g are the modulus of elasticity and moment of inertia of the concrete columns, and E_m is the modulus of elasticity of the infill.

2. The shear force carried by the FRP reinforcement can be computed from the following expression:

$$R_f = 0.5 \left(\frac{Af}{s} \right) f^*_{fu}\, d_v \qquad (5)$$

where:

A_f = cross-sectional area of FRP shear reinforcement

s = spacing of reinforcement

d_v = actual depth of masonry in direction of shear considered

f^*_{fu} = tensile strength of the rods reported by the manufacturer

The factor of 0.5 is estimated empirically by MSJC (2001) for the shear strength contribution of steel reinforcement in beams, piers and columns. Similarly, the factor 0.5 in FRP structural repointing intends to account for the observed

mechanism of failure by assuming an effective stress in the rods equal to half of the ultimate strength. However, it is recognized that this factor can change with future research.

Changes to the masonry standards proposed by MSJC (2001) suggest a reduction factor ϕ equal to 0.8 when considering shear with or without axial load.

Since long-term exposure to various types of environments may reduce the tensile properties of the FRP reinforcement, the material properties used in design equations should be reduced based on the environmental exposure condition by an appropriate environmental reduction factor C_E (ACI-440, 2000). Thus:

$$f_{fu} = C_E f_{fu}^*$$
(6)

The environmental reduction factors given in Table 4.2.1a are conservative estimates based on the relative durability of each fiber type.

Table 4.2.1a *C_E Factor for Various Fibers and Exposure Conditions*

Exposure Condition	Fiber Type	C_E
Enclosed Conditioned Space	Carbon	1.00
	Glass	0.80
	Aramid	0.90
Unenclosed or Unconditioned Space	Carbon	0.90
	Glass	0.70
	Aramid	0.80

Design Example

A RC frame is infilled with a 6 in. hollow concrete block masonry wall with dimensions of 8 ft. long by 8 ft. high. The surrounding RC columns are 6 in. wide and 12 in. deep. Due to increased load demand, the load to be resisted by the infill wall has been computed as 20 kips. Assume the wall has the masonry units face shell mortar bedded. Determine if the infill wall can resist the required load. If the demand is exceeded, use FRP structural repointing to upgrade the shear capacity.

Masonry Properties: $f'_m = 1500$ psi

$E_m = 900 \, f'_m = 1'350,000$ psi (MSJC, 1999)

Concrete Properties: $f'_c = 4000$ psi

$E_m = 57,000 \sqrt{f'_c} = 3'605,000$ psi (ACI-318, 1999)

FRP Properties: $f^*_{fu} = 120$ ksi

$A_{rod} = 0.05$ in^2

- Estimate the critical diagonal force in the masonry infill

Diagonal Tension Failure:

Length and height of infill panel are $l_m = 8$ ft. and $h_m = 8$ ft., respectively. Thus, the diagonal can be computed as: $d_m = 11.31$ ft.

The shell mortar bedded thickness of 1.0 in. for 6 in. block results in the effective area:

$A_n = 2 \, (1.0 \text{ in.})(8 \text{ ft})(12 \text{ in}) = 192$ in^2

Then, the diagonal force initiating cracking can be estimated from equation 2b as:

$$R_d = 1.5\sqrt{1500\,\text{psi}}\,(192\,\text{in}^2)\left(\frac{11.31\,\text{ft.}}{8\,\text{ft.}}\right) = 15770\,\text{lbs} = 15.77\,\text{kips}$$

The load demand of 20 kips exceeds R_d, therefore the infill panel needs to be strengthened.

Sliding Shear Failure:

The MSJC provisions suggest the use of τ_o equal to 37 psi, and μ equal to 0.45. Thus the diagonal force initiating shear sliding is estimated from equation 3c as:

$$R_s = \frac{(37\,\text{psi})(192\,\text{in}^2)(11.31\,\text{ft.})}{(8\,\text{ft.}) - (0.45)(8\,\text{ft.})} = 18270\,\text{lbs} = 18.27\,\text{kips}$$

Compression Failure of Diagonal Strut:

The cross section of the RC columns is specified as 6 in. wide and 12 in. deep. Thus, the moment of inertia is estimated as: $I_g = 864 \text{ in.}^4$. The vertical contact length, z, between infill and column is estimated from equation 4b as:

$$z = \frac{\pi}{2}\left(\frac{4(3605\,\text{ksi})(864\,\text{in.}^4)(8\,\text{ft.})(12\,\text{in.})}{(1350\,\text{ksi})(5.625\,\text{in.})(\sin 2(45^\circ))} \right) = 31.29\,\text{in.}$$

The force to cause compression failure of the diagonal strut is computed by equation 4a:

$$R_c = \frac{2}{3}(31.29\,\text{in.})(5.625\,\text{in.})(1500\,\text{psi})(\sec 45^\circ) = 248930\,\text{lbs} = 548.93\,\text{kips}$$

- Determine the amount of FRP reinforcement

The shear demand was specified to be 20 kips; therefore considering a ϕ factor equal to 0.8, the nominal shear force R_f to be entirely carried by the FRP reinforcement is:

$$R_f = \frac{20\,\text{kips}}{0.8} = 25\,\text{kips}$$

The ultimate strength is calculated as: $f_{fu} = C_E f_{fu}^* = 0.8(120\,\text{ksi}) = 96\,\text{ksi}$

The environmental factor C_E equal to 0.8 is determined from Table 4.2.1a for enclosed conditioned space and for glass fibers.

The spacing of reinforcement is estimated from equation 5 as:

$$s = 0.5\left(\frac{A_f}{R_f} \right)f_{fe}d_v = 0.5\left(\frac{(0.05\,\text{in.}^2)}{(25\,\text{kips})} \right)(96\,\text{ksi})(96\,\text{in.}) = 9.2\,\text{in.}$$

$\therefore$ Use 11 # 2 GFRP rods, place them at every joint (spacing = 8.0-in.)

5.
CONCLUSIONS AND FUTURE WORK

The present investigation has demonstrated that FRP composites offer great benefits for the strengthening of masonry elements. FRP systems have been proven to increase remarkably flexure and shear capacities of URM elements. Provisional design protocols and recommendations for proper engineering and installation procedures, which are key to success, are presented.

5.1 MASONRY WALLS UNDER IN-PLANE LOADING

The following conclusions can be drawn from the walls strengthened by FRP Structural Repointing (Section 3):

- Remarkable increases in shear capacity and pseudo-ductility, ranging between 30% and 80%, can be achieved in concrete units walls. These increment levels should not be generalized for walls built with clay bricks, where different masonry characteristics (i.e. compressive strength) and wall geometries are observed (i.e. number of wythes and number of layers).

- For Series COW, two failure phases were identified: in-plane and out-of-plane. For Series CLW other two: vertical and horizontal. The in-plane component as well as the horizontal were observed to be the most critical.

- The out-of-plane phase is pronounced in walls having reinforcement eccentricity (i.e. only one side of the wall was strengthened). In those walls a reduction in pseudo-ductility was observed. The investigation of this condition was important because in field applications most of the times only one wall side is accessible.

- Walls where not every joint was strengthened failed by shear sliding. This mode of failure may be avoided by placing vertical reinforcement. However, shear sliding no necessarily occurs for masonry walls built with clay bricks strengthened with FRP laminates

- In contrast with URM walls, strengthened walls were stable after failure. In a real building, this fact can avoid injuries or loss of human life due to collapse.

- By assuming that the effective stress developed in the FRP rods is equal to a half of the ultimate stress, a provisional design protocol was presented.

This assumption needs to be verified studying different strengthening schemes and masonry typology.

5.2 MASONRY WALLS UNDER OUT-OF-PLANE LOADING

The following conclusions can be drawn from the walls strengthened by FRP laminates:

- FRP laminates have been proven to remarkably increase the flexural capacities of URM walls. Significant increases in flexural capacities, compared to the less strengthened wall, ranging between 50% and 300%, can be achieved in concrete and clay walls.

- Different modes of failures were observed in the tested specimens. According to previous researches, debonding of the FRP laminates has been proven to be the controlling mechanism of failure. The test results showed a critical relationship between the effective strain values in the laminates and debonding, which is profoundly related to the porosity of the masonry surfaces and their preparation prior to the application of the FRP reinforcement. No visible relationships were detected between delamination and type of laminate. Clay surfaces demonstrated to exhibit the best engagement for FRP sheets; in fact for this material ruptures of the laminates were observed. For concrete and clay masonry, where a large amount of FRP was provided, shear failures occurred.

- Analytical models were presented for determining the flexural capacity of the strengthened walls and the effective bonded lengths of the laminates. The models showed adequate correlation with the experimental results.

- Based on the previous analysis it was recommended to assume an effective strain of 0.008 in./in. in order to prevent debonding failures. A design protocol was so implemented, assuming that debonding is the governing mode of failure: for this reason, the amount of FRP reinforcement is limited, in order to prevent unexpected shear failures.

5.3 FUTURE WORK

The following recommendations for future work are formulated:

- For masonry strengthened with FRP laminates, there's a urgent need to correlate the debonding phenomenon with the porosity and the preparation of the masonry surfaces

- Boundary conditions such as presence of surrounding frames or slabs should be investigated to understand which are the critical factors that may affect the flexural strength of the masonry walls (slenderness ratios, masonry properties, etc.)

- For masonry walls strengthened by FRP structural repointing, the effective strain developed in the rods needs to be estimated as done in this experimental program for different strengthening schemes and masonry typologies

- For FRP structural repointing, more economical embedding materials to encapsulate the FRP rods in the mortar joints need to be explored. This materials might be mortars with improved bond properties, which can transfer tensile stresses to the reinforcement

- It is important to investigate the interaction of strengthened walls with the surrounding structural elements (i.e. beams and columns) since the effectiveness of the strengthening may be dangerously overestimated due to premature failures in the masonry or structural elements

- Investigation on surface preparation methods and amount of impregnating resins is also needed

APPENDIX A

MATERIAL CHARACTERIZATION

A.0 **Materials used in the experimental program**

This section presents the properties of the materials used in the experimental program. These materials included concrete blocks, clay bricks, mortar, GFRP rods, AFRP and GFRP laminates, epoxy paste, primer, putty and saturant.

Standard tests were performed to determine the compressive strength of mortar cubes and concrete and clay prisms. Bonding tests in order to calculate the anchorage length of AFRP laminates on concrete and clay masonry surfaces were conducted in laboratory environment. Tests on concrete unit and clay unit triplets were performed for the purpose of measuring the shear strength along mortar bed joints.

A.1 CONCRETE BLOCKS

A.1.1 OUT-OF-PLANE

Compression tests following ASTM C1314 standard protocol were performed. The concrete masonry units involved in this investigation are commonly employed in a particular masonry typology called infill panels, utilised as exterior walls in reinforced concrete frame structures to form part of the building envelope. A Tinius Olsen Universal Testing Machine was used to apply the compression load. The nominal dimensions of the concrete units are 4x8x12in. (0.102x0.203x0.305 m) (Fig. A.1.1). The specified block dimensions are 3/8 in. (10 mm) less than the nominal values to allow for a standard mortar joint thickness.

Fig. A.1.1a *Concrete block unit*

Four prisms consisting of two units incorporating one full mortar bedding in 3/8 in. (10mm) flush joint were constructed and tested (Fig. A.1.1b).

Fig. A.1.1b *Concrete prisms in lab environment*

In order to create a uniform distribution of compression stresses on the edges of the specimens two plywood strips were cut and inserted between the edges and the two cross-heads of the machine, as shown in Fig. A.1.1c; in this manner undesirable crushing failures at the borders were also prevented.

Fig. A.1.1c *Test preparation*

An extensometer was also bonded to one of the prism face shells in order to register the average vertical strain of the masonry sample. Applied load and strain values were recorded by a data acquisition system, consisting of Data general Conditioner Rack and LABTECH (Laboratory Technologies Corp.) data acquisition software. The sampling rate was set to 1 Hz. Fig. A.1.1c illustrates the test setup. Table A.1.1a gathers concrete unit geometrical data. Table A.1.1b summarises test results.

Fig. A.1.1c *Test setup*

Table A.1.1a *Concrete unit specifications*

Designation	Concrete hollow two-cells unit
Nominal dimensions (in.-mm)	4x8x12-102x203x305
Gross Area (in^2-mm^2)	42.37-2.73 E+04
Net Area (in^2- mm^2)	27.75-1.79 E+04
Percentage of solid (%)	65

Table A.1.1b *Test results*

Prism #	Compressive Strength f'$_m$ (psi-MPa)
1	1585-10.92
2	1189-8.19
3	1369-9.43
4	1513-10.42

Average compressive strength f'$_m$ (Net Area): 1414 psi (9.74 MPa)
Standard deviation: 151 psi (1.04 MPa)
Modulus of elasticity :900f'$_m$ =1272.6 ksi (8768 MPa) from MSJC Code (1999)

A.1.2 IN-PLANE

Similarly to 4 in. thick concrete block prisms, four samples built with the same geometry were subjected to compression tests; at the same time seven triplets were constructed in order to estimate shear stresses along mortar bed joints. In the latter case it was decide to apply three different confinement stresses, corresponding to the action carried by one, two and three masonry storages respectively.

Details of the concrete units are exposed in Table A.1.2a and in Fig. A.1.2a.

Table A.1.2a *Concrete unit specifications*

Designation	Concrete hollow two-cells unit
Nominal dimensions (in.-mm)	6x8x16-152x203x406
Gross Area (in^2-mm^2)	84.89-5.47 E+04
Net Area (in^2- mm^2)	54.89-3.54 E+04
Percentage of solid (%)	65
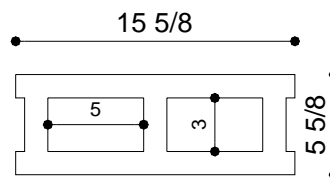
Fig. A.1.2a *Concrete block cross section (dimensions in inches)*

Fig. A.1.2b-c *Compression test: prism before (left) and after (right) failure*

As shown in Fig. A.1.2b, compression tests were performed under a Baldwin Test machine and the load values were recorded by means of a suitable data acquisition system, consisting of Data general Conditioner Rack and LABTECH (Laboratory Technologies Corp.) data acquisition software.

Test results are presented in Table A.1.2b.

Table A.1.2b *Compression: test results*

Prism #	Compressive Strength f'$_m$ (psi-MPa)
1	2608-17.99
2	2230-15.36
3	1989-13.70
4	2889-19.90

Average compressive strength f'$_m$ (Net Area): 2430 psi (16.74 MPa)
Standard deviation: 345 psi (2.37 MPa)
Modulus of elasticity :900f'$_m$ =2187 ksi (15068 MPa) from MSJC Code (1999)

In order to estimate shear stresses developed along bed mortar joints seven triplets were constructed as shown in Fig. A.1.2d. Cohesion and coefficient of friction according to Coulomb criterion expression $\tau=\tau_o+\mu\sigma_n$ were calculated by means of linear interpolation of the data provided by the tests.
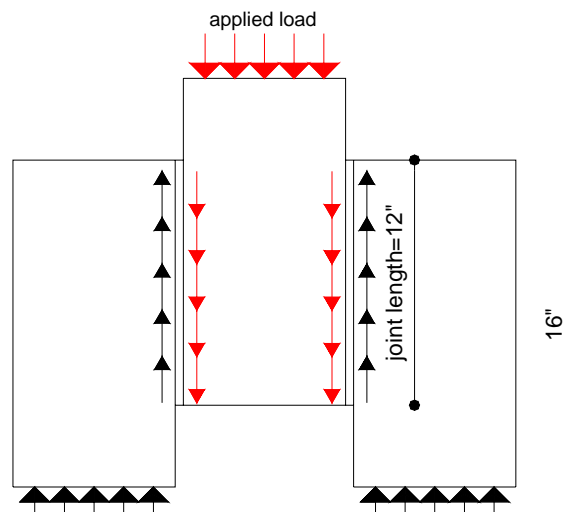
Fig. A.1.2d *Scheme of bed joint shear test*

The three confinement stresses resulted 72 psi, 144 psi, 216 psi respectively, correspondent to 0.5 MPa, 1 MPa and 1.5 MPa. As shown in Fig. A.1.2e it was obtain, according to Coulomb criterion: $\tau=57.43+0.6679\sigma_n$ (psi) for $\sigma_n<216$ psi.
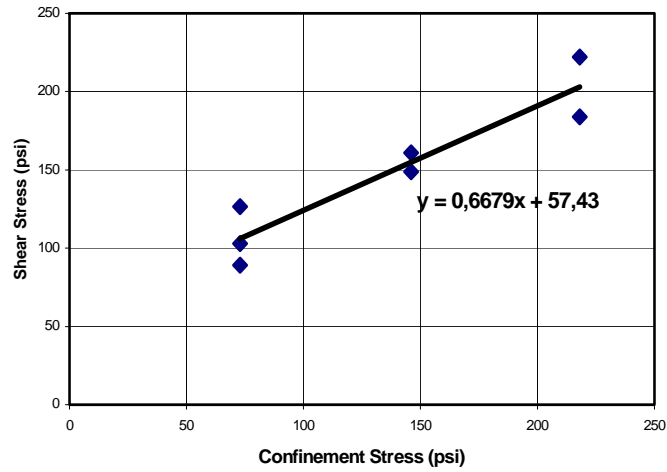
Fig. A.1.2e *Test results from concrete triplets*

Fig. A.1.2f *Concrete block triplet under loading*

A.2 CLAY BRICKS

A.2.1 OUT-OF-PLANE

Compression tests were performed on four prisms made of dark molded bricks. Modern clay units often have compressive strengths much higher than required to satisfy product specifications and generally exceed by large margins the requirements for member design strengths. However, in order to calculate the correct amount of FRP reinforcement for wallettes subjected to out-of-plane loading, this type of tests was required by the experimental program.

Table A.2.1a *Specifications for clay bricks*

Designation	Clay solid unit
Nominal dimensions (in.-mm)	4x8x2.5-102x203x64
Gross Area (in^2-mm^2)	27.64-1.78 E+04
Net Area (in^2- mm^2)	23.20-1.42 E+04
Percentage of solid (%)	84
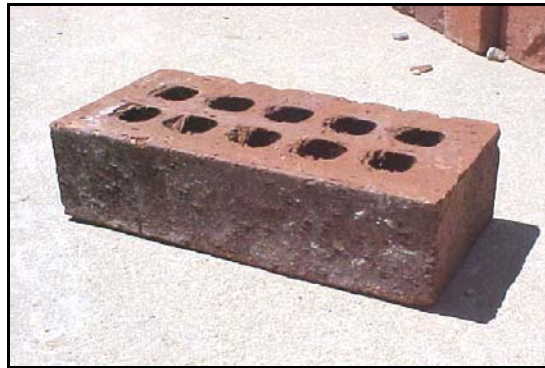
Fig. A.2.1a *Dark molded clay brick unit*

ASTM C1314 standard protocol was followed. Similarly to compression tests on concrete coupons a Tinius Olsen machine was used. Applied load and average vertical strain of the masonry specimens were recorded with the same instrumentation. The tests were performed in displacement control mode. Test results are illustrated in Table A.2.1a.

Table A.2.1b *Dark bricks: test results*

Prism #	Compressive Strength f'$_m$ (psi-MPa)
1	2435-16.77
2	2550-17.60
3	2600-17.91
4	2520-17.36

Average compressive strength f'$_m$ (Net Area): 2500 psi (17.23 MPa)
Standard deviation: 50 psi (0.35 MPa)
Modulus of elasticity :700f'$_m$ =1750 ksi (12057 MPa) from MSJC Code (1999)

Fig. A.2.1b-c *Dark clay prism before (left) and after failure (right)*

A.2.2 IN-PLANE

Compression tests were also performed using light extruded bricks. No differences were applied in the test procedure. Nominal dimensions, gross area, net are and percentage of solid correspond to dark brick specifications. The only difference are the manufacturing process and the type of clay. Test results are presented in Table A.2.1b.

Table A.2.1c *Clay prisms: test results*

Prism #	Compression Strength f'$_m$ (psi-MPa)
1	2161-14.89
2	2431-16.75
3	1940-13.37
4	1982-13.66

Average compression strength f'$_m$ (Net Area): 2129 psi (14.67 MPa)
Standard deviation: 193 psi (1.33 MPa)
Modulus of elasticity :700f'$_m$ =1490 ksi (10266 MPa) from MSJC Code (1999)
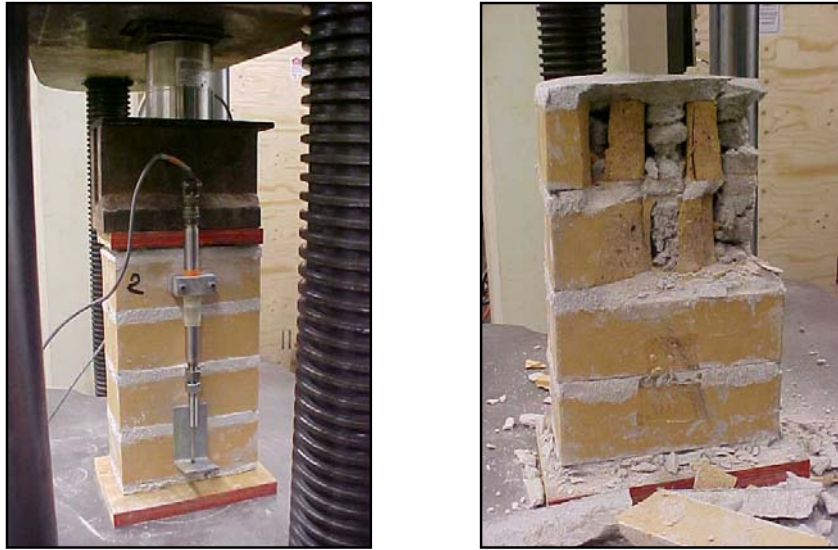
Fig. A.2.1d-e *Light clay prisms before (left) and after (right) failure*

Nineteen triplets were also constructed in order to extimate the shear stresses along the bed mortar joints. Four confinement stresses were chosen: 7 psi, 14 psi, 42 psi, 70 psi, corresponding to 0.05, 0.1, 0.3, 0.5 MPa. Test results are showed in Fig. A.2.1b. According to Coulomb criterion $\tau = 119.57 + 1.35\sigma_n$ (psi) for $\sigma_n < 70$ psi
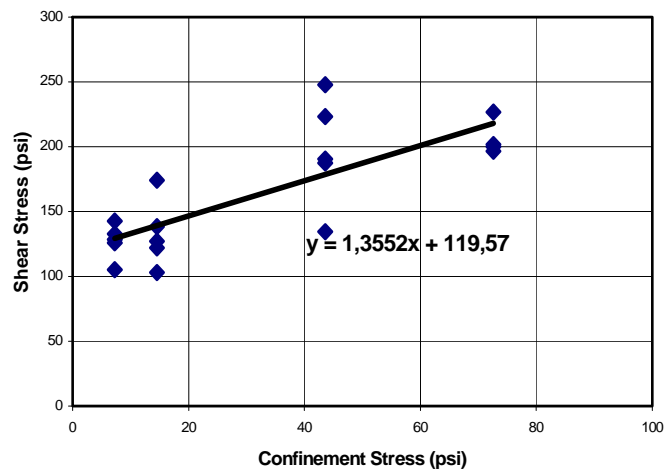
Fig. A.2.1f *Test results from clay triplets*

Fig. A.2.1g *Clay triplet under loading*

A.3 MORTAR

   The mortar used for the wallettes was available in bags in a dry premixed composition of cement and sand, and was classified as Type N according to the standard ASTM C270. Table A.3a illustrates property specifications requirements for Type N masonry mortar.

Table A.3a *Specifications for type N masonry mortar*

Mortar	Type	Average compressive strength at 28 days (psi-Mpa)	Water Retention (%)	Air Content (%)
Masonry cement	N	750-5.2	75	20

According to ASTM C1019 two groups consisting of six cubes 2x2x2 in. each were built using a special plastic grid. Series A was created utilizing mortar used for the construction of clay and concrete block wallettes for out-of-plane tests and for concrete block panels for in-plane tests, whereas Series B referred to the construction of clay panels for in-plane experimental program.

The load was applied by means of a Tinius Olsen Machine: strain gages were bonded on the face shells of the cubes in order to estimate the vertical and horizontal strains when loading, and in ultimate analysis to calculate the Poisson ratio value.

Test results are illustrates in Table A.3b.

Table A.3b *Mortar: test results*

Prism #	Compression Strength f'$_m$ (psi-MPa)
A1	950-6.55
A2	700-4.82
A3	705-4.85
A4	638-4.40
A5	850-5.86
A6	1100-7.58
B1	1480-10.20
B2	1790-12.33
B3	1640-11.29
B4	1606-11.06
B5	1195-8.23
B6	1313-9.05

Series A
Average compressive strength f'$_m$: 823 psi (5.67 MPa)
Standard deviation: 161 psi (1.10 MPa)
Series B
Average compressive strength f'$_m$: 1504 psi (10.36 MPa)
Standard deviation: 203 psi (1.40 MPa)

As shown in Table A.3b big differences in values were observed between Series A and Series B. This may be explained because of different handworkers involved in the preparation of the specimens.
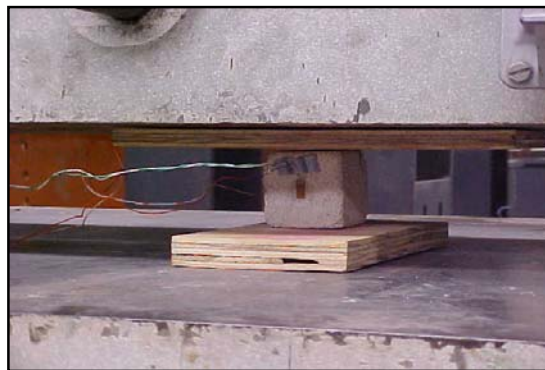
Fig. A.3a *Mortar cube under loading*

A11

A.4 FRP MATERIALS

A.4.1 AFRP AND GFRP LAMINATES

Mechanical properties of AFRP (Aramid) and GFRP (Glass) fabrics used at the beginning of the experimental program are presented in Table A.4.1a. All the data were provided by the manufacturers.

Table A.4.1 *Mechanical properties for Aramid and E-Glass Fabrics*

Designation	Fiber Type	Guaranteed Ultimate Strength, ksi (MPa)	Load per Sheet width, lbs/in (kN/mm)	Tensile Modulus, ksi (MPa)	Guaranteed Ultimate Strain (%)
AK60	Aramid	290(1998)	3190(0.56)	17000(117130)	1.7
EG 900	E-Glass	220(1516)	3050(0.53)	10500(72345)	2.1

A.4.2 PRIMER, PUTTY, SATURANT

In Table A.4.2 mechanical properties of primer, putty and saturant are exposed. Similarly to Section A.4.1, all the data were provided by the manufacturers.

Table A.4.2 *Mechanical properties for primer, putty and saturant*

Material	Tensile Strength, psi, (kPa)	Tensile Elastic Modulus, ksi (MPa)	Tensile Strain (%)	Compressive Strength psi, (kPa)	Compressive Modulus ksi, (MPa)	Bond Strength psi, (MPa)
Primer	1800 (12400)	105 (723.5)	3	3500 (24100)	95 (654.5)	NA
Putty	1800 (12400)	260 (1791.4)	1.5	3500 (24100)	155 (1068.0)	NA
Saturant	7900 (54400)	440 (3031.6)	2.5	12500 (86100)	380 (2618.2)	NA

A.4.3 GFRP RODS

In Table A.4.2 mechanical properties of GFRP rods utilised as Near Surface Mounted (NSM) rods are illustrated. As for AFRP and GFRP laminates, the data were provided by the manufactures.

Table A.4.2 *Mechanical properties of GFRP rod #2*

BAR SIZE # (mm)	Cross-Sectional Area, $in^2 (mm^2)$	Nominal Diameter, in (mm)	Tensile Strength, ksi (MPa)	Tensile Modulus of Elasticity, ksi (MPa)	Max Bond Stress to Concrete psi (kPa)
2(6)	0.0515 (33.23)	0.250 (6.35)	110 (760)	5920 (40789)	1679 (11568)

A.4.4 AFRP AND GFRP LAMINATES/LAB TESTS

In order to verify the mechanical properties provided by the manufacturers of AFRP and GFRP laminates, tensile tests on thin flat strip of material having a constant rectangular cross section were performed in laboratory environment, following specifications provided by ASTM D3039.

Laminate panels were fabricated by the well known wet lay-up technique (Fig. A.Aa) and coupons were cut from the panels after complete cure. A 610x460x16 mm plywood sheet was set as the base of the mold which was a rectangular plastic plate covered with a thin polyethylene film as the release agent. After the mold was prepared, a thin layer of saturant was placed on it with a roller. Then the aramid and glass fiber plies were spread on the saturant layer and a plastic roller was used to remove air entrapped between fiber plies and saturant.

Fig. A.4.4a *Final impregnation of laminate plies*
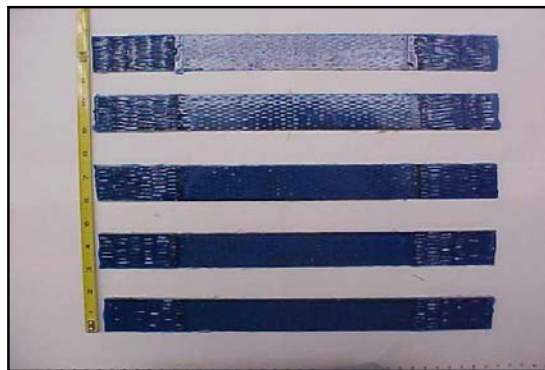
Fig. A.4.4b *Coupons to be tested*

After approximately 30 minutes, a second layer of saturant was applied and the plastic roller was used again to work the resin into the fibers. The wet laminates were left to

cure for seven days and then released from the mold. The laminate panels were then ready to be cut into coupons along predetermined lines in order to obtain equal widths of 1.5 in. (38 mm). All the specimens had a gage length of 15 in. (381 mm) as shown in Fig. A.4.4b. Strain gages were attached to the mold-side surface of the specimens in the longitudinal and transverse directions. The load was acquired by the built-in hydraulic pressure transducer of the INSTRON 4485 machine. In this testing frame, as shown in Fig. A.4.4c, the loading head is rotationally self-aligning, which eliminates the potential of bending and twisting the specimen. The wedge grips are self-tightening, to keep a constant pressure, so the clamping conditions do not change due to laminate contraction. All specimens were tested under displacement control with a constant loading speed of 2mm/min (*ASTM* 1995; *Tarnopol'skii and Kincis* 1985).

Fig. A.4.4c *Test setup*   **Fig. A.4.4d** *Coupon failure*

In Table A.4.4a-b test results for AFRP and GFRP laminates respectively are presented.

Table A.4.4a *AFRP laminates: test results*

Designation	Maximum Strain (%)	Maximum Stress ksi (GPa)	Modulus of Elasticity ksi (GPa)
A1	1.48	242.3(1.67)	16981(117)
A2	1.64	281.5(1.94)	20464(141)
A3	1.52	255.4(1.76)	17417(120)
A4	1.74	300.4(2.07)	17126(118)
A5	1.76	287.3(1.98)	16836(116)
A6	1.66	269.9(1.86)	16546(114)

A14

Table A.4.4b *GFRP laminates: test results*

Designation	Maximum Strain (%)	Maximum Stress ksi (GPa)	Modulus of Elasticity ksi (GPa)
G1	2.14	253.9(1.75)	11321(78)
G2	1.63	246.7(1.70)	11901(82)
G3	2.16	249.6(1.72)	12337(85)
G4	1.59	243.8(1.68)	12337(85)
G5	1.80	217.7(1.50)	12046(83)
G6	1.60	256.9(1.77)	12046(83)

AFRP
Average maximum strain: 1.633%
Standard deviation: 0.114%

Average maximum stress: 272.8 ksi (1.88 GPa)
Standard deviation: 20.8 ksi (0.144 GPa)

Average modulus of elasticity: 17576 ksi (121.1 GPa)
Standard deviation: 1442.6 ksi (9.94 GPa)

GFRP
Average maximum strain: 1.820%
Standard deviation: 0.266%

Average maximum stress: 245.3 ksi (1.69 GPa)
Standard deviation: 14.0 ksi (0.097 GPa)

Average modulus of elasticity: 12065 ksi (83.13 GPa)
Standard deviation: 361.4 ksi (2.49 GPa)

A.5 CHARACTERIZATION OF FRP LAMINATES
     BONDED TO MASONRY SURFACES

A.5.1 Background

FRP laminates are successfully used for strengthening of existing RC and PC structures. Bond of the external FRP reinforcement to the concrete substrate is of critical importance for the effectiveness of this technique. Bond mechanism consists of shear transfer mechanism and local region tension at the interface between the concrete and FRP. Delamination before ultimate FRP strain may be encountered.

In the case of masonry, have shown that debonding of FRP laminates is the predominant mode of failure. Therefore, the issue of bond is also one of the ultimate states to consider in the design of strengthening with externally bonded FRP laminates. To date there has been few bond research conducted on masonry elements (*Roko et al.,* 1999); the objective of this section is to develop an analytical model to determine the proper bonded length for FRP laminates.

A.5.2 Test specimens

Standard hollow concrete blocks and clay brick specimens were tested, to investigate the bond behavior of AFRP sheets on different types of masonry surface. Mechanical properties of AFRP laminates, primer, putty and saturant are illustrated in the previous section.

To determine the effective bonded length several lengths were investigated; different widths of AFRP sheets were employed to evaluate the different behavior and size effect. Depending on these variables, the configurations of the blocks were different, as shown in Fig. A.5.2a.

(A)   (B)   (C)   (D)
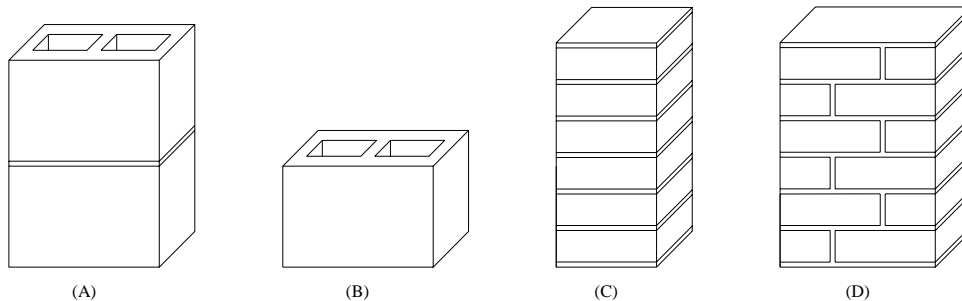
Fig. A.5.2a *Specimens configuration*

Two prisms were used for each test; Fig. A.5.2b shows the configuration utilised for the tests explaining in what way the generic blocks (X and Y) were positioned:

SIDE VIEW OF THE SPECIMENS
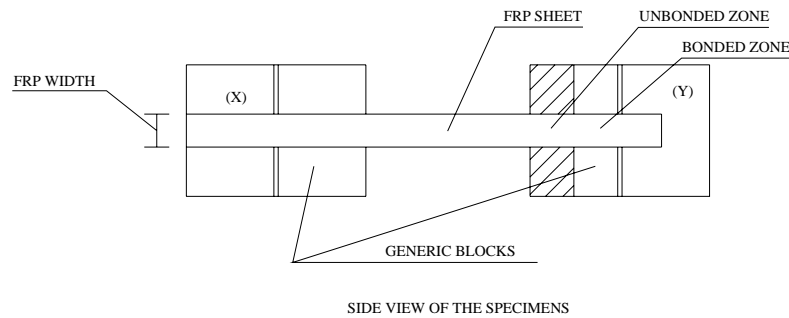
Fig. A.5.2b *Generic test configuration*

Tables A.5.2a and A.5.2b summarises the test configurations:

Table A.5.2a *Test configuration for concrete blocks*

Test name	FRP width (mm)	Bonded length (mm)	Unbonded length (mm)	Blocks used (X - Y)
CA3-4	76.2	101.6	101.6	A - B
CA3-8	76.2	203.2	101.6	A - A
CA3-12	76.2	304.8	101.6	A - A
CA6-4	152.4	101.6	101.6	A - B
CA6-8	152.4	203.2	101.6	A - A
CA6-12	152.4	304.8	101.6	A - A

Note: 1 mm = 0.03937 in

Table A.5.2b *Test configuration for clay bricks*

Test name	FRP width (mm)	Bonded length (mm)	Unbonded length (mm)	Blocks used (X - Y)
BA3-4	76.2	101.6	101.6	C - C
BA3-8	76.2	203.2	101.6	C - C
BA3-12	76.2	304.8	101.6	C - C
BA6-4	152.4	101.6	101.6	D - D
BA6-8	152.4	203.2	101.6	D - D
BA6-12	152.4	304.8	101.6	D - D

Note: 1 mm = 0.03937 in

The dimensions of the blocks are described in Section A.1.1. One FRP sheet was applied to each face of the blocks in the longitudinal direction, connecting the two blocks together. Only one block was instrumented, this area called *test region* had the

A17

AFRP laminate with a limited bonded length and being unbonded the remaining part (using adhesive tape) to force the delamination in the test region. Length and position of the bonded part were the same on both faces of the test block. However, to avoid failure in the non-instrumental regions, transversal sheets were applied as shown in Fig. A.5.2c.
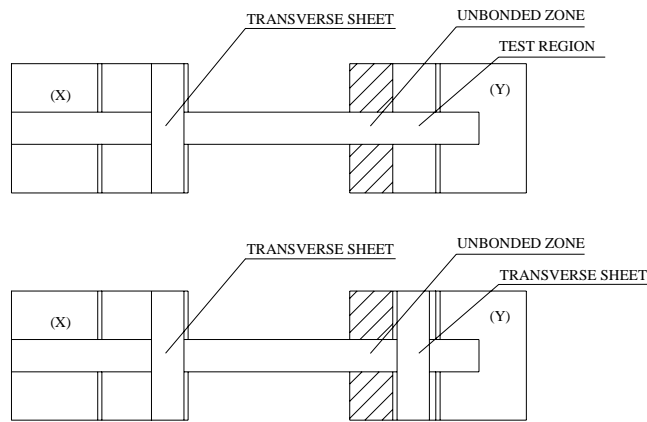
Fig. A.5.2c *Side views of the specimens*

The test specimens were laid on the floor, after they were aligned along the major axis (Fig. A.5.2d).

Fig. A.5.2d *Specimens aligned*

Then, the specimens were prepared using the well-known wet lay-up technique.
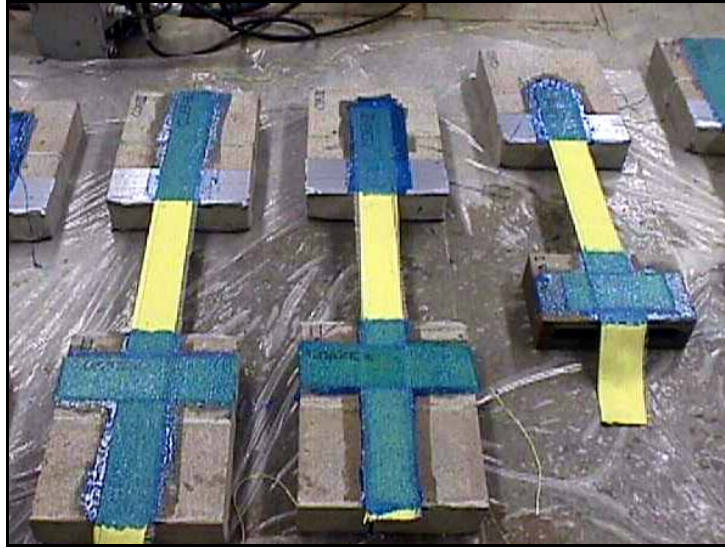
Fig. A.5.2e *Specimens to be tested*

The only difference between concrete blocks and bricks were the application of putty on the bricks surfaces, but in the test region it was applied only to cover the surface irregularities, to not influence significantly the bond behavior.

Strain gages were applied on the AFRP laminates to monitor the strain distribution along the laminate during the tests. All the strain gages had a gage length of 12.7 mm (1/2 inch) to ensure localized strain measurement. The surface of laminate was smoothed and conditioned to assure a perfect bond between strain gage and sheet.

Two strain gages were applied on the unbonded region at 25.4 mm (1 in.) from the beginning of the unbonded region; their spacing was 50.8 mm (2 in.). The unbonded regions were taken 101.6 mm (4 in.) for all the specimens.

The others strain gages in the bonded region were applied from 25.4 mm (1 in.) by the beginning of this region, their distance were 50.8 mm (2 in.) except for the bond length of 101.6 mm (4 in.) where the distance was only 25.4 mm (1 in.).

Fig. A.5.2f illustrates the typical location of the strain gages on the AFRP laminates.
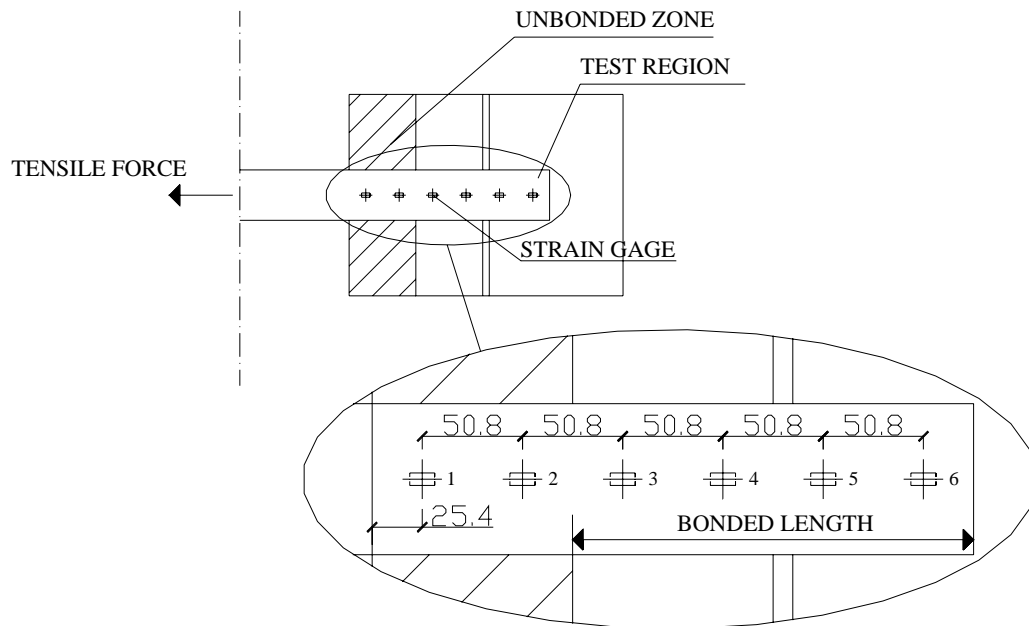
Fig A.5.2f *Strain gage location*

A.5.3 Test Setup

The test bed consisted of a steel plate with dimensions 1524 mm (5 ft.) by 609.6 mm (2 ft.) and thickness of 3.175 mm (1/8 in.). Five steel angles were bolted on the plate to delimitate the position where the blocks had to be placed. The purpose of the plate was to ensure the proper positioning of the specimens during preparation and testing. Grease was placed between the plate and the bottom surface of the blocks, in order to minimize the friction between the two surfaces during testing.

Load was applied by means of a 12-ton hydraulic jack connected to a hydraulic pump. The jack was placed horizontally between the two blocks.

A Sensotek pressure transducer connected to the hydraulic jack recorded the load. Load and strains were all recorded with a one-Hertz sampling rate by a LABTECH data acquisition system. Figures A.5.3a and A.5.3b illustrate the test setup.
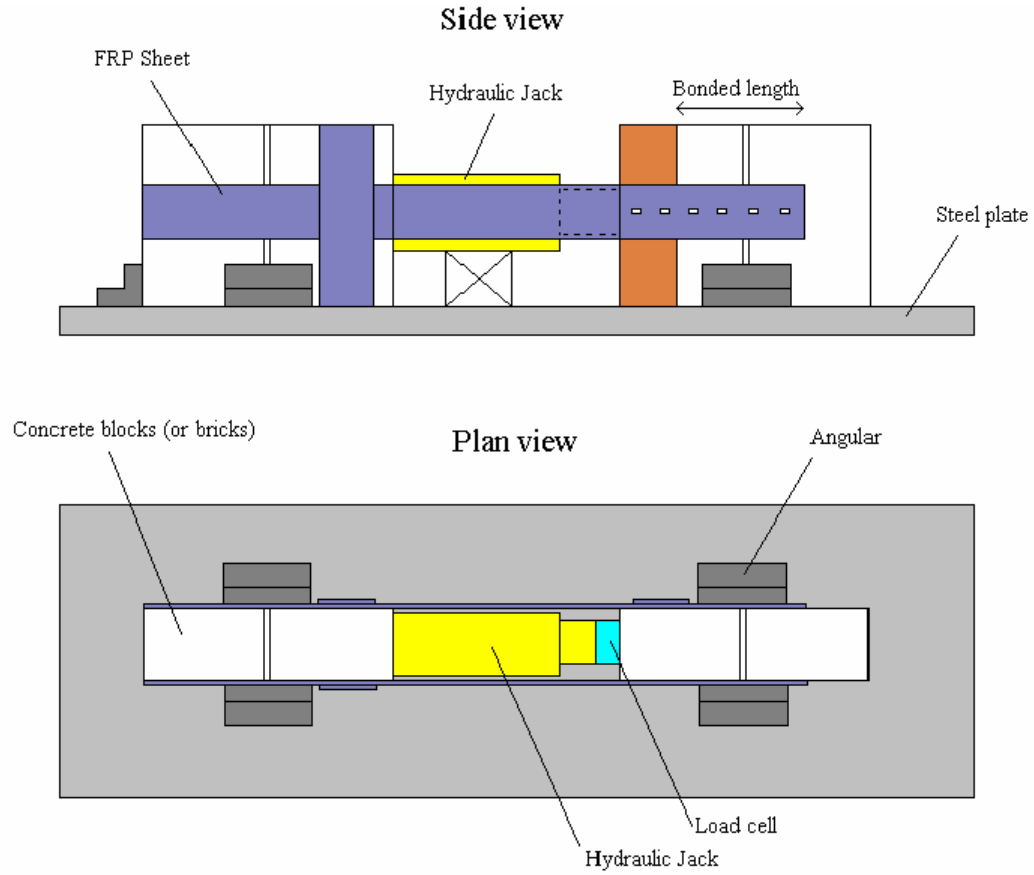
Fig. A.5.3a *Test setup scheme*

Fig. A.5.3b *Test setup*

A21
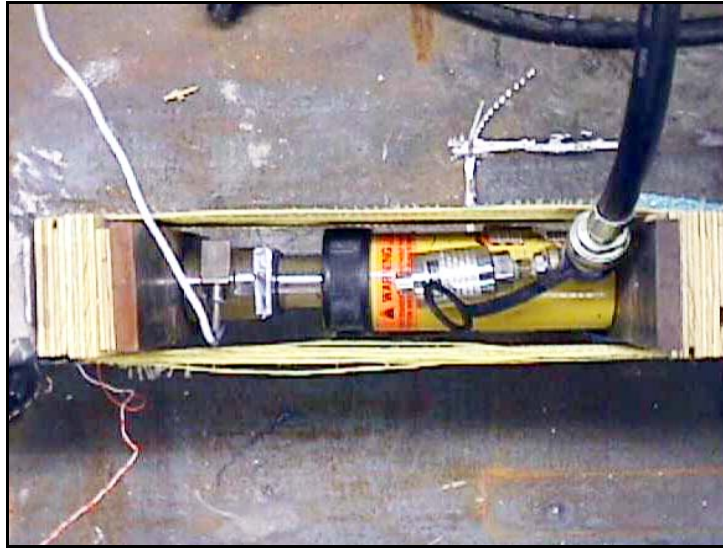
Fig. A.5.3c *Detail of hydraulic jack and pressure transducer*

A.5.4 Test Results

Test results in terms of ultimate load and failure mode are summarized in Table A.5.4a and A.5.4b. The value of the ultimate load was obtained dividing by two the maximum load registered by the load cell.

Table A.5.4a *Test results for Concrete Masonry*

Test name	Sheet width (mm)	Bonded length (mm)	Ultim. load (kN)	Failure mode
CA3-4	76.2	101.6	23.7	D
CA3-8	76.2	203.2	26.5	D
CA3-12	76.2	304.8	24.6	R+D
CA6-4	152.4	101.6	37.5	D
CA6-8	152.4	203.2	48.2	D
CA6-12	152.4	304.8	48.9	D

Table A.5.4b *Test results for Clay Masonry*

Test name	Sheet width (mm)	Bonded length (mm)	Ultim. load (kN)	Failure mode
BA3-4	76.2	101.6	29.0	D
BA3-8	76.2	203.2	27.9	D
BA3-12	76.2	304.8	24.0	R+D
BA6-4	152.4	101.6	46.4	D
BA6-8	152.4	203.2	31.3	D
BA6-12	152.4	304.8	46.6	D

Legend: D = Delamination ; R = Fiber rupture   Note: 1 mm = 0.03937 in ; 1 kN = 0.2248 kips

As indicated in Tables A.5.4a and A.5.4b, two different failure modes were observed. In the specimens CA3-12 and BA3-12 with 304.8 mm (12 in.) of bonded length, failure occurred by fiber delamination (not complete, the fiber did not detach completely from the specimens) in the test region followed by fiber rupture on the other side. This can be explained as follows: during delamination process, load switched in the backside of the specimens because of eccentricity causing suddenly the fiber rupture.
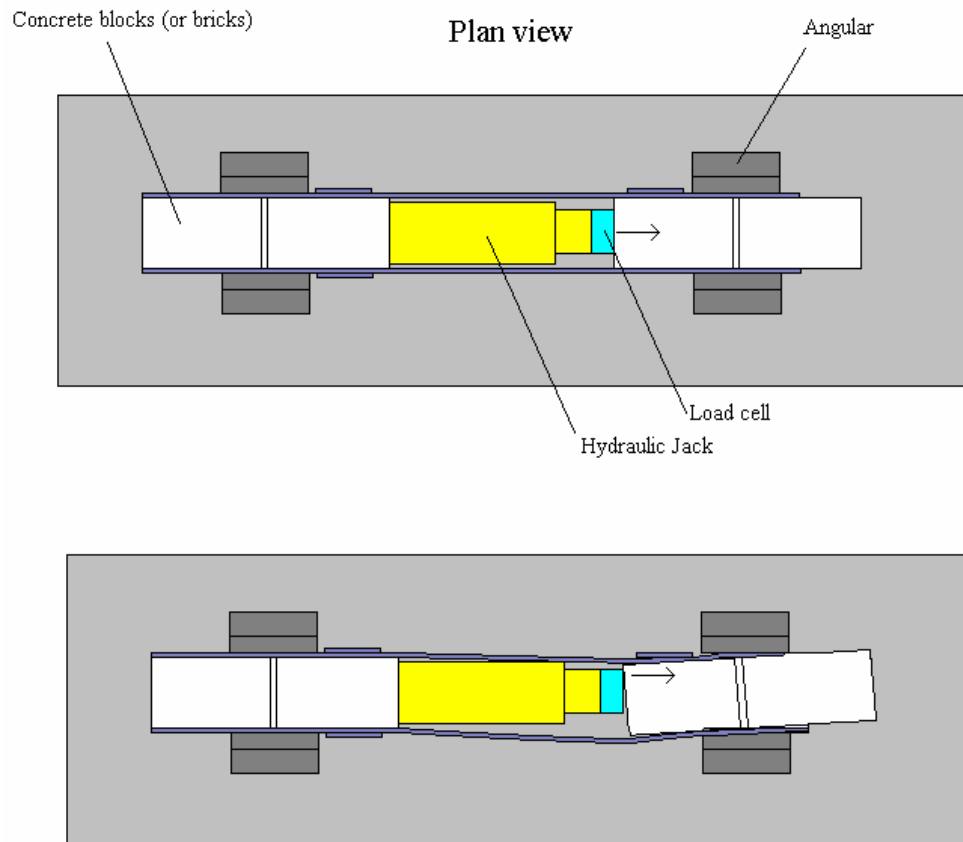
Fig. A.5.4a *Cause of failure in tests CA3-12 and BA3-12*

In the remaining specimens failure occurred only for delamination. Due to geometrical imperfections, the tensile force was not perfectly centered. These imperfections were evident when the specimens were not perfectly aligned. This eccentrical force introduced an additional bending moment. Previous study on this phenomenon (*Van Gemert D. et al.*, 2001) had shown that no significant differences were recorded. Due to the eccentricity, a premature peeling off of the FRP laminates could be observed, which can explain the mode of failure observed in specimens CA6-4 and BA6-8.

Fig. A.5.4b illustrates the debonding for several specimens; it can be seen also that some concrete blocks and masonry bricks surrounding the fiber were damaged, meaning that a good engagement was created between FRP laminates and masonry surface.

(a) Test CA3-8

(b) Test CA6-4

(c) Test BA6-12

(d) Test BA6-8

(e) Damage in masonry bricks

(f) Damage in concrete blocks

Fig. A.5.4b *Failure modes*

A.5.5 Strain Data

Strain gages were placed at various locations to monitor the strain distribution along the laminate during the test. The strain gages were numbered starting from one in the unbonded region towards the sheet free end.

The two strain gages in the unbonded region were used to determine the tensile modulus of elasticity of the FRP laminate. Assuming the strain the average between the two strain gages in the unbonded region and building the load-strain diagram the axial stiffness EA can be found (Fig. A.5.5a).
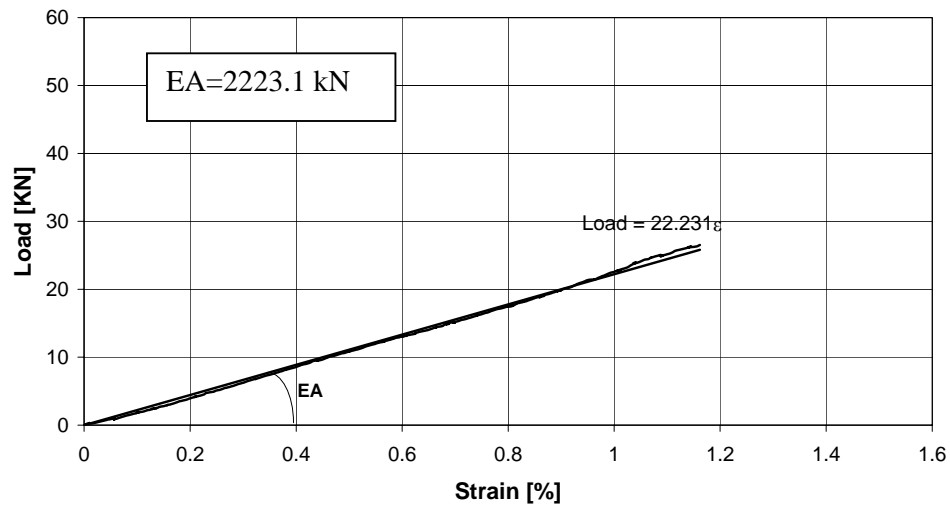
Fig. A.5.5a *Axial stiffness for CA3-8*

Then, can be calculated the FRP tensile modulus simply dividing the axial stiffness by the FRP area relating to that test.

Tables A.5.5a and A.5.5b show the values of the AFRP tensile elastic modulus calculated for all the specimens.

Table A.5.5a *Experimental tensile modulus of elasticity for AFRP on concrete blocks*

Specimen	Width (mm)	Bond Length (mm)	Thickness* (mm)	Axial Stiffness EA (kN)	E (GPa)
CA3-4	76.2	101.6	0.28	2263.1	106.1
CA3-8	76.2	203.2	0.28	2223.1	104.2
CA3-12	76.2	304.8	0.28	2236.9	104.8
CA6-4	152.4	101.6	0.28	3826.5	89.7
CA6-8	152.4	203.2	0.28	4701.8	110.2
CA6-12	152.4	304.8	0.28	3985.9	93.4

Note:1 mm = 0.03937 in; 1 KN = 0.2248 Kip; 1 MPa = 145 Psi * = Values from manufacturer

Table A.5.5b *Experimental tensile modulus of elasticity for AFRP on masonry bricks*

Specimen	Width [mm]	Bond Length [mm]	Thickness* [mm]	Axial Stiffness [KN]	E [GPa]
BA3-4	76.2	101.6	0.28	N/A	N/A
BA3-8	76.2	203.2	0.28	2381.4	111.6
BA3-12	76.2	304.8	0.28	1855.7	87.0
BA6-4	152.4	101.6	0.28	4081.4	95.6
BA6-8	152.4	203.2	0.28	N/A	N/A
BA6-12	152.4	304.8	0.28	4518.4	105.9

Note:1 mm=0.03937 in; 1 KN=0.2248 kip; 1 MPa=145 Psi
* = Values from manufacturer; N/A = Not available

The experimental tensile modulus of elasticity is computed as by the average of all these values and it is equal to 100.80 GPa (14616 ksi).

This value is lower that provided by manufacturer value that is 117.20 GPa (17000 ksi). The strain gages in the bonded region were used to determine the bond behavior for the FRP sheet.

Assuming that the strain at the beginning of the bonded region at determinate values of load is:

$$\varepsilon_b = \frac{N}{E_t A}$$

where:

N = load

E_t = experimental modulus of elasticity (average)

A = AFRP area

The strain-location graphics can be found.

Fig. A.5.5b and A.5.5c show strain-location graphics for two specimens; from the experimental results, it can be observed that the strain vs. location graphics for concrete blocks and masonry bricks have similar behavior and that the bonded length does not significantly influence the ultimate load.
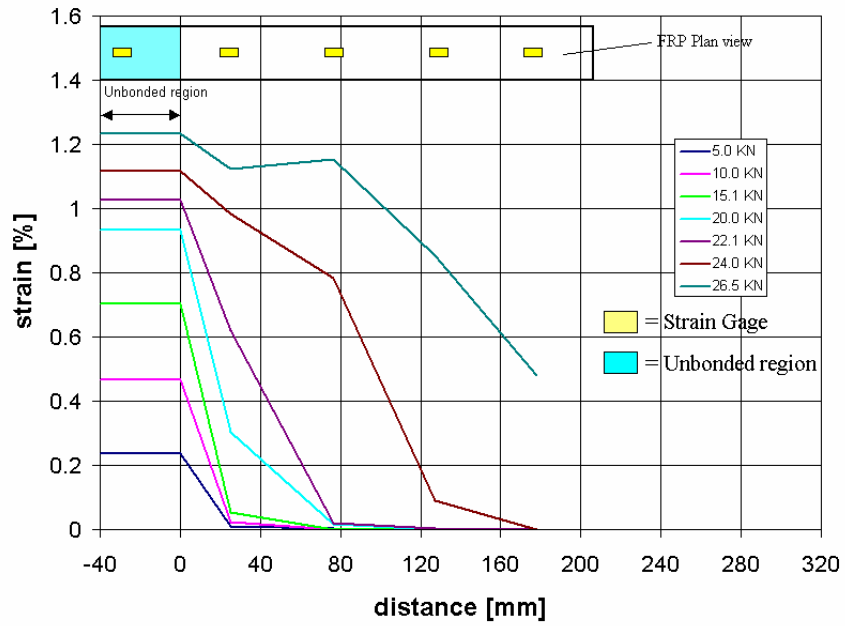
Fig. A.5.5b *Typical strain vs. location graph for concrete blocks (specimen CA3-8)*
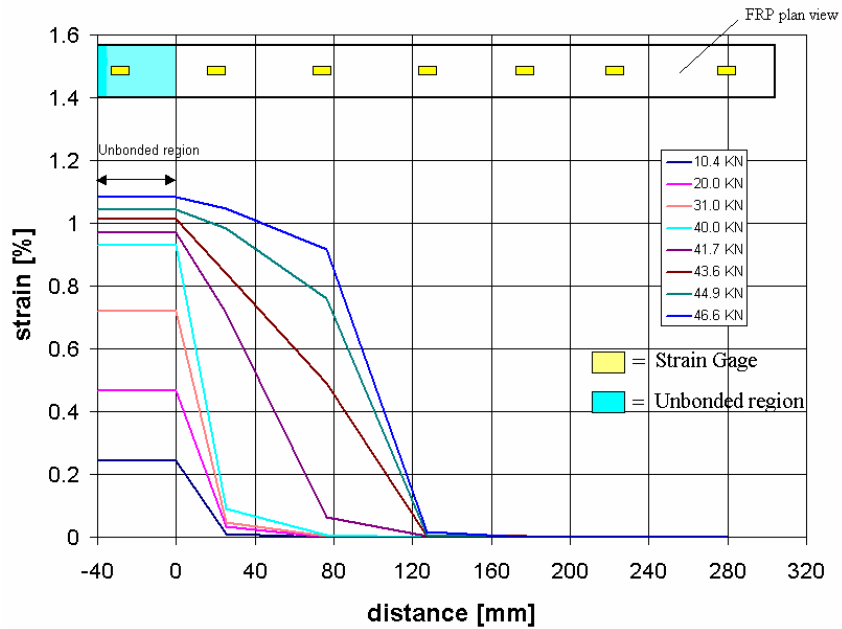
Fig. A.5.5c *Typical strain-location graph for masonry bricks (specimen BA6-12)*

In order to determine the effective bond length, the ultimate load is not very significant because FRP is already detached at this value of load. Peeling load is the load when the fiber starts the delamination. It is identified as the load level at which the strain distribution becomes linear. Fig. A.5.5d shows different theoretical stages.

It can be observed that after the peeling load the effective bond length slips towards the end of the fiber, but presents always the same length.
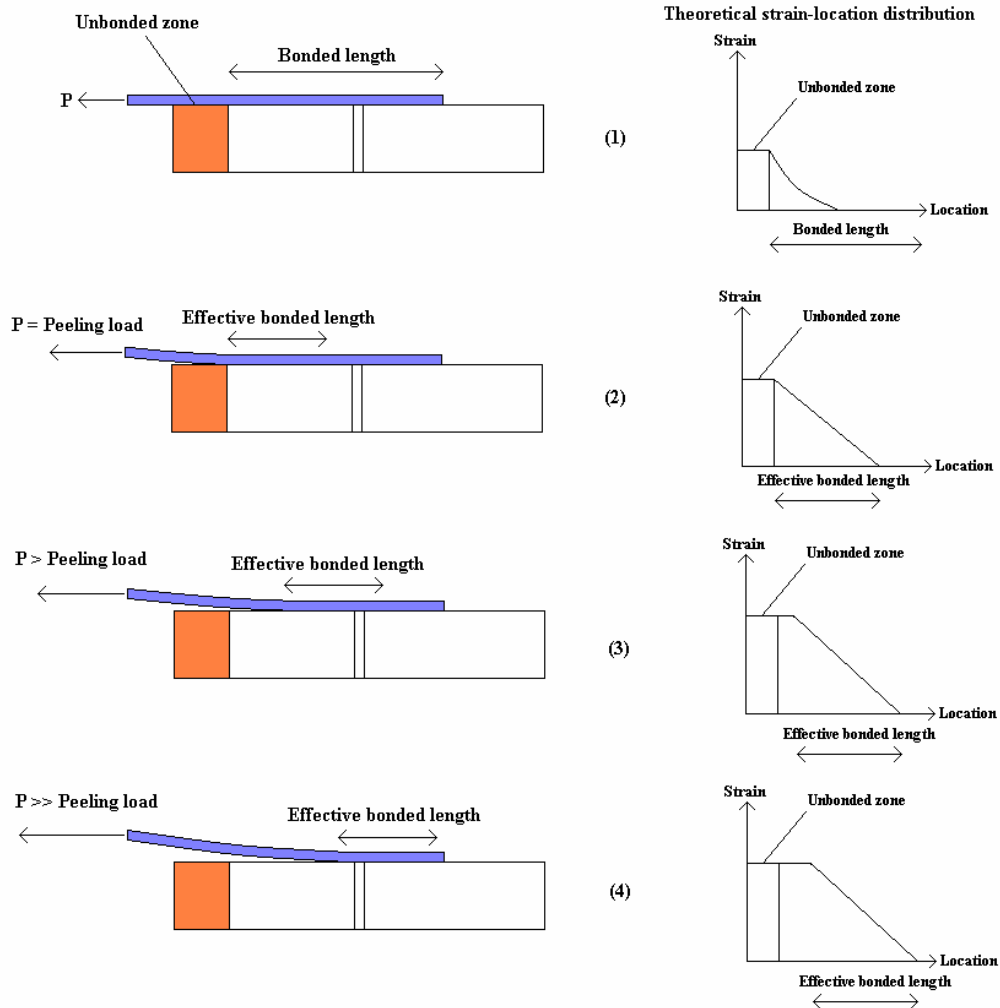
Fig. A.5.5d *Theoretical peeling load*

Fig. A.5.5e illustrates how the load corresponding to imminent peeling is determined. To that effect specimen CA3-8 was used. From Fig. A.5.5d the theoretical behavior after the peeling load can be assumed parallel to the straight line that characterize the peeling load. The theoretical behavior after the peeling load can be found following the

experimental behavior. Fig. A.5.5e shows that the fiber is already detached, like the theoretical behavior explains. Tracking the parallel lines the peeling load can be found and also the imminent peeling load that is the closest experimental behavior.
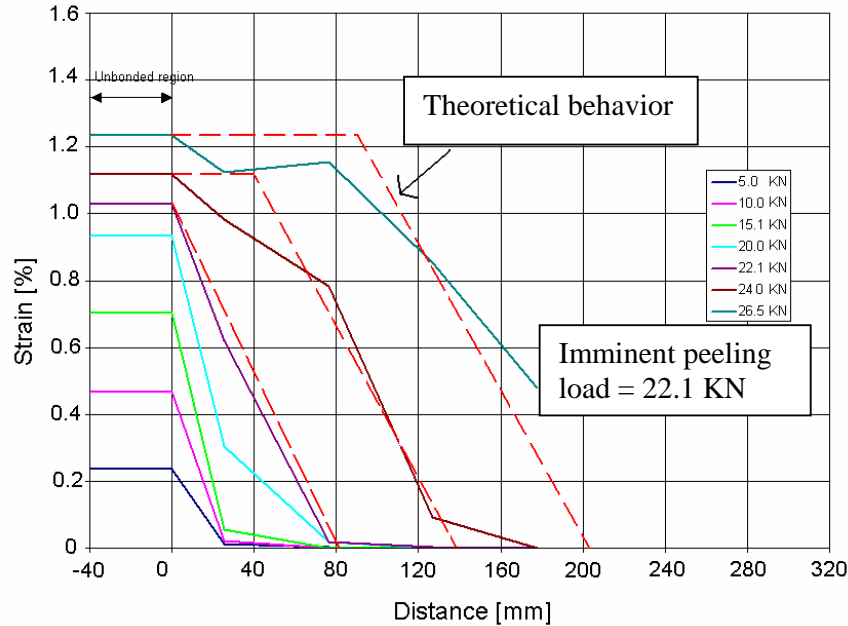
Fig. A.5.5e *Determination of imminent peeling load for specimen CA3-8*

Table A.5.5c shows the imminent peeling load values estimated for the test specimens

Table A.5.5c *Imminent peeling load estimated for the specimens*

Specimen	Imm. peeling [kN]	Specimen	Imm. peeling [kN]
CA3-4	22.1	BA3-4	N/A
CA3-8	22.1	BA3-8	24.2
CA3-12	24.0	BA3-12	N/A
CA6-4	37.4	BA6-4	N/A
CA6-8	44.0	BA6-8	41.7
CA6-12	46.4	BA6-12	N/A

Note:1 kN = 0.2248 kips

Because of imperfections in the clay masonry specimens (such as misalignment of the laminate), it was not possible to clearly determine the strain distribution over the bonded length of the FRP laminate. Also, it was not possible to determine the peeling load for several specimens. As a consequence, the analytical model proposed in the next paragraph could not be validated in this case. However, the overall test trends indicated the following:

- The bonded length does not significantly influence the ultimate load

- The bonded length could be about 100 mm (4 in.)

- In some specimens, the strain versus location behavior is similar to that specimens made with concrete blocks

A.5.6 Analytical study

The bond issue is an important limit stated to consider in the strengthening design of externally bonded FRP laminates. When failure is bond-controlled, the maximum stress in the FRP cannot be considered equal to the tensile strength of the FRP material. To reach a possible design, the ACI committee 440 seems to indicate a reduced ultimate strain level in the FRP reinforcement:

$$\varepsilon_{ub} = k_r \cdot \varepsilon_u \qquad (5.6.1)$$

Where:

ε_u = ultimate strain of the FRP laminate

k_r = reduction factor

In order to determine the k_r coefficient and then the bonded length, a model developed by *De Lorenzis et al.* (2000) can also be used for masonry, since the hypotheses are fundamentally the same:

- The adhesive is only exposed to shear forces

- The thickness of the adhesive is constant throughout the bond line

- The width of the FRP sheet is constant throughout the bond line

The bond failure load can be found using non-linear fracture mechanics approach (*Taljsten*, 1994). It has been observed that with an energy approach, the same results of classical Volkersen's theory can be found. This theory was used like starting point for the bond.

$$P_{ub} = b_f \sqrt{2 \cdot E_f \cdot t_f \cdot G_f} \qquad (5.6.2)$$

Where:

b_f, E_f, t_f = width, tensile elastic modulus and thickness of FRP sheet

G_f = fracture energy per unit area of the joint

The energy needed to bring a connection with a certain area to failure is called fracture energy and it is determined building the τ-slip curve. The fracture energy is the area underneath this graphic ($G_f = \int \tau \, ds$).

τ   τ

γ

h $s = \gamma \, h$

τ   τ

Undeformed   Deformed
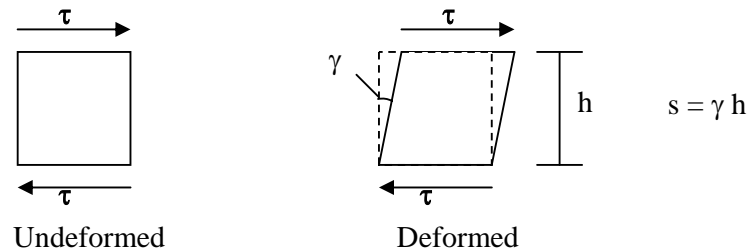
Fig. A.5.6a *Infinitesimal part of adhesive layer subjected to angular distorsion*

Because the slip "s" value is more used in civil engineering than the "γ" value, it was decided to was use the τ-slip relationship rather than the τ-γ relationship, also because the slip value is much easier to record experimentally, and the thickness of the glue layer "h" is in most cases unknown or it is difficult to determine.

The local τ-slip curve can be obtained from the experimental data. The bond stress (τ) can be found by equilibrium of forces:

τ

P_1 P_2

dx
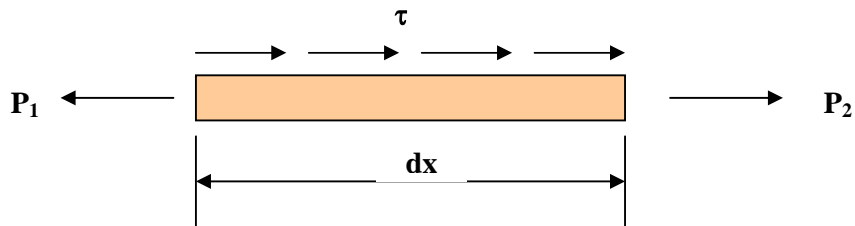
Being the generic force P equal to:

$$P = \sigma_f \cdot t_f \cdot b_f \tag{5.6.3}$$

The follow equation can be obtained:

$$P_1 - P_2 = \tau(x) \cdot b_f \cdot dx \tag{5.6.4}$$

The force P can be expressed in terms of strain (elastic-linear behavior):

$$P = \varepsilon_f \cdot E_f \cdot t_f \cdot b_f \tag{5.6.5}$$

So the equation (5.6.4) becomes:

$$(\varepsilon_1 - \varepsilon_2) \cdot E_f \cdot t_f \cdot b_f = \tau(x) \cdot b_f \cdot dx \tag{5.6.6}$$

Substituting $(\varepsilon_1 - \varepsilon_2)$ with $d\varepsilon_f(x)$ and solving for $\tau(x)$ the average bond stress can be obtained:

$$\tau(x) = t_f \cdot E_f \cdot \frac{d\varepsilon_f(x)}{dx} \tag{5.6.7}$$

Where ε_f is the strain in the FRP laminate. Therefore, the τ - location can be obtained from equation of the strain-location multiplied by the elastic modulus E_f and the thickness t_f of FRP sheet. To calculate the $\varepsilon_f(x)$ is used a cubic approximation for the experimental results with the hypothesis that the strain to the end of the fiber is zero $(\varepsilon_f(L) = 0)$. Fig. A.5.6a shows a typical approximation for $\varepsilon_f(x)$ obtained with Maple 6.0.
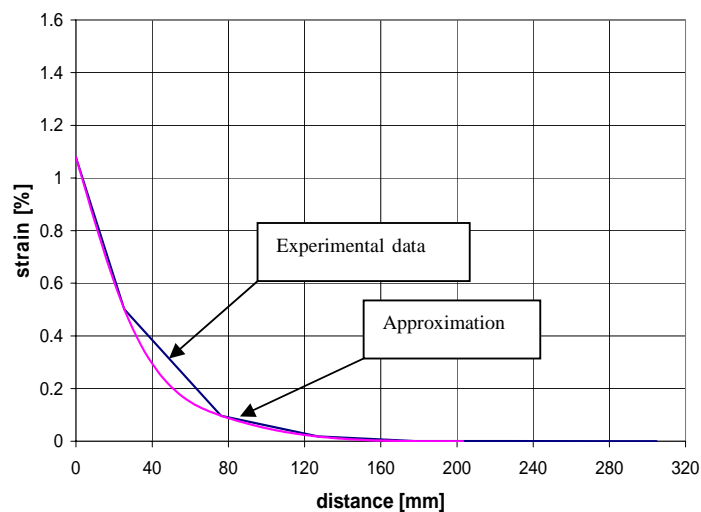
Fig. A.5.6b Approximation of ε(x) for the specimen CA6-12

A32

The graphics were developed at imminent peeling load level, because after this load the G_f is not significant since the first part of fiber is already detached. As an example shown the τ versus location behavior for specimen CA3-8 is shown in Fig. A.5.6b:
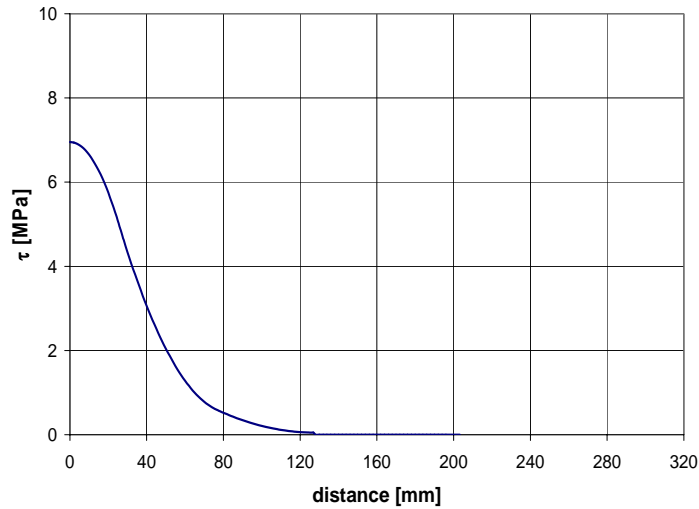
Fig. A.5.6c *τ versus location at peeling load for the specimen CA6-8*

For the slip "s" it can be assumed that the strain in masonry is negligible compared to the FRP strain, so the follow equation can be used to measure the slip:

$$\frac{ds}{dx} = \varepsilon_f \qquad\qquad (5.6.8)$$

from which:

$$s(x) = s(0) + \int_0^x \varepsilon_r(x)dx \qquad\qquad (5.6.9)$$

Assuming s(0) the slip at the end of the laminate equal to zero (can be consider negligible prior to delamination), the slip-location diagram can be obtained only from the integration of the strain-location curve. Fig. A.5.6d shows the behavior for specimen CA3-8:
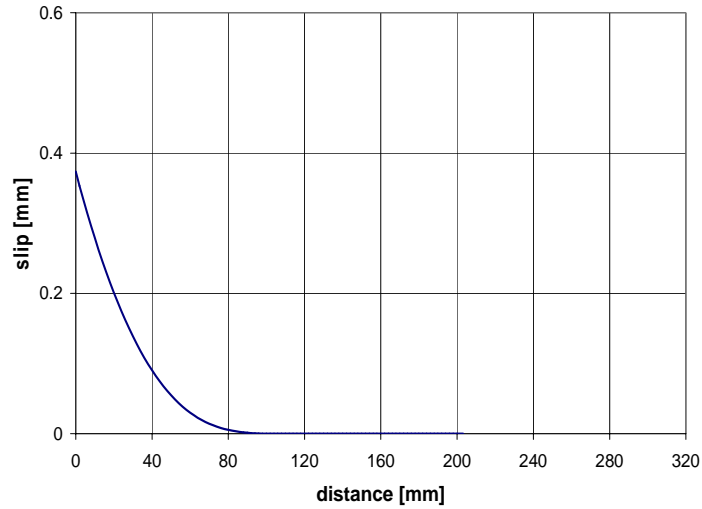
Fig. A.5.6d *Slip versus location behavior for specimen CA3-8*
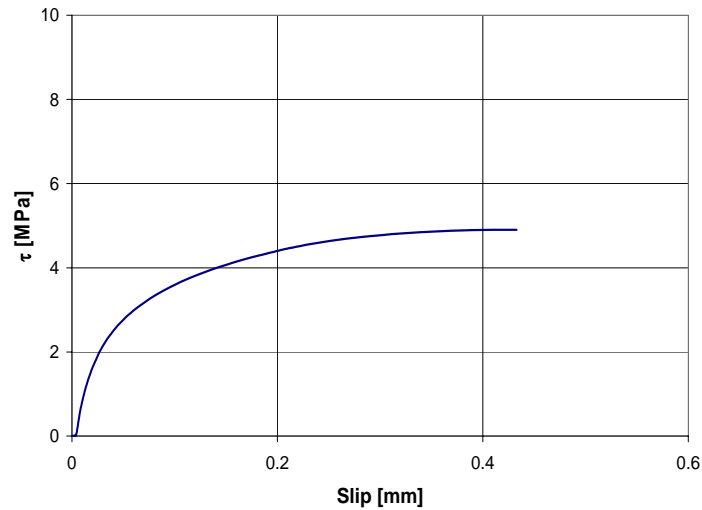
Fig. A.5.6e *τ versus slip behavior for the specimen CA3-12*

To the end, the local τ-slip relationship can be achieved by combining the two curves $\tau(x)$ and $s(x)$. This diagram can be done for all the loads; Fig. A.5.6e shows the τ-slip curves of the tested specimens at a load level corresponding to imminent peeling.

Following this procedure the experimental graphics for all the specimens can be found. Fig. A.5.6f and following show the comparison from the experimental data.
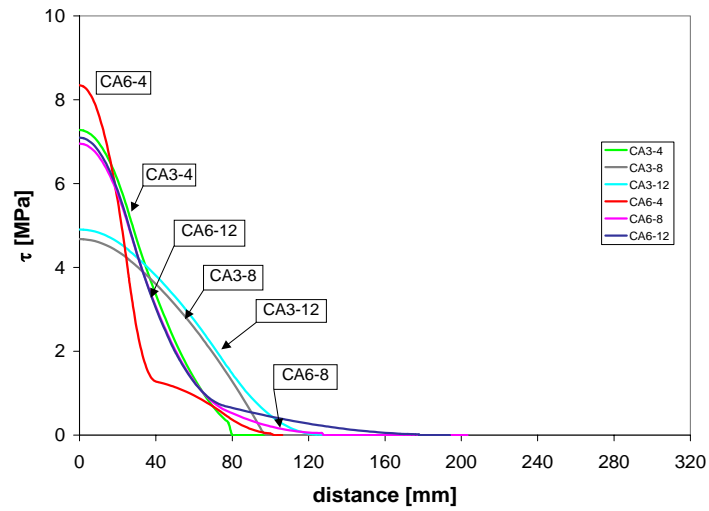
Fig. A.5.6f *Comparison among the experimental results in terms of τ vs. location for the concrete blocks*
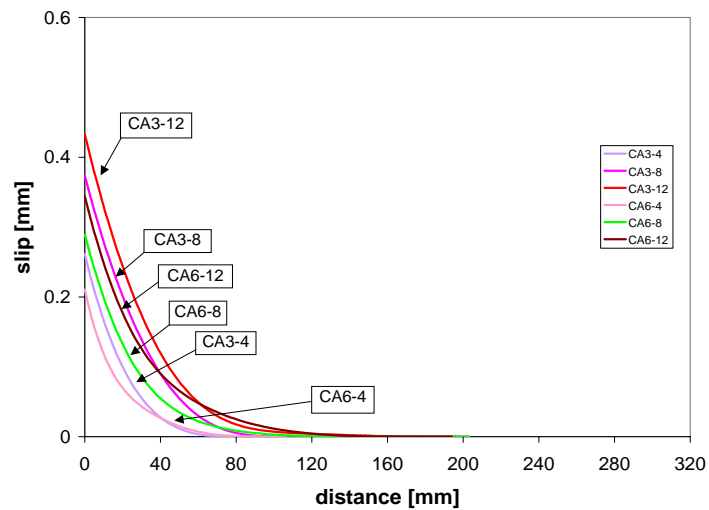
Fig. A.5.6g *Comparison among the experimental results in terms of slip vs. location for concrete blocks*
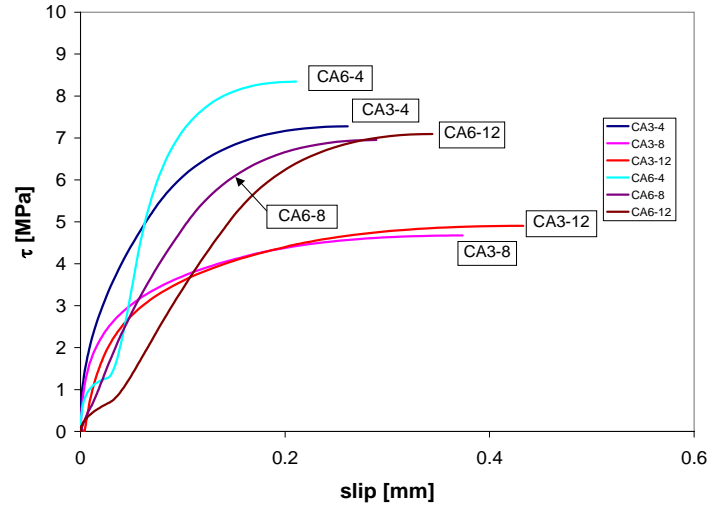
Fig. A.5.6h *Comparison among the experimental results in terms of τ vs. slip for concrete blocks*

Fig. A.5.6h illustrates the τ-slip curves obtained for the specimens at load level corresponding to imminent peeling. An ascending branch is followed by a second region characterized by plastic or softening behavior, until an ultimate value of slip is reached. The plastic branch of the curve explains the attainment of a linear strain distribution close to peeling. The limited value of ultimate slip suggests a brittle behavior of the joint, that is, the localization of load transfer within a short effective area even for long bonded lengths.

The fracture energy per unit area of the bonded joint "G_f", its corresponding slip "S_m" and the value of "τ_m" (i.e. the maximum value of τ in the τ-slip curve) can be found.

Table A.5.6a *Values of G_f , S_m, and τ_m for the concrete blocks*

Specimen	G_f (N*mm/mm^2)	S_m (mm)	τ_m (MPa)
CA3-4	1.500	0.261	7.278
CA3-8	1.486	0.374	4.674
CA3-12	1.757	0.433	4.905
CA6-4	1.252	0.211	8.346
CA6-8	1.477	0.289	6.954
CA6-12	1.642	0.344	7.095

Note: 1 Nmm/mm^2 = 5.71 lbs in./in^2; 1 mm = 0.03937 in; 1 MPa = 145 psi

A36

It can be noted that the fracture energies are almost the same for all the specimens. To determine the FRP ultimate strain (see equation 5.6.1) the follow procedure can be used: being $\sigma_{ub} = E_f \cdot \varepsilon_{ub}$ (assuming a elastic-linear behavior) the ultimate peeling strength, combining the last equations and the 5.6.2 the equation for ultimate strain of FRP laminate before peeling ε_{ub} can be found:

$$\varepsilon_{ub} = \sqrt{\frac{2 \cdot G_f}{E_f \cdot t_f}} \qquad (5.6.10)$$

Using the G_f average "G_{fm}" for the concrete block specimens, the ultimate strain before peeling can be found. Being $G_{fm} = 1.519$ N*mm/mm^2 (8.67 lbs *in/in^2) ε_{ub} becomes:

$$\varepsilon_{ub} = \sqrt{\frac{2 \cdot 1.519}{100800 \cdot 0.28}} = 0.0104 = 1.04 \ \%$$

So, the experimental reduction factors can be found with the equation shown below:

$$k_r = \frac{\varepsilon_{ub}}{\varepsilon_u} = \frac{1.04}{1.7} = 0.61 \qquad (5.6.11)$$

Previous works on reinforced concrete (*Chajes et al.*, 1999; *Maeda et al.,* 1997; *Talijsten*, 1994; and *De Lorenzis*, 2000) have shown that the reduction factor k_r becomes very low if the stiffness of the laminate increases. From this, is evident that further research on this area needs to be considered. Anyway, the value of k_r found at Et = 28224 N/mm (160.7 kips/in) is in according with the previous researches.

A.5.7 Effective bond length

The effective bond length can be expressed as follows:

$$l_{eff} = \frac{\varepsilon_{ub}}{\left.\dfrac{d\varepsilon}{dx}\right|_{peel}} \tag{5.6.12}$$

The τ-slip curve can be modeled having an initial ascending branch followed by a perfectly plastic behavior at value τ_m then:

$$\left.\frac{d\varepsilon}{dx}\right|_{peel} = \frac{\tau_m}{E_f \cdot t_f} \tag{5.6.13}$$

Using equations 5.6.10, 5.6.12 and 5.6.13, equation 5.6.10 can be modified:

$$l_{eff} = \frac{\sqrt{2 \cdot E_t \cdot G_{fm}}}{\tau_m} \tag{5.6.14}$$

Using the average of τ_m (τ_{ma}) the effective bonded length can be found. Taking τ_{ma} equal to 6.54 MPa (948 psi) the effective bond length is:

$$l_{eff} = \frac{\sqrt{2 \cdot 100800 \cdot 1.533}}{6.54} = 85 \text{ mm (3.35 in.)}$$

A.5.8 Conclusions

Several specimens were prepared to study bond between masonry and FRP sheets. Failure occurred in the masonry-adhesive interface, sometimes with signs of damage into the masonry. The experimental bonded length did not affect the ultimate load, as shown in previous works on concrete specimens (i.e. *L. De Lorenzis et al.*, 2000). This confirms the existence of an effective bonded length beyond which no stress is transferred after peeling occurs. No significance increase in resistance to peeling is attainable.

A.5.9 Design

To date, there are few investigations conducted on the bond between FRP sheets and masonry; the reported work represents intends to establish a limit for the FRP strain and for determination of an effective development length. The extent of the experimental work is not sufficient for the calibration of the model but allows for its validation.

It can be seen from the experimental results that the τ values are included in a range of values between 8.346 MPa (1210 psi) and 4.674 MPa (678 psi) (see Fig. A.5.9a)
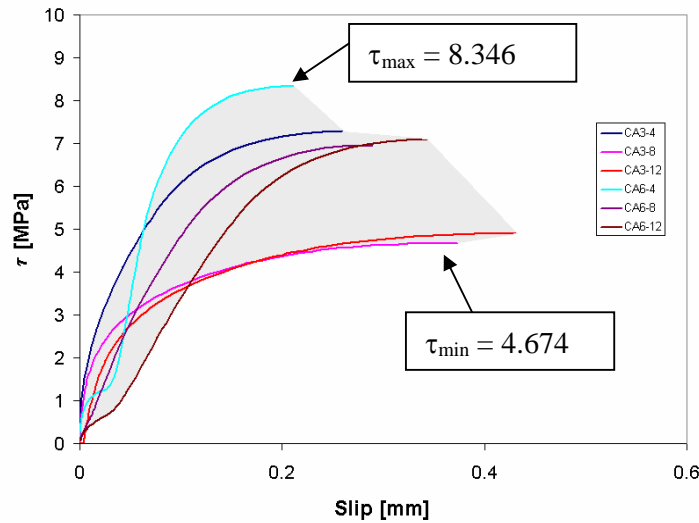
Fig A.5.9a *τ versus slip fuse*

For a conservative design, the τ values corresponding to the lower boundary of the experimental results can be adopted. Considering a safety factor equal to 2 it is suggested a maximum value of:

$$\tau = \frac{4.674}{2} \cong 2.2 \text{ MPa } (319 \text{ psi})$$

Correspondingly, based on average fracture energy value G_{fm} the minimum development length becomes:

$$l_{min} = \frac{\sqrt{2 \cdot 100800 \cdot 1.533}}{2.2} = 253 \text{ mm } (10 \text{ in.})$$

Furthermore, being the ultimate strain before peeling equal to $\varepsilon_{ub} = 1.04$ %, to avoid debonding from the masonry surface it is recommended that the ultimate design strain should not exceeded $\varepsilon_{ub} = 0.8$ %, because of the presence of the normal component of stress due to flexural behavior. This recommendation is similar to the strain limit adopted by a previous work on flexural strengthening of masonry elements (*Tumialan*, 2001).

APPENDIX B

CYCLES-CRACK PATTERNS

B.1 OUT-OF-PLANE LOAD CYCLES
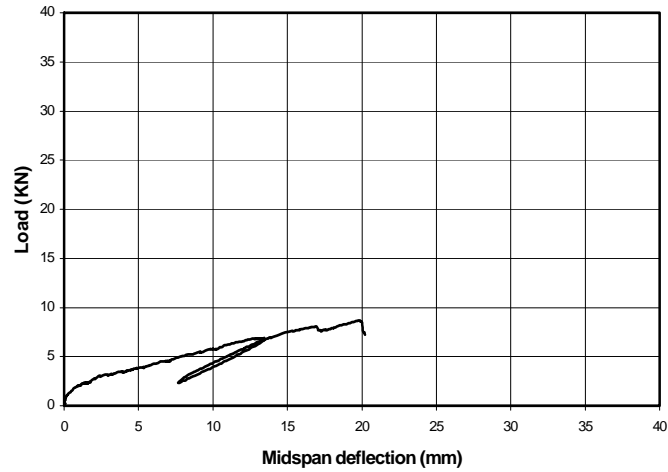
Load vs. Midspan net deflection Curve-Wall COG3
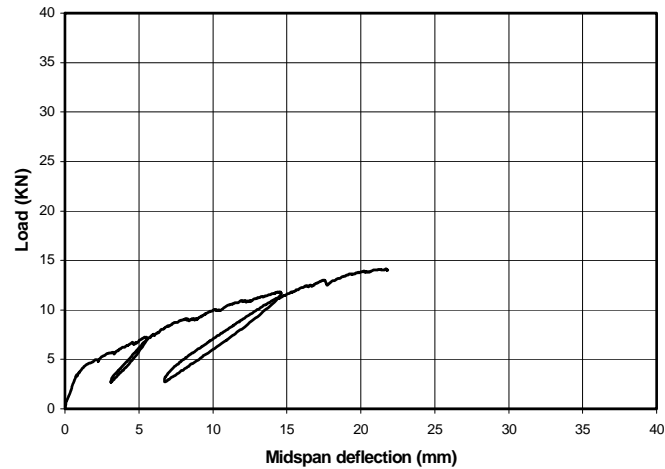
Load vs. Midspan net deflection Curve-COG5
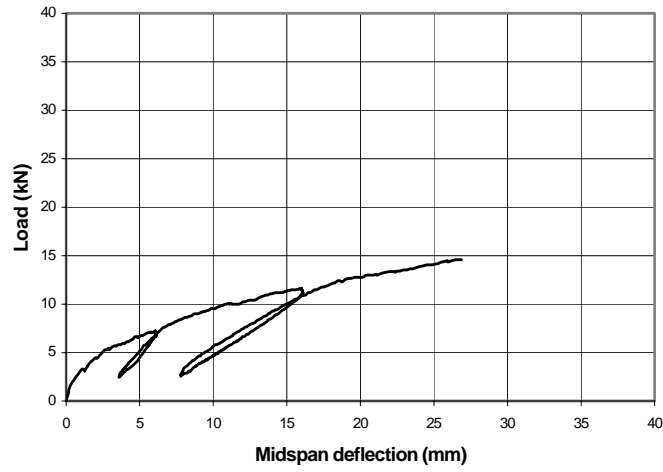
Load vs. Midspan net deflection Curve-COG5R
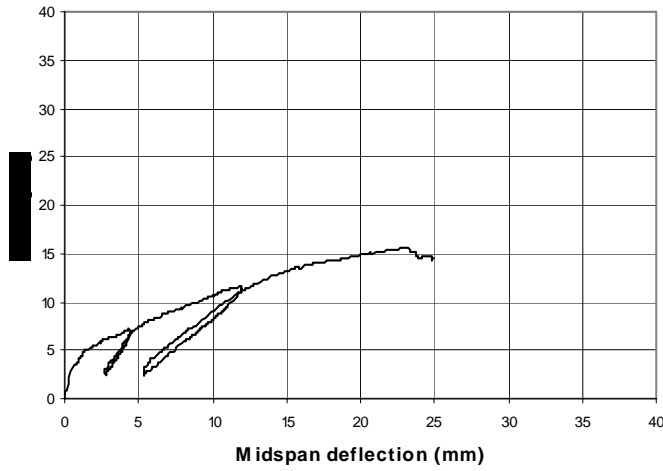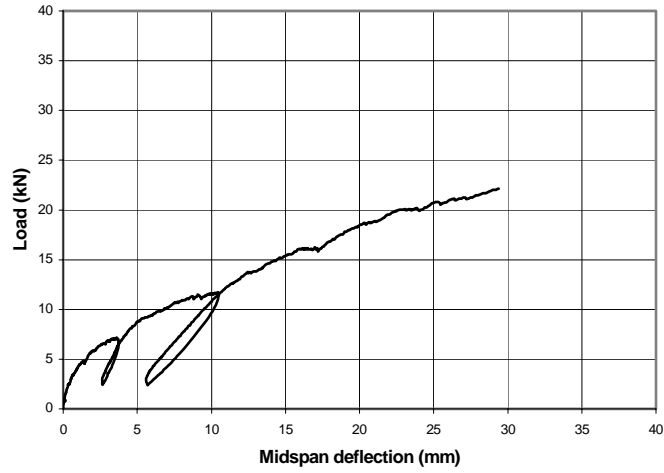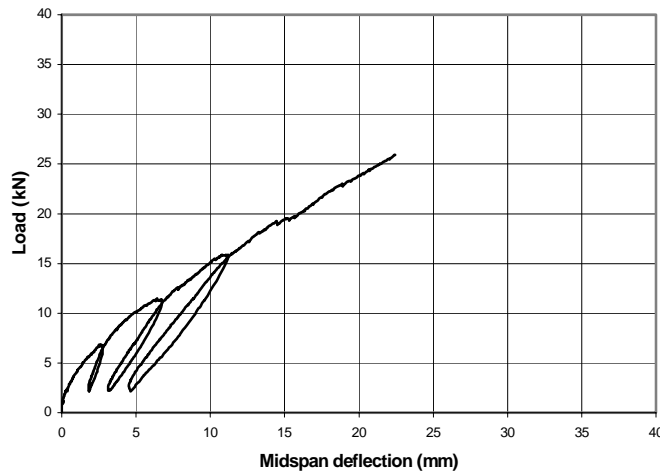

Load vs. Midspan net deflection Curve-COG5A
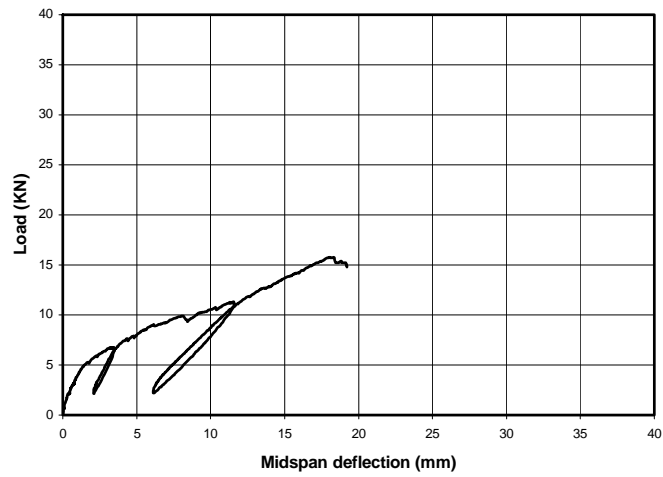
Load vs. Midspan net deflection Curve-COG7
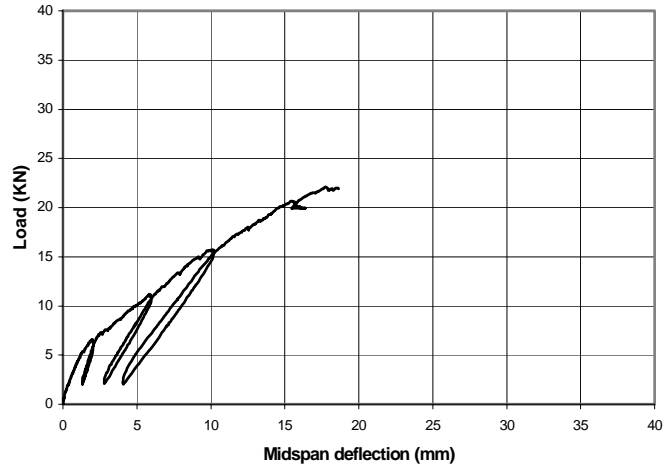
Load vs. Midspan net deflection Curve-COG9
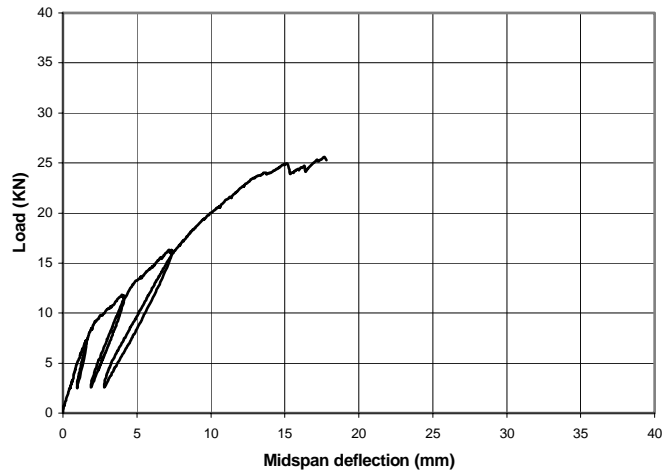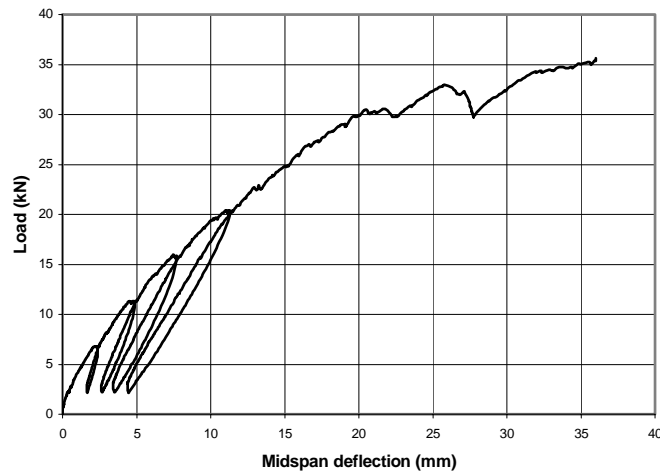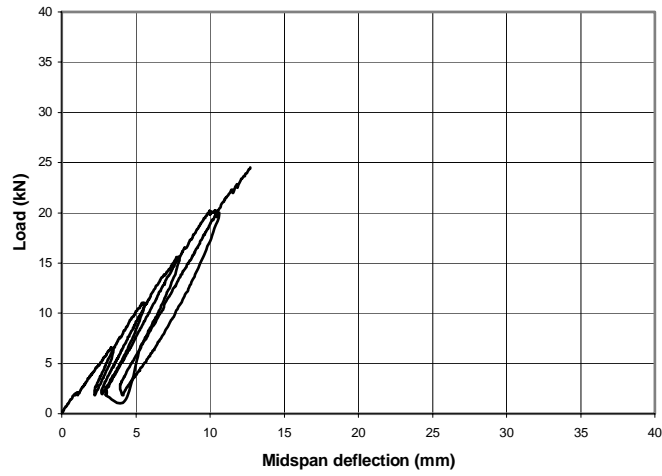

Load vs. Midspan net deflection Curve, COG12
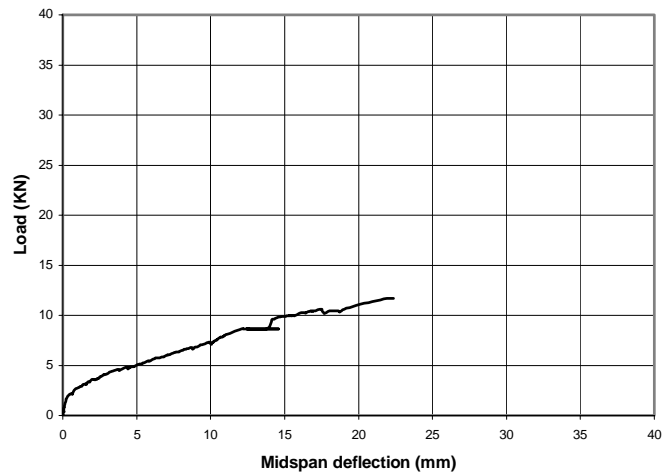
Load vs. Midspan net deflection-COA3
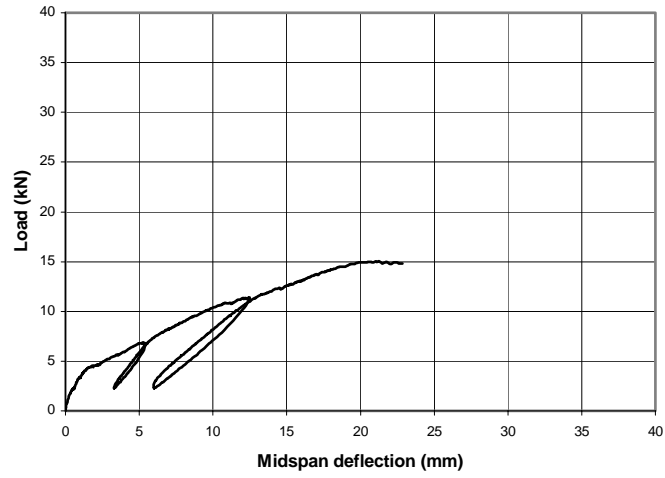
Load vs. Midspan net deflection Curve-*COA5*
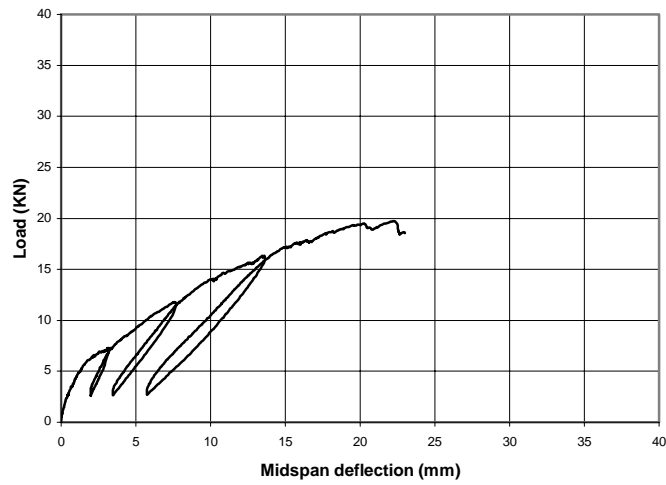
Load vs. Midspan net deflection Curve-COA7
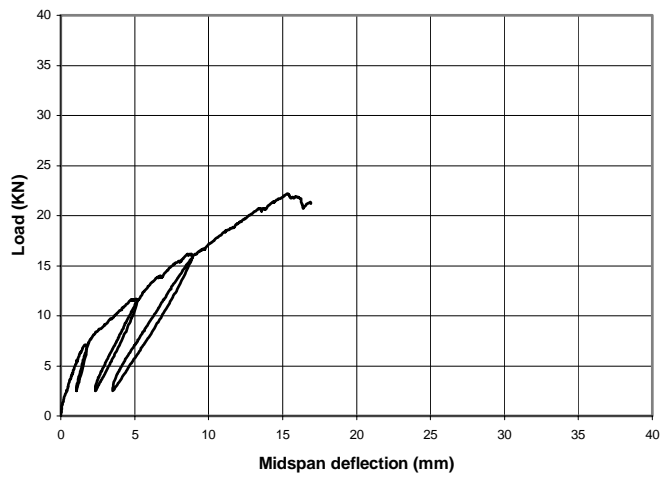
Fig. 2.3.5g* *Load vs. Midspan net deflection Curve-COGA9*
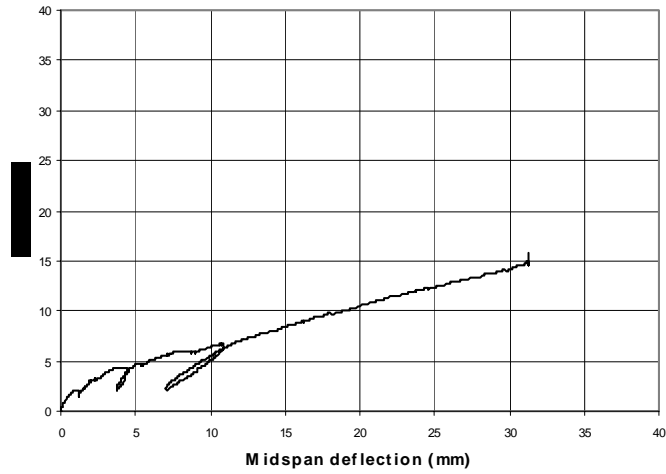
Load vs. Midspan net deflection Curve-CLG3
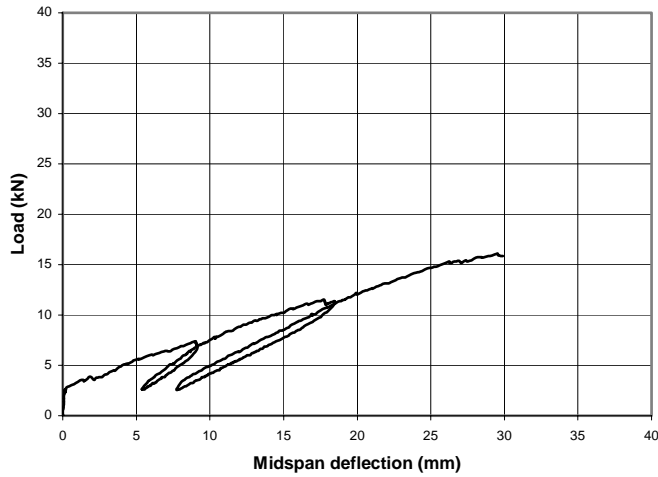
Load vs. Midspan net deflection Curve-CLG3R

Load vs. Midspan net deflection Curve-CLG5

B5
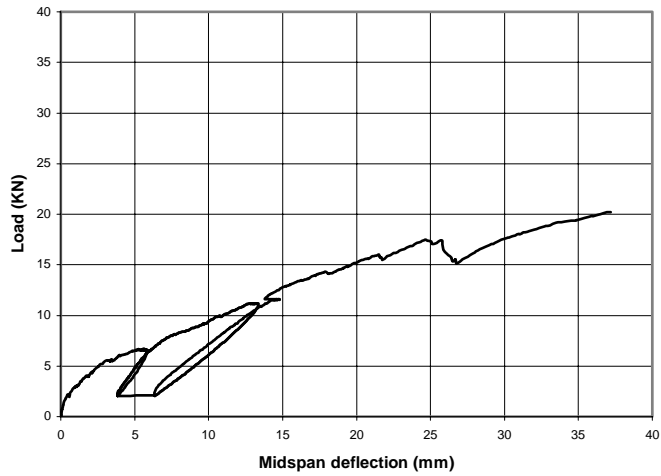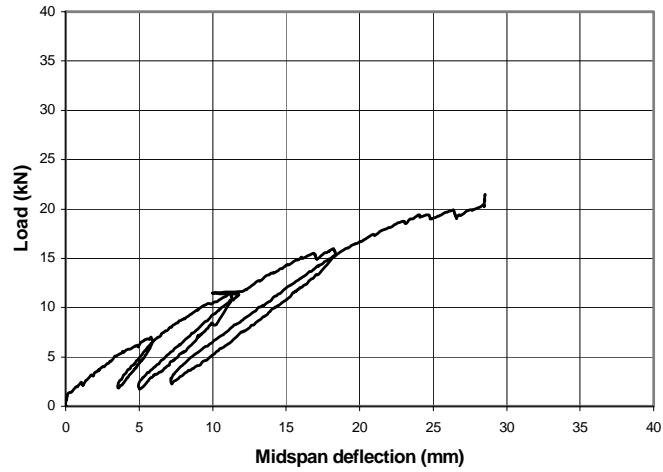
Load vs. Midspan net deflection Curve-CLG5R
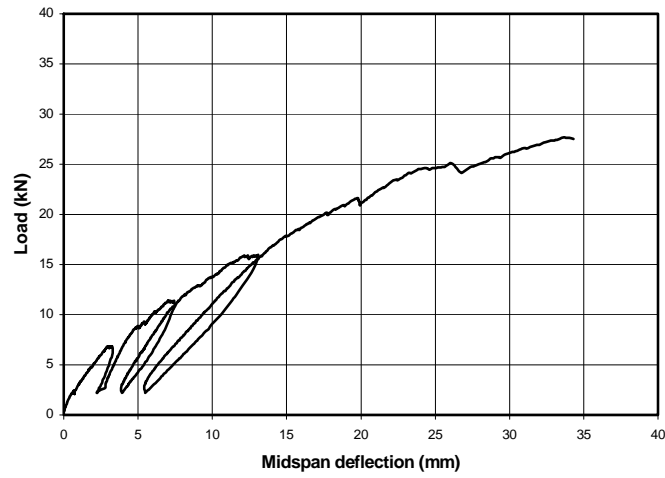

Load vs. Midspan net deflection-CLG7

Load vs. Midspan net deflection Curve, CLG7R

B6
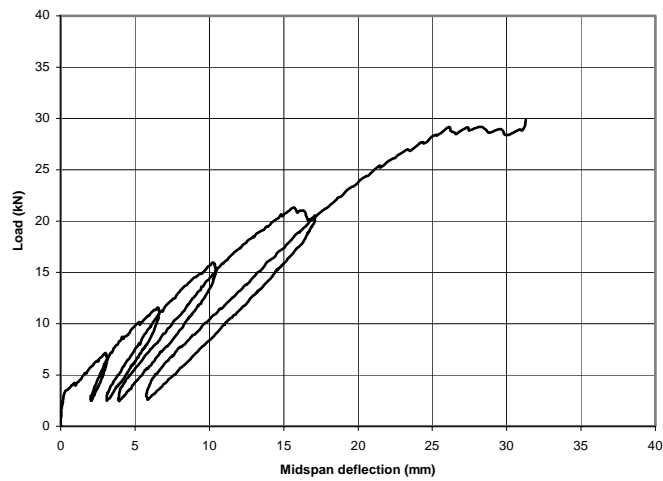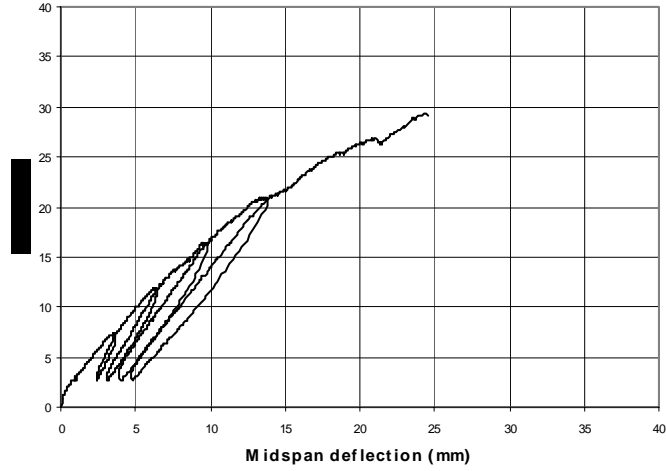
Load vs. Midspan net deflection Curve-CLG9
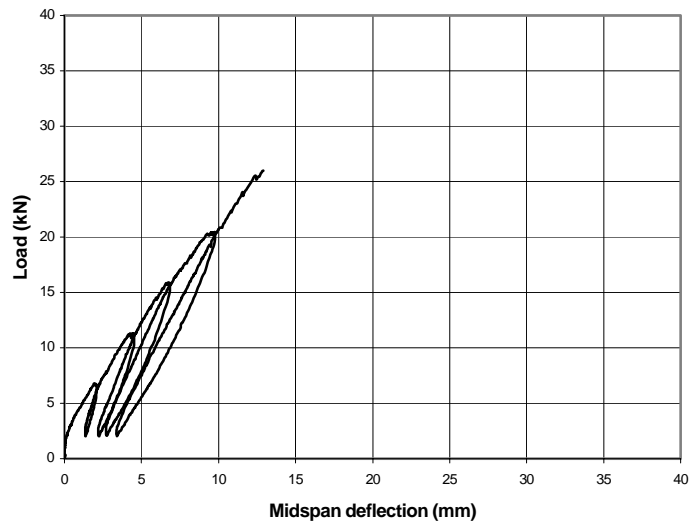
Load vs. Midspan net deflection Curve,CLG12

Load vs. Midspan net deflection Curve, CLA3

B7
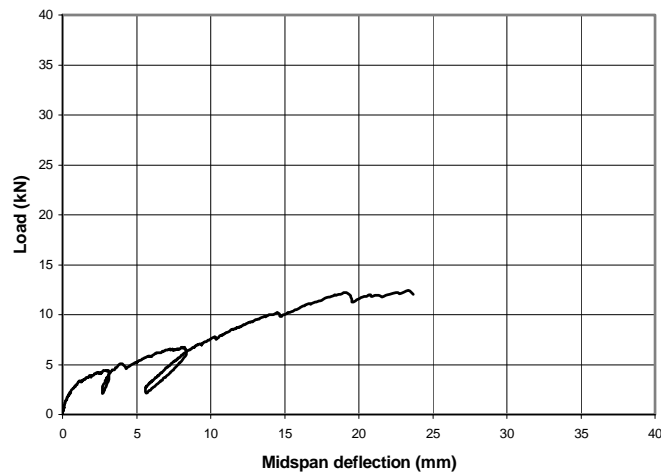
Load vs. Midspan net deflection Curve, CLA5

Load vs. Midspan net deflection Curve, CLA7
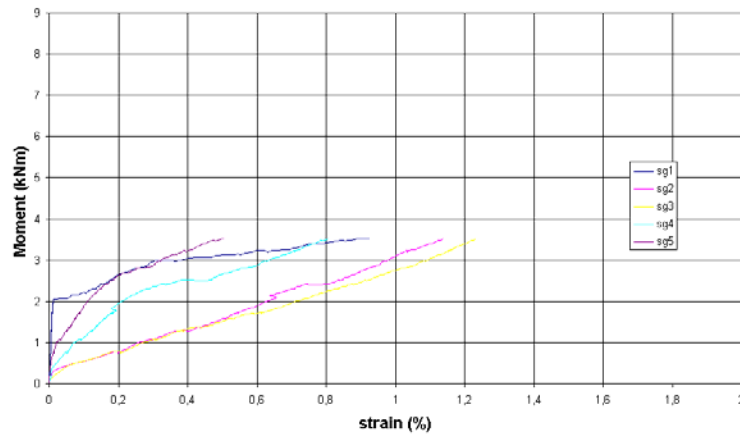

Load vs. Midspan net deflection Curve-CLA9
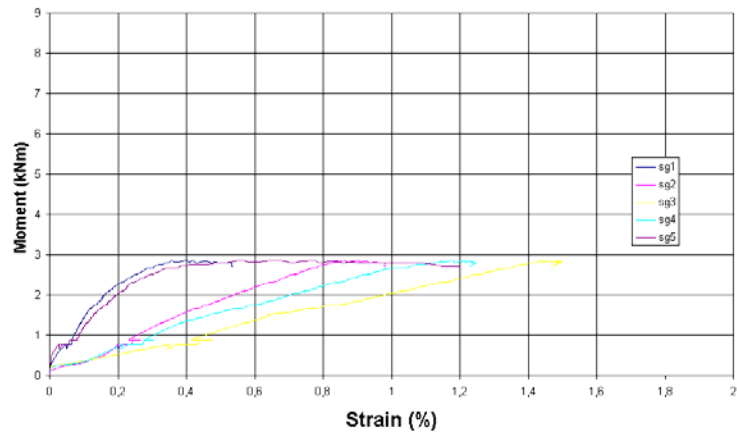
B8

Load vs. Midspan net deflection Curve-CLA12
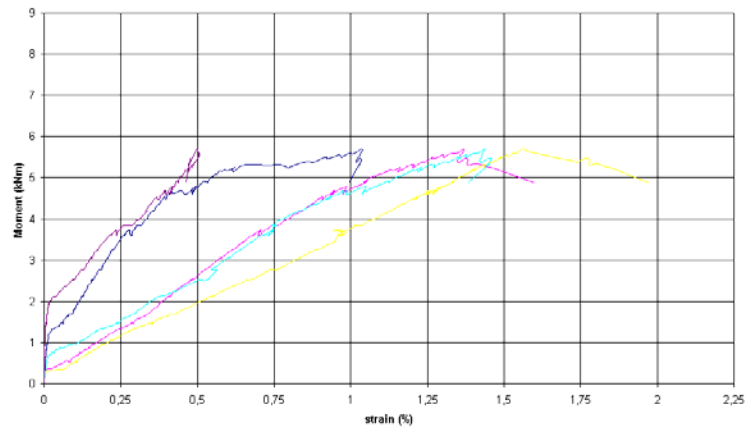
STRAIN VALUES FOR SERIES CO AND CL

STRAINS-COG5R

B9
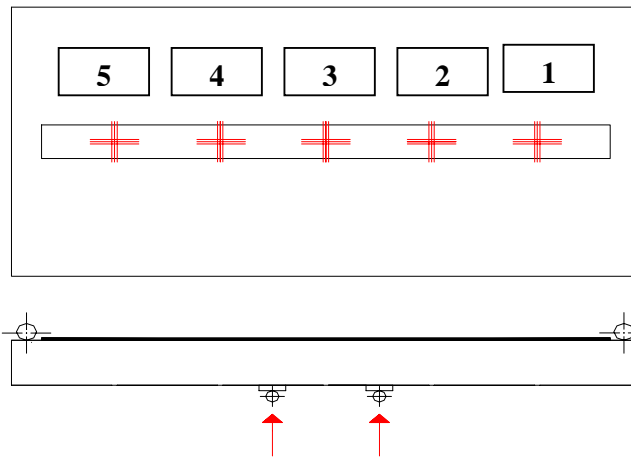
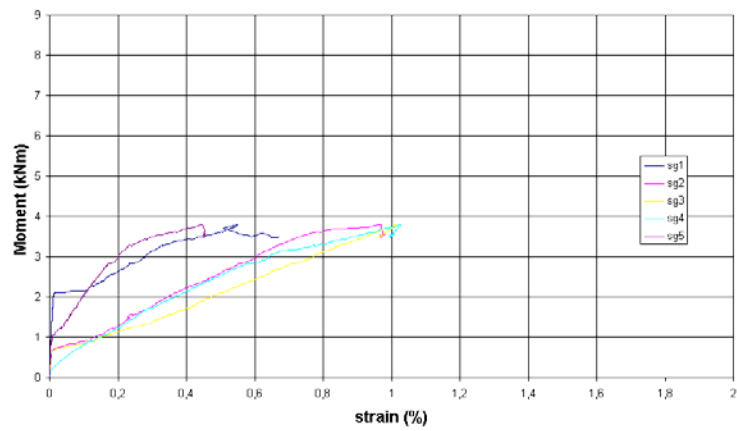**STRAINS-COG3R**
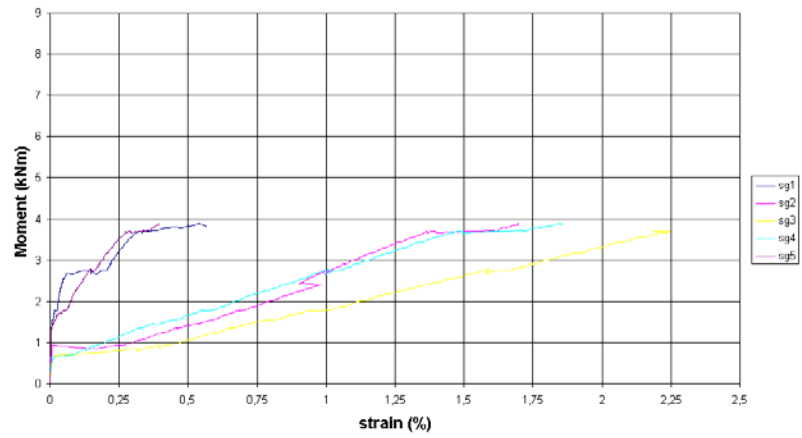

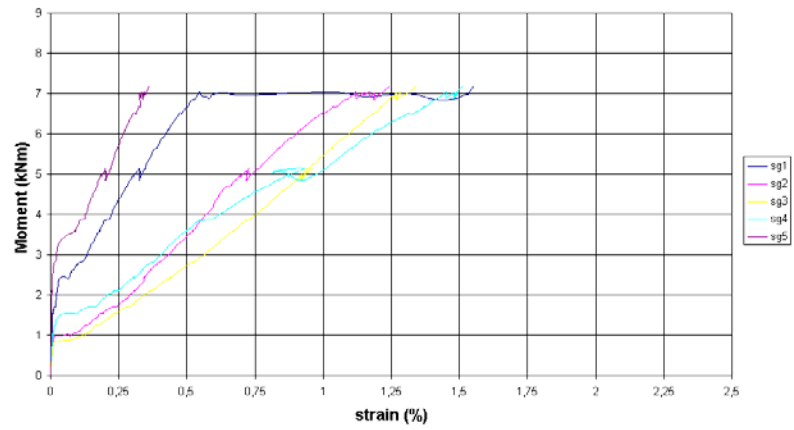**STRAINS-CLG5R**

STRAINS-COG5A

STRAINS-CLG3R

STRAINS-CLG7R

B11

B.2 IN-PLANE CRACK PATTERNS

COW1 FRONT-BACK

COW2 FRONT

COW2 BACK

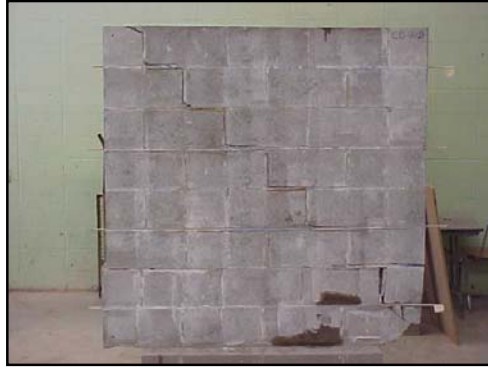
COW3 FRONT

COW3 BACK

COW4 FRONT   **COW4 BACK**

COW5 FRONT   **COW5 BACK**
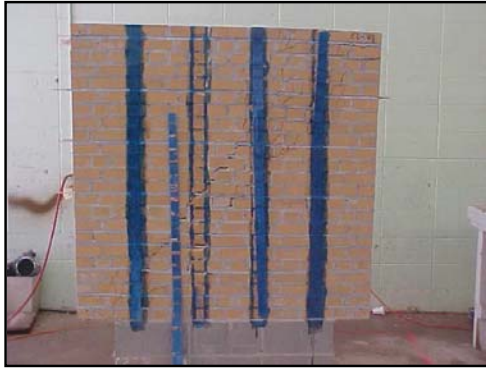

COW6 FRONT   **COW6 BACK**
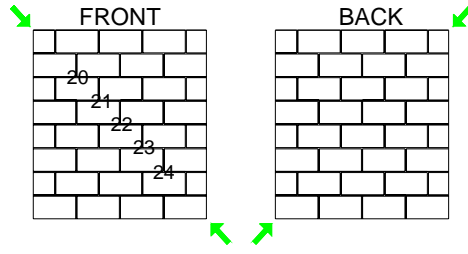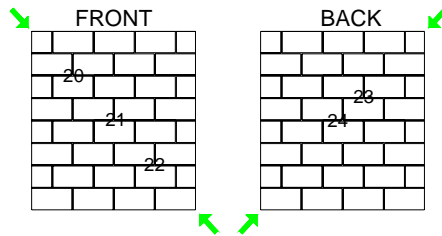
CLW1 FRONT-BACK

CLW3 FRONT

CLW3 BACK

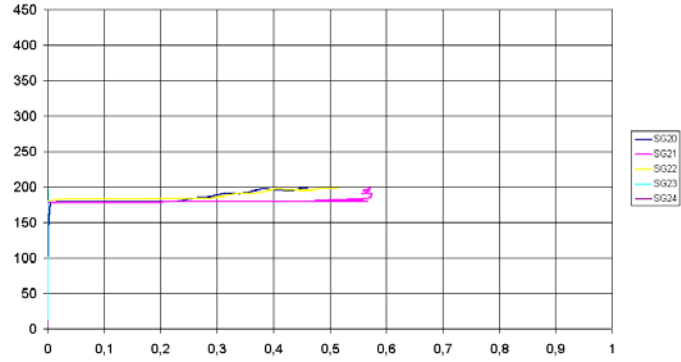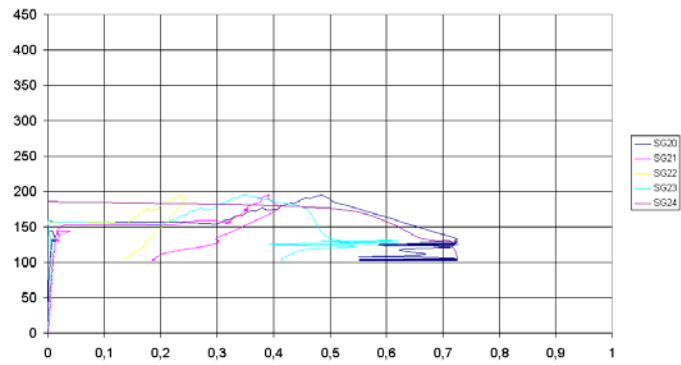

CLW4 BACK

CLW4 FRONT
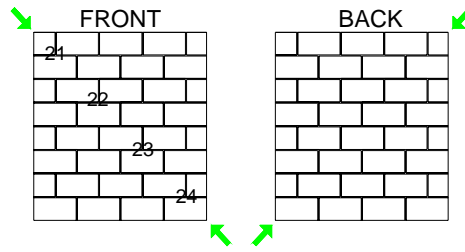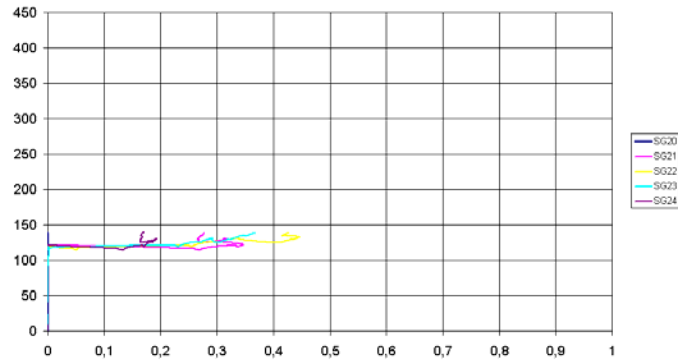
STRAINS-COW2

STRAINS-COW3

B15

For COW5 and COW6, as well as for Series CL, no useful data were recorded in order to determine the effective strain in GFRP rods or laminates.

APPENDIX C

SUPPORTING CALCULATIONS

C.1 Determination of ρ_b for Series CO

Masonry	Concrete		Masonry	Concrete	
$t_m=$	4	in	$t_m=$	4	in
$b=$	24	in	$b=$	24	in
$\varepsilon_m=$	0,025	in/in	$\varepsilon_m=$	0,025	in/in
$f_m=$	1,5	ksi	$f_m=$	1,5	ksi
FRP	**Glass**		**FRP**	**Aramid**	
$t_f=$	0,014	in	$t_f=$	0,011	in
$\varepsilon_f=$	0,021	in/in	$\varepsilon_f=$	0,017	in/in
$f_f=$	220	ksi	$f_f=$	290	ksi
$c=$	0,54	in	$c=$	0,60	in
$A_f=$	0,06	in^2	$A_f=$	0,05	in^2
$w=$	7,02	in	$w=$	7,31	in

C.2 Determination of ρ_b for Series CL

Masonry	Clay		Masonry	Clay	
$t_m=$	4	in	$t_m=$	4	in
$b=$	24	in	$b=$	24	in
$\varepsilon_m=$	0,035	in/in	$\varepsilon_m=$	0,035	in/in
$f_m=$	3	ksi	$f_m=$	3	ksi
FRP	**Glass**		**FRP**	**Aramid**	
$t_f=$	0,014	in	$t_f=$	0,011	in
$\varepsilon_f=$	0,021	in/in	$\varepsilon_f=$	0,017	in/in
$f_f=$	220	ksi	$f_f=$	290	ksi
$c=$	0,63	in	$c=$	0,67	in
$A_f=$	0,13	in^2	$A_f=$	0,11	in^2
$w=$	9,35	in	$w=$	9,72	in

C.3 Correlation between experimental and theoretical results with ε_{eff}=0.008 %
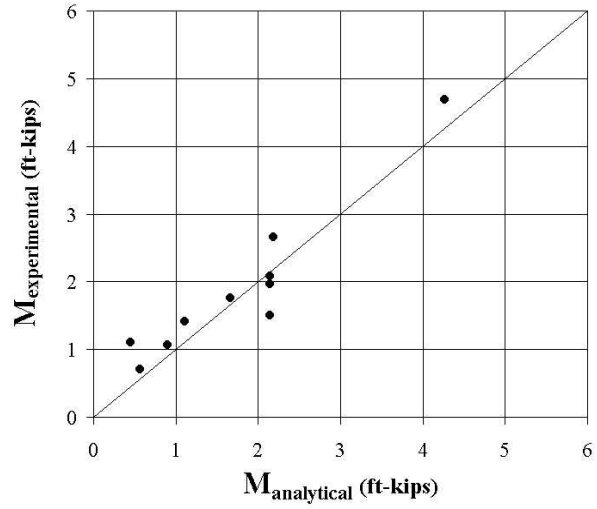
REFERENCES

[1]
Asplund
STRENGHTENING BRIDGE SLABS WITH GROUTED REINFORCEMENT
Journal of the American Concrete Institute, v20 #6 January 1949, pp. 397-406

[2]
Prawel, Reinhorn
SEISMIC RETROFIT OF STRUCTURAL MASONRY USING A FERROCEMENT OVERLAY
Proceedings of the Third North American Masonry Conference, Arlington, Texas, June 1985, pp. 50-1 to 50-19

[3]
Abboud, Hamid, Harris
SMALL-SCALE MODELING OF CONCRETE BLOCK MASONRY STRUCTURES
ACI Structural Journal, v87 #2 March April 1990, pp.145-155

[4]
El-Metwally, Ashour, Chen
BEHAVIOUR AND STRENGHT OF CONCRETE MASONRY WALLS
ACI Structural Journal, v88 #1 January February 1991, pp.42-48

[5]
Paulay, Priestley
SEISMIC DESIGN OF REINFORCED CONCRETE AND MASONRY BUILDINGS
John Wiley & Sons Inc., New York, 1992

[6]
Angel, Abrams, Shapiro, Uzarski, Webster
BEHAVIOR OF REINFORCED CONCRETE FRAMES WITH MASONRY INFILLS
Structural Research Series Report No. 589, Department of Civil Engineering, University of Illinois at Urbana-Champaign, March 1994

[7]
Rahman, Anand
EMPIRICAL MOHR-COULOMB FAILURE CRITERION FOR CONCRETE BLOCK-MORTAR JOINTS
ASCE Journal of Structural Engineering, v120 #8 August 1994

[8]
Riddington, Jukes
MASONRY JOINT SHEAR STRENGHT TEST METHOD
Proceedings of the Institution of Civil Engineers, v104 #3 August 1994, pp.267-274

[9]
Anand, Rahman
ACCURATE ESTIMATION OF INTERFACE SHEAR STRESSES IN COMPOSITE MASONRY WALLS
ASCE Journal of Structural Engineering, v120 #3 March 1994, pp.998-1015

[10]
Engebretson, Sen, Mullins, Hartley
STRENGHTENING CONCRETE BLOCK WALLS USING CARBON FIBER
Proceedings of the Materials Engineering Conference for the New Millennium
Proceedings of the 1996 4th Materials Engineering Conference Part2 (of 2)
10-14 November 1996,pp.1592-1600

[11]
Sayed-Ahmed, Shrive
NONLINEAR FINITE-ELEMENT MODEL OF HOLLOW MASONRY
ASCE Journal of Structural Engineering, v122 #6 June 1996, pp.683-690

[12]
Hamilton, Holberg, Caspersen, Dolan
STRENGHTENING CONCRETE MASONRY WITH FIBER REINFORCED POLYMERS
Proceedings of the First International Conference on Composites in Infrastructure
(ICCI 1996),Tucson,Arizona, pp.1103-1115

[13]
Wang, Goto, Joh
BOND STRENGHT OF VARIOUS TYPES OF FIBER REINFORCED PLASTIC RODS
Proceedings of the First International Conference on Composites in Infrastructure
(ICCI 1996),Tucson,Arizona, pp.1117-1130

[14]
Roko, Boothby, Bakis
FAILURE MODELS OF SHEET BONDED FIBER REINFORCED POLYMER APPLIED TO BRICK MASONRY
Proceedings of the First International Conference on Composites in Infrastructure
(ICCI 1996),Tucson,Arizona, pp.305-311

[15]
Marshall, Sweeney, Trovillion
SEISMIC REHABILITATION OF UNREINFORCED MASONRY WALLS
Proceedings of the First International Conference on Composites in Infrastructure (ICCI 1996),Tucson,Arizona, pp.287-295

[16]
Tomazevic, Lutman, Petkovic
SEISMIC BEHAVIOUR OF MASONRY WALLS: EXPERIMENTAL SIMULATION
ASCE Journal of Structural Engineering, September 1996, pp.1040-1047

[17]
Tomazevic, Lutman
SEISMIC BEHAVIOUR OF MASONRY WALLS: MODELING OF ISTERETIC RULES
ASCE Journal of Structural Engineering, September 1996, pp.1048-1054

[18]
Ehsani, Saadatmanesh, Al-Saidy
SHEAR BEHAVIOUR OF URM RETROFITTED WITH FRP OVERLAYS
ASCE Journal of Composites for Construction, v1 #1 February 1997, pp.17-25

[19]
Triantafillou, Fardis
STRENGHTENING OF HISTORIC MASONRY STRUCTURES WITH COMPOSITE MATERIALS
Materials and Structures, v30 #202 October 1997, pp.486-496

[20]
Dajun
STUDIES ON BRICK MASONRY UNDER COMPRESSION
Materials and Structures, v30 #198 May 1997, pp.247-252

[21]
Atkinson, Hammons
TENSION STIFFENING BEHAVIOUR OF REINFORCED MASONRY
ASCE Journal of Structural Engineering, v123 #5 May 1997, pp.597-603

[22]
Mojsilovic, Marti
STRENGHT OF MASONRY SUBJECTED TO COMBINED ACTIONS
ACI Structural Journal, v94 #6 November December 1997, pp.633-642

[23]
Khalaf
BLOCKWORK MASONRY COMPRESSED IN TWO ORTHOGONAL DIRECTIONS
ASCE Journal of Structural Engineering, v123 #5 May 1997

[24]
Brosens, Van Gemert
ANCHORING STRESSES BETWEEN CONCRETE AND CARBON FIBER REINFORCED LAMINATES
Proceedings of the Third International Symposium on Non-Metallic(FRP) Reinforcement for Concrete Structures, v1, Japan Concrete Institute, Japan,1998, pp. 271-278

[25]
Maeda, Asano, Sato, Ueda, Kakuta
A STUDY ON BOND MECHANISM OF CARBON FIBER SHEET
Proceedings of the Third International Symposium on Non-Metallic(FRP) Reinforcement for Concrete Structures, v1, Japan Concrete Institute, Japan, 1998,pp. 279-286

[26]
Bernardini, Modena, Valluzzi
LOAD TRANSFER MECHANISMS IN MASONRY:FRICTION ALONG A CRACK WITHIN A BRICK
Materials and Structures, v31, January-February 1998, pp.42-48

[27]
Gilstrap, Dolan
OUT-OF-PLANE BENDING OF FRP-REINFORCED MASONRY WALLS
Composites Science and Technology, v58 #8 August 1998, pp.1277-1284

[28]
Trantafillou
COMPOSITES: A NEW POSSIBILITY FOR THE SHEAR STRENGHTENING OF CONCRETE, MASONRY AND WOOD
Composites Science and Technology, v58 #8 August 1998, pp.1285-1295

[29]
Trantafillou
STRENGHTENING OF MASONRY STRUCTURES USING EPOXY-BONDED FRP LAMINATES
ASCE Journal of Composites for Construction, v2 #2 May 1998, pp.96-103

[30]

American Concrete Institute, Masonry Standard Joint Committee
CODE, SPECIFICATION AND COMMENTARIES, ACI-530-99/ASCE 5-99/ TMS 402-99
American Concrete Institute, American Society of Civil Engineering, The Masonry Society, Detroit, New York and Boulder, 1999

[31]

Miller, Nanni
BOND BETWEEN CFRP SHEETS AND CONCRETE
Proceedings,ASCE 5th Materials Congress, Cincinnati,OH, May 10-12 1999,pp. 240-247

[32]

Drysdale, Hamid, Baker
MASONRY STRUCTURES, BEHAVIOR AND DESIGN
The Masonry Society, 2nd edition, Boulder Colorado(CO),1999

[33]

Yan, Miller, Nanni, Bakis
CHARACTERIZATION OF CFRP RODS USED AS NEAR-SURFACE-MOUNTED REINFORCEMENT
Proceedings of the 8th International Structural Faults and Repair Conference, Engineering Techniques Press, Edinburgh, Scotland,1999, pp.340-350

[34]

Binda, Modena, Valluzzi, Zago
MECHANICAL EFFECTS OF BED JOINT STEEL REINFORCEMENT IN HISTORIC BRICK MASONRY STRUCTURES
Structural Faults+Repair-99,8th International Conference and Exhibition ,London,England, July 13-15,1999

[35]

Ehsani, Saadatmanesh, Velasquez-Dimas
BEHAVIOUR OF RETROFITTED URM WALLS UNDER SIMULATED EARTHQUAKE LOADING
ASCE Journal of Structural Engineering, August 1999, pp.134-142

[36]

Roko, Boothby, Bakis
FAILURE MODES OF SHEET BONDED FIBER REINFORCED POLYMER APPLIED TO BRICK MASONRY
Fourth International Symposium on Fiber Reinforced Polymers (FRP) for RC structures, Baltimore (Maryland), November 1999, pp. 305-311

189

[37]
American Concrete Institute (ACI), Committee 440
GUIDE FOR THE DESIGN AND CONSTRUCTION OF EXTERNALLY BONDED FRP SYSTEMS FOR STRENGTHENING CONCRETE STRUCTURES
July 2000 (document under review)

[38]
American Concrete Institute (ACI), Committee 318
BUILDING CODE REQUIREMENTS FOR REINFORCED CONCRETE AND COMMENTARY
American Concrete Institute, Detroit, Michigan, 1999

[39]
Focacci, Nanni, Bakis
LOCAL BOND-SLIP RELATIONSHIP FOR FRP REINFORCEMENT IN CONCRETE
ASCE Journal of Composites for Construction, February 2000, pp. 24-31

[40]
De Lorenzis, Miller, Nanni, Bakis
BOND OF FRP LAMINATES TO CONCRETE
ACI Structural Journal, July 2000

[41]
Marshall, Sweeney, Trovillion
PERFORMANCE TESTING OF FIBER-REINFORCED POLYMER COMPOSITE OVERLAYS FOR SEISMIC REHABILITATION OF UNREINFORCED MASONRY WALLS
US Army Corps of Engineers, Engineer Research and Development Center, June 2000

[42]
Velasquez-Dimas, Ehsani, Saadatmanesh
OUT-OF-PLANE BEHAVIOUR OF BRICK MASONRY WALLS STRENGHTENED WITH FIBER COMPOSITES
ACI Structural Journal, v97 #3 May June 2000, pp.377-386

[43]
FINITE ELEMENT MODEL OF NONLINEAR DYNAMIC ANALYSIS FOR SMALL-SIZE CONCRETE HOLLOW BLOCK MASONRY
Journal of Northeastern University, v21 #1 2000

[44]
Jai,Springer,Kollar,Krawinkler
REINFORCING MASONRY WALLS WITH COMPOSITE MATERIALS-MODEL
Journal of Composite Materials,v34 #18 2000,pp.1548-1581

[45]
Azevedo, Eeri, Sincraian, Lemos
SEISMIC BEHAVIOUR OF BLOCKY MASONRY STRUCTURES
Earthquake Spectra, v16 #2 May 2000, pp. 337-365

[46]
De Lorenzis
STRENGTHENING OF RC STRUCTURES WITH NEAR SURFACE MOUNTED RODS
MS Thesis, Department of Civil Engineering, The University of Missouri – Rolla
Rolla (MO), 175 pp., May 2000

[47]
Velasquez-Dimas, Ehsani,
MODELING OUT-OF-PLANE BEHAVIOUR OF URM WALLS RETROFITTED WITH FIBER COMPOSITES
ASCE Journal of Composites for Construction, v4 #4, November 2000, pp.172-181

[48]
Stratford, Pascale, Manfroni, Bonfiglioli
SHEAR STRENGHTENING OF MASONRY PANELS WITH GFRP: PRELIMINARY EXPERIMENTAL RESULTS
Proceedings of National Conference on Mechanics of Masonry Structures Strengthened with FRP Materials, Venice, Italy,December 7-8 2000, pp.19-30

[49]
Valluzzi, Tinazzi, Modena
SHEAR TESTS ON MASONRY PANELS REINFORCED WITH FRP SHEETS
Proceedings of National Conference on Mechanics of Masonry Structures Strengthened with FRP Materials, Venice, Italy,December 7-8 2000, pp.31-40

[50]
Marfia, Sacco
MECHANICAL RESPONSE OF MASONRY REINFORCED WITH FRP MATERIALS
Proceedings of National Conference on Mechanics of Masonry Structures Strenghtened with FRP Materials, Venice, Italy,December 7-8 2000, pp.111-120

[51]
De Lorenzis, Tinazzi, Nanni
NEAR-SURFACE MOUNTED RODS FOR MASONRY STRENGHTENING: BOND AND FLEXURAL TESTING
Proceedings of National Conference on Mechanics of Masonry Structures Strenghtened with FRP Materials, Venice, Italy,December 7-8 2000, pp.7-18

[52]
Tumialan, Huang, Nanni, Silva
STRENGTHENING OF MASONRY WALLS BY FRP STRUCTURAL REPOINTING
CIES Report, University of Missouri-Rolla, Rolla(MO), June 2000, 10 pp.

[53]
Tumialan, Tinazzi, Myers, Nanni
FIELD EVALUATION OF UNREINFORCED MASONRY WALLS STRENGTHENED WITH FRP COMPOSITES SUBJECTED TO OUT-OF-PLANE LOADING
CIES Report, University of Missouri-Rolla, Rolla (MO), November 1999, 14 pp.

[54]
Albert, Elwi, Cheng
STRENGTHENING OF UNREINFORCED MASONRY WALLS USING FRPs
ASCE Journal of Composites for Construction, v5 #2, May 2001, pp. 76-84

[55]
Barbieri
INTERVENTI STRUTTURALI SU EDIFICI STORICI IN MURATURA: ELEMENTI PRESSOINFLESSI, RINFORZATI CON MATERIALE COMPOSITO
Ph.D. Thesis, Innovation Engineering Department-University of Lecce (Italy), May 2001

[56]
Hamoush, McGinley, Mlakar, Scott, Murray
OUT-OF-PLANE STRENTHENING OF MASONRY WALLS WITH REINFORCED COMPOSITES
ASCE Journal of Composites for Construction, v5 #3, August 2001, pp.139-145

[57]
Hamilton, Dolan
FLEXURAL CAPACITY OF GLASS FRP STRENGTHENED CONCRETE MASONRY WALLS
ASCE Journal of Composites for Construction, v5 #3, August 2001, pp.170-178